AN INVESTIGATION

INTO

THE ELECTRICAL AND OPTICAL PROPERTIES

OF

THIN FILMS OF NIOBIUM-TIN ALLOYS

by

N. MANGKORNTONG , B.Sc.(Hons), M.Sc.

A thesis submitted to the University of Aston

in Birmingham for the degree of

DOCTOR OF PHILOSOPHY

November, 1977

AN INVESTIGATION INTO THE ELECTRICAL AND OPTICAL PROPERTIES OF THIN FILMS OF NIOBIUM TIN-ALLOYS

by

N. MANGKORNTONG , B.Sc.(Hons), M.Sc.

A thesis submitted for the degree of Doctor of Philosophy of the University of Aston in Birmingham.

November, 1977

SUMMARY

1) Thin films of niobium-tin alloys were prepared in an ultra high vacuum system by a diffusion and alloying technique.For films alloyed at temperatures below 650°C , mixed phases of Nb_6Sn_5 and $NbSn_2$ were observed , while higher alloying temperatures yielded single phase of Nb_3Sn (β-tungsten structure) which had the lattice parameter ranging from 5.28 to 5.29 Angstroms.

2) Electrical properties of the normal and superconducting states were studied in the temperature range 2 - 300°K by using a four point probe technique. The highest transition temperatures(T_c) for Nb_3Sn and mixed phases (of Nb_6Sn_5 and $NbSn_2$) were 18.2°K and 2.8°K , respectively. A correlation between the resistivity ratio (ρ_{300}/ρ_{20}) and T_c was observed for Nb_3Sn films, having resistivity ratios in the range 1 to 4 for film thicknesses in the range 27-510 nm.

3) From the ellipsometric measurements at a radiation wavelength of 549 nm , the optical constants , n and k , of Nb_3Sn were 2.35 ± 0.2 and 2.6 ± 0.1 , respectively.

4) Oxide growth on the surfaces of some Nb_3Sn films was stimulated by heating the specimens in the atmosphere, which enabled the following phenomena to be studied :

a) Depression of T_c due to decrease in film thickness.In attempts to explain this effect , a model of film structure was proposed and was found applicable to the depression of T_c caused by other processes of induced damage such as alpha-particle and neutron bombardment.

b) Electron mean-free-path (m.f.p.) as a function of temperature. From observations on a film of Nb_3Sn, the resistivity was estimated to be saturated at temperatures above 600°K when the effective m.f.p. is comparable with the atomic spacing.

c) Refractive index of grown oxide layers. The refractive index of oxide , as evaluated from the change of the ellipsometric parameters due to the oxide growth, at the radiation wavelength of 549 nm , was 2.5 ± 0.2.

Index terms : **********

superconductivity
thin films
beta-tungsten
cryostats
ellipsometry

Objectives of the Present Investigation

During the last decade, considerable interest has been shown in the alloys Nb_3X (X = Sn, Ga,Ge and Si) having β-tungsten structure because of their high critical temperature(T_c), either measured or expected. Among these alloys, Nb_3Sn is the only compound in which β-tungsten structure can be easily prepared by several methods such as sintering (Matthias et al.,1954) , chemical vapour deposition (Hanak et al.,1964) and solid state diffusion (Kunzle et al.,1961 , Mangkorntong and Neal,1977), and is the most studied material so far, owing to its various applications, e.g., in high magnetic field and power transmission lines. In particular, at the Technical University of Wupperal in West Germany, experiments on resonators ultilizing superconducting surface layers of Nb_3Sn have been undertaken in an attempt to produce electron accelerators (private communication). A thin layer of the alloy has been formed on the surface of niobium by heating the metal under vacuum conditions in tin vapour at a temperature in the region of 900°C. Surface layers with high T_c have been obtained, although it is not easy to determine the characteristics of these layers independently, particularly if they are very thin.

One of the objectives of the present work was to prepare such layers in the form of thin films (Mangkorntong and Neal, 1977) which enable independent investigation of the structural, electrical and optical properties of the films.

A second objective was to investigate any correlation between the (normal to superconducting) transition temperature

and other electrical properties as had already been observed in this department. Previous studies in this laboratory on thin films of niobium (Salter,1973) and tantalum(Aguado Bombin,1975) show that there is a correlation between the transition temperature (T_c) and the resistivity ratio, ρ_{300}/ρ_{10}. Consequently, two empirical expressions have been proposed by Aguado Bombin and Neal(1976) to establish this correlation.

Since optical properties had elucidated interesting features in tantalum films (Neal and Aguado Bombin,1977),it was also decided to investigate the optical properties of the films of Nb_3Sn.

****

CONTENTS

LIST OF TABLES

Table | Page No.

CHAPTER 1 : INTRODUCTION

1.1 Phenomenon of Superconductivity

The disappearance of the electrical resistance of mercury at the normal boiling point of helium was first observed by Kammerlingh Onnes in 1911. He called this phenomenon 'Superconductivity'. Since then, it has been extensively studied, both experimentally and theoretically, and is now well established as a macroscopic manifestation of quantum effects. A theoretical survey of the nature and origin of superconductivity will be presented in Section 2.6. The temperature at which a material becomes superconducting in the absence of a magnetic field is called the transition temperature or critical temperature (T_c).

Since 1911, a large number of metals, alloys and compounds have been found to be superconducting. A comprehensive list of superconducting materials discovered up to 1964 has been published in Ben Roberts's Compilation (1964). A recent review article about these materials in various forms, e.g., powders, thin films and solid solutions has been up-dated by the same author (Roberts,1976).

1.2 Materials With High Critical Transition Temperatures

The history of high T_c superconductors began in 1954 when Hardy and Hulm (1954) found V_3Si to be superconducting at 17 ^{o}K. Matthias et al.(1954) subsequently reported a T_c of 18 ^{o}K in Nb_3Sn. Since then , higher T_cs have been observed, mostly in niobium based compounds with β-tungsten structure. Alekseevskii et al.(1966) were able to show that the ternary alloy, $Nb_3Al_{0.8}Ge_{0.2}$, had a higher T_c

than the constituent compounds, Nb_3Al (T_c=19°K) and Nb_3Ge (T_c=7°K). Later, Matthias et al.(1967) obtained a T_c of 21°K with this alloy. Webb et al.(1971) have achieved T_c's above 20°K in Nb_3Ga. At the present, the highest critical temperature has been observed in Nb_3Ge sputtered films (T_c=23°K). In 1973, Gavaler provided an important advance in obtaining T_c of 22.3°K in Nb_3Ge sputtered on to hot substrates at high argon pressures. This was later increased to T_c onset* of 23°K by Testardi et al.(1974) and Gavaler et al.(1974).

1.3 Compounds in the Niobium-Tin System

The system of niobium-tin is of interest owing to the existence of the superconducting compound Nb_3Sn. The first attempt at constructing a phase diagram was made by Agafonova et al.(1959). They reported the peritectic decomposition of Nb_3Sn at about 2000°C. Later on several compounds and various forms of Nb-Sn diagrams were proposed. Reed et al.(1962) reported that Nb_3Sn, Nb_3Sn_2 and Nb_2Sn_3 could be present. Wyman et al.(1962) found Nb_4Sn, Nb_3Sn, Nb_2Sn and Nb_2Sn_3. Enstrom et al.(1962) observed the presence of Nb_3Sn, Nb_3Sn_2 and Nb_2Sn_3. Kogan et al.(1963) reported that apart from Nb_3Sn another compound, rich in tin, Nb_5Sn_3 could exist. In abstracts reported by Courtney et al.(1964) and by Schadler and Rosenbaum(1964), three compounds Nb_3Sn, Nb_2Sn_3 and $NbSn_2$ were mentioned. Ellis and Wilhelm (1964) observed Nb_3Sn_2 and Nb_2Sn_3 as the additional phases to Nb_3Sn.

* The temperature at which a material starts becoming superconductor. This term is usually used for specimens having broad transition curves.

van Vucht et al.(1965) investigated the niobium-tin phase diagram very extensively and concluded that three compounds exist , namely Nb_3Sn , Nb_6Sn_5 and $NbSn_2$.

According to van Vucht et al.(1965) , Nb_6Sn_5 and $NbSn_2$ are present below 1200°C. The crystal structure of Nb_6Sn_5 is isomorphous to β -Ti_6Sn_5 (i.e., body-centred orthorhombic) with unit cell a=16.81 Å, b=9.2057 Å and c=5.6549 Å. The peritectic decomposition has been observed at 930°C. $NbSn_2$ is also orthorhombic with unit cell a=9.852 Å, b=5.654 Å and c=19.126 Å and peritectic decomposition is at 840°C. Above 1200°C, their phase diagram is similar to that observed by Vieland(1964) who reported the peritectic decomposition of Nb_3Sn at 2130°C. The dominant crystal structure is β -tungsten type with lattice constant ranging from 5.280 to 5.291 Å.

The compounds observed by various workers are summarized in Table(1.1). The complete phase diagram and some physical properties of the compounds proposed by van Vucht et al.(1965) and Vieland(1964) are presented in Fig.(1.1) and Table(1.2), respectively.

1.4 The Alloy Nb_3Sn

According to Matthias(1971) high transition temperatures above 12°K have been mostly found in the β -tungsten, NaCl and Pu_2C_3 structures. The compounds with β -tungsten structure, particularly Nb_3Sn, have been the most extensively studied because of their usefulness in the production of high magnetic fields and other applications.

The intermetallic compound Nb_3Sn was first synthesized by Matthias et al.(1954). They observed a superconducting transition

Table 1.1 The compounds in the niobium-tin system according to various authors.

Compound	Stability temperature (^{o}C)	Concentration (at% of Nb)	Observers
Nb_3Sn	Room-2000	75%	Agafonova et al.(1959)
Nb_3Sn	Room-2000	75%	Kogan et al.(1963)
Nb_5Sn_3	Room-850	——	" "
Nb_3Sn	not given	not given	Kolbe and Rosner (1963)
Nb_3Sn_2	" "	" "	" "
Nb_2Sn_3	" "	" "	" "
Nb_4Sn	Room-2050	20.8-22.6%	Wyman et al.(1962)
Nb_3Sn	Room-730	25.1-26.8%	" "
Nb_2Sn	Room-690	30.2%	" "
Nb_2Sn_3	Room-863	39-41.3%	" "
Nb_3Sn	860-2000	——	Reed et al.(1962)
Nb_3Sn_2	755-890	60%	" "
Nb_2Sn_3	Room-850	40%	" "
Nb_3Sn	775-2000	75-80%	Enstrom et al.(1963)
Nb_3Sn_2	600-1175	56.1%	" "
Nb_2Sn_3	Room-1050	38.6-40%	" "
Nb_3Sn	775-2000	75-79%	Courtney et al.(1964)
Nb_3Sn_2	600-925	54.5-56.1%	" "
$NbSn_2$	Room-850	35-40%	" "

Table 1.1 (Continued.)

Compound	Stability temperature (^{o}C)	Concentration (at% of Nb)	Observers
Nb_3Sn	——	78.5%	Schadler and Rosenbaum (1964)
Nb_3Sn_2	below 915	59%	" "
$NbSn_2$	below 840	33%	" "
Nb_3Sn	Room-2130	——	Ellis and Wilhelm (1964)
Nb_3Sn_2	Room-915	——	" "
Nb_2Sn_3	Room-820	——	" "
Nb_3Sn	805-2000	——	Levinstein and Buehler (1964)
Nb_3Sn_2	805-925	——	" "
$NbSn_2$	Room-950	——	" "
Nb_3Sn	——	75%	Enstrom et al.(1962)
Nb_3Sn_2	——	56%	" "
Nb_2Sn_3	——	38%	" "
Nb_3Sn	——	——	Reed and Gatos (1962)
Nb_3Sn_2	775-875	——	" "
Nb_2Sn_3	Room-875	——	" "
Nb_3Sn	Room-1980	75-80%	van Vucht et al.(1965)
Nb_6Sn_5	Room-930	54.5%	" "
$NbSn_2$	Room-840	33%	" "

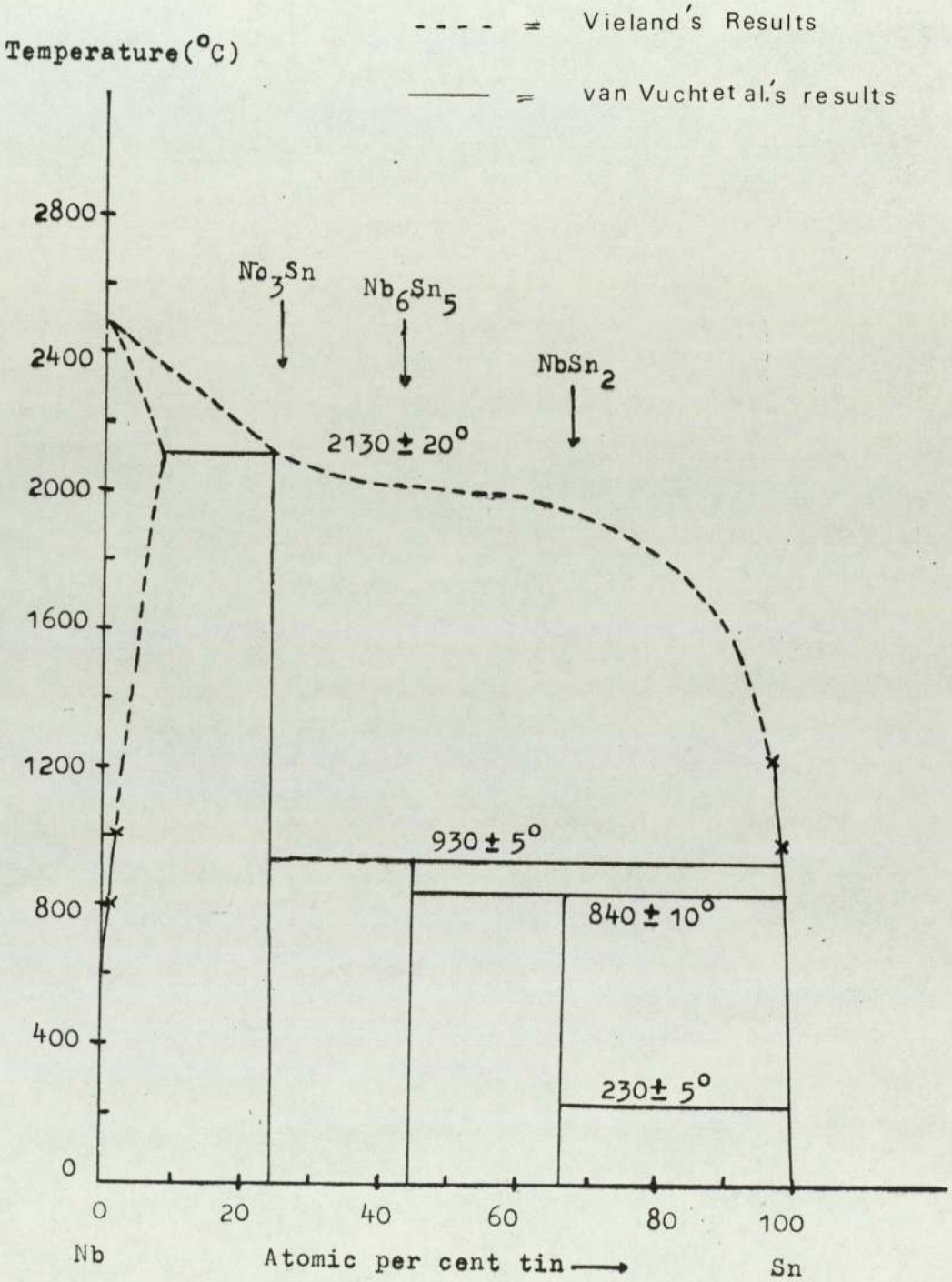

Fig. 1.1. Phase diagram of the system Nb-Sn combining the high temperature measurements of Vieland(1964) and van Vucht et al. (1965).

Table 1.2 Some physical properties of intermetallic compounds in the niobium-tin system (After van Vucht et al.(1965)).

Compound	Physical properties
Nb_3Sn	β-tungsten type (A15) cubic unit cell a=5.2902 - 5.2816 Å peritectic decomposition at 1980 ± 10°C d_o=8.95 ± 0.05 g/cm^3, d_c=8.92 g/cm^3, Z=2 T_c=18.3°K
Nb_6Sn_5	isomorphous to β-Ti_6Sn_5 b.c. orthorhombic unit cell a=16.814 ± 0.001 Å b=9.2057 ± 0.0004 Å c=5.6549 ± 0.0005 Å d_o=8.6 ± 0.1 g/cm^3, d_c=8.74 g/cm^3, Z=4 peritectic decomposition at 930 ± 15°C T_c < 0.3°K
$NbSn_2$	Mg_2Cu type orthorhombic unit cell a=9.852 ± 0.001 Å b=5.645 ± 0.001 Å c=19.126 0.003 Å d_o=8.08 ± 0.03 g/cm^3, d_c=8.26 g/cm^3, Z=16 space group F ddd peritectic decomposition 840 ± 10°C T_c=2.6°K

temperature of 18.05°K in the sintered Nb_3Sn with the β-tungsten structure. It was considered that this alloy was formed by a peritectic reaction between about 1200°C and 1500°C. Later Geller et al.(1955) made a more accurate determination of the lattice constant and obtained $a_o = 5.289 \pm 0.002$ Å.

In 1960, Bozorth et al. discovered that the critical magnetic field for Nb_3Sn was unusually high, 7 Teslas, at 4.2°K, compared to less than 2 Teslas observed in niobium. A year later Kunzler et al. (1961) succeeded in solving the problem of preparing Nb_3Sn wires for superconducting coils, because of its extreme brittleness. They obtained the critical current density of the order of 10^5 Amp/cm^2 in a magnetic field of 8.8 Teslas, at 4.2°K. A short time later, Arp et al. (1961) observed superconductivity at 1.6°K in pulse magnetic field of 18.5 Teslas. Later the superconductivity of Nb_3Sn in even higher fields has been reported. A critical field of the order of 20 Teslas at 4.2°K has been made by Hart et al.(1962) and by Montgomery (1965).

1.5 Preparation of Thin Films of Nb_3Sn

The crucial part of the present work was the preparation of thin films of Nb_3Sn. Prior to this work, there have been a number of reports on the techniques utilized in preparation. Nb_3Sn films were first prepared by Hanak (1963) who developed a chemical vapour-deposition process involving the simultaneous reduction of gaseous chlorides of niobium and tin by hydrogen. Elevated substrate temperatures, in the neighbourhood of 1000°C were required. Neugebauer (1964) used a codeposition method to prepare niobium-tin films in a vacuum system. It was observed that the cubic phase Nb_3Sn

was the predominant product when the deposition rate of Nb:Sn was near 3:1 regardless of substrate temperatures. Initial exploration of the formation of Nb_3Sn layers was done by Jackson and Hooker (1969), using low-energy electron-diffraction (LEED). Extensive studies of ultra thin films of Nb_3Sn has been reported by Dickey et al.(1971). Thin layers of tin about 100 Å thick were deposited on niobium foils,heated to form Nb_3Sn, and then its transition temperature was measured in situ in a vacuum chamber. Recently Strozier et al. (1973) re-investigated the surface effects on the formation of the structure using LEED and Auger electron spectroscopy. They observed that the Nb_3Sn layers decomposed at temperatures above about 980°C, as was observed by Dickey et al. (1971), but they argued that the loss of tin was by sublimation into the vacuum rather than diffusion into the niobium surface.

In the present investigation only codeposition and solid state diffusion (of tin into niobium) methods were possible with the equipment available in this laboratory. After several initial runs, it was found that the solid state diffusion method was to be preferred for films of good quality, i.e., those with which a high T_c could be obtained. The codeposition method was abandoned because the ratio of evaporation rates of niobium:tin could not be manually controlled by a simple mechanism to be 3:1 which has been found by Neugebauer (1964) to be crucial factor for the formation of Nb_3Sn.

* * * * * * * * * * * * * * * * * * *

CHAPTER 2 : THEORETICAL FOUNDATIONS

2.1 Film Formation

One of the most common methods employed for preparing thin films is by means of condensation. Atoms condense from the vapour phase of a material to form three dimensional nuclei which then grow to form a continuous film by a diffusion-controlled process. The structural behaviour and properties of films can largely be ascribed to this growth process (Chopra,1969).

At the earliest stage of film formation, the condensation of vapour atoms is determined by their interaction with the surface on which they impinge. The vapour atoms which are then physically absorbed (called 'adatoms') may migrate over the surface during their lifetime to form pairs which, in turn, act as condensation centres for other atoms.

The characteristic sequential growth stages are : (1) randomly distributed three-dimentional nuclei are first formed and rapidly approach a saturation density. These nuclei then grow to form observable islands, (2) as islands increase their size by further deposition and come closer to each other, the larger ones appear to grow by coalescence of the smaller ones, (3) when the islands distribution reaches a critical state, a rapid large-scale coalescence of the islands results in a connected network structure and (4) the final stage of growth is a slow process of filling spaces between islands.

The influence of the deposition parameters on film growth may be understood in terms of their effects on the sticking coefficient, the nucleation density and the surface mobility of adatoms. Their

effects are felt in some aspects of physical structure of thin films, such as grain size, lattice constants, crystalline structure and orientated growth.

2.2 Survey of the Theory of Electrical Conduction

Shortly after Thomson's discovery of the electron, a universal theory of metallic conductivity based on the average velocity of free electrons in a 'free electron gas' was developed by Drude (1900). This enabled him to give a theoretical derivation of the empirical law of Wiedemann and Franz, i.e., the ratio of the electrical and thermal conductivities at a given temperature is the same for all metals. According to Drude, the Wiedemann-Franz ratio is :

$$K/\sigma = LT \qquad (2.1)$$

where L is the Lorenz number, K and σ are the thermal and electrical conductivities respectively and T is the absolute temperature. In 1905, Lorentz used the Boltzmann transport equation and a simplified model for the collision between the electrons and atoms in the lattice. Although the transport problems are immensely simplified when a relaxation time, τ , is established in the solution of the Boltzmann equations, Lorentz's theory was unable to produce reasonable results for thermal and magnetic effects associated with metallic conduction, such as specific heat and the paramagnetism of metals. It was left to Sommerfeld to show that many of the most serious difficulties of the Drude-Lorentz theory could be reconciled if the distribution of electrons is governed by Fermi-Dirac statistics instead of classical statistics (Sommerfeld, 1928).

2.3 A Model of the Electrical Conduction Mechanism

From the macroscopic point of view , the electrical conductivity of a metal is defined by

$$J_x = \sigma E_x \qquad (2.2)$$

where J_x is the current density resulting from an applied electrical field E_x in the x-direction. In the case of an anisotropic solid, the conductivity depends on direction and becomes a tensor (see for example Dekker,1962). By assuming an isotropic solid, the conductivity becomes scalar and the current density, from an atomic view point, is

$$J_x = - ne\langle v_x \rangle \qquad (2.3)$$

where n is the number of electrons per unit volume, -e is the electronic charge and $\langle v_x \rangle$ is the average velocity of the electrons in the x-direction.

Consider a simple model of the electrical conduction mechanism which shows the essential features of the theory of conductivity. In its simplest phenomenological form, the interaction of the electrons with the lattice may be described in the following manner: when an electric field is applied, the energy gained by an electron from the external field is assumed to be wholly given up at a collision so that the drift velocity momentarily becomes zero and then motion of the electron immediately afterwards can be taken as being entirely random. Furthermore, a quantity τ is also introduced such that the probability for an electron to collide with the lattice during a small time interval dt is dt/τ. For simplicity, it is

assumed that τ is constant, independent of the energy of the electron and of the direction of motion. Under the terms of the model specified above, the rate of change of the average velocity in the x-direction due to the field alone is

$$(\partial \langle v_x \rangle / \partial t)_{field} = -eE_x/m \qquad (2.4)$$

Also, the rate of change of $\langle v_x \rangle$ due to collisions with the lattice alone is

$$(\partial \langle v_x \rangle / \partial t)_{coll.} = -\langle v_x \rangle / \tau \qquad (2.5)$$

since $1/\tau$ is the probability for a collision per second and after the collision the velocities are random. Thus, in the steady state

$$d\langle v_x \rangle / dt = 0 = (\partial \langle v_x \rangle / \partial t)_{field} + (\partial \langle v_x \rangle / \partial t)_{coll.} \qquad (2.6)$$

From equations (2.4), (2.5) and (2.6) it follows that the average drift velocity in the field direction is given by

$$\langle v_x \rangle = (-e\tau/m)E_x \qquad (2.7)$$

From equations (2.3) and (2.7) the conductivity is given by

$$\sigma = ne^2\tau/m = ne^2 l/m\langle v_x \rangle \qquad (2.8)$$

where the mean free path of the collisions, $l = \tau \langle v_x \rangle$.

Suppose that under the influence of an electric field E_x, the electrons have a certain average drift velocity and that at the instant t=0 the field is suddenly switched off. As a result of the collisions with the lattice the average drift velocity will gradually approach zero, since the rate of change of $\langle v_x \rangle$ by collisions alone is given by equation (2.5) , the average drift

velocity at time t>0 will be

$$\langle v_x(t>0) \rangle = \langle v_x(0) \rangle e^{-t/\tau} \qquad (2.9)$$

where $\langle v_x(0) \rangle$ is the average drift velocity at t=0. Because of the exponential form of equation (2.9), the quantity τ is called the relaxation time.

Although the argument so far is based on the simple model specified above, the expression of the conductivity in equation (2.8) is still valid for the more sophisticated theory of conductivity, providing some appropriate adjustments are made. For example, when the Boltzmann Transport Equation is employed (see, for example, Dekker, 1962), the relaxation time, τ, is governed by the distribution function in the expression

$$(f - f_o)_{t>o} = (f - f_o)_{t=o} e^{-t/\tau} \qquad (2.10)$$

where f_o and f are the distribution functions of the electrons in the thermal equilibrium in the absence and presence of the external field, respectively.

Following Sommerfeld(1928), the Fermi-Dirac statistics is now applied to the problem, obtaining the conductivity in the form similar to that of equation (2.8), i.e.,

$$\sigma = \frac{ne^2 l_F}{m^* v_F} \qquad (2.11)$$

where n is the number of conduction electrons per unit volume , v_F is the average velocity of the electrons at the surface of the Fermi distribution, l_F is the mean free path of the conduction electrons. The effective mass m* arises from the modern theory of solids initiated by Bloch (1928) in which a conduction electron in a metal under influence of an electric field can be treated as a

free particle having an effective mass(Kittel, 1971):

$$m^* = \bar{h}^2/(d^2E/dk^2) \qquad (2.12)$$

where h is Planck's constant and $\bar{h} = h/2\pi$. E is the energy of the electron corresponding to the wave vector of the state k.

The resistivity is defined by

$$\rho = 1/\sigma = m^*v_F/ne^2l_F = m^*/ne^2\tau_F \qquad (2.13)$$

This relation is correct at least for an isotropic monovalent metal which has a simple conduction band model.

2.4 Matthiessen's Rule

According to Bloch(1928), an electron can move freely through a perfect crystal lattice without resistance. The actual cause of the resistivity must therefore be sought in deviations from the periodicity of the potential in which the electrons move. These deviations may be due to :

(i) Lattice vibrations

(ii) Lattice defects, such as vacancies, interstitial atoms and dislocations.

(iii) Foreign impurity atoms

(iv) Boundaries

In general, the temperature dependence of resistivity is due to the lattice vibrations and is proportional to absolute temperature, T, at high temperatures and as a good approximation to T^5 at very low temperatures. The residual resistivity is mainly due to the scattering processes of types (ii) and (iii) mentioned above. Denoting the relaxation times associated with each of these

processes by τ_{res} and τ_{th} for the residual and thermal resistivities respectively, the resulting relaxation time, τ , according to Matthiessen's rule, is given by

$$1/\tau = 1/\tau_{res} + 1/\tau_{th} \qquad (2.14)$$

since the probabilities for scattering in this simple model are additive and they are proportional to the reciprocals of the relaxation times. An alternative to the above expression for the resistivity of a metal containing small amounts of impurities is

$$\rho(T) = m^*/ne^2\tau = m^*/ne^2(1/\tau_{res} + 1/\tau_{th})$$

$$= \rho_o + \rho_1(T) \qquad (2.15)$$

where the residual resistivity ρ_o is a constant which increases with increasing impurity content and the resistivity $\rho_1(T)$ is the temperature-dependent part of the total resistivity, arising from the thermal motion of the lattice.

In the case of thin films the scattering at boundaries can be important,and the expression in (2.14) and (2.15) may be written as follows :

$$1/\tau = 1/\tau_{res.} + 1/\tau_{th.} + 1/\tau_{bou.} \qquad (2.16)$$

and

$$\rho_F(T) = \rho_o + \rho_1(T) + \rho_{bou.} \qquad (2.17)$$

2.5 Size Effect on Electrical Resistivity

As the thickness of a metal film becomes comparable in magnitude with the mean free path of electrons (m.f.p.), the film boundaries impose a geometrical limitation on the movement of the

conduction electrons resulting in a higher electrical resistivity for a film than that for the same metal in the bulk. Physical effects arising because of this geometrical limitation of the m.f.p. are called "mean-free-path" or "size" effects.

A size-effect theory was initially proposed by Thomson(1901). The modern size-effect theory for a free-electron model has been established by Fuchs(1938) for a metal with a spherical Fermi surface and extended by Sondheimer(1950,1952) to include galvanomagnetic effects. Lucas(1965) generalized Fuchs' calculation to the case of scattering from the two surfaces with different specularity parameters. Fuchs' treatment is a statistical analysis based on the Boltzmann equation for the distribution function, f , of the conduction electrons which is formed by equating the rate of change of f due to external fields to the rate of change due to the collision mechanism. In the presence of an electric field, $\vec{E}$, and a magnetic field, $\vec{H}$, the Boltzmann equation for quasi-free electrons takes the form:

$$-e/m(\vec{E} + \vec{v} \times \vec{H}) \ \text{grad}_v f + v \ \text{grad}_r f = (\partial f/\partial t)_{coll} \qquad (2.18)$$

where f is the Fermi-Dirac function of the velocity vector, $\vec{v}$, and the space vector, $\vec{r}$, and m is the mass of an electron.

The term $(\partial f/\partial t)_{coll}$ can be determined by the time taken for the distribution function, f, to relax to the steady undisturbed state, f_o, when the external constraint is removed. The approach to equilibrium is then given by

$$(f - f')_t = (f - f_o)_{t=o} e^{-t/\alpha} \qquad (2.19)$$

where f' is the distribution function at time t.

Since $\partial f_o/\partial t = 0$,

$$(\partial f/\partial t)_{coll.} = -(f - f_o)/\tau \qquad (2.20)$$

If v is the mean velocity of these electrons to which τ refers, the corresponding free path l is defined by $l = v\tau$.

In order to find the solution of equation (2.3), i.e., to determine the current density, for metal films, consider a metal film of thickness t with the z axis perpendicular to the film and an electrical field, $\vec{E}$, applied in the x-direction. The distribution function may be written in the form

$$f = f_o + f_1(v,z) \qquad (2.21)$$

To the first order of approximation the product of $\vec{E}$ with f in equation (2.18) can be neglected (i.e., the terms causing deviation from Ohm's law) and the Boltzmann equation reduces to

$$\partial f_1/\partial z + f_1/\tau v_z = e\vec{E}/mv_z(\partial f_o/\partial v_x) \qquad (2.22)$$

The general solution of this equation is

$$f_1(v,z) = e\vec{E}\tau/m(\partial f_o/\partial v_x)(1 + F(v)\exp(-z/\tau v_z)) \qquad (2.23)$$

where F(v) is an arbitrary function of v determined by the boundary conditions. Assume the boundary condition that every free path is terminated by collision at the surface (diffuse scattering) so that the distribution function of the electrons leaving each surface must then be independent of direction, and further that the relaxation process for surface scattering is the same as for the bulk. This first condition is satisfied if F(v) is chosen so that $f_1(v,0) = 0$ for all v such that $v_z > 0$ and $f_1(v,t) = 0$ for all v such that $v_z < 0$. Thus, there are two values for f_1, depending on

whether electrons are moving away from ($v_z>0$),or moving toward ($v_z<0$) the surface. These may be written as

$$f_1^+(v,z) = eE\tau/m(\partial f_o/\partial v_x)(\ 1 - \exp(-z/\tau v_z)) \qquad (2.24a)$$

$$f_1^-(v,z) = eE\tau/m(\partial f_o/\partial v_x)(\ 1 - \exp((t-z)/\tau v_z)) \qquad (2.24b)$$

for $v_z>0$ and $v_z<0$, respectively.

The current density for a position z is given by

$$J(z) = -2e(m/h)^3\iiint v_x f_1 dv_x dv_y dv_z \qquad (2.25)$$

which can be simplified by introducing polar co-ordinates (v,Θ,ϕ) in the v space (with $v_z = v\cos\Theta$) and remembering that f_o depends only on the magnitude of v. The total current density is obtained by integrating equation (2.25) with respect to z. The current density J_B in bulk metal may be obtained by putting $z = \infty$ in the integration of equation (2.25). Since the effective conductivity is $\sigma = J/E$, the ratio of the conductivities is given by an expression

$$\sigma_B/\sigma_F = \rho_F/\rho_B = \phi(\tau)/\tau \qquad (2.26)$$

here $\tau = d/l_B$, and

$$1/\phi(\tau) = 1/\tau - 3/8\tau^2 + 3/2\tau^2\int_1^\infty (1/a^3 - 1/a^5)e^{-\tau a}da \qquad (2.27)$$

The limiting form for large τ ($\tau>1$) is given by

$$\sigma_B/\sigma_F = \rho_F/\rho_B = 1 + 3/8\tau \qquad (2.28)$$

and for very thin films ($\tau\ll1$)

$$\sigma_B/\sigma_F \approx \frac{4}{3\tau(\ln(1/\tau) + 0.4228)} \qquad (2.29)$$

Fig.(2.1) shows plots of equations (2.28) and (2.29).

So far the assumption is only for completely diffused

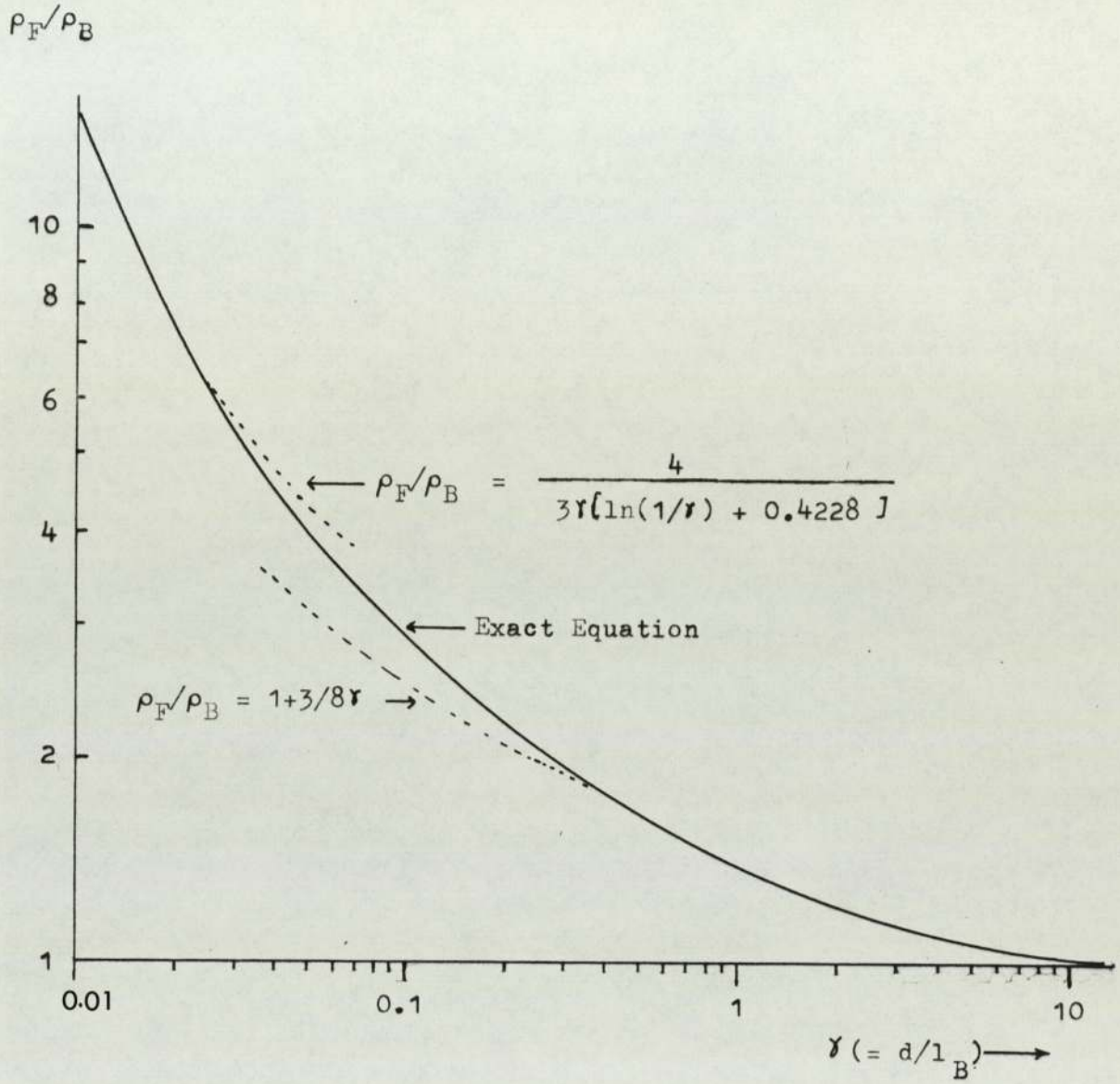

Figure 2.1 Theoretical variation of the film-to-bulk resistivity ratio (ρ_F/ρ_B) with reduced thickness , d/l_B .

scattering processes.If the scattering is not entirely diffuse the specularity parameter,p,has to be employed. This parameter, initially introduced by Fuchs(1938), is a measure of the size-effect deviation from the bulk behaviour which ranges from zero for perfect specular scattering (p=1) to the minimum value for perfect diffused scattering(p=0) (see, for example,Cirkler,1957 and Niebuhr, 1952). For simplicity of calculations, p is considered to be a constant. The general solution of equation (2.23) is still valid but to determine F(v) the boundary conditions are controlled by the specularity parameter p. The factor F(v) is chosen so that the distribution function of the electrons satisfy the boundary conditions below :

$$f_1^+(v,z=0) = pf_1^-(-v_z,0) \qquad (2.30a)$$

$$f_1^-(v,z=t) = pf_1^+(-v_z,t) \qquad (2.30b)$$

which yields,

$$f_1^+(v,z) = eE\tau/m(\partial f_o/\partial v_x)\left(1- \frac{(1-p)\exp(-z/\tau v_z)}{1-p\exp(-t/\tau v_z)}\right) \qquad (2.31a)$$

$$f_1^-(v,z) = eE\tau/m(\partial f_o/\partial v_x)\left(1- \frac{(1-p)\exp((t-z)/\tau v_z)}{1-p\exp(t/\tau v_z)}\right) \qquad (2.31b)$$

for $v_z > 0$ and $v_z < 0$, respectively.

The effective conductivity is calculated as before. The function $\phi(\tau)$ defined by equation (2.27) is now replaced by

$$1/\phi(\tau) = 1/\tau - 3/2\tau^2(1-p)\int_1^\infty (1/a^3-1/a^5)\left(\frac{1-e^{\tau a}}{1-pe^{-\tau a}}\right)da \qquad (2.32)$$

The limiting forms of equation (2.32) for thick and thin films yield,

$$\sigma_B/\sigma_F = \rho_F/\rho_B = 1 + 3(1-p)/8\tau \qquad (\tau>1) \qquad (2.33)$$

and $$\rho_F/\rho_B \approx \frac{4}{3}\frac{(1-p)}{(1+p)}\frac{1}{\tau(\ln(1/\tau) + 0.4228)} \qquad (2.34)$$

$(\tau \ll 1)$

which reduces to equations (2.28) and (2.29) respectivly, when p = 0

2.6 Superconductivity

From 1911 until Meissner and Ochsenfeld's work in 1933 , superconductivity was consider to be infinite conductivity and attempts were made to try to understand the apparent lack of scattering. An early step towards a phenomenological theory of superconductivity was made by Gorter and Casimir(1934,a) who showed that the thermodynamic properties of superconductors could be accounted for by assuming that their conduction electrons were divided into two fluids or phases. The electrons in one phase were considered to retain their normal properties (n_n) but a proportion ($n_s/(n_n+n_s)$) was assumed to be condensed into a lower free energy phase in which conduction takes place without dissipation of (Joule) heat. This proportion ($n_s/(n_n+n_s)$) was assumed to be unity at the absolute zero of temperature and zero at the critical temperature, T_c.

2.6.1 The London Theory

Before the discovery of the Meissner effect in 1933, Becker et al.(1933) predicted that there could be a magnetic field (H_o) trapped inside a superconducting specimen if H_o had been stored while the specimen was in the normal state. The argument is as follows when an electric field, $\vec{E}$, is applied to an electron mass, m, and charge, e, there would be an acceleration according to the equation

$$m\dot{\vec{v}} = e\vec{E} \tag{2.35}$$

with the current density

$$\vec{J} = n\vec{v}e \tag{2.36}$$

where n is the density of the conduction electrons.

Differentiating equation (2.36) and eliminating $\dot{\vec{v}}$ using equation (2.35) to obtain

$$\vec{E} = (m/ne^2)\dot{\vec{J}} = (4\pi\lambda^2/c^2)\dot{\vec{J}} \tag{2.37}$$

where $$\lambda^2 = mc^2/4\pi ne^2 \tag{2.38}$$

Using Maxwell's equation for a region where $\mu = 1$, to obtain

$$\text{curl } \vec{E} = (-1/c)\dot{\vec{H}} \tag{2.39}$$

Substituting $\vec{E}$ from equation (2.38) into equation (2.39)

$$(4\pi\lambda^2/c)\text{curl } \dot{\vec{J}} + \dot{\vec{H}} = 0 \tag{2.40}$$

$\vec{J}$ can be eliminated by considering another of Maxwell's equations

$$\text{curl } \vec{H} = (4\pi/c)\vec{J} \tag{2.41}$$

Making use of the vector identity

$$\text{curl}(\text{curl } \vec{A}) = \text{grad}(\text{div } \vec{A}) - \text{div}(\text{grad}\vec{A}),$$

equation (2.14) becomes

$$\nabla^2 H = -(4\pi/c)\text{curl } \vec{J} \tag{2.42}$$

Since grad(div H) is identically zero, then

$$\nabla^2 \dot{\vec{H}} = -(4\pi/c)\text{curl } \dot{\vec{J}} \tag{2.43}$$

Using the relation of equation (2.40) to obtain

$$\pi^2 \nabla^2 \dot{\vec{H}} = \dot{\vec{H}} \tag{2.44}$$

and integrating equation (2.44) with respect to time yields

$$\lambda^2 \nabla^2 (\vec{H} - \vec{H}_o) = \vec{H} - \vec{H}_o \qquad (2.45)$$

where $\vec{H}_o$ is a constant. By solving equation (2.45) for a semi-infinite body whose surface is at x=0, it can be shown that the internal field, H_{in}, at a distance x from the surface is

$$H_{in} = H_o + (H_{ext} - H_o)e^{-x/\lambda} \qquad (2.46)$$

Here H_{ext} is the external field and H_o is any field present in the superconducting specimen. According to equation (2.46) the external field falls off exponentially inside a zero-resistance material to a 'trapped' field H_o (which could be stored before the specimen passes to the superconducting state). This was the theoretical prediction. However, in 1933 Meissner and Ochsenfeld measured the flux distribution outside tin and lead specimens which had been cooled below their transition temperatures while in a magnetic field. They found that the expected situation of equation (2.46) did not occur, but that at their transition temperatures the specimen spontaneously became perfectly diamagnetic, even though they had been cooled in a magnetic field. This effect, whereby the flux density inside a bulk superconducting material is zero even when in an applied magnetic field is called the' Meissner effect'.

In 1935, F. and H. London showed that the Meissner effect could be incorporated into the Becker-Heller-Santer theory if equation (2.40) was replaced by the equation

$$(mc/n_s e^2) \text{ curl } \vec{J}_s + \vec{H} = 0 \qquad (2.46)$$

where n_s and J_s are interpreted respectively as the volume density and current density of the superconducting portion of the conduct-

ion electrons. Substituting for curl $\vec{J}$ from equation (2.41) to obtain

$$\lambda^2 \nabla^2 \vec{H} = \vec{H} \qquad (2.47)$$

which when solved for a semi-infinite region gives

$$H_{in} = H_{ext} e^{-x/\lambda_L} \qquad (2.48)$$

The penetration depth , λ_L , given by equation (2.38) which is known to be the correct order of magnitude at absolute zero, is retained by the London theory, provided that n_s approaches n at absolute zero , i.e., all the conduction electrons become superconducting as $T \to 0$. At higher temperatures λ_L is known to approach infinity.

To account for the zero-resistance phenomenon, the London theory retains equation (2.37) for the superconducting portion n_s of the conduction electrons , that is ,

$$\vec{E} = (m/n_s e^2) \dot{\vec{J}} = \Lambda (T) \dot{\vec{J}}/c \qquad (2.49)$$

where $$\Lambda(T) = mc/ n_s(T)e^2 = 4\pi\lambda_L^2(T)/c \qquad (2.50)$$

and assumes that the remainder interact with the lattice according to Ohm's law , so that for the normal state :

$$\vec{J}_n = \sigma(T) \vec{E} \qquad (2.51)$$

and the total current density

$$\vec{J} = \vec{J}_s + \vec{J}_n \qquad (2.52)$$

An intimation that the London equations are of more fundamental significance , is provided by the fact that when combined with the thermodynamic treatment of the two-fluid model of Gorter and Casimir (1934b), they yield the empirically determined temperature dependence of the penetration depth , that is

$$\lambda_L(T) = \lambda_L(0) \left(1 - (T/T_c)^4 \right)^{-\frac{1}{2}} \qquad (2.53)$$

(see, for instance, Shoenberg, 1960).

2.6.2 Basis of the Microscopic Theory of Superconductivity

Any successful microscopic theory of superconductivity must be able to explain these following phenomena :

(i) Superconductivity is essentially bound up with some profound change in the behaviour of the conduction electrons which is marked by the appearance of long range order and a gap in their energy spectrum of the order of 10^{-4} eV.

(ii) The crystal lattice does not show any change of properties , but must nevertheless play a very important part in establishing superconductivity because the critical temperature depends on the atomic mass (the isotope effect; see, for example, Maxwell(1950), Reynolds et al.(1950))

(iii) The superconducting-to-normal transition is a phase change of the second order - at the absolute zero and at the critical temperature when the latent heat is zero. At other temperatures in the presence of a magnetic field a latent heat is involved.

An early step forward in the search for a microscopic theory came in 1950 when Fröhlich(1950) pointed out that the electron-phonon interaction was able to couple two electrons together in such a way that they behaved as if there was a direct interaction between them. .

The Fröhlich interaction is schematically illustrated in

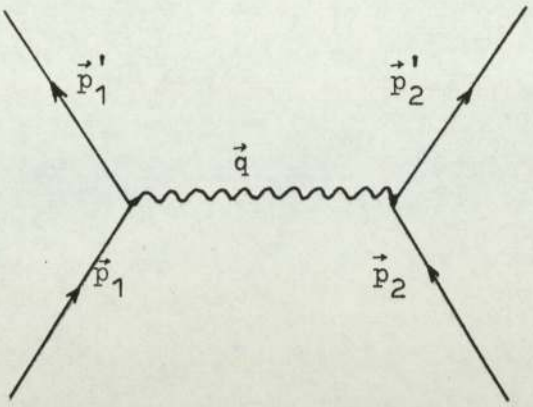

Fig 2.2 Schematic representation of electron-electron interaction transmitted by a phonon.

Fig.(2.2). During the process of phonon emission , momentum is conserved , i.e.,

$$\vec{p}_1 = \vec{p}_1' + \vec{q} \qquad (2.54)$$

where $\vec{p}_1$, $\vec{p}_1'$ are its momenta before and after scattering, respectively and $\vec{q}$ is the phonon momentum with magnitude $q=h\nu_q/v_s$, where ν_q is the phonon frequency and v_s is the velocity of sound.

Then the phonon is quickly absorbed by the second electron,

$$\vec{p}_2 + \vec{q} = \vec{p}_2' \qquad (2.55)$$

Equations (2.54) and (2.55) yield

$$\vec{p}_1 + \vec{p}_2 = \vec{p}_1' + \vec{p}_2' \qquad (2.56)$$

showing that momentum is conserved between the initial and final states. The energy transfer between the pair of electrons is thus via the intermediate phonon (lattice vibration). Fröhlich's

suggestion that the interaction responsible for superconductivity is one which involves lattice vibration enabled him to predict the isotope effect before it had been discovered experimentally(Maxwell, 1950). The next important step was taken by Cooper(1956) who showed that conduction electrons in metals could form a bound pair in the presence of an attractive interaction. Two electrons in the bound pair , called the Cooper pair , have equal and opposite momenta and spin. Stability of the pair is ensured , no matter how weak the interaction is , by the presence of other electrons in the metal. This is in contrast with the case of two isolated electrons in the presence of attractive interaction. Any attractive interaction can bind a pair of electrons , if it is sufficiently strong.

Cooper's work established that Fröhlich-type of interaction produces a profound correlation between electrons having equal and opposite momenta and energy of two electrons is lowered by going over to the correlated pair state. Thus the Fermi sea is unstable against formation of Cooper pairs.

This prompted Bardeen , Cooper and Schrieffer(1957) to assume that the superconducting ground state is one in which all electrons are paired among themselves. The model proposed by them (BCS) is a true many-body one. Existence in a metal of a large number of states having almost the same energy appeared to rule out a conventional configuration-mixing type of calculation and nobody knew how to solve the model. Here , BCS suggested the variational form of superconducting ground state function which was a linear combination of normal metal configurations in which electronic states were occupied in pairs.

Following self-consistent variational procedure , they calculated the energy difference between normal and superconducting phases and showed that there was an energy gap in the electron density of states between these phases. Physically , the BCS state is one in which Cooper pairs are scattered by electron-phonon-interaction against each other such that momenta of the pairs are conserved, the net momentum of the pair being zero . Hence many pairs with individual momenta can be formed. The resistanceless state is actually due to inhibition of random scattering of the pairs by the existence of an energy gap. BCS also extended their calculation to higher temperatures and showed that their theory could explain almost all of the experimental data collected on superconductors. Further , the BCS function introduces in a natural way long range correlation between electrons of opposite spin which extends over distances of order 10^{-4} cm in real space. Since common value of the momentum is the same everywhere , there is also long-range correlation of average momentum similar to that suggested by F. and H. London(1935).

2.6.3 Transition Temperature

Matthias(1957) had emphasized a number of interesting regularities in the appearance of superconductivity in the periodic system , the principal of which are the following:

(1) Superconductivity has been observed only for metallic substances for which the number of valence electrons,Z,lies between about 2 and 8.

(2) In all cases involving transition metals , the

variation of T_c with the number of valence electrons shows sharp maxima for Z = 3, 5 and 7.

(3) For a given value of Z , certain crystal structures seem more favourable than others. These crystal structures are β-tungsten (A15) , b.c.c. and f.c.c. structures. In addition the transition temperature is inversely proportional to the atomic mass (isotope effect).

These regularities could be incorporated into empirical rules for predicting whether a new material would be superconducting and for estimating the critical temperature. However, they give no indication of the mechanism responsible for superconductivity, whereas , by a detailed study of the interactions which give rise to superconductivity, it should be possible to predict the value of the transition temperature with some degree of accuracy.

The microscopic theory proposed by BCS yields an energy gap of the right order of magnitude and reasonable values for other superconducting parameters such as T_c , provided one fixes a certain parameter , V , which measures the average strength of the net interaction between electrons very close to the Fermi surface. Both the screened Coulomb repulsion between the electrons and the phonon-induced electron-electron interaction contribute to V. The criterion for superconductivity is that V be negative , i.e., that the phonon-induced attractive interaction must predominate over the short range Coulomb repulsion.

In the BCS theory, the critical temperature , T_c , is given by :

$$k_B T_c = 1.14 \langle \hbar w \rangle_{av.} \left[\exp -1/(N(0)V) \right] \qquad (2.57)$$

where w is the phonon cut-off frequency of the lattice vibration ,

k_B is the Boltzmann constant , $\langle \hbar\omega \rangle_{av.}$ is the average energy of the phonons which scatter electrons at the Fermi surface and N(0) is the density of energy of electron states on that surface. At 0^oK , the energy gap which has the value $2\epsilon(0)$ is given by :

$$2\epsilon(0) = 2\langle \hbar\omega \rangle_{av.} / \sinh(1/N(0)V)$$

$$\simeq 4\langle \hbar\omega \rangle_{av.} \exp(-1/N(0)V) \qquad (2.58)$$

Combining equations (2.56) and (2.57) yields for the width of the energy gap at 0^oK :

$$2\epsilon(0) = 3.52\, k_B T_c \qquad (2.59)$$

This is in remarkable quantitative agreement with experimental values obtained from a wide variety of measurements (see for example, Lynton, 1969).

2.6.4 Type I and Type II Superconductors

There is no difference in the fundamental mechanism of superconductivity in type I and type II superconductors. In both types, the mechanism is the electron-phonon-interaction. Both types have similar thermal properties at the superconducting-to-normal transition in zero magnetic field , but the magnetic properties are different in the two types. A good type I superconductor excludes a magnetic field until superconductivity is destroyed suddenly and completely, after which the field penetrates completely (Fig 2.4). A good type II superconductor excludes the field completely only for relatively weak fields up to a field H_{c1} . Above H_{c1} , the field is partially excluded (Fig 2.3) but the specimen remains electric-

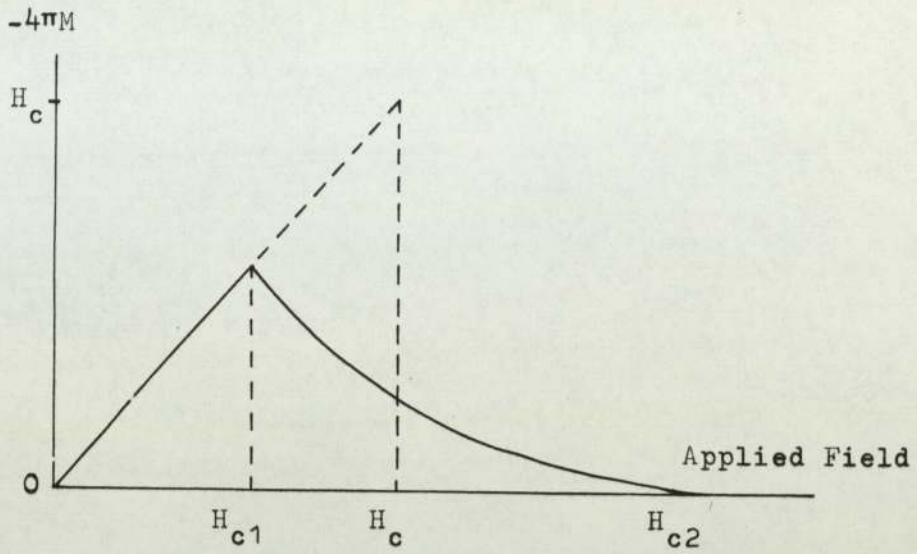

Figure 2.3 Magnetic behaviour of Type II superconductor in an external magnetic field.

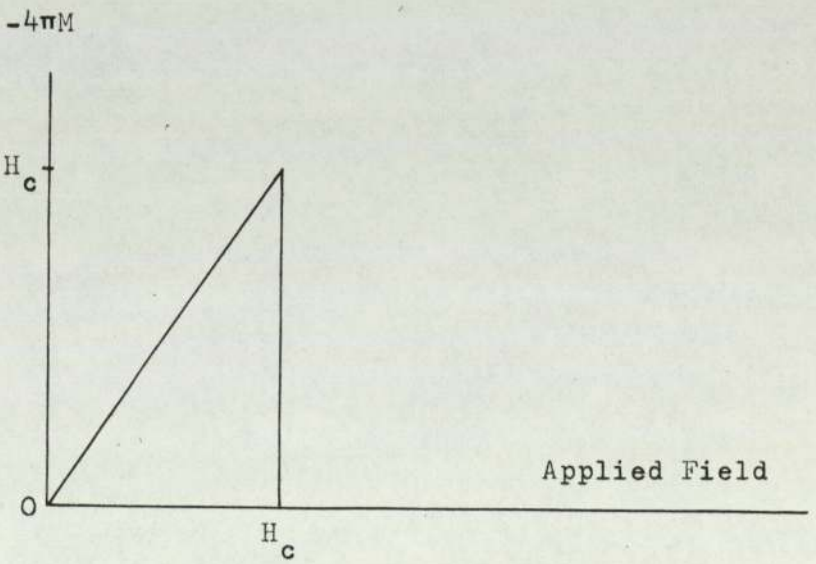

Figure 2.4 Magnetic behaviour of Type I superconductor in an external magnetic field.

ally superconducting at a much higher field (H_{c2}) , sometimes 10 Tesla or more , and, at this value of field, the flux penetrates completely and all superconductivity vanishes.

In the Ginzburg-Landau (G-L) theory(1950) , the superfluid (superconducting portion of the conduction electrons) flow , $\rho_s v_s$, is described in terms of an effective wave function with amplitude, $\psi(r)$, and phase , $\varkappa(r)$; the superfluid density, ρ_s , is assumed to be proportional to $|\psi(r)|^2$ where:

$$\psi(r) = |\psi(r)|^2 e^{i\varkappa(r)} \qquad (2.60)$$

From this wave function, the existence of an interface between a region in the superconducting state and a region in the normal state in a superconductor is explicitly realised.The boundary has an extra energy associated with it called surface energy. The surface energy , which may be positive or negative, decreases as the applied magnetic field is increased. A superconductor is type I if the surface energy is always positive and type II if the surface energy becomes negative as the magnetic field increases beyond H_{c1} (see Fig. 2.3) . The sign of the surface energy is shown to depend on the ratio of the penetration depth ,λ_L , to the coherence length, ξ . The results are usually expressed in terms of the Ginburg-Landau parameter, K_{G-L} :

$$K_{G-L} = \frac{\lambda}{\xi\sqrt{2}} \qquad (2.61)$$

The G-L theory predicts a negative surface energy (type II superconductors) when $K_{G-L} \geq 1/\sqrt{2}$ and that a type II superconductor with a negative surface energy would remain superconducting up to a magnetic field , H_{c2} , of :

$$H_{c2} = \sqrt{2}\, k\, H_c \qquad (2.62)$$

Superconductors which satisfy $K_{G-L} < 1/\sqrt{2}$, having positive surface energy , are termed type I superconductors. However films of some materials of type I may exhibit type II behaviour below a critical thickness , d_c.

2.6.5 Critical Current Density

In a flat superconducting film carrying current, an intense magnetic field is created near the film edges which has a complex effect on the current-induced transition. For simplicity , only the geometry in which the current is distributed uniformly over the whole film will be considered here so that edge effects are negligible. Two examples of such geometries are a film deposited on a cylinder much longer than its radius , which, in turn, is much larger than the film thickness, and a film adjacent and parallel to a much larger superconducting plane of higher critical temperature.

In the case of a current carrying film of thickness greater than λ_L , deposited on a cylinder, the current flows in an outer region of approximate depth $3\lambda_L$. In accordance with Silsbee's Rule (1916) the critical current in this case is that which produces a surface field , H_c , outside the cylinder. The field on the inside surface of the film should be zero for all currents since the current is assumed to be distributed uniformly around the cylinder. For a film much thinner than λ_L , the current is distributed approximately uniformly throughout the film thickness and the surface field, H , induced correspondingly to the critical current, is smaller than H_c. The transition to the normal state occurs when

the critical velocity , which causes the virtual electron pairs to split up, is exceeded. To calculate the critical current at finite temperatures , a thermodynamic method established by Bardeen(1958) based on the BCS theory will be employed.

It is assumed that in a thin film the kinetic energy of the electrons at the critical current value equals the difference in the free energies of the normal and superconducting states. The increase in the kinetic energy of the superconducting portion , n_s, of the conduction electrons with drift velocity , v_s , is :

$$E = \frac{1}{2} n_s m v_s^2 \qquad (2.63)$$

Using the relation between $\vec{v}_s$ and $\vec{J}_s$ in the equation (2.3) , $\vec{v}_s = \vec{J}_s/en_s$, then :

$$E = \frac{1}{2} (m/e^2 n_s) J_s^2 \qquad (2.64a)$$

$$= \frac{1}{2} \Lambda J_s^2/c \qquad (2.64b)$$

where Λ $(=mc/n_s(T)e^2)$ is the parameter of the London theory defined in equation (2.49).

According to the assumption above , the current-induced superconducting-to-normal transition will take place when the kinetic energy of the current-carrying electrons just cancels out the free energy that accompanies the transition to the normal state. That is,the transition causes no change in the magnetic field energy which is valid for a film much thinner than the penetration depth. If the critical current density for the film is J_c , then the corresponding kinetic energy is :

$$E_c = \frac{1}{2} \Lambda J_c^2/c \qquad (2.65)$$

Due to the conservation of energy , this increase of kinetic energy is associated with the energy of $H_c^2/8\pi$ which is stored in the penetration field , H_c , where H_c is the critical field of the bulk material. Hence :

$$H_c^2/8\pi = \frac{1}{2}\Lambda J_c^2/c = \frac{1}{2}(mc/n_s e^2)J_c^2/c \qquad (2.66a)$$

i.e. , $$J_c = cH_c/4\pi\lambda_L \qquad (2.66b)$$

Using the solution of London theory , equation (2.48) , which is : $H_{in} = H_{ext}e^{-x/\lambda_L}$, where the x-axis is taken at right angles to the surface and , for the simple geometry under consideration , $|\text{curl } \vec{H}| = d\vec{H}/dx$, it can be shown that Maxwell's equation :

$$\text{curl } \vec{H} = (4\pi/c)\,\vec{J}_s \qquad (2.67)$$

will yield: $$\vec{J}_s = -(cH_{ext}/4\pi\lambda)e^{-x/\lambda_L} \qquad (2.68)$$

The transition occurs when $J_s \rightarrow J_c$ and $H_{ext} \rightarrow H_c$, with the result that the magnetic field is the same for all x , i.e., $H(x=0) = H_c$, resulting in $J_s = (cH_{ext}/4\pi\lambda_L)e^{-x/\lambda_L} \rightarrow J_c = (cH_c/4\pi\lambda_L)$, which is identical to equation (2.66b).

According to Rose-Innes and Rhoderick(1976) the critical field , H_c, has been found to fall off almost as the square of the temperature , i.e.,

$$H_c(T) = H_c(0)(\,1 - (T/T_c)^2\,) \qquad (2.69)$$

where $H_c(0)$ is the critical field at absolute zero and T_c is the transition temperature. If we substitute $H_c(T)$, from equation (2.69) and $\lambda_L(T)$, from equation(2.53) into equation (2.66b), we

obtain the relation below :

$$J_c(T)/J_c(0) = (1 - T_R^2)(1 - T_R^4)^{\frac{1}{2}} \qquad (2.71)$$

$$= (1 - T_R^2)^{\frac{3}{2}}(1 + T_R^2)^{\frac{1}{2}} \qquad (2.72)$$

where $T_R = T/T_c$.

2.7 Optical Properties of Thin Films : Ellipsometry

The measurement of the changes in polarization upon the reflection of light from a surface is a very sensitive technique for studying the properties of a surface and/or surface films. This technique is commonly called "Ellipsometry" since it involves measurement of the state of polarization of elliptically polarized light. The basic equations for analyzing elliptical polarization based on the Fresnel formulas was initiated by Drude(1889,a) . Although the exact Drude's equations are cumbersome in form, recent developments in instrumentation and computation techniques makes ellipsometry a more attractive tool for surface examination. A review article about ellipsometry and its application has been given by Neal and Fane(1973).

2.7.1 Reflection and Transmission of Light at a Plane Boundary

Consider light incident at a plane boundary between two media as shown in Fig.(2.5) . The analysis of Maxwell's equations for homogeneous isotropic and non-absorbing media leads to the following results (Vasicek,1960) :

(a) Law of Reflection

$$\phi_o = \phi_o' \qquad (2.73)$$

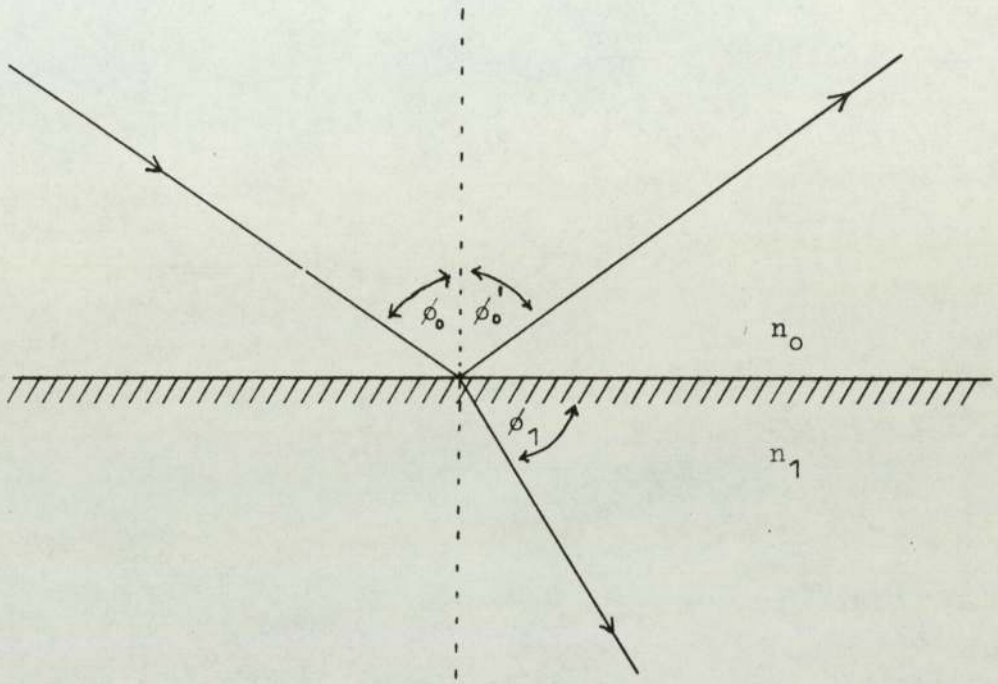

Figure 2.5 Reflection and refraction of light at a plane boundary between two media having refactive indices n_o and n_1 respectively.

(b) Snell's Law of Refraction

$$n_o \sin\phi_o = n_1 \sin\phi_1 = n_2 \sin\phi_2 = \ldots . \qquad (2.74)$$

(c) Fresnel Reflection and Transmission Coefficients*

$$\frac{E^-_{o(p)}}{E^+_{o(p)}} = \frac{n_1\cos\phi_o - n_o\cos\phi_1}{n_1\cos\phi_o + n_o\cos\phi_1} = r_{o1(p)} \qquad (2.75)$$

$$\frac{E^+_{1(p)}}{E^+_{o(p)}} = \frac{2n_o\cos\phi_o}{n_1\cos\phi_o + n_o\cos\phi_1} = t_{o1(p)} \qquad (2.76)$$

$$\frac{E^-_{o(s)}}{E^+_{o(s)}} = \frac{n_o\cos\phi_o - n_1\cos\phi_1}{n_o\cos\phi_o + n_1\cos\phi_1} = r_{o1(s)} \qquad (2.77)$$

$$\frac{E^+_{1(s)}}{E^+_{o(s)}} = \frac{2n_o\cos\phi_o}{n_o\cos\phi_o + n_1\cos\phi_1} = t_{o1(s)} \qquad (2.78)$$

* See Appendix A for the optical notations.

When both media are transparent the optical constants are their respective refractive indices , given by:

$$n_i = \sqrt{\frac{\mu_i \epsilon_i}{\mu' \epsilon'}} \qquad (2.79)$$

where ϵ' and μ' are dielectric permeability and magnetic permeability , respectively, of free space. Thus all terms in the Fresnel equations are real. For the case of an absorbing medium, the equations (2.74) - (2.78) above are still valid if the refractive index of the medium is replaced by the 'complex refractive index' , N, defined by : $N = n - ik$ (2.80)

where n and k fulfill the following relationships :

$$n^2 - k^2 = \frac{\mu\epsilon}{\mu'\epsilon'} = \frac{\epsilon}{\epsilon'} = \epsilon_r \qquad (2.81)$$

and $$nk = \frac{\mu\sigma}{2w\mu'\epsilon'} = \frac{\sigma}{2w\epsilon} \qquad (2.82)$$

for $\frac{\mu}{\mu'} = 1$; here w is the angular frequency of the light.

Giving :

$$n^2 = \frac{\epsilon_r}{2}\left[1 + \left(1 + \frac{\sigma^2}{w^2\epsilon^2}\right)^{\frac{1}{2}}\right] \qquad (2.83)$$

$$k^2 = \frac{\epsilon_r}{2}\left[1 - \left(1 + \frac{\sigma^2}{w^2\epsilon^2}\right)^{\frac{1}{2}}\right] \qquad (2.84)$$

here σ and ϵ_r are the conductivity and the permittivity at the optical frequency , respectively and generally are not equal to their respective d.c. or low frequency values.

2.7.2 Ellipsometric Equation of Single Layer Films

For the general case , consider a parallel beam of plane polarized light of unit amplitude incident at angle ϕ_o on a film of index N_1(real for non absorbing film) and thickness d_1 , as shown in Fig.(2.6) , lying on a flat substrate of index N_2. The reflectance and transmittance may be conveniently determined in terms of the Fresnel coefficients of reflection and transmission at the N_o/N_1 and N_1/N_2 interfaces, according to equations (2.75)-(2.78).

The complex amplitudes of the successive beams reflected and transmitted by the film are as shown in Fig.(2.6) , δ_1 which is the phase change of the light amplitude in traversing the film once, is given by :

$$\delta_1 = 2\pi N_1(d_1/\lambda_o)\cos\phi_1 = 2\pi d_1/\lambda_o(N_1^2 - \sin\phi_o^2)^{\frac{1}{2}} \qquad (2.85)$$

where λ_o is the wave length of light in vacuum. The total reflected amplitude of the whole system is determined by summation of the multiply reflected and transmitted beams, taking account of the phase difference δ_1, i.e.,

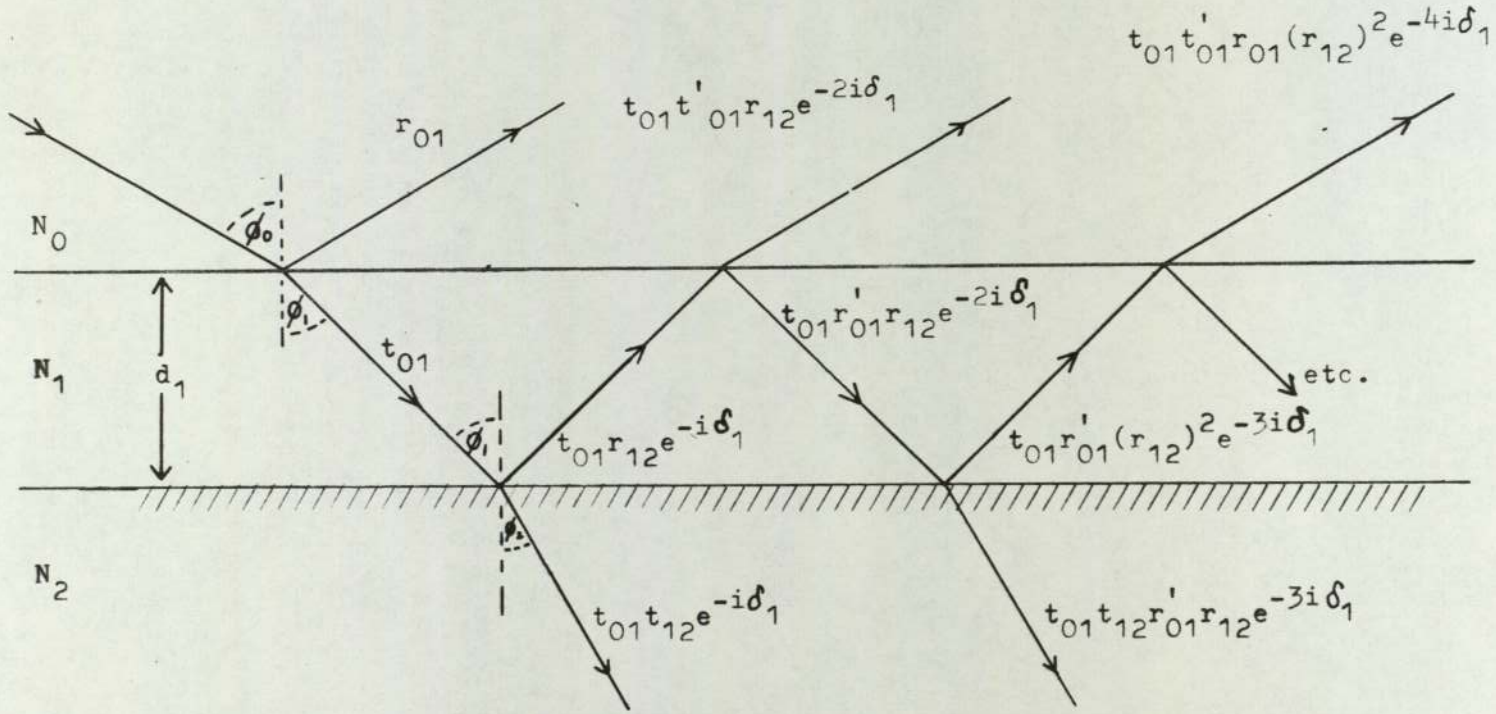

Figure 2.6 Reflectance and transmittance of single film of thickness d_1.

$$r_{o2} = r_{o1} + t_{o1}t'_{o1}r_{12}e^{-2i\delta_1} - t_{o1}t'_{o1}r_{o1}(r_{12})^2e^{-4i\delta_1} + \ldots \quad (2.86)$$

$$= r_{o1} + t_{o1}t'_{o1}r_{12}e^{-2i\delta_1}/(1 + r_{o1}r_{12}e^{-2i\delta_1}) \quad (2.87)$$

It follows from the conservation of energy that $t_{o1}t'_{o1} = 1-(r_{o1})^2$ and substituting this into equation (2.86) :

$$r_{o2} = (r_{o1} + r_{12}e^{-2i\delta_1})/(1 + r_{o1}r_{12}e^{-2i\delta_1}) = \rho' e^{i\Delta'} \quad (2.87)$$

where ρ' is the amplitude ratio and Δ' is the difference in phase of the reflected light compared to the incident light. Two identical expressions exist for the (p) and (s) components although the numerical values are different due to different expression of the Fresnel coefficients. The ellipsometric equation is given by :

$$\mathrm{Tan}\Psi\, e^{i\Delta} = r_{o2(p)}/r_{o2(s)} = \left[\rho'_{(p)}/\rho'_{(s)}\right]e^{i(\Delta'_p - \Delta'_s)} \quad (2.88)$$

where $r_{o2(p)}$ and $r_{o2(s)}$ are the (p) and (s) components of the reflected beam, respectively, $|\mathrm{Tan}\Psi| = |r_{o2(p)}/r_{o2(s)}|$ and $\Delta = \Delta'_p - \Delta'_s$.

2.7.3 Solution of the Ellipsometric Equation

Although the experimental procedure for determining ellipsometric parameters, Ψ and Δ for a film-free surface and a film-covered surface is identical, the calculation of solutions for the latter is far more lengthy :

(1) For the film-free case , the explicit solutions can be obtained from equations (2.74)-(2.78), (2.80) , (2.87) and (2.88) by setting the thickness of the film, $d_1=0$,resulting in :

$$n_2^2 - k_2^2 = \sin^2\phi_o \left[\frac{1+\tan^2\phi_o(\cos^2 2\bar{\psi} - \sin^2 2\bar{\psi} \sin^2\bar{\Delta})}{(1+\sin 2\bar{\psi}\cos\bar{\Delta})^2} \right] \qquad (2.89)$$

$$2n_2k_2 = \frac{\sin^2\phi_o \tan^2\phi_o \sin 4\bar{\psi} \sin\bar{\Delta}}{(1+\sin 2\bar{\psi}\cos\bar{\Delta})^2} \qquad (2.90)$$

where the bars over ψ and Δ indicate a film-free surface.

For metal films , the optical constants depend on the angle of incidence , ϕ_o , and hence the angle of refraction ϕ_1 , because the light waves propagating in a metal are nonhomogeneous. Therefore it is necessary to calculate these optical constants always for the normal incidence of light. According to Vasicek(1960) , they are related to each other by the following formulae :

$$\bar{n}^2 = ((A^2 + B^2)^{\frac{1}{2}} + A)/2 \qquad (2.91)$$

$$\bar{k}^2 = ((A^2 + B^2)^{\frac{1}{2}} - A)/2 \qquad (2.92)$$

$$A = n^2 - k^2 = \bar{n}^2 - \bar{k}^2 \qquad (2.93)$$

$$B = 2nk\cos\phi_1 = 2\bar{n}\bar{k} \qquad (2.94)$$

and $$\cos^2\phi_1 = (n^2 - n_o^2\sin^2\phi_o)/n^2 \qquad (2.95a)$$

$$= \frac{\tan^2\phi_o \cos^2 2\psi}{1+\sin 2\bar{\psi}\cos\bar{\Delta})^2 + \tan^2\phi_o\cos^2 2\bar{\psi}} \qquad (2.95b)$$

where n, k , $\bar{n}$, and $\bar{k}$ are optical constants at angle of incidence ϕ_o and at normal incidence respectively.

(2) For the film-covered surface , the derivation of n and k , and d_1 for the film using exact Drude's equation(equation (2.88) is extremely laborious , so that an electric computer is

essential. However , the film thickness of a very thin film ($d_1 < 10$ nanometers) can be simply determined from the Drude's first approximation formulae(Drude,1889b) , provide $\bar{\Psi}$ and $\bar{\Delta}$ of the clean surface as well as n and k for the film are known by other means. Drude expanded the exponential terms in the equations (2.86)-(2.88) in a power series of (d_1/λ_o) , to the first approximation , obtained :

$$\Delta = \bar{\Delta} - \alpha d_1 \qquad (2.96)$$

$$\Psi = \bar{\Psi} + \beta d_1 \qquad (2.97)$$

where $$\alpha = \frac{4\pi}{\lambda_o} \frac{\cos\phi_o \sin^2\phi_o (\cos^2\phi - a)(\frac{1}{n_1^2} - 1)}{(\cos^2\phi_o - a)^2 + a_1^2} \qquad (2.98)$$

$$= \frac{2\pi}{\lambda_o} \frac{\cos\phi_o \sin 2\bar{\Psi} \sin^2\phi_o (1 - n_1^2 \cos^2\phi_o) a_1 (\frac{1}{n_1^2} - 1)}{(\cos^2\phi_o - a)^2 + a_1^2} , \qquad (2.99)$$

$$a = \frac{n_2^2 - k_2^2}{(n_2^2 + k_2^2)^2} , \qquad (2.100)$$

and $$a_1 = \frac{2n_2k_2}{(n_2^2 + k_2^2)^2} \qquad (2.101)$$

If the optical constants of the film are not known or thickness is not small compared with λ_o (say larger than 10 nm), then the exact equation must be used. For example, Archer(1962) and McCrackin et al.(1963) have applied computer techniques to evaluate the solution of the exact equation.

In the present work Algol programmes , as fully described by O'Shea(1971), employing the exact equation , were used to determine

the optical constants of some of the niobium-tin alloy films. The method of measuring Ψ and Δ is given in section (4.5.1)

****

CHAPTER 3 : EXPERIMENTAL EQUIPMENT

Introduction

The superconducting properties of thin films can be influenced by gaseous impurities . The extent by which the critical temperatures of niobium and tantalum films are reduced from bulk values by these impurities has been demonstrated by De Sorbo and more recently in this laboratory by Salter(1973) and Aguado Bombin(1975).

Because the method of preparing the alloyed films of Nb_3Sn in the present work involved evaporation of niobium and tin and alloying of the two elements at high temperatures , the gaseous inclusion could be included at any of the stages mentioned below, namely : (a) During the deposition of niobium.

(b) During the evaporation of tin.

(c) During the alloying process when the films were heated to high temperature (above $400^{\circ}C$).

In order to keep the inclusion to a minimum it was necessary to satisfy the following conditions :

(1) The vacuum system should be capable of providing a base pressure of less than 10^{-8} torr in the evaporation chamber.

(2) The rate of deposition should be high enough so that the number of metal atoms striking the substrates per second was much greater than the number of gaseous atoms striking per second.

(3) The substrates should be maintained at an elevated

temperature to reduce the sticking coefficient of gaseous molecules that would impinge on the films during deposition.

By incorporating all these three conditions in the evaporation unit , it was possible to deposit niobium films of the required superconducting characteristics with minimum gaseous impurities and subsequently to prepare the alloy films.

3.1 Vacuum System

The arrangement of the vacuum system is shown in Fig.(3.1). The ultra high vacuum (U.H.V.) was obtained by means of a 200 lit/sec. Ultek Sputter Ion Pump attached to the vacuum chamber. The rough vacuum elements were connected to a 25 mm diameter manifold which could be isolated from the vacuum chamber by a bakeable U.H.V. valve. The initial rough pumping of the vacuum chamber was by means of a 250 lit/sec. Edwards single stage rotary pump , followed by an oil diffusion pump. A liquid nitrogen trap was interposed between the pump and the manifold to prevent backstreaming of oil vapour from the diffusion pump and rotary pump into the vacuum chamber. This trap was of the glass disc type which has been fully described elsewhere (Haller,1964).

In order to achieve the vacuum of better than 10^{-8} torr , the ion pump was surrounded by an oven containing two 500 watt heater elements controlled by a Variac . This enabled the pump to be baked at a temperature of 200 ^{o}C . Controlled heater tapes were also positioned around the vacuum chamber.

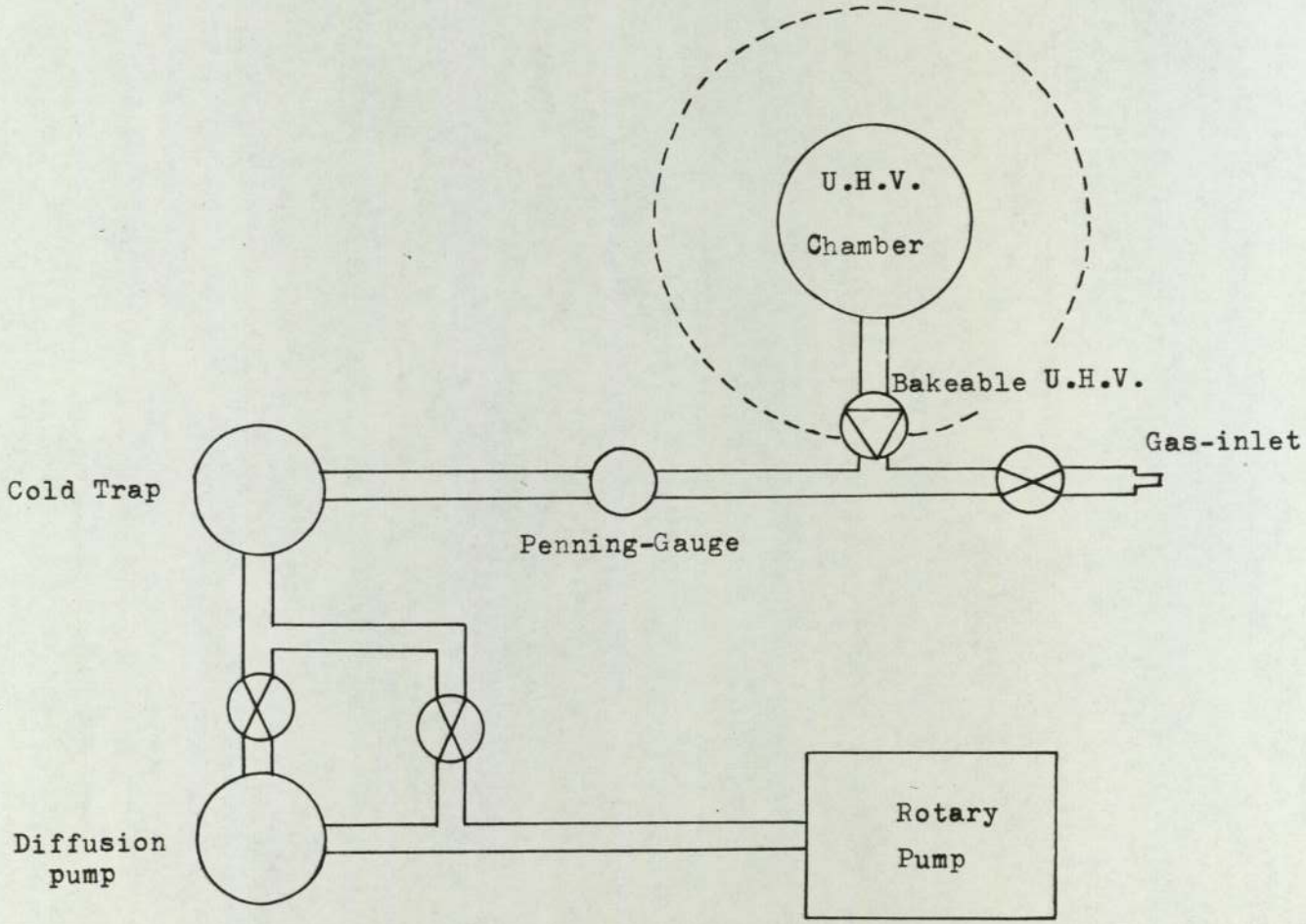

Figure 3.1 Diagram of the Vacuum System.

3.2 Vacuum Chamber

The stainless steel vacuum chamber was constructed by Ferranti Ltd. The chamber consisted of a cylinder , 250 mm in diameter and 600 mm long , fitted with a number of flanges , as shown in Fig.(3.2) and Plate (3.1). The top flange and the five 16.5 mm diameter flanges were sealed by means of aluminium wire seals(Halder et al.,1959). The eleven removable flanges were standard 70 mm diameter copper gasket flanges. A reducing flange , 250 mm to 170 mm was used to connect the chamber to the ion pump beneath it. Aluminium wire and copper gasket seals were interposed on the large diameter side and the smaller diameter side respectively.

One 16.5 mm diameter flange, A , in Fig.(3.2) was fitted with an observation port to enable the sample holder , the shutter assembly and the evaporation sources to be viewed. The latter was viewed indirectly via a stainless steel mirror positioned inside the chamber. Flange B was used for mounting a bellows type linear motion drive , which was designed to operate the shutter mechanism. Another flange , C , carried the electron beam evaporator in conjunction with cooling water for the hearth. In preliminary tests by Salter(1973) , on the vacuum system , it was found that radiation from the electron beam evaporator produced unacceptably high temperatures on the walls of the chamber during the evaporation of niobium, thus resulted in considerable outgasing. To overcome this problem , a water cooled stainless steel tube was employed and coiled around the evaporator , supported by the opposite flange , D. The shielding substantially reduced the amount of radiant heat from the molten niobium sample to the walls of the chamber and it

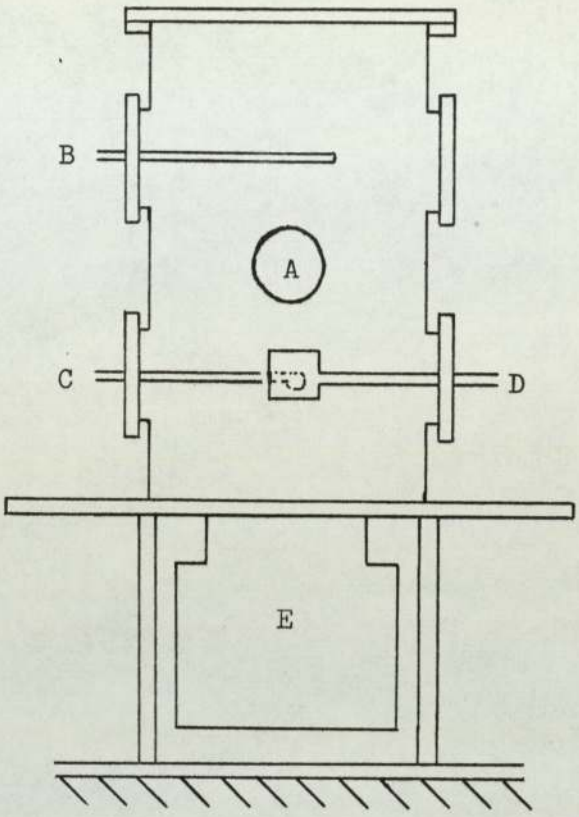

A - Observation Port

B - Linear Movement Bellow

C - Water Coolant Tubes for Electron-gun Evaporator

D - Water Coolant Tubes for Shielding

E - Ion Pump

Figure 3.2 Diagram of the U.H.V. chamber.

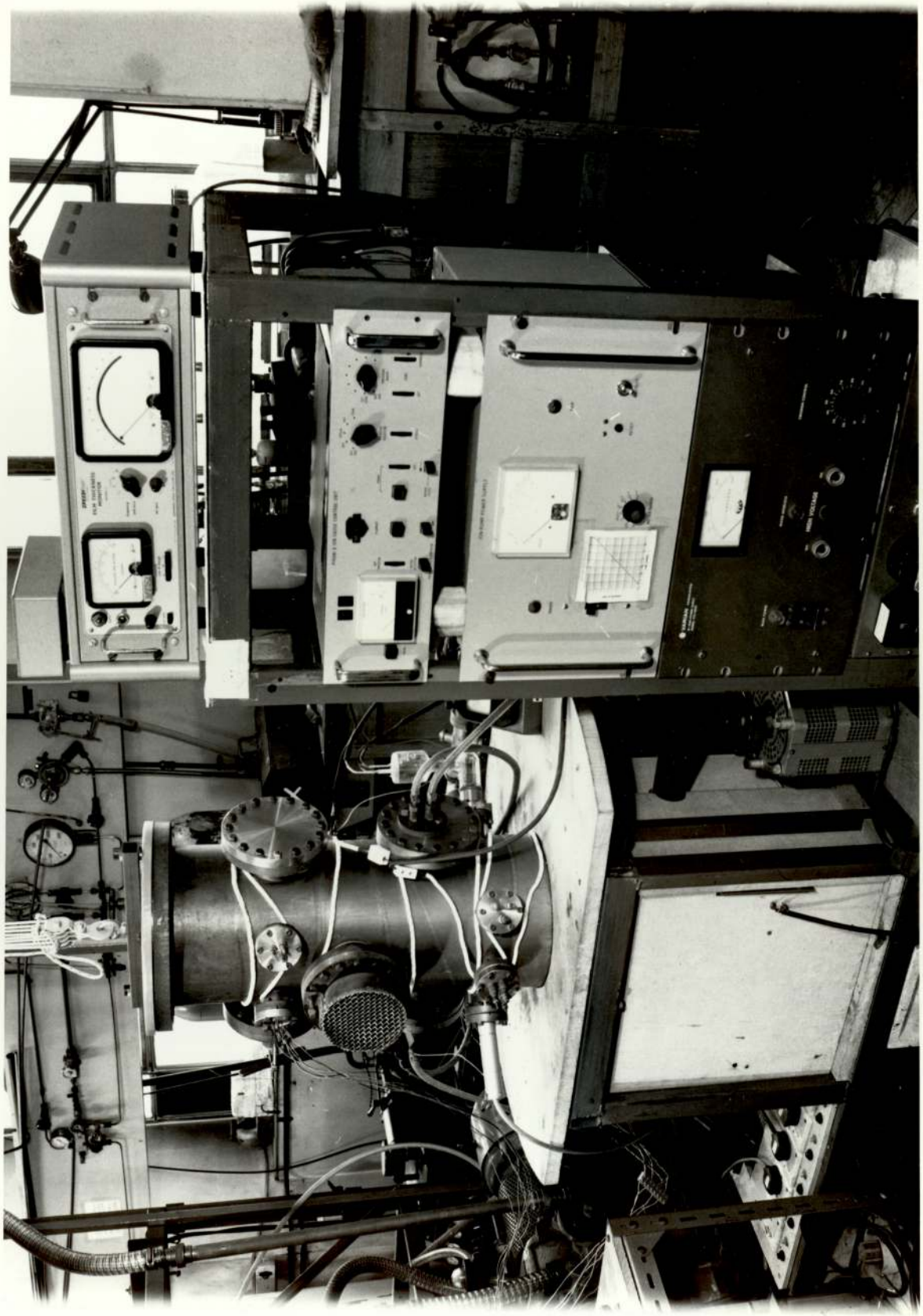

PLATE 3.1a EVAPORATION SYSTEM

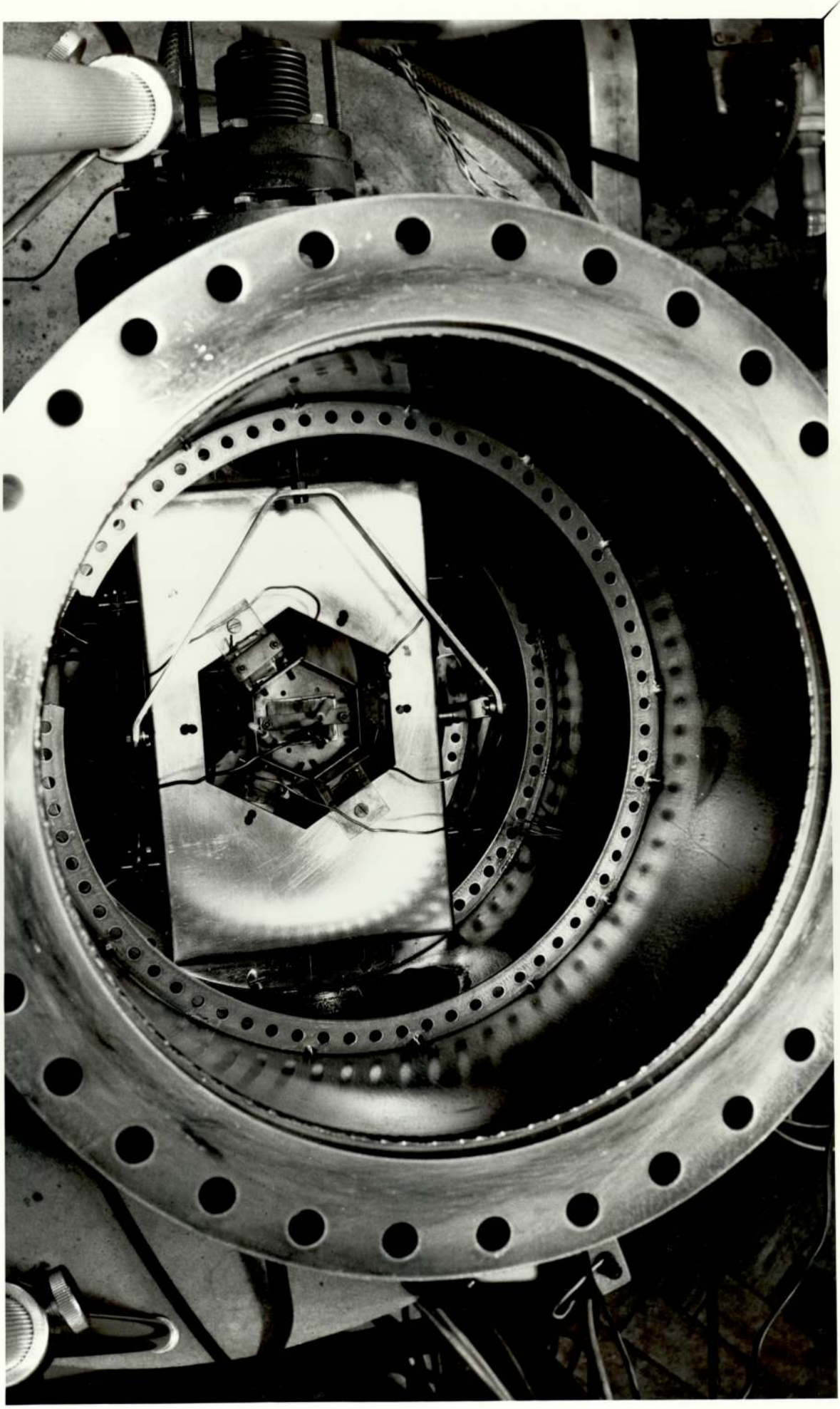

PLATE 3.1b INSIDE VIEW OF VACUUM CHAMBER

also provided a cooler surface for the deposition of niobium for gettering prior to and during deposition of the sample.

Two of the 70 mm flanges adjacent to the flange C were used to carry electrical lead throughs for the electron beam evaporator. Four flanges of the same size were fitted with 3-way lead throughs which carried all the electrical connections to the substrate heaters and the tin crucible heater. The remaining flanges were used for auxiliary electrical leads, for the film thickness monitor crystal and thermocouples. An ion gauge type Mullard IOG 12 was used for pressure measurements and a mass spectrometer head for partial pressure measurements.

3.3 Electron Beam Evaporator

Niobium has a melting point of about 2500°C and in order to obtain a reasonable evaporation rate, temperatures of the order of 3500°C are required. The electron beam evaporator can provide not only these sort of temperatures but also has the advantage of not contaminating the source which is held on a water cooled copper hearth.

A Varian No. 980-0001 electron beam evaporator was mounted in the chamber so that the niobium source on the hearth was about 200 mm from the substrate holder. The evaporator was supported by stainless steel tubes which carried the water coolant for the crucible. Electrical connections between the evaporator and the lead through were made by bare 12 SWG copper wires.

The electron beam current could be varied by a potential variac from 0 to 500 mA , giving up to 2000 watt beam power. The

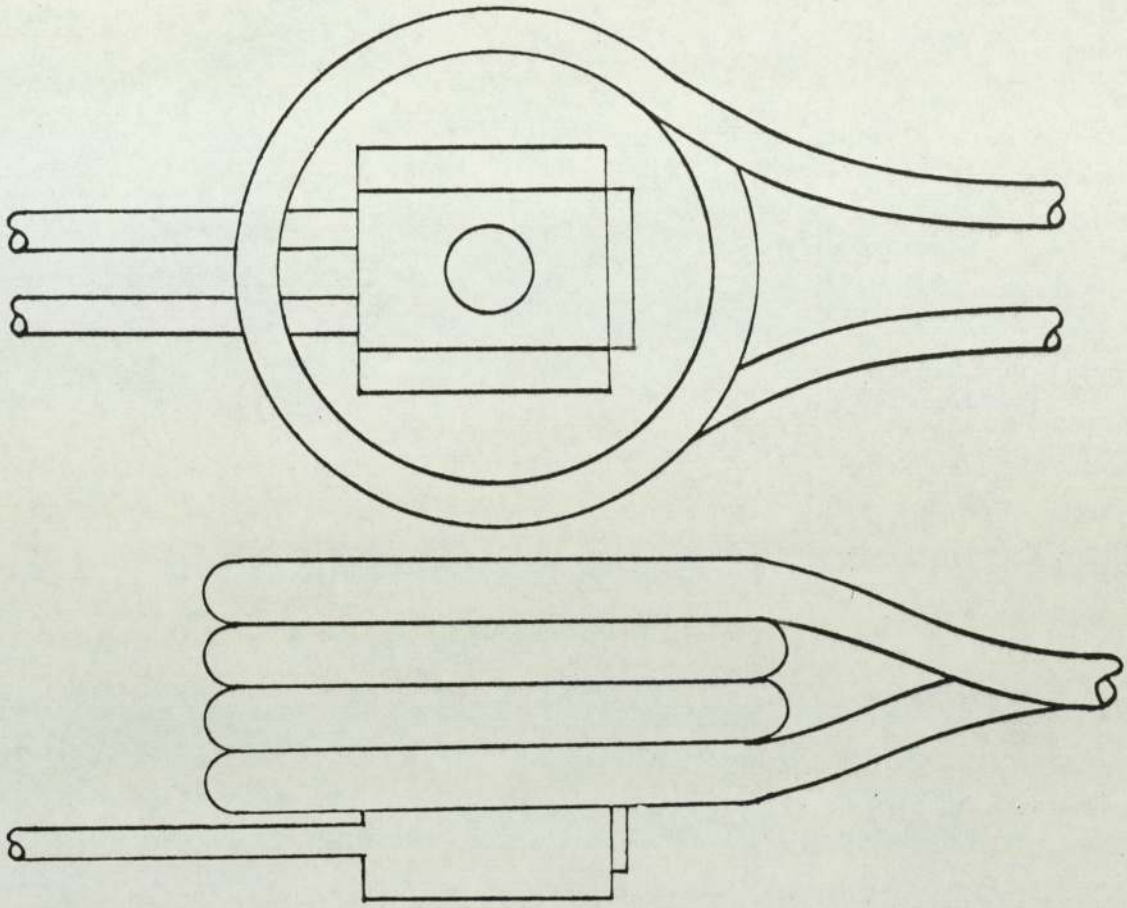

Figure 3.3 Positioning of the water cooled shield around the e-gun evaporator.

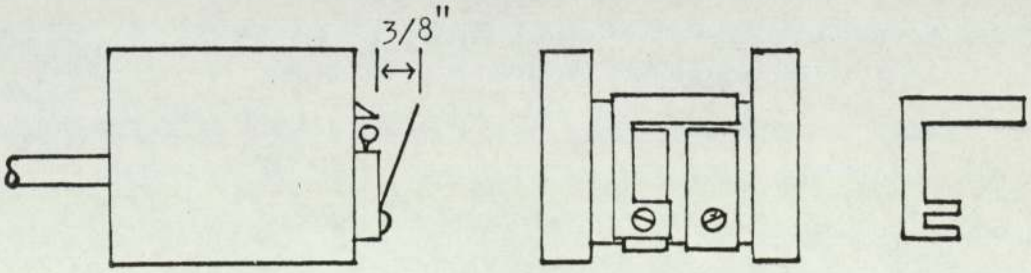

Figure 3.4 Position of the 'overspray' shield as fitted to the e-gun evaporator.

rates of evaporation were considerably improved by the fitting of an 'overspray' shield fixed to the evaporator by a factor of 5 at maximim power. The shield was cut from 0.5 mm thick molybdenum sheet and fixed to the evaporator as shown in Fig. (3.4).

3.4 Evaporator for Tin

Initially attempts were made to produce the tin layer on the niobium surface by preparing niobium films in the vacuum chamber previously described and then transferring the films to another subsidiary evaporator unit for the subsequent processes of overlaying with tin, diffusion and alloying. The films produced were not superconducting and the film surfaces were contaminated due most probably to the inclusion of oxygen. Therefore it was decided to carry out the process of preparation of niobium-tin alloy films in situ whilst still maintaining the ultra high vacuum.

Subsequently a crucible for the tin evaporation process was included in the main vacuum chamber. The crucible , as shown in Fig.(3.5),was made of a high purity quartz tube of 6 mm in diameter and 1 mm thick. It was constructed into a 'T' shape and wound with a heating element made of a tantalum strip 2 mm wide , cut from a tantalum sheet of 0.1 mm thick. Surrounding this , quartz tubes of slightly larger diameter served as a thermal and electrical insulators.The whole was wrapped with a tantalum shielding sheet of 0.1 mm thick , held inside another slightly larger quartz tube. The assembly was held together by a molybdenum wire of 0.5 mm in diameter. It was then attached to the outer side of the electron

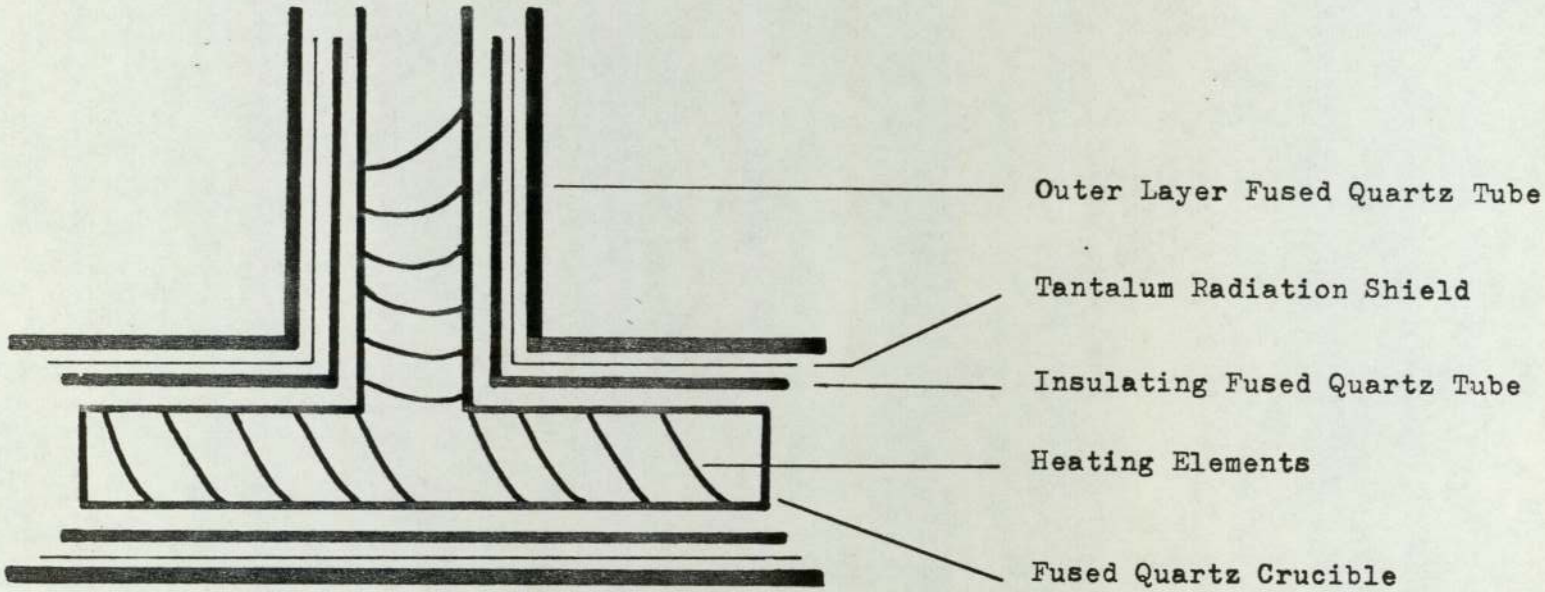

Figure 3.5 Cross-section of the tin evaporator.

beam radiation shield with molybdenum wires. The electrical leads were bare 18 SWG copper wires.

3.5 Substrate Holder

The substrate holder was initially designed by Aguado Bombin(1975). The purpose was that a set of films could be prepared under identical vacuum conditions , but :

(a) with varying thicknesses

(b) with the same thickness

(c) at the same substrate temperature

(d) at different substrate temperatures

It was arranged geometrically in such a way that up to eight films with the same or different thicknesses could be prepared simultaneously depending on the separation of source and substrates. The body of the holder was made of stainless steel and consisted of a plate 240 mm long , 90 mm wide and 0.75 mm thick with an hexagonal hole in the middle , as shown in Plate (3.2). Attached to every side of the hexagonal , there was a mounting bracket , carrying a mask and a substrate which could be placed in three different positions , i.e. , three different distances from the sources , so that films of different thicknesses could be prepared at the same time. The uniform thickness of the films was achieved by having the normals from the centres of symmetry of the masks in each of the three position intersect at the electron gun hearth.

The mounting bracket at the centre which was big enough to hold two masks , also served to join the six mounting brackets

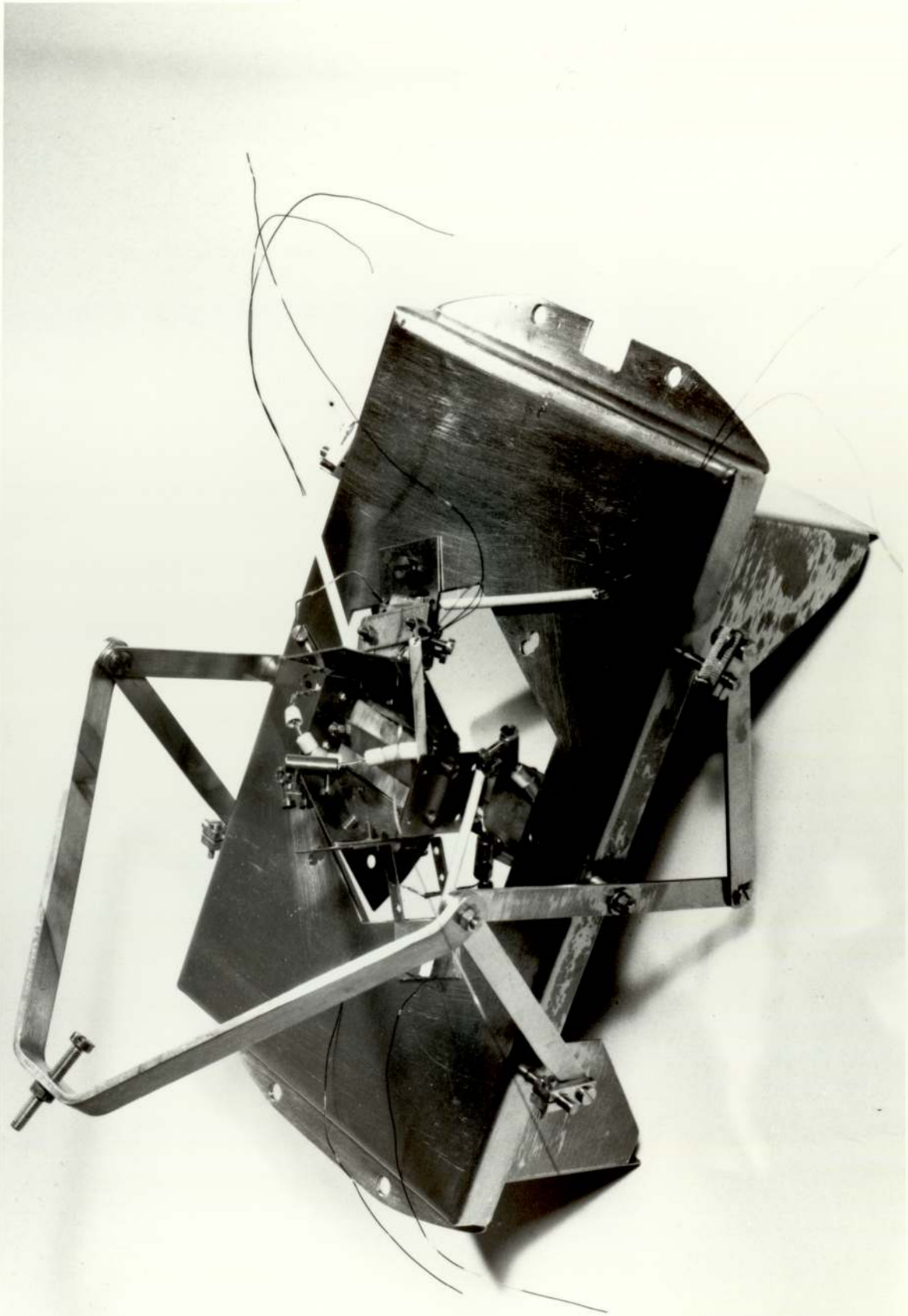

PLATE 3.2 SUBSTATE HODER

together. The distance from the source to these two samples was about 200 mm.

In the early runs a single shutter was used but its size was more than half the chamber diameter , when opened the far edge was too close to the niobium source. To eliminate this problem , a two-halved shutter was fabricated from stainless steel and joined to the holder assembly with stainless steel which also served for converting the 20 mm linear movement into a 90 degrees rotation about a horizontal axis.

3.6 Substrate Heaters

A necessary condition for the preparation of niobium- tin samples was to maintain the substrate temperatures up to about 1000°C for long periods of time without causing an excessive pressure rise in the chamber. This difficulty was overcome to some extent by using localised heaters. These heaters were made of silica plates (19x14x1 mm) wrapped around with tantalum strips, 15 mm wide and 0.1 mm thick. Temperatures of the substrates could be controlled separately by means of Variac controlled transformers and were monitored by means of alumel/chromel thermocouples.

3.7 Apparatus For Low Temperature Experiments

The apparatus for the low temperature measurements of thin film resistivity was designed to fulfil the following requirements :

(a) Production and measurement of temperatures from 300°K to 2°K.

(b) Vary temperatures over a small range of about $1^{o}K$ in the region $2^{o}K$ to $25\ ^{o}K$ for critical temperature and critical current measurements.

(c) Maintain the low temperatures for periods of up to 6 hours to enable an experiment to be completed without replenishing the liquid helium.

The apparatus used consisted of :

(1) A liquid helium cryostat and helium recovery system.

(2) A sample holder cryostat.

(3) Electrical contacts to the samples.

Plate (3.3) shows a general view of the system. The low temperature cryostats are illustrated in Fig.(3.6) and Plate (3.4).

3.7.1 Liquid Helium Cryostat

The outer cryostat used in the low temperature experiments was a standard helium cryostat manufactured by Oxford Instrument Co. The liquid nitrogen jacket has a capacity of 5.5 liters and the liquid helium chamber has a usable volume of 3.5 litres. The heat leak into the helium reservoir was less than 0.1 watt. Thus the experimental enclosure could be maintained at near liquid helium temperature for 10 to 15 hours. A copper pipe was linked to the helium chamber for two purposes, firstly for collecting helium gas into the recovery bag and , secondly, for lowering the temperature inside the chamber by reducing the pressure over the liquid helium with a single stage 250 lit/sec. rotary pump. In this way it was possible to cool the liquid helium to a temperature of about $1.5^{o}K$ when required.

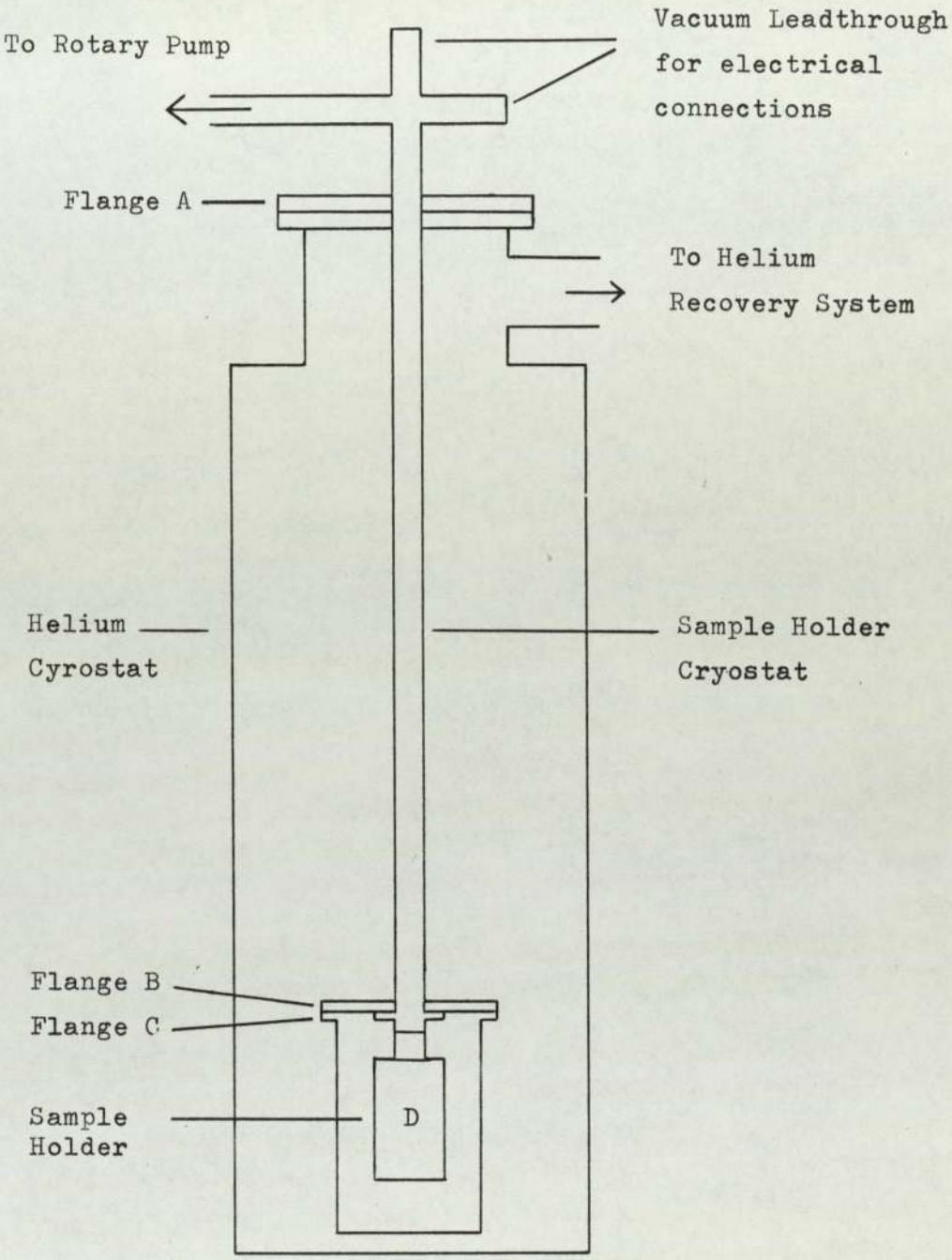

Figure 3.6 Diagram of low temperature cryostats.

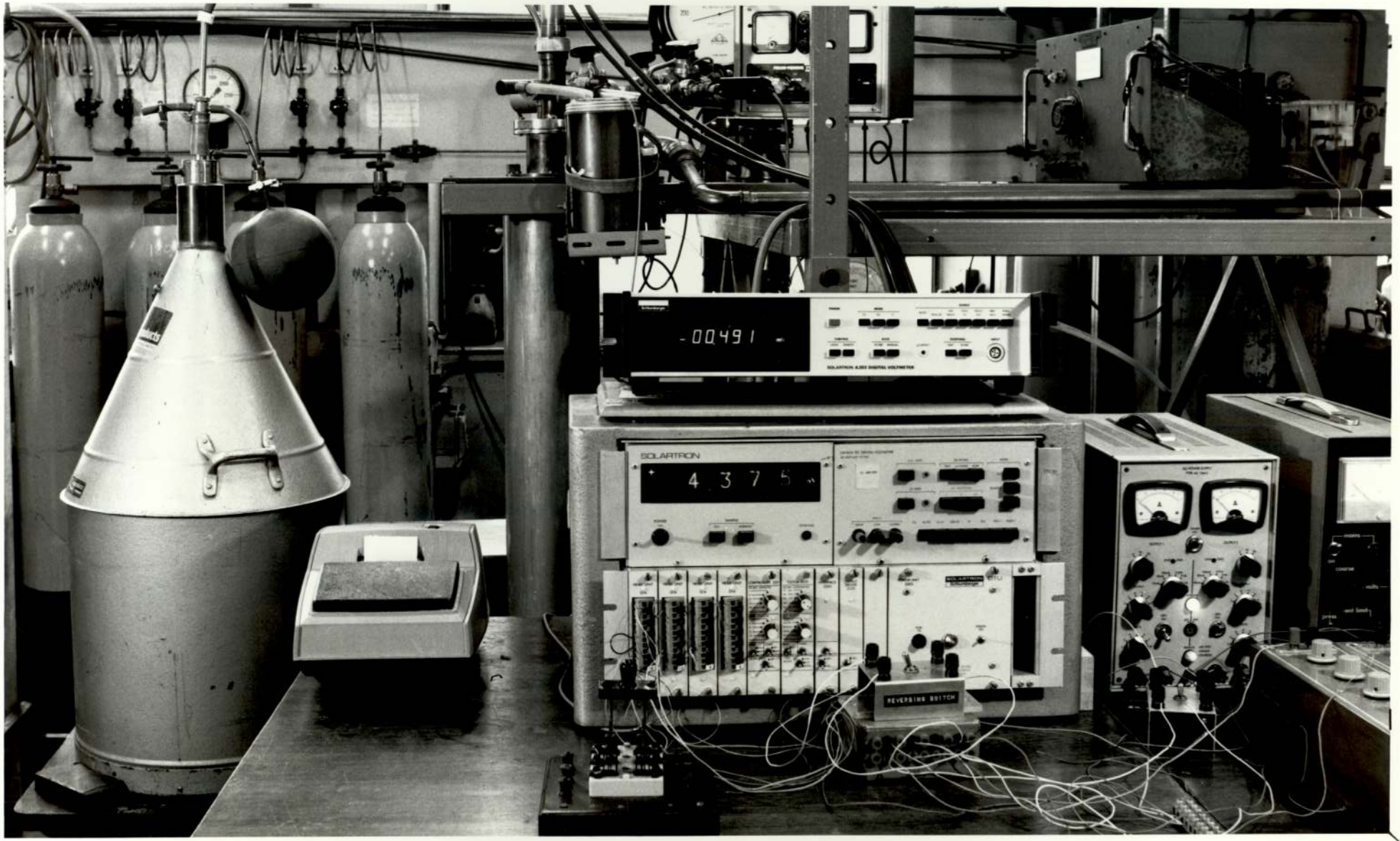

PLATE 3.3 GENERAL VIEW OF LOW TEMPEPATURE EXPERIMENT

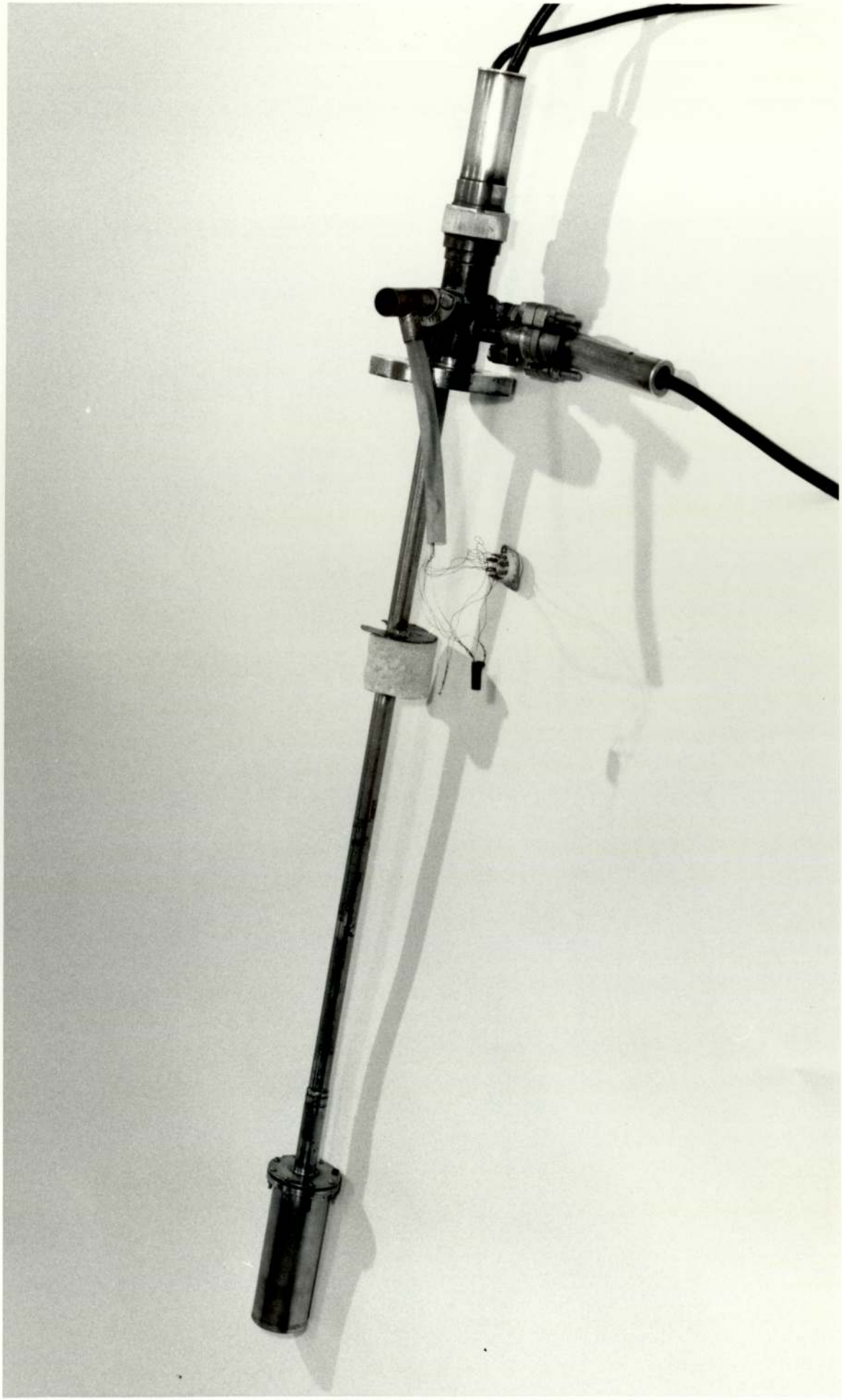

PLATE 3.4 LOW TEMPERATURE CRYOSTAT

3.7.2 Sample Holder Cryostat

The sample cryostat utilized for resistivity measurements in this work was designed to accommodate up to four samples at the same time. It was made of a stainless steel tube of 20 mm in diameter , suspended (when in used) at the centre of the liquid helium cryostat from a brass flange , A , of 125 mm in diameter, as shown in Fig.(3.6). The top end of the tube was branched for electrical lead throughs, thermocouples and evacuation. A sample holder, as shown in Fig.(3.7), designed for resistivity experiments was secured to the copper flange B at the other end of the stainless steel tube by two 8 B.A. bolts. The holder consisted of a rectangular copper block 25 x 25 x 45 mm which could be heated to a desired temperature by means of heater H_1. The heater was made of a 350 ohms eureka wire,wound around the copper rod and capable of maintaining a temperature difference of 30°K between the holder and the flange B (at liquid helium temperature). The sample holder assembly was enclosed in a copper can sealed at one end and with a copper flange C at the other. A vacuum seal was made between B and C using indium wire of 1 mm in diameter and eight 8 B.A. bolts round their circumferences.

3.7.3 Electrical Contacts to the Samples

All of the film samples studied in the resistivity experiments were deposited through stainless steel masks of the same configurations. Fig.(3.8) illustrates the dimensions of a film.

A and B were current contact areas and C, D, E and F were contact areas for the measurements of the potential difference

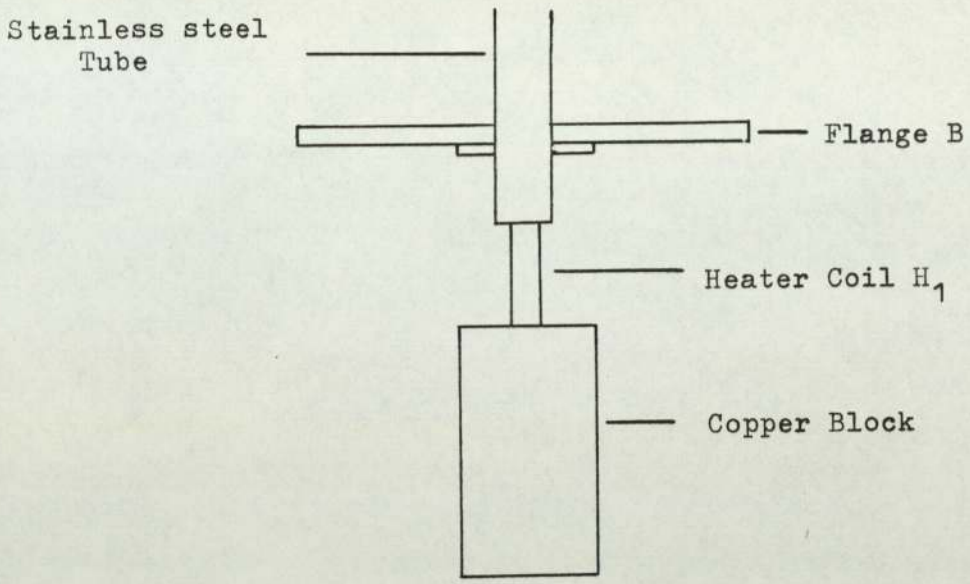

Figure 3.7 Diagram of the sample holder cryostat.

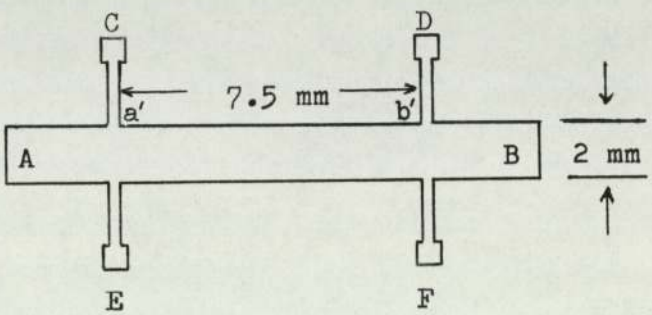

Figure 3.8 Film configuration.

between a' and b' arising from the resistance of the film when a current was passing through.

To measure the electrical resistance of a sample, six gold plated copper strips were used. The arrangement of these strips is shown in Fig.(3.10) . Pressure was applied to the electrical contact areas by spring loaded steel ball-bearings, 3 mm in diameter. Each spring was fixed in a hole drilled into the copper block (10 mm deep and 3 mm in diameter) and held by lightly centre punching the top edge of the hole. Fig.(3.9) shows the cross-section of a sample mounting surface. Insulation between a gold-plated strip and the block was made by means of low temperature varnish G.E. 7031 . The sample could be held against the spring-loaded bearings by means of a stainless steel backing plate which was secured to the block by two fixing screws.

Two additional ball-bearings enabled a thermocouples junction to be held against the substrate so that the surface temperatures of the sample could be monitored. The thermocouples used were Au-0.03 at % Fe / chromel wires , 1 mm in diameter. Liquid nitrogen was used at the reference junction. All of the four pairs of the thermocouples were calibrated against rhodium-iron and germanium resistance thermometers in the range 300 -30^{o}K and 30-2^{o}K respectively. The accuracy of the thermocouples was to within 0.07^{o}K.

The current and voltage leads were enamelled copper wires of 36 S.W.G. and 40 S.W.G. ,respectively. The surface of the copper flange B(in Fig.(3.6))was used as a thermal anchor of all the wires including thermocouples.

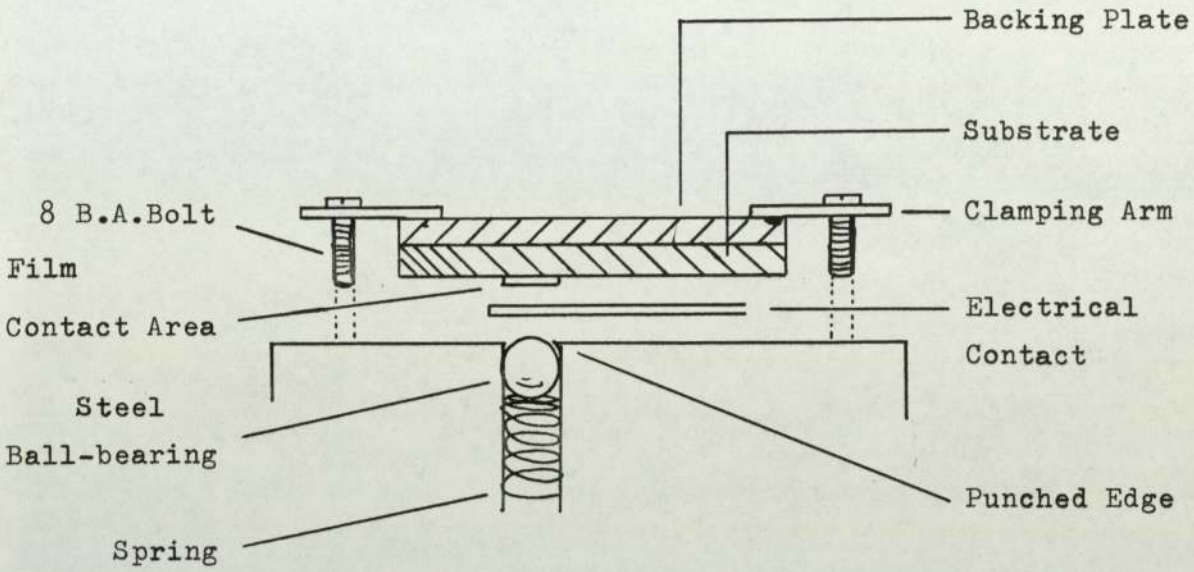

Figure 3.9 Cross-section of a sample mounting surface.

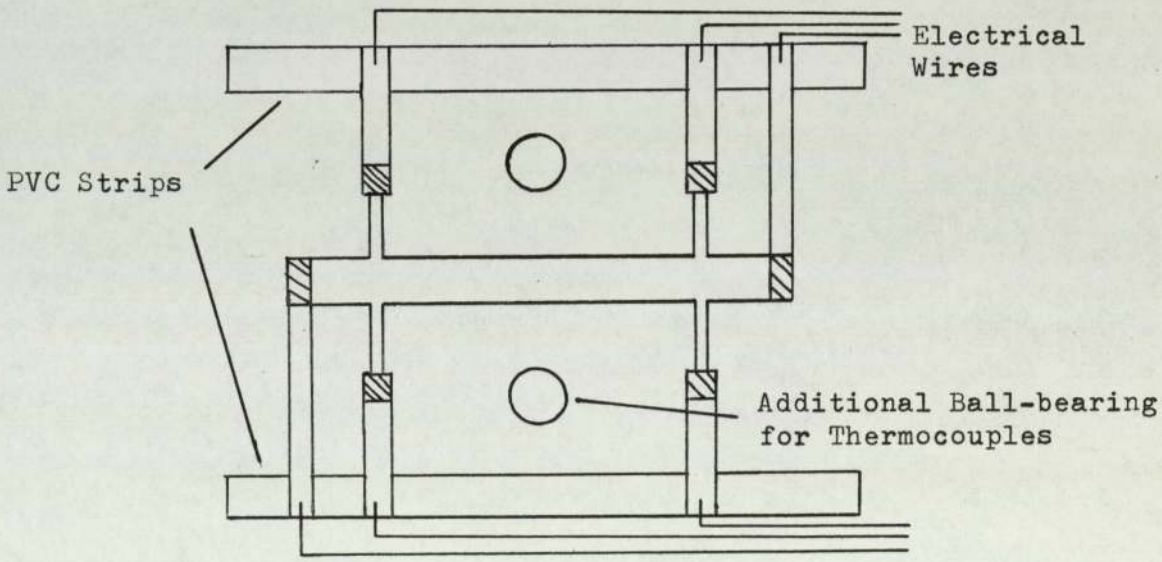

Figure 3.10 Arrangement of the electrical contacts.

3.8 The Ellipsometer

The ellipsometer employed in the present work was one with facilities for making measurements at two angles of incidence. It comprised the basic compcnents similar to other ellipsometers described elsewhere(O'Shea,1971) but had two optical benches on the analyser side which enabled measurements to be carried out at two different angles of incidence.

Three triangular optical benches were set to make angles of approximately 90° , 120° and 150° to one another. Plate (3.5) illustrates the two angle of incidence ellipsometer. The light source , collimator , filter and polarizer were mounted on the fixed bench. The other two could be moved $\pm 5^{\circ}$ about the centre positions. This permitted the angle of incidence to vary between 55° and 75°. These benches, together with their components on sliding saddles were lined up as shown in Plate (3.5). The light source was from a 24 volt , 150 watt projector lamp, type A1/212, operated from a 25 volts 200 VA Variac controlled transformer.

The optimum angle of incidence , for determination of optical constants , has been calculated by Miller et al.(1970) and found to be in the region of 74° , for n less than 3.0 and k less than 3.2. Thus the two angles used in the present work were set at 61° and 73° so that a significant difference between ψ and Δ readings for the two angles could be achieved without departing too much from the region of maximum sensitivity.

Two of the modified type P3 polariser heads,purchased from Bellingham and Stanley Ltd.,were used interchangeably as a polarizer or analyser. Each head carried a modified calcite Glan Thomson

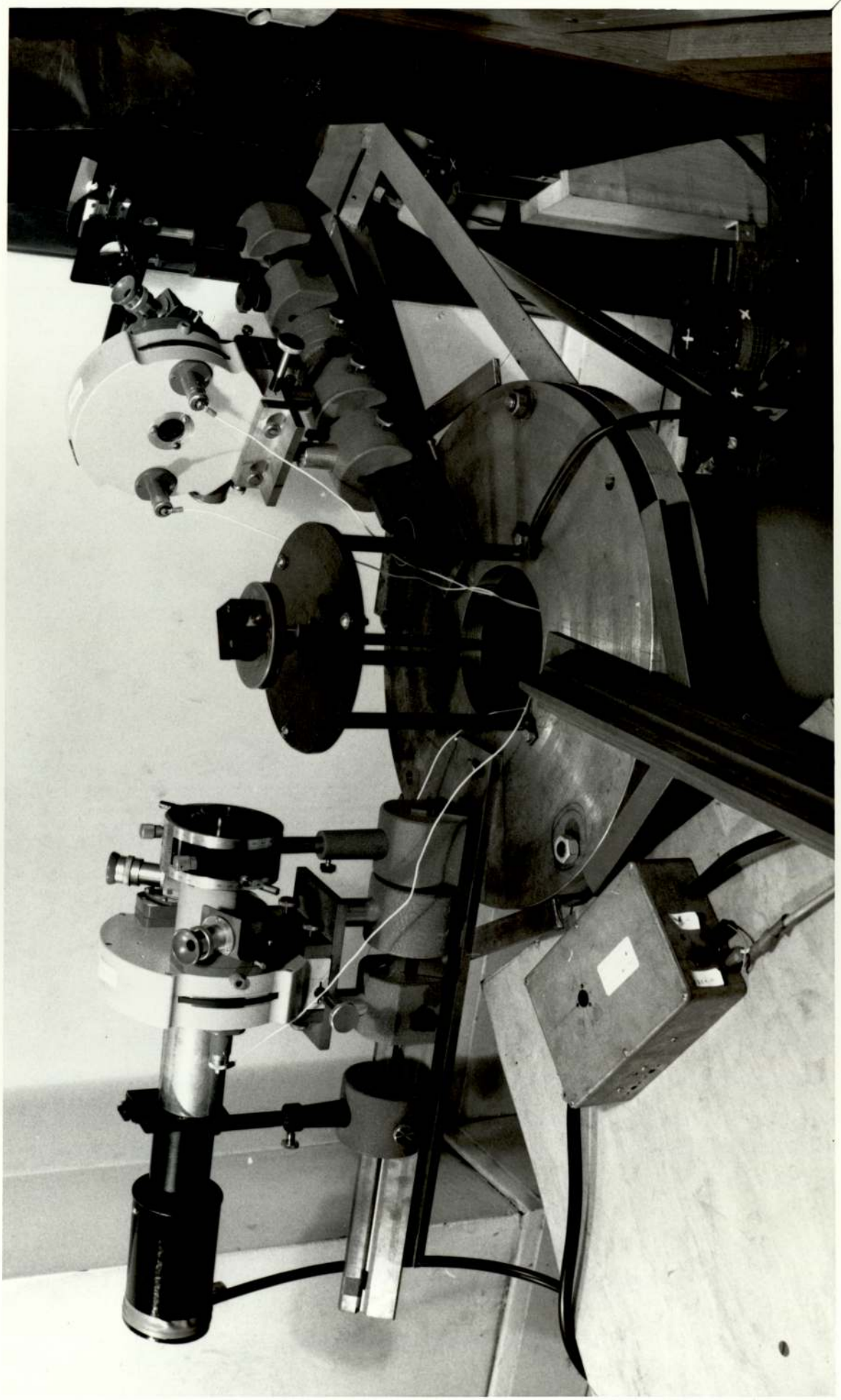

PLATE 3.5 TWO ANGLE OF INCIDENCE ELLIPSOMETER

prism giving a high degree of precision of polarisation. A single index line actuated by a micrometer screw divided drum was incorporated into the head , enabling the 1/4 degree division on the scale to be subdivided directly to 0.01 degrees and by estimation to 0.002 degrees. It also carried two scale readings with telescopes to provide readings at 180 degrees apart to eliminate any centring errors. The scale illumination is provided from low voltage bulbs supplied from a 6 volt transformer , placed inside the ellipsometer base.

The detector used was a type 6094 B photomultiplier tube supplied by E.M.I. Electronics Ltd. and was employed in conjunction with a stabilised power supply type 532/D from Isotope Development Ltd. A Solartron digital voltmeter type A203 which had a sentivity of 1 microvolt was utilized for observing the voltage drop across a standard 1000 ohm resistance , enabling currents of less than 10^{-9} Amperes to be detected.

3.9 X-ray Diffractometer

The apparatus used for identifying the composition of the film samples was a Philips PW105 difractometer, Plate(3.6) , in conjunction with a Philips 1010 x-ray generator. The radiation used was CuKα radiation of wavelength , λ , = 1.5405 $\mathring{A}$. The diffraction patterns of the niobium-tin system and their oxides are listed in Appendix B.

The facilities also available to use in conjunction with the diffractometer were :

(1) Automatic step scanning capabilities which allowed

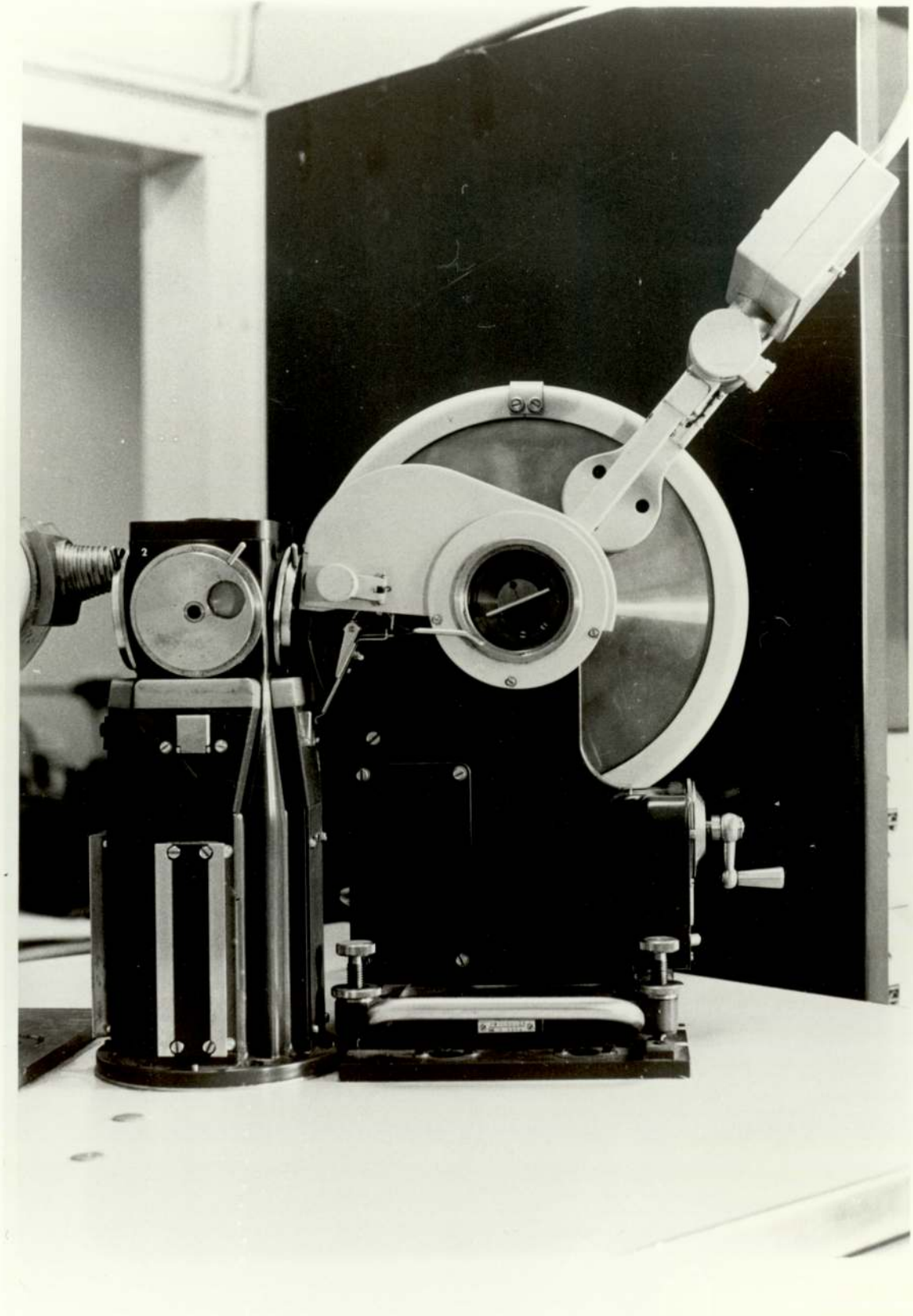

PLATE 3.6 X-RAY DIFFRACTION

the collection of data across the line profiles to be performed.

(2) Standard counting equipment including pulse height analyser.

(3) A printer and 8-hole punch tape out fit to register measured intensity values.

* * * * * * * * * * * * * * * * *

CHAPTER 4 : EXPERIMENTAL PROCEDURE

4.1 Consideration For Substrates

In order to prepare niobium-tin films which could be used for both optical and electrical measurements , substrates were chosen with properties which satisfied the following criteria :

(1) Due to high alloying temperatures of Nb_3Sn (minimum about 650°C) which has been reported to have optimum temperatures in the region of 800-900°C(Dickey et al.,1971) , the substrates should be able to withstand temperatures in excess of 1000°C.

(2) The surface of a substrate should be as near optically flat as possible (preferably with precisely known optical refractive index for the ellipsometric measurements, particularly measurements on very thin films.

(3) To study the electrical properties in the temperature range from 300°K down to liquid helium temperatures the films were required to have good adhesion to the substrates.

Taking into account these conditions , fused quartz was considered as an appropriate material. Not only could it withstand the required high temperature but the variation of refractive index with the wave length of light in the visible region has been precisely determined(Kaye and Laby,1973). The initial trial showed that good adhesion of a set of films after a few thermal cycles from room temperature to liquid helium temperatures was achieved.

All the substrates used in the present work were clear fused quartz of dimensions 19 x 14 x 1 mm , purchased from Qua drant

Glass Ltd. In order to prevent stray reflections from the back of the substrates in the ellipsometric experiments (particularly if thin films were examined) most of the substrates were ground on the reverse side with grade 200 carborundum powder.

The substrates were cleaned prior to mounting in the evaporation unit , according to the procedure below :

(1) Boiled for 20 minutes in a 5% detergent solution.

(2) Rinsed five times with distilled water (follow each time by ultrasonic cleaning also in distilled water)

(3) Boiled for five minutes in iso-propyl alcohol and then slowly removed through the iso-proply alcohol vapour.

4.2 Establishment of a Vacuum

Initial rough pumping of the vacuum chamber was carried out by means of a rotary pump , see Fig.(3.1) . A liquid nitrogen cold trap was included between the diffusion and rotary pumps. The diffusion pump could be switched on when the pressure of the system was less than 10^{-1} torr. Then the chamber was heated gradually to a temperature of about 200°C after the pressure of less than 5×10^{-4} torr had been established. The pressure of less than 5×10^{-5} torr could be achieved in about 15 hours after the diffusion pump had been switched on. At this pressure, the ion pump could be started and the rough vacuum pumping system was then isolated from the chamber by the U.H.V. valve. A set of Pirani and Penning gauges were used to monitor the pressure prior to isolation, but after that a Mullard IOG 12 gauge having a lower limit of 10^{-10} torr was utilized.

In order to outgas the substrates, the temperatures of the substrate heaters were gradually increased and maintained at a temperature of 800°C for a few hours. When the whole system cooled to room temperature, the pressure would fall to less than 10^{-8} torr. A further reduction in the pressure was achieved by outgassing the niobium slug and tin crucible, pre-evaporation of these sources and utilizing the gettering action of freshly deposited niobium and tin to produce a vacuum of less than 10^{-9} torr.

4.3 Preparation of Nb-Sn Alloy Films

Two preparation techniques were primarily examined in the present work, namely , co-deposition of niobium and tin , and solid state diffusion of tin into niobium layers followed by alloying.

The co-deposition method has been employed for preparing Nb_3Sn films by several workers.(For example, Hammond,1975). The process was considered to be simpler and less time consuming than the diffusion method. Once the required deposition rates of both niobium and tin had been reached then the substrates could be exposed to the sources until the required thickness was obtained. The disadvantage of this method in the present work was that the deposition rates of both sources could not be controlled to be 3:1. This ratio has been reported by Neugebauer(1964) to be the crucial factor for the formation of Nb_3Sn. Furthermore, the prepared films were found to have cracks on the surfaces,suggesting that the films were either inhomogeneous or not firmly attached to the substrates. Films prepared by diffusion were found to be superior

in that the surfaces were smooth and a good crystalline structure could be achieved. In addition preparation conditions could be more easily reproduced. Therefore the co-deposition method was abandoned after a few preliminary runs.

4.3.1 Solid State Diffusion

There were four main stages in preparing a set of films by this method. Following preliminary experiments , each stage of the preparation of superconducting Nb_3Sn was optimised.

4.3.1(a) Evaporation of Niobium Films

High purity niobium, 99.99 % was obtained from Metals Research Ltd. in the form of slugs , weighing about 6-7 grams each. A niobium slug was gradually heated with the electron beam after a pressure of less than 10^{-6} torr had been established in the chamber. Input power of the beam was controlled so that the pressure in the chamber was not higher than the maximum safety pressure for the tungsten filament of the electron gun,of 1×10^{-5} torr. At a power input of about 1000 watts the niobium would melt and it was held just above the melting point for a few hours. During this time there would be some evaporation of the niobium and the pressure would fall to less than 10^{-8} torr.

To achieve a niobium deposition rate of 250 $\mathring{A}$ $min.^{-1}$ on a substrate positioned 200 mm above the source , an evaporation rate of about 0.08 $gm.min.^{-1}$, corresponding to an electron current of 420 mA was needed. Once the required evaporation rate had been reached the pressure in the chamber was allowed to stabilize for several

minutes . At this point the substrates were exposed to the evaporation source by opening the shutter and then when the required thickness of films had been deposited the shutter was closed. The electron beam evaporator was gradually cooled down and finally switched off. Simultaneously, the substrates which were heated to a temperature of about 200°C during the deposition were gradually cooled down to room temperature. After about 2 hours the pressure would fall to less than 1×10^{-9} torr and could be maintained indefinitely if no further heating was created.

4.3.1(b) Evaporation of Overlay Tin Films

Tin wire (99.999 %) also purchased from Metals Research Ltd. was used for the tin overlay deposition. After the tin source had been gradually heated up to a temperature of about 1000°C for several minutes, the shutter was opened so that tin vapour would deposit on to the previously deposited niobium films which were held at room temperature. The pressure in the chamber could be maintained at 3×10^{-7} torr during the deposition. When a required thickness had been reached the shutter was closed again and the tin crucible was gradually cooled down.

4.3.1(c) Diffusion of Tin into Niobium

The next step was to diffuse tin in the overlay into the niobium surfaces. The samples which consisted of niobium and tin layers were heated to a temperature of about 400°C and held at this temperature for a period from a few hours to 24 hours depending on the thickness of the niobium films previously prepared (and which

in turn determined the thickness of the niobium-tin alloy layers).

4.3.1(d) Alloying At High Temperatures

The substrates were finally heated individually by the localized heaters and kept at higher temperatures ranging between 650°C and 1000°C to form the alloys. The temperature was maintained for more than 8 hours so that excess surface tin would evaporate.

4.4 Structural Determination of Nb_3Sn

The identification of film samples was made by means of x-ray diffraction and superconductivity observations. The x-ray diffraction technique was simpler to employ since it could be performed in a shorter time , but was suitable only for films of thickness greater than 100 nm. For thinner films , resistivity measurement was the alternative way of identifying the presence of Nb_3Sn since this is the only compound in the niobium-tin system which has transition temperature above 4.2°K(Enstrom,1966)

To observe the x-ray diffraction pattern of a film, the sample was mounted on to the diffractometer target holder. The counter was set to scan from $2\theta = 20^\circ$ to 140° with a constant angular speed of 1°/min.The diffraction intensities as a function of 2θ were recorded on a paper chart , using a plotter provided. The d-spacings of the observed peaks were compared with those of niobium, tin, their compounds and their oxides. The A.S.T.M. index cards of these materials have been listed in Appendix B.

For a well crystallized Nb_3Sn film , its lattice constant was obtained by a conventional method. Firstly, a common factor would be found from the d-spacings of the observed peaks and

consequently, the indices (h, k, l) of these d-spacings were established. Then the plot of $\sin^2\theta$ against $N^2(=h^2+k^2+l^2)$ would yield the lattice constant of Nb_3Sn from the slope of the graph. (the wavelength of the CuK_α radiation used in the calculation was 1.5405 $\mathring{A}$).

4.5 Ellipsometric Experiment

The ellipsometer used was the two angle of incidence ellipsometer described in the previous chapter (Section 3.8). The essence of the experiment was to obtain Ψ and Δ (at a given angle of incidence) from which the optical characteristics of the specimen under examination could be determined. Then these observed values were evaluated according to the conditions explained in Section (2.7.3) , e.g., equations (2.89) - (2.95b) were used for the case of film-free surfaces.

4.5.1 Evaluation of Ψ and Δ Using Compensation Method

The method of compensation utilized in the present work was that due to Winterbottom(1955), employing a quarter wave plate as the compensator. Principally the quarter wave plate can be constructed from any bi-refringent material inwhich the refractive index for the ordinary ray, n_o , differs from that of the extra-ordinary ray, n_e. The phase difference between these two rays after passing through the plate will be given by :

$$\delta = \frac{2\pi}{\lambda}(n_e - n_o)\, h \qquad (4.1)$$

$$= \pi/4 \quad \text{for a quarter wave plate}$$

where h is the thickness of the plate.

The basis of the compensation method is illustrated in Fig.(4.1). Plane polarized light produced by the polarizer P, is incident on the specimen with azimuth Ψ , i.e., its plane of polarization inclined at an angle Ψ to the plane of incidence. On reflection from the specimen the difference in amplitude reduction and the difference in phase change between the (p) and (s) components gives rise to reflected light which is, in general, elliptically polarized. This elliptically polarized light then passes through the compensator, which consists of a bi-refringent sheet of mica, of a quarter wave thickness for the particular wavelength of light used (549 nm). If the fast axis of the compensator is arranged to be parallel to the major axis of the reflected ellipse, the vibrations along the major and minor axes of the ellipse (for which a phase difference of 90 degrees exists) are again brought into phase, and plane polarized light results. Then the light passes through the analyser, A, which may be rotated until its transmission axis is perpendicular to the plane of polarization. In this condition the light intensity received by the photomultiplier detector is zero.

To evaluate the parameters Ψ and Δ for the general representation of elliptically polarized light as shown in Fig.(4.2), three parameters are required :

(a) The ratio of minor to major axes, or ellipticity

$$b/a = \tan \gamma \quad \text{(say)} \qquad (4.2)$$

(b) The azimuth of the major axis, Ψ

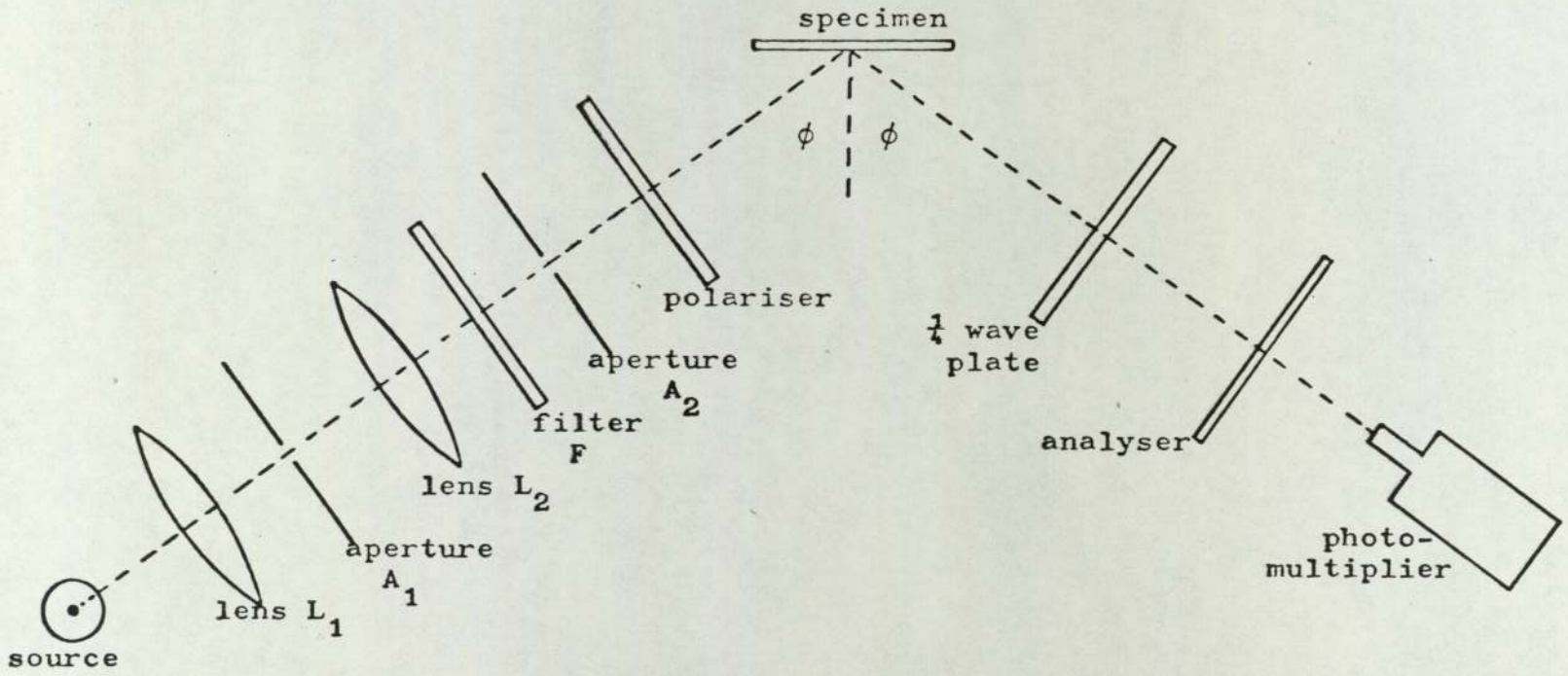

Figure 4.1 Arrangement of the ellipsometer components.

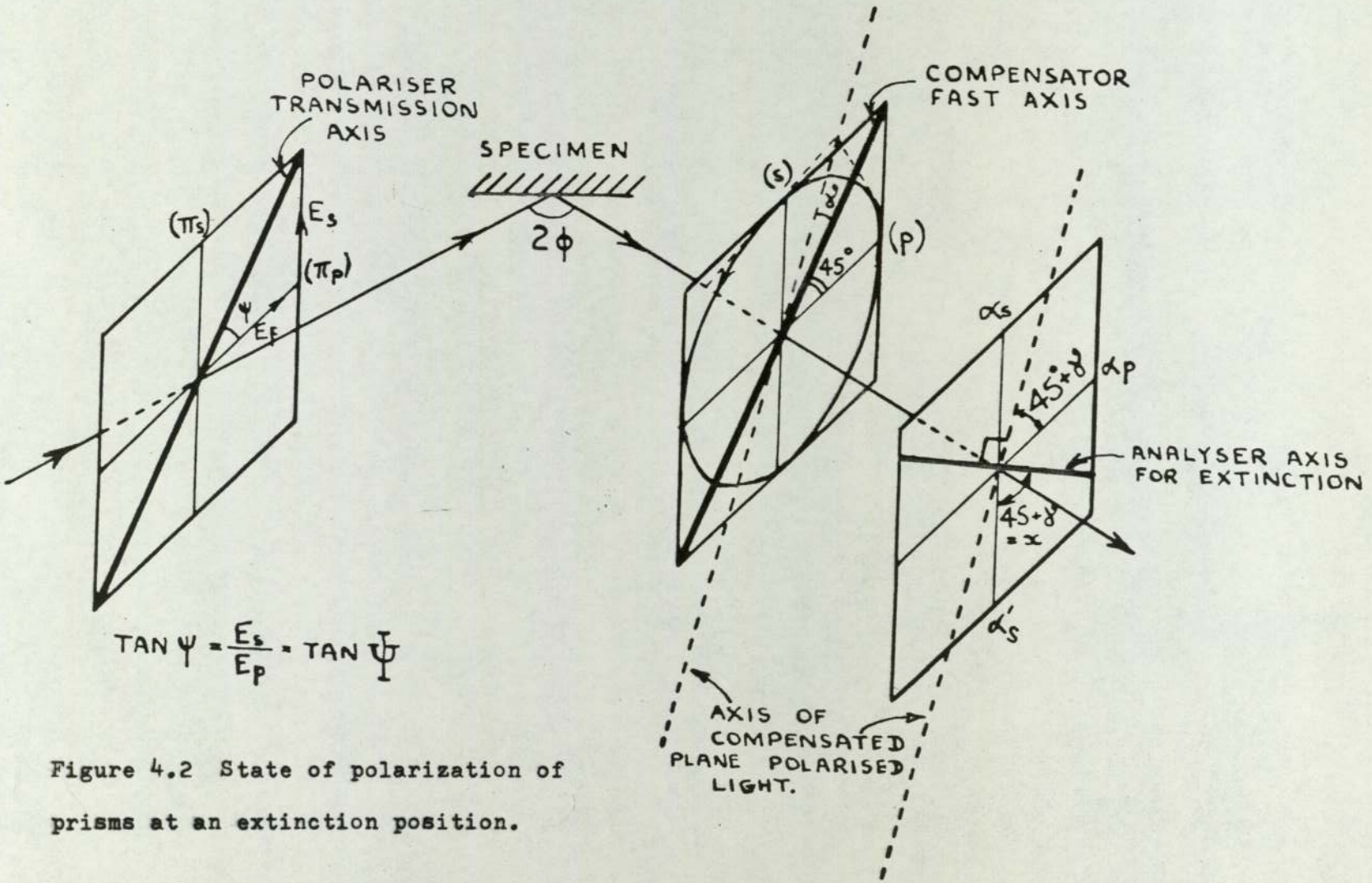

Figure 4.2 State of polarization of prisms at an extinction position.

(c) The rotation direction, conventionally positive if anti-clockwise looking towards the on coming light. (see Appendix A).

According to the experimental procedure, the compensator was first locked with its fast axis at exactly 45 degrees to the plane of incidence. Light emerging through the compensator would be plane polarized only if the azimuth of the reflected ellipse was also 45 degrees to the plane of incidence.

The azimuth ψ of the polarizer was then equal to the parameter Ψ mentioned in equation (2.88) , for , from Fig.(4.3) :

$$\tan\psi = E_s^+/E_p^+ \qquad (4.3)$$

But , $$\mathrm{Tan}\Psi e^{i\Delta} = r_{o2(p)}/r_{o2(s)}$$

$$= \frac{E_p^-/E_p^+}{E_s^-/E_s^+} = \frac{E_p^-/E_s^-}{E_p^+/E_s^+} \qquad (4.4)$$

Since from above, $$E_p^-/E_s^- = 1 \qquad (4.5)$$

then equation (3.4) becomes,

$$\mathrm{Tan}\,\Psi = E_s^+/E_p^+ \qquad (4.6)$$

Hence , from (3.3) $\tan\psi = \mathrm{Tan}\,\Psi$

i.e. , $$\psi = \Psi \qquad (4.7)$$

The ellipticity is related to the phase difference between the (p) and (s) components. In general, it may be shown that:

$$\tan\Delta = \tan 2\gamma/\sin 2\psi \qquad (4.8)$$

Since , from above $\psi = 45^\circ$, $\sin 2\psi = 1$

and thus $\tan\Delta = \tan 2\gamma$

i.e. , $\Delta = 2\gamma$ (4.9)

The ellipticity γ and hence the phase difference Δ was determined from the analyser azimuth , as shown in Fig.(4.3). The azimuth of the compensated light was $45+\gamma$, so that the azimuth of the analyser in its extinction position would be $45+\gamma$ with respect to α_s' (a reference azimuth inwhich plane polarized light with its electric vector parallel to the plane of the incidence could not pass through), the perpendicular to the plane of incidence. It was this quantity , marked x , which was measured experimentally.

Since $x = 45 + \gamma = 45 + \Delta/2$ (4.10)

then $\Delta = 2x - 90$ (4.11)

4.5.2 Determination of Reference Azimuths

The readings on the divided circles of the polarizer and analyser which correspond to the transmission axes of the Glan Thomson prisms , i.e., parallel and perpendicular to the plane of incidence are known as the reference azimuths. In this work the experimental azimuths were expressed relative to the plane of incidence. Assuming that the ellipsometer was aligned, approximate values were obtained by removing the polarizing and analysing prisms in turn from the ellipsometer and arranging for light from a lamp to be reflected at approximately 56 degrees from a glass plate, placed flat on a bench, and to pass through the prism. As shown in Fig.(4.4) , the transmission axis was approximately vertical when minimum light was observed through the prism. On returning the prisms to the ellipsometer, the transmission axes were therefore set roughly perpendicular to the plane of incidence

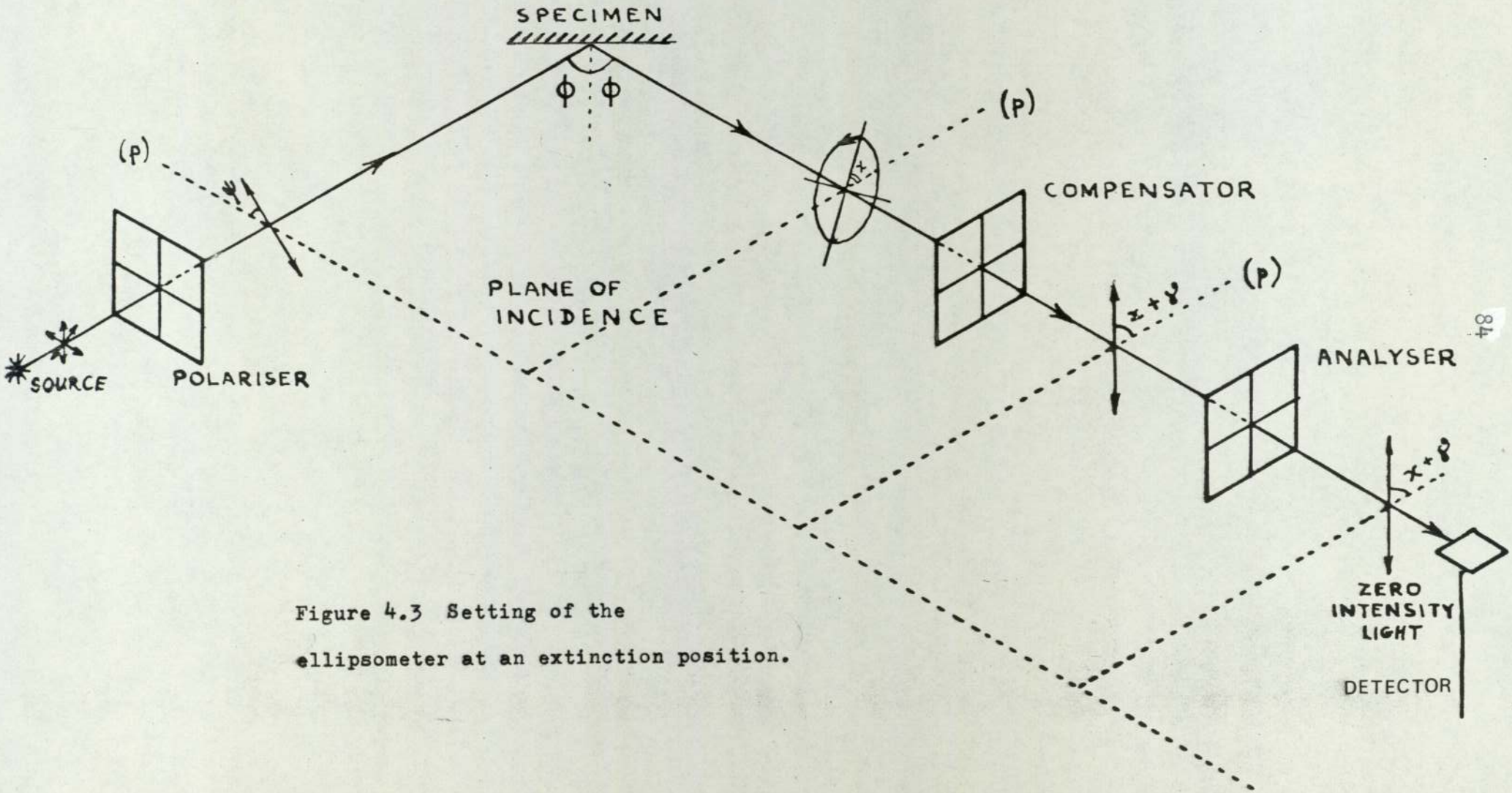

Figure 4.3 Setting of the ellipsometer at an extinction position.

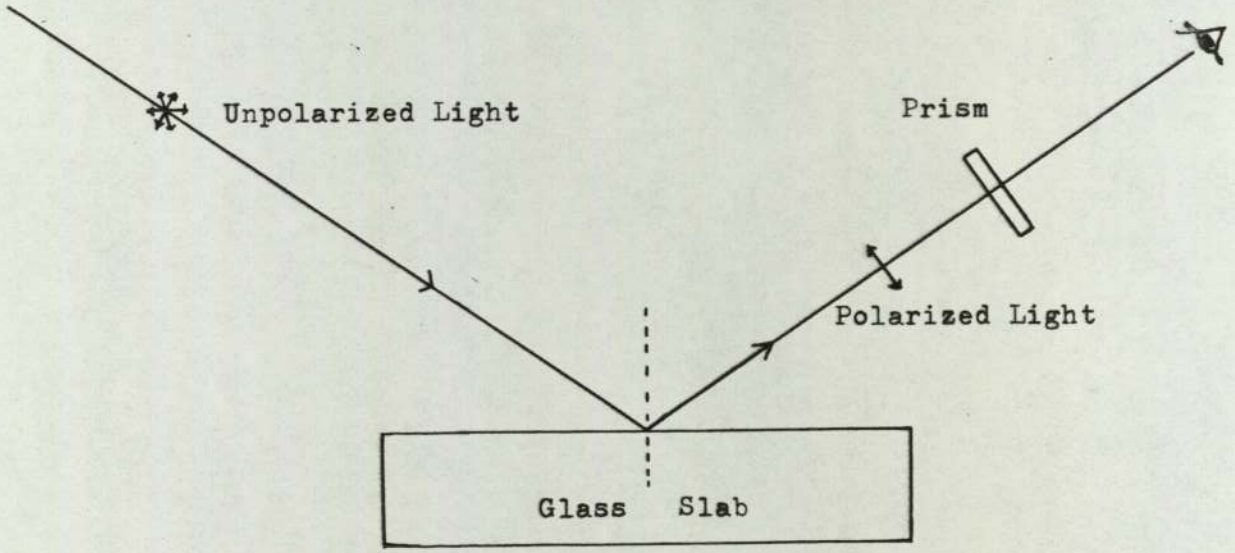

Figure 4.4 Approximate oreintation of the prism polarization

which was horizontal.

The compensator was next removed from the ellipsometer and the polarizer was rotated through 90 degrees so that the transmission axis was horizontal (i.e. , parallel to the plane of incidence). With the light being reflected from a metal surface (i.e. , from a metal film mounted on the sample holder of the ellipsometer), a small voltage was applied to the photomultiplier. A slight adjustment of polarizer and then analyser served to reduce the light intensity to a minimum.The process repeated, with the voltage increasing, until the limiting value of 1500 volts was reached. To get extinction the incident light was either polarized parallel or perpendicular to the plane of incidence. All other positions non-extinctions resulted. Then the exact polarizer azimuth for extinction was obtained by averaging a set of pairs of the azimuths at equal intensities on each side of the minimum. With the polarizer set at its extinction position the analyser extinction position was obtained in the same manner.

From a set of pairs of azimuths, taken at equal intensities on each side of the extinction position it would be realized that light intensities as a function of the polarizer azimuth was symmetical about its extinction position for an analyser setting and and vice versa for a polarizer setting. Taking the advantage of this symmetrical property of intensities of light, a technique called " Bracketting " was used to locate the exact position of extinction, i.e., minimum output from the photomultiplier. By rotating of 5 to 10 degrees on either side of a minimum it was sufficient to attain the greatest accuracy.

The polarizer and analyser reference azimuths now cor-

responded to positions known as π_p and α_s , respectively . Both polarizer and analyser were then rotated through 90 degrees in a positive sense (i.e., anti-clockwise looking towards the on-coming light) and the entire process repeated. These alternative positions corresponded to azimuths π_s and α_p and would be 90 degrees exactly from the first positions for correctly alinged apparatus. There were also non-significant positions at 180 degrees to each scale reading, indicated by the dash(') e.g., π'_p , α'_s , etc. For other polarizer positions, the reflected light was elliptically polarized and could be extinguished by the analyser only when used in conjunction with the compensator.

To obtain a reference position for the compensator (when in use) the polarizer and analyser were set to a pair of related extinction positions and the compensator returned to the ellipsometer in the position shown in Fig.(4.1). By rotating the compensator through the minimum, using the bracketting technique, a reference azimuth of the compensator was found. This position corresponded to either the fast or slow axis of the compensator being parallel to the plane of incidence because only when the light incident on the compensator was plane polarized in a direction parallel to either the fast or slow axis would the light emerging through the compensator be plane polarized, resulting in extinction by the analyser. The procedure is repeated for the alternative reference azimuth which would be 90 degrees from the first position for an exact quarter wave plate (i.e., one which changes relative phase by $\pi/4$). Once again, there were non-significant positions at 180 degrees to both reference positions. The whole procedure was repeated for the other angle of incidence so that the reference azimuths at that

angle of incidence for the polarizer, analyser and compensator were observed.

4.5.3 Determination of Ψ_{exp} and Δ_{exp}

The procedure was as follows :- the compensator was locked at 45 degrees to a reference positon. The polarizer and analyser were then successively turned to give minimum light intensity. Using the bracketting technique, the extinction positions of the polarizer and analyser would be found at, say , P_1 and A_1, respectively. The setting procedure was repeated for a polarizer azimuth in the next quadrant, giving readings P_2 and A_2 on the polarizer and analyser, respectively. It could be found that at other two polarizer positions , say, P_3 and P_4, 180 degrees to P_1 and P_2 , there would be extinction with the corresponding analyser positions A_3 and A_4, respectively.

The compensator was then rotated through 90 degrees with respect to the plane of incidence and four different pairs of polarizer and analyser settings could be obtained in the same way. In practice it was not necessary to made the measurements in all four zones, only those pairs of results designated 1 and 2 were recorded for each compensator setting.

In general, the polarizer setting are symmetrically placed about the plane of incidence, i.e., $P_1 - \pi_p$ should be equal to $\pi_p - P_2$. Therefore in the present investigation, the average was taken,

$$\frac{(P_1-\pi_p) + (\pi_p-P_2)}{2} = \Psi_{exp} \qquad (4.12)$$

or

$$\frac{P_1- P_2}{2} = \Psi_{exp} \qquad (4.13)$$

Using the Poincare' Sphere (O'Shea,1971) , the value of x in equation (4.11) should be either equal to $\alpha_s - A_1$ or $\alpha_p - A_2$, where the angle 2x - 90 gave the relative phase retardation, between the (p) and (s) components. Again, the average value was taken,

$$\frac{(\alpha_s - A_1) + (\alpha_p - A_2)}{2} = x \qquad (4.14)$$

and

$$2x - 90 = \Delta_{exp} \qquad (4.15)$$

4.5.4 Determination of the Optical Constants and Film Thickness

After the parameters Ψ_{exp} and Δ_{exp} had been evaluated from experimental observations, they were compared with theoretical ones and the unknown parameters n and k were determined. In the case of very thin films (less than 50 nm) their thicknesses could also be determined. The following procedure was adopted :

(a) Determination of Ψ_{exp} and Δ_{exp} were made at both angles of incidence.

(b) An initial guess was made by calculating the 'psuedo constants' , n_o and k_o , from the Ψ_{exp} and Δ_{exp} , using the ellipsometric equations for the film-free surface.

(c) A mesh of points (n_{cal} and k_{cal}) was established with a reasonable interval around the trial point (n_o,k_o). The theoretical Ψ_{cal} and Δ_{cal} were then evaluated from the exact equation , described in Section (2.7.3). (The details of computation technique have been described by O'Shea,1971 and Aguado Bombin,1975). The tabulated values for a given angle of incidence were compared with the corresponding experimental ones, retaining those values of thickness for which a numerical correspondence was fulfilled.

Thus for a given angle and for each choice of the constants, n_{cal} and k_{cal} there would be a set of Ψ_{cal} defined by (Aguado Bombin and Neal,1977) :

$$\Psi_{exp} - \varepsilon \leq \Psi_{cal} \leq \Psi_{exp} + \varepsilon \qquad (4.16)$$

and an independent set of Δ_{cal} values defined by

$$\Delta_{exp} - \mu \leq \Delta_{cal} \leq \Delta_{exp} + \mu \qquad (4.17)$$

where Ψ_{exp} and Δ_{exp} were those obtained from the experiment with experimental error ε and μ respectively. In the present work the experimental errors used were ; ε = 0.1 degrees and μ = 0.1 degrees, respectively.

The intersection of these two sets gave the value of thickness that ensured a simultaneous coincidence between the two theoretical quantities and the corresponding measurements for the angle specified. In general, there would be a definite spread of the constants n_{cal} and k_{cal} corresponding to this solution.Any ambiguity could be lifted by repeating the operation using the results obtained for the second angle of incidence.

4.6 Determination of Film Thickness

Film thickness is an important parameter in the calculation of the electrical properties and it is also necessary to evaluate the optical constants for thin films when the measured values of Ψ_{exp} and Δ_{exp} are dependent on the thickness of the films. Film thickness for metals and their oxides of the present work could be evaluated by several methods depending on the circumstances :

(1) Interferometry

(2) Electrical resistivity

(3) Quartz crystal thickness monitor

(4) Changes of ellipsometer parameters Ψ and Δ (see Section (4.5.4)).

4.6.1 The Interferometry Method

The principal technique used was that of the multiple beam interferometry. The thickness of the films was measured after removal from the ultra-high vacuum system, using an Interference Microscope supplied by Hilger and Watts Ltd.,see Plate (4.1). The method used for determining the thickness followed that suggested by Tolansky(1949), using fringes of equal chromatic order.

A cross-sectional diagram of a specimen, for film thickness determination by interferometry, has been illustrated in Fig.(4.6). The edge of the film, A,was first overlayed by a film B, of a highly reflecting material such as aluminium or silver (in this work aluminium was used for it could maintain a high reflectivity for a prolonged period of time).The 'step' formed over the edge of the film was independent of the thickness of the overlay and had equal reflectivity on either side. A semi-reflecting optically flat, C,was then placed over the step. An air gap was formed between the surfaces. An incident beam of white light on to the system would cause interference to take place between the light reflected from either side of the step and the semi-reflecting surface.If the gap thickness was a multiple of $\lambda/2$ (where λ was the wavelength of light) then destructive interference for that particular wavelength occurred .When the arrangement was viewed through

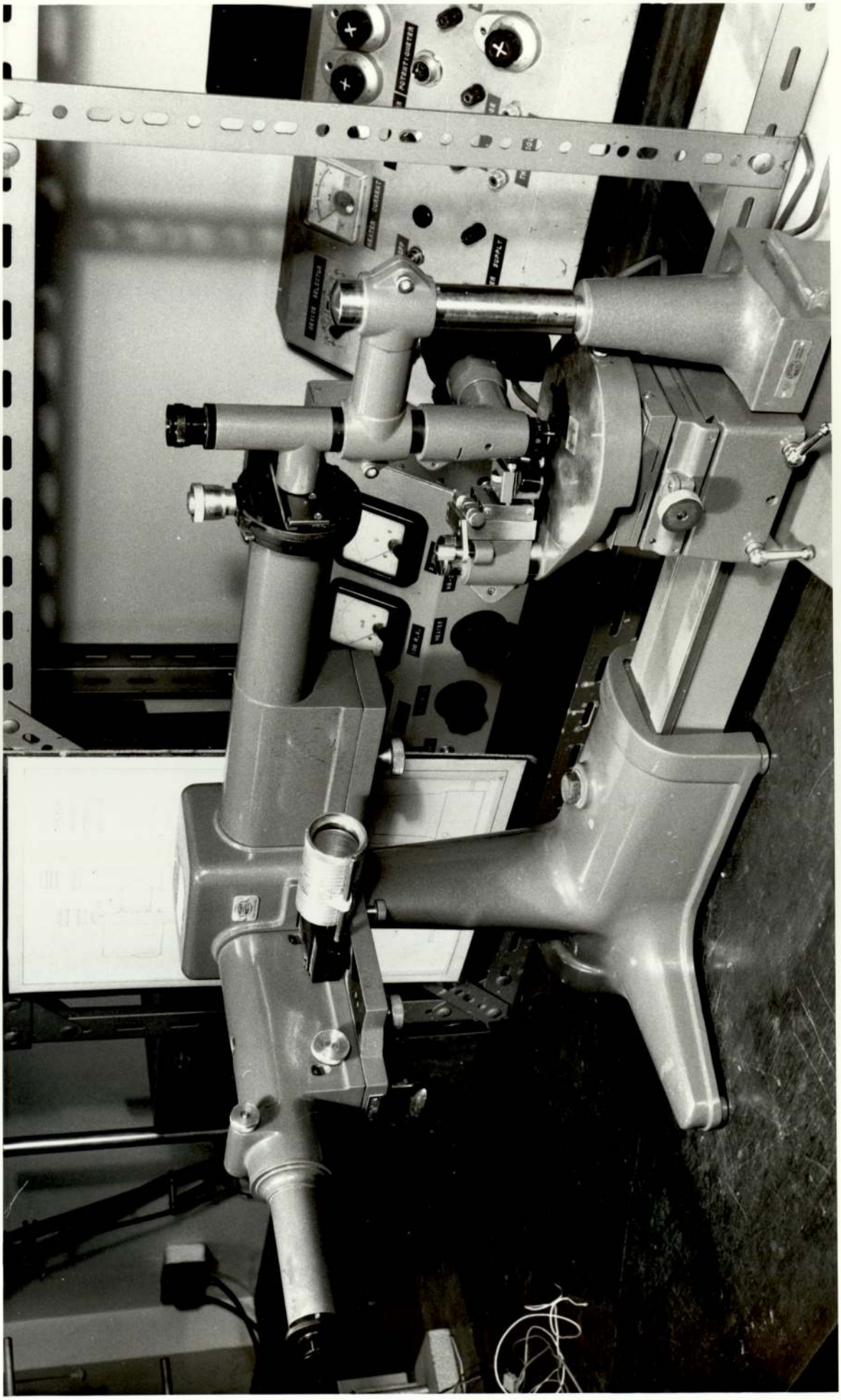

PLATE 4.1 INTERFEROMETER FOR FILM THICKNESS MEASUREMENTS

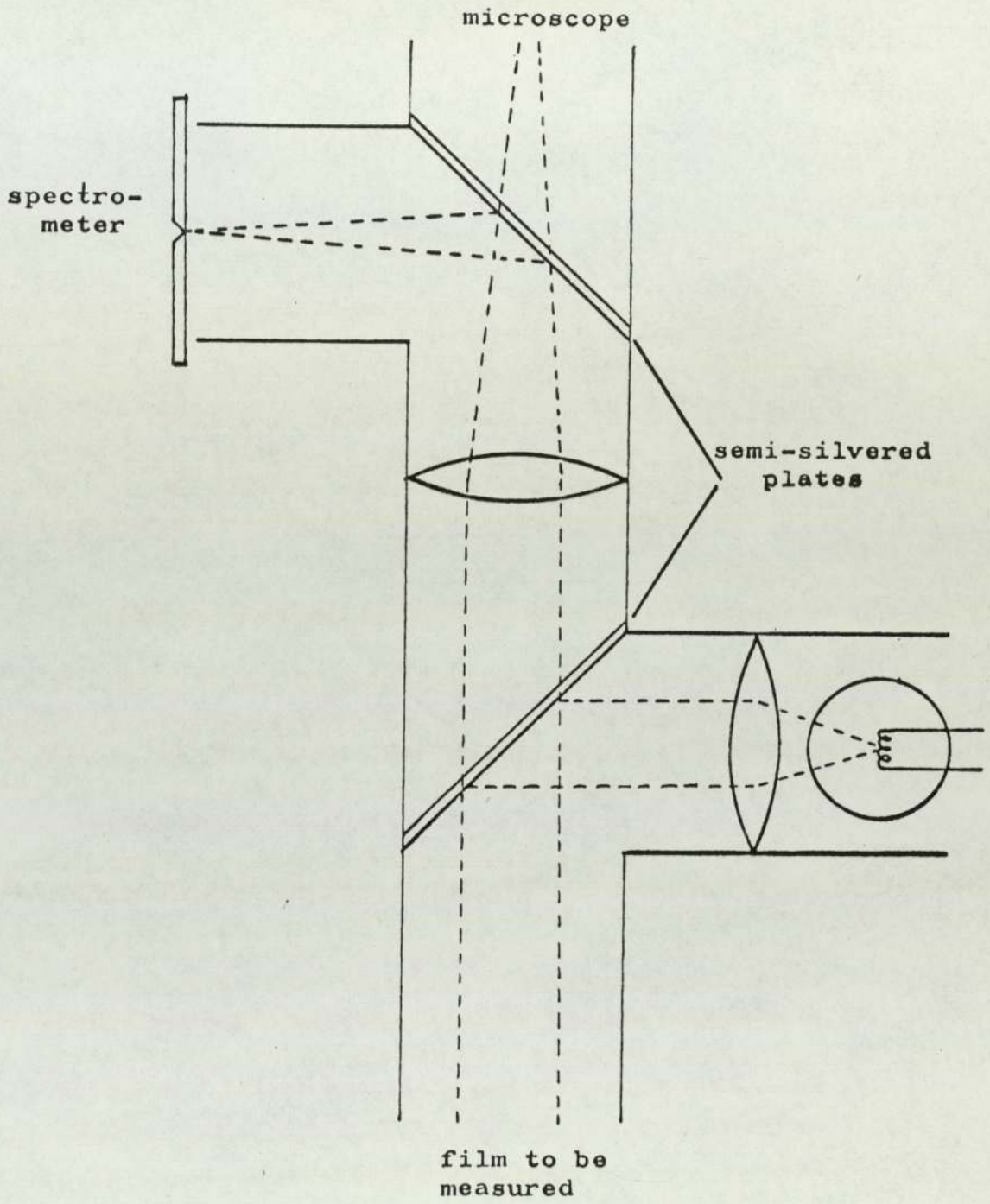

Figure 4.5 Thin film measuring microscope.

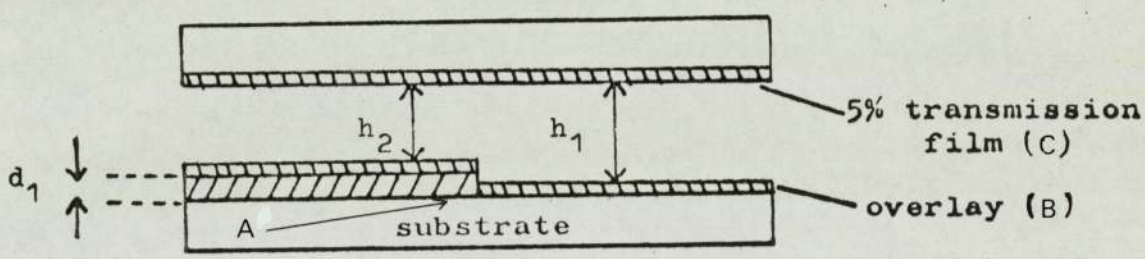

Figure 4.6 Position of a specimen for the fringe formation.

the spectrometer, for white light, dark fringes appeared in the field of view corresponding to wavelengths satisfying the above criteria. The fringes have a ' kink ' due to the discontinuity in the air gap from h_1 to h_2, caused by the step (i.e., due to the film thickness), as shown in Fig.(4.7) below.

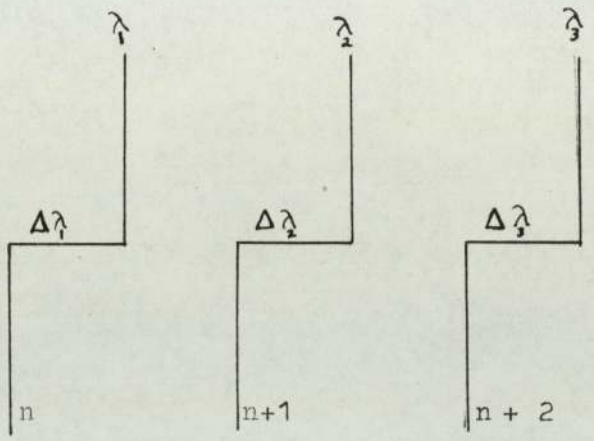

Figure 4.7 Field of view showing three fringes of equal chromatic order.

The fringes produced were of equal chromatic order (i.e., the order of the top and bottom of each fringe were the same) and the consecutive fringes differed in order by unity.

Consider fringes produced at wavelengths λ_1,λ_2 andλ_3 with order n, n+1, and n+2,respectively. The conditions for the occurrence of these fringes were :

$$2h_1 = n\lambda_1 \qquad (4.18)$$

$$2h_1 = (n+1)\lambda_2 = (n+2)\lambda_3 \qquad (4.19)$$

which yield

$$n = \lambda_2(\lambda_1 - \lambda_2) \qquad (4.20)$$

Next consider the displacement of the fringe formed at λ_1, this shifted part has the same order n , but has interference corresponding to a wavelength $\lambda_1 - \Delta\lambda_1$ caused by interference in the gap h_2 ,i.e.,

$$2h_2 = n(\lambda_1 - \Delta\lambda_1) \qquad (4.21)$$

Substracting this equation from equation (4.18) we obtain :

$$2h_1 - 2h_2 = n\Delta\lambda_1 \qquad (4.22)$$

thus the film thickness is

$$d_1 = h_1 - h_2$$

$$= n\Delta\lambda_1/2 \qquad (4.23)$$

4.6.2 The Electrical Method

According to Matthiessen's rule (equation (2.15)), the total resistance of a bulk specimen is :

$$\rho_B = \rho_o + \rho_1(T) \qquad (4.24)$$

and of a film is :

$$\rho_F = \rho_o + \rho_1(T) + \rho_{bou.} \qquad (4.25)$$

Differentiating these two equations with respect to temperature,T, yields :

$$\rho_B/dT = \rho_F/dT \qquad \text{if } \rho_o + \rho_{bou.} \leq \rho_1(T) \qquad (4.26)$$

To determine the film thickness, consider the relationship below :

$$R = \rho_F \frac{\text{film length}}{\text{width} \cdot \text{thickness}} \qquad (4.27a)$$

where R is the resistance of the film. Differentiating the equation (4.26) above with respect to T, we obtain :

$$dR/dT = d\rho_B/dT \cdot \frac{\text{film length}}{\text{width} \cdot \text{thickness}} \qquad (4.27b)$$

since $\rho_B/dT = \rho_F/dT$ and is constant for a particular material. The film thickness can be estimated from measured value of dR/dT if the width and the length of the film are known and provided that Matthiessen's rule holds for that thickness, i.e., the boundary effect is small.

4.6.3 The Quartz Crystal Thickness Monitor Method

During the deposition of thin films it is usually necessary to measure their thickness or to detect small mass changes and it is often preferable to do this whilst the film is growing rather than outside the vacuum system after the deposition. A convenient method is to use a thickness monitor of the ' AT ' cut oscillating quartz crystal type. Details of the thickness monitor has been described by Lawson(1967).

In the present work, a Film Thickness Monitor, model 1 , supplied by Edwards High Vacuum Ltd. was used for this purpose. The complete unit consisted of a 6.0 MHz monitor crystal and a 6.5 MHz reference crystal, both were AT cut quartz crystals, a power supply and an oscillator unit.

The relationship between the thickness of a quartz crystal of an AT cut and its resonance frequency has been derived by Mason (1956) to be:

$$f = 1.67 \times 10^3/t \qquad (4.28)$$

where f is frequency in Hz and t is the thickness of the crystal in Angstroms.

To calibrate the monitor crystal, an absolute optical

method, such as interferometry, is required. This calibration should be carried out for each :

a) monitor crystal

b) change in monitor crystal or substrate distance relative to the evaporant

c) change in monitor crystal position relative to the substrate.

According to the above conditions, the crystal would have to be calibrated for precision monitoring of the film thickness. Only the approximate thickness of niobium films was required during deposition . The more precise thickness of Nb_3Sn films could be observed outside by other means. Therefore an estimation of film thickness of niobium deposited on to the monitor, $\Delta t(\mathring{A})$, was obtained from the equation :

$$\Delta f = \Delta t \cdot p \qquad (4.29)$$

where p in this case is the bulk density in gm/cm^3 and Δf is the frequency shift of the monitor in Hz.

To prepared a set of films, the following procedure was used :

Let d_1 be the required thickness of niobium films. Suppose the distance between the quartz crystal and the evaporation source is r_q and that of substrate and the source is r_s. Then the film thickness of the niobium layer deposited on to the crystal is related to the thickness of the films on the substrates by :

$$\Delta t = d_1(r_s/r_q)^2 \qquad (4.30)$$

Substituting equation (4.30) into equation (4.29), yields,

$$\Delta f = p \cdot d_1 (r_s/r_q)^2 \qquad (4.31)$$

Therefore by observing the predetermined frequency shift, Δf, the film of thickness d_1 , could be obtained. The bulk densities of niobium and tin utilized in the preliminary determinations were 8.57 and 7.28 gm/cm^3, respectively.

4.7 Film Oxidation

In general the resistivity ratio of a film decreases with decreasing thickness and the residual resistivity increases for thin films. Two possibilities exist for changing resistivity ratio:

1) prepare films of different thickness

2) reduce the thickness of a film in stages

Since the oxides of metals are nonconducting electrically, one method of reducing the effective thickness of a metal film is to grow an oxide layer which uses up some of the metal of the film. The advantage of this method to investigate changes of resistivity with thickness is that the sample condition should be the same and any observed differences are real and can be attributed only to variation in thickness.

Originally film thickness reduction by this technique was considered as a possible means of establishing the correlation between the resistivity ratio and T_c of a film having identical preparation conditions. Later it was found applicable for the ellipsometric experiments as well since an oxide layer could be grown faster at higher temperatures.

Film oxidation was performed by heating samples in the atmostphere for a period of 10-60 minutes, using a laboratory oven.

The temperature of the oven was initially set at 100°C and was gradually raised up to 250°C after a series of oxidations because of the declining rate of the oxide growth with time at a given temperature. The film thickness reduction was monitored via the resistance increase (typically 5 to 20 % increase in each run) from the previous value before oxidation. The ellipsometric and resistivity measurements were carried out after each oxidation.

4.8 Low Temperature Measurements

The electrical properties of films were investigated by means of the cryostats previously described. The resistance of a set of four films could be simultaneously measured over the temperature range 1.5°K to 300°K, using liquid nitrogen and liquid helium.

The sample holder cryostat was first evacuated and then helium exchange gas was admitted. Readings were taken at 10 minute intervals while the cryostat was being cooled down gradually from room temperature to below 100°K, using liquid nitrogen. The equilibrium would reach in about 6-8 hours and then liquid helium was introduced into the helium cryostat by means of a liquid helium syphon. A rotary pump was used to obtain temperatures below the normal boiling point of the liquid helium. The temperature of the samples could be raised above 4.2°K by means of a heater coil provided but the sample holder cryostat had to be evacuated first.

The normal resistive properties of a film was determined by passing a constant current through the electrical contacts A and B , as shown in Fig.(3.8) and observing the potential

difference across the sample at C and D, and E and F. The resistivity could then be determined from the film configuration given in Fig.(3.8) when the film thickness was known. Current densities of the order of 10 to 100 Amp./cm^2 were used (e.g. about 100 microamp. for a film of 100 nm thick).

The critical temperature was roughly observed while the film was being cooled down to 4.2^{o}K or below. Then the temperature of the film was raised up slowly by means of the heater coil provided so that a more precise transition temperature of the film would be observed. The critical currents of some Nb_3Sn films were also determined at various temperatures above 4.2 ^{o}K , using D.C. currents.

****

CHAPTER 5 : EXPERIMENTAL RESULTS

The experimental results of over eighty samples prepared during this programme of work are presented in this chapter. These results have been divided into three parts ; the first part , sections (5.1) and (5.2),deal with the preparation conditions and x-ray data respectively, section (5.3) contains results from resistivity measurements in the temperature range 2 to 300 ^{o}K and finally section (5.4) gives results of the ellipsometric measurements.

5.1 Preparation Conditions

All of the films were deposited on clear fused quartz substrates and were cleaned prior to mounting on to the substrate holder by the method of cleaning described in section (4.1). Substrate temperatures were kept at about 200 ± 100 ^{o}C during the deposition of niobium films (except films prepared by codeposition) with a deposition rate of about 20 nm/min. and were varied between 400-900^{o}C during the diffusion and alloying processes. The summary of the deposition conditions are shown in Table (5.1).

5.2 X-ray Diffraction Results

There are three compounds existing in the niobium-tin system, namely; Nb_3Sn , Nb_6Sn_5 and $NbSn_2$. In the present work these compounds were identified according to their A.S.T.M. index cards, as listed in Appendix B. Single phase of Nb_3Sn was observed

for films alloyed at temperatures above 650 ± 100°C. Below this temperature, mixed phases of Nb_6Sn_5 and $NbSn_2$ were observed.

X-ray diffraction revealed that the Nb_3Sn films prepared in the present investigation had a crystal structure of β-tungsten (A-15) type with lattice parameter, a_o, ranging from 5.28-5.29 Angstroms. X-ray diffraction data of a film of Nb_3Sn are shown in Table (5.2). NbO was observed in some of Nb_3Sn films in the proportion of as high as 40 at %. The x-ray diffraction results of these films have been shown in Table (5.3) and Plates (5.1)-(5.2).

Films alloyed at temperatures below 650°C contained mixed phases of Nb_6Sn_5 and $NbSn_2$. Their x-ray diffraction results are shown in Table (5.4) with their possible (hkl)'s. The lattice parameters; a, b and c were calculated from the relations (Lipson and Steeple, 1970) below :

$$\lambda = 2d_{hkl} \sin\theta_{hkl} \qquad (5.1)$$

and

$$\sin^2\theta_{hkl} = (\lambda^2/4)(h^2/a^2 + k^2/b^2 + l^2/c^2) \qquad (5.2)$$

where λ is the wavelength of the x-ray radiation and d_{hkl} and θ_{hkl} are the d-spacing and diffracting angle corresponded to the indices (hkl).

Table 5.1 Preparation Conditions.

A) Evaporation of Niobium

Sample Set No.	Base Pressure (torr)	Evaporation Pressure(torr)	Substrate Temperature(°C)	Remark
1	3×10^{-9}	3×10^{-8}	200 ± 50	
2	3×10^{-9}	3×10^{-7}	300 ± 100	Codeposition
3	2.5×10^{-9}	2×10^{-7}	750 ± 100	Codeposition
4	4×10^{-9}	4×10^{-8}	200 ± 50	Niobium only
5	4×10^{-9}	3×10^{-7}	850 ± 100	Codeposition
6	5×10^{-9}	5×10^{-8}	250 ± 50	
7	4×10^{-9}	5×10^{-8}	200 ± 50	
8	4×10^{-9}	4×10^{-8}	200 ± 50	
9	3×10^{-9}	3×10^{-8}	200 ± 50	
10	3×10^{-9}	4×10^{-8}	200 ± 50	
11	2×10^{-9}	4×10^{-8}	200 ± 50	
12	2×10^{-9}	3×10^{-8}	200 ± 50	
13	4×10^{-9}	5×10^{-8}	200 ± 50	
14	4×10^{-9}	6×10^{-8}	200 ± 50	
15	4×10^{-9}	3×10^{-8}	200 ± 50	
16	2×10^{-9}	3×10^{-8}	200 ± 50	

Table 5.1 Preparation conditions (continued.)

B) Evaporation of Tin and Alloying

Sample Set No.	Base Pressure (torr)	Evaporation Pressure (torr)	Diffusion		Alloying	
			Temperature (°C)	Time (hr)	Temperature (°C)	Time (hr)
1	2×10^{-9}	2×10^{-7}	450 ± 100	12	750 ± 100	4
2	3×10^{-9}	← Codeposition →				
3	1.5×10^{-9}	← Codeposition →				
4	2×10^{-9}	← Niobium only →				
5	2×10^{-9}	← Codeposition →				
6	3×10^{-9}	3×10^{-7}	400 ± 100	16	800 ± 100	8
7	3×10^{-9}	5×10^{-7}	450 ± 100	14	700 ± 100	20
8	2×10^{-9}	3×10^{-7}	450 ± 100	40	600 ± 100	24
9	2×10^{-9}	3×10^{-7}	400 ± 100	20	700 ± 100	18
10	1.5×10^{-9}	4×10^{-7}	450 ± 100	20	800 ± 100	8
11	1.5×10^{-9}	5×10^{-7}	450 ± 100	24	800 ± 100	20
12	2×10^{-9}	1×10^{-7}	450 ± 100	24	700 ± 100	12
13	3×10^{-9}	1×10^{-7}	450 ± 100	20	850 ± 100	8
14	3×10^{-9}	1×10^{-7}	450 ± 100	20	800 ± 100	10
15	3×10^{-9}	2×10^{-7}	450 ± 100	20	900 ± 100	4
16	1.5×10^{-9}	3×10^{-7}	450 ± 100	20	850 ± 100	6

Table 5.2 X-ray diffraction data of a film of Nb_3Sn.

$d_{obs.}$ (Å)	$d_{cal.}$ (Å)	Indices(hkl)	$I/I^*_{max.}$
3.73	3.74	1 1 0	1
2.64	2.64	2 0 0	100
2.36	2.36	2 1 0	80
2.16	2.16	2 1 1	15
1.32	1.32	4 0 0	6
1.20	1.25	4 2 0	11
Lattice constant, a_o = 5.29 ± 0.01 Å .			

$I/I^*_{max.}$ = ratio of observed intensities.

Table 5.3 X-ray diffraction data of Nb_3Sn films with the present of NbO.

Sample No.	$d_{obs.}$ (Å)	(hkl)	$I/I_{max.}$	Remark
112	4.23	100	4	NbO
	2.65	200	100	Nb_3Sn
	2.44	111	8	NbO
	2.37	210	50	Nb_3Sn
	2.16	211	3	Nb_3Sn
	2.11	200	10	NbO
	1.32	400	8	Nb_3Sn
	$a_o(Nb_3Sn) = 5.29 \pm 0.01$ Å.			
114	4.21	100	50	NbO
	2.64	200	100	Nb_3Sn
	2.43	111	41	NbO
	2.36	210	77	Nb_3Sn
	2.15	211	10	Nb_3Sn
	2.11	200	41	NbO
	1.32	400	15	Nb_3Sn
	1.18	420	15	Nb_3Sn
	a_o $(Nb_3Sn) = 5.28 \pm 0.01$ Å.			

Table 5.4 Observed x-ray data of Nb_6Sn_5 and $NbSn_2$ (mixed phases) and their possible indices's.

Sample No.	$d_{obs.}$ (Å)	(hkl) (Nb_6Sn_5)	(hkl) ($NbSn_2$)	$I/I_{max.}$
82	3.01	031,123	511	14
	2.81	—	113	42
	2.70	—	220	5
	2.67	—	602	65
	2.59	—	313	45
	2.45	125	—	2
	2.38	—	800,711	80
	2.34	017,204	—	100
	2.31	222	—	72
	2.18	042	422	38
		a = 5.59 Å b = 9.10 Å c = 16.62 Å	a = 19.08 Å b = 5.63 Å c = 9.83 Å	
83	3.00	031,123	—	5
	2.81	—	113	11
	2.59	—	313	2
	2.42	116	—	3
	2.39	—	800,711	50
	2.34	017,204	—	100
	2.31	222	—	42
	2.27	134,035	—	10

Table 5.4 (continued)

Sample No.	$d_{obs.}$ (Å)	(hkl) (Nb_6Sn_5)	(hkl) ($NbSn_2$)	$I/I_{max.}$
83	2.02	141,215	—	68
	1.43	—	11.1.3	35
		a = 5.67 Å	a = 19.01 Å	
		b = 9.23 Å	b = 5.61 Å	
		c = 16.85 Å	c = 9.80 Å	

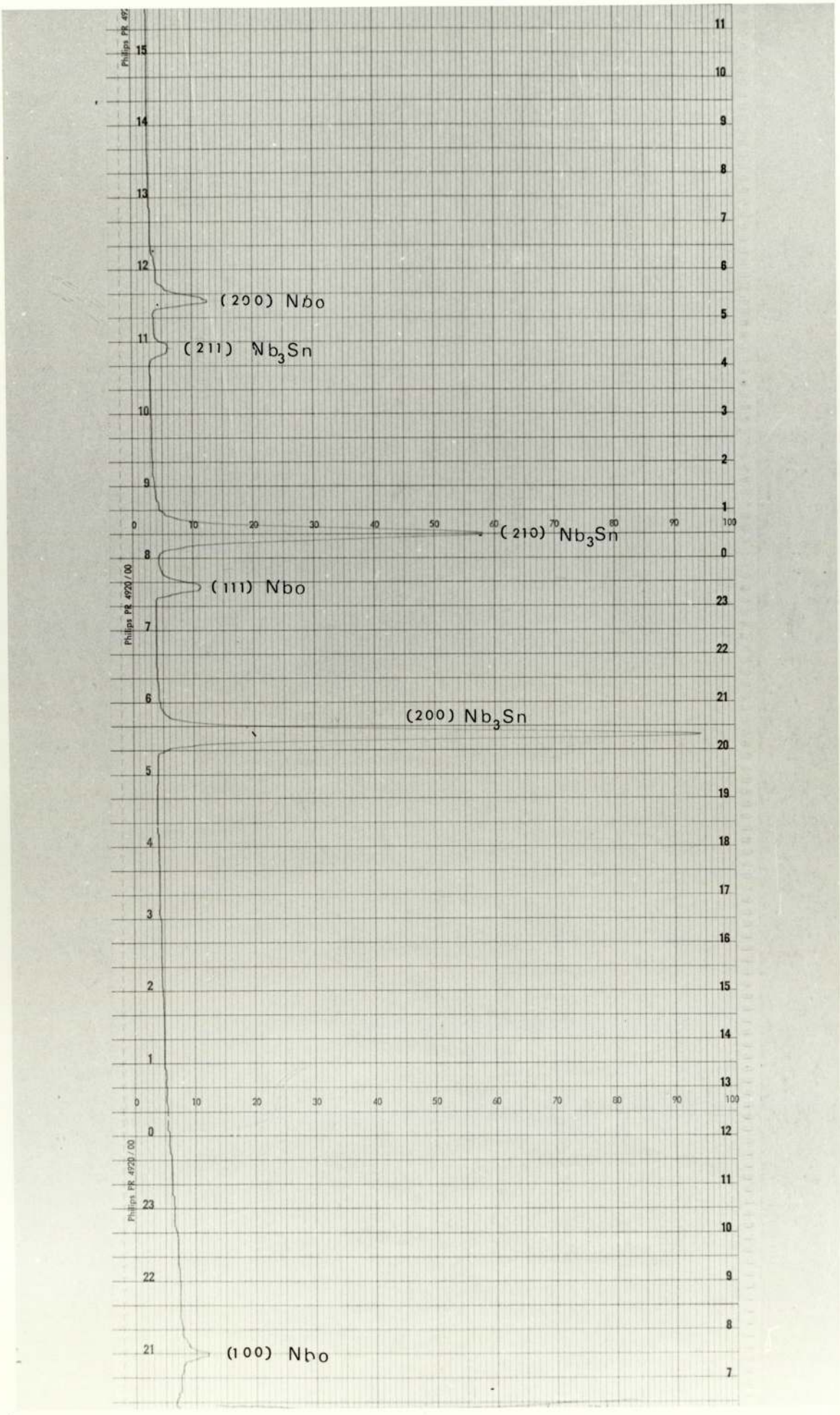

PLATE 5.1 X-RAY DIFFRACTION PATTERN OF Nb_3Sn No. 112

PLATE 5.1 CONTINUED

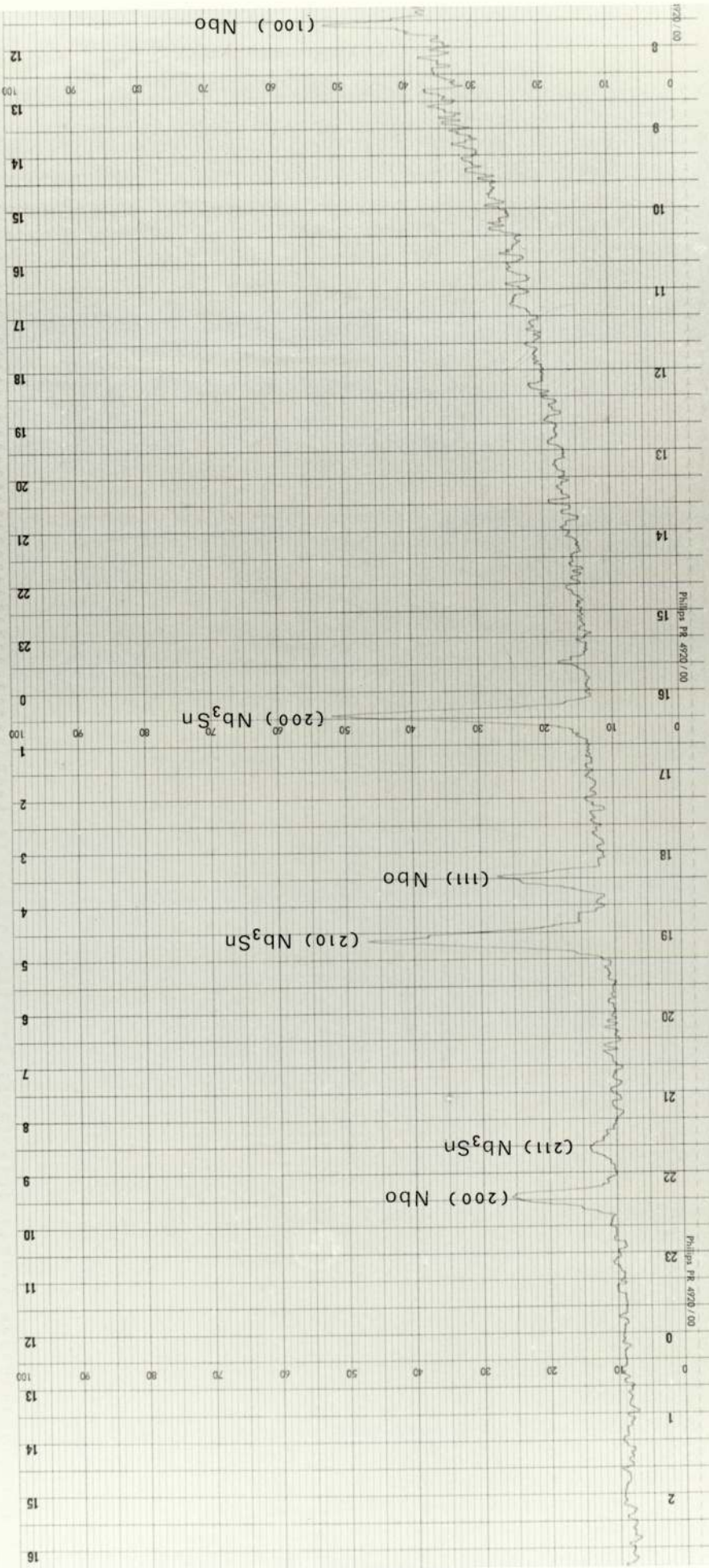

PLATE 5.2 X-RAY DIFFRACTION PATTERN OF Nb_3Sn FILM No.114

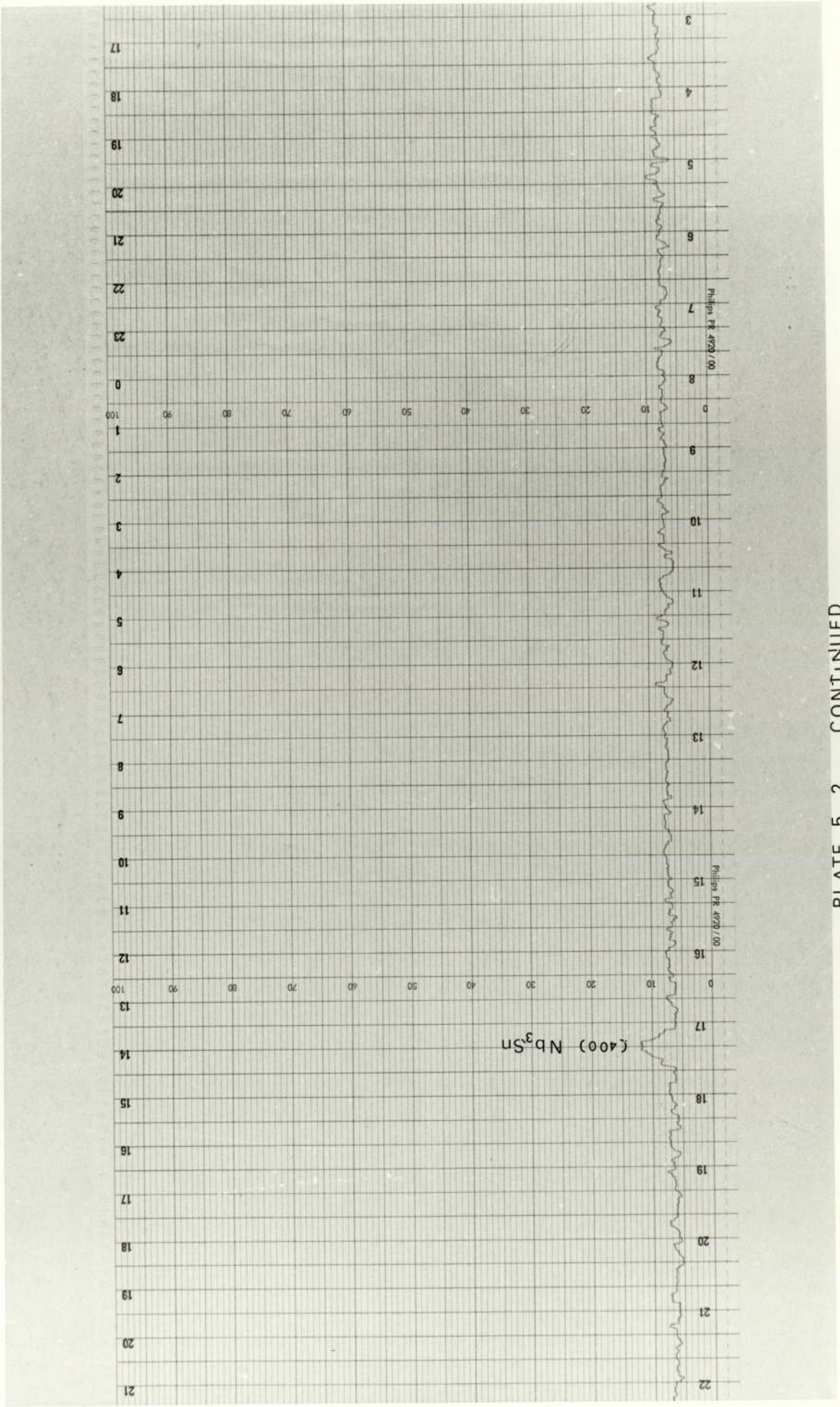

PLATE 5.2 CONTINUED

5.3 Resistive Measurements

The normal and superconducting properties of the (electrically) continuous films were observed by means of resistive measurements, using the four point probe technique, as described in section (3.7.3). The resistance at a given temperature of a film was the average, evaluated from the potential difference, measured on both sides of the film (see Fig (3.8)). The residual resistivities of samples ($\rho_{res.}$) were taken from the horizontal part of resistivity-temperature curves near the critical temperatures, i.e., at 20°K , 10°K and 4.2°K , for Nb_3Sn films, niobium films and Nb_6Sn_5 and $NbSn_2$ (mixed phases) films, respectively. Some films exhibited irreversible temperature-dependent resistance due to thermal cycling, Fig.(5.1) , while most of the specimens were reversible, Fig. (5.2). Transition temperatures of samples were defined as 0.9 of the residue resistivity of samples.

It was possible to observe the film thickness dependence of the transition temperature by oxidation. A set of niobium and Nb_3Sn films were chosen for this purpose. The results are presented in Tables (5.6) and (5.7), and Figures (5.15)-(5.18). More details of discussion and comparision with the depression of T_c by other methods , reported by several workers, are presented in section (6.3) In the recent years, there has been considerable interest shown in film resistivity ratio, $\rho_{300}/\rho_{res.}$ and the variation of this parameter with respect to T_c . Fig. (5.11) shows this correlation for Nb_3Sn films of various thicknesses. Contrast to this, Figures (5.19)-(5.23) illustrate the correlation observed in a set of oxidized films of niobium and Nb_3Sn , taken from a series of

measurements on each specimen. Electron mean free paths were determined, Table (5.8) , from the change of resistivity due to oxidation of film No.12 in which the Nb_3Sn layer was deduced from the corresponding ellipsometric measurements, Table (5.12).

The critical currents of some Nb_3Sn films were determined in the zero magnetic field by means of D.C. currents. The results obtained from these measurements are illustrated in Figures (5.25) and (5.26).

Table 5.5 Results from electrical measurements of film samples in the temperature range of 300°K to liquid helium temperatures.

A) Normal state

Sample No.	ρ/d (300°K) Ω	ρ/d (250°K) Ω	ρ/d (200°K) Ω	ρ/d (150°K) Ω	ρ/d (100°K) Ω	ρ/d (50°K) Ω	ρ/d (res.) Ω
6	3.04	2.62	2.32	1.97	1.58	1.24	1.09
11	14.68	13.97	12.65	10.33	8.43	6.01	4.57
12	12.86	11.99	10.80	9.47	7.89	5.43	3.95
13	13.61	12.85	12.00	10.68	8.92	5.60	3.74
14	22.46	19.79	17.56	15.33	12.67	10.67	10.35
15	7.93	7.07	6.12	5.16	4.14	3.20	2.95
16	16.20	14.72	14.03	12.65	10.53	7.15	5.23
33	47.95	51.20	53.87	51.15	50.27	39.33	24.59
42	1.05	0.92	0.81	0.67	0.52	0.37	0.32
44	0.89	0.75	0.65	0.55	0.41	0.30	0.28
57	2.22	2.02	1.95	1.84	1.69	1.52	1.50
62	3.68	3.45	3.11	2.70	2.25	1.65	1.22
63	69.33	82.4	81.18	79.33	76.80	74.66	63.87
82	2.34	2.19	2.04	1.78	1.42	0.79	0.30
83	5.65	5.51	5.43	5.12	4.37	2.89	1.56
84	2.32	2.11	1.92	1.70	1.32	0.80	0.34
93	5.17	6.11	6.64	6.93	6.77	5.23	2.45

Table 5.5 (Continued.)

Sample No.	ρ/d (300°K) Ω	ρ/d (250°K) Ω	ρ/d (200°K) Ω	ρ/d (150°K) Ω	ρ/d (100°K) Ω	ρ/d (50°K) Ω	ρ/d (res.) Ω
101	8.04	7.93	7.73	7.27	6.53	5.45	5.14
102	1.99	1.86	1.71	1.53	1.34	1.18	1.14
103	4.40	4.16	3.89	3.65	3.34	3.07	2.99
104	20.70	20.42	20.04	19.22	17.95	16.63	15.95
111	15.01	14.16	13.61	12.80	11.52	9.82	9.45
112	3.00	2.65	2.28	1.86	1.41	0.91	0.68
113	2.35	2.06	1.71	1.36	1.02	0.70	0.66
114	4.09	3.59	3.07	2.51	1.92	1.32	1.11
133	2.34	2.08	1.81	1.45	1.12	0.82	0.62
134	1.93	1.80	1.56	1.33	1.10	0.88	0.83
141	2.09	1.92	1.60	1.33	0.97	0.71	0.61
142	1.83	1.59	1.34	1.33	0.80	0.56	0.51
143	2.55	2.31	2.02	1.68	1.27	0.77	0.55
151	11.07	10.54	9.85	8.63	7.55	5.35	3.96
152	2.57	2.24	1.91	1.56	1.19	0.89	0.79
153	7.23	6.96	6.58	6.00	5.55	3.57	2.67
161	33.09	31.53	28.80	28.50	19.92	11.69	7.82
162	70.69	74.27	73.20	69.90	62.45	49.14	39.36

Table 5.5 (Continued.)

B) Superconducting state

Sample No.	Film Thickness (nm)	ρ_{300} μΩ-cm	$\rho_{res.}$ μΩ-cm	$\rho_{300}/\rho_{res.}$	T_c (^oK)	Remark
6	187	56.85	20.40	2.79	16.1	
11	55.6	81.62	25.43	3.21	16.7	
12	58.2	74.82	22.99	3.27	16.3	
13	56.6	77.04	21.17	3.64	17.4	
14	57.1	128.25	59.09	2.17	—	
15	68.9	54.62	20.32	2.69	15.4	
16	55.0	89.10	28.75	3.09	16.9	
33	32.0	153.43	78.68	1.95	15.3	
42	166.5	17.40	5.33	3.27	8.8	Niobium Film
44	188	16.79	5.32	3.16	8.7	" "
57	–	–	–	1.48	–	
62	–	–	–	3.02	14.5	
63	–	–	–	1.09	16.6	
82	372	87.05	11.16	7.80	2.8	Nb_6Sn_5, $NbSn_2$
83	320	180.74	49.82	3.63	2.6	" "
84	361	83.77	12.16	6.88	2.8	" "
93	35	18.11	8.56	2.11	–	

Table 5.5 (Continued.)

Sample No.	Film Thickness (nm)	ρ_{300} μΩ-cm	$\rho_{res.}$ μΩ-cm	$\rho_{300}/\rho_{res.}$	T_c (^oK)	Remark
101	–	–	–	1.57	12.5	
102	–	–	–	1.75	10.8	
103	187	82.27	55.86	1.49	13.9	
104	–	–	–	1.30	13.5	
111	488	73.20	46.11	1.59	12.2	
112	321	96.42	21.69	4.45	17.8	
113	510	119.68	33.83	3.54	16.5	
114	423	172.92	46.83	3.69	18.2	
133	170	39.85	10.56	3.78	18.1	
134	162	31.23	13.40	2.33	14.8	
141	116	24.30	7.03	3.45	17.4	
142	126	23.08	6.41	3.60	17.0	
143	159	40.61	8.74	4.64	17.2	
151	126	139.44	49.89	2.80	17.1	
152	148	38.12	11.67	3.27	15.8	
153	141	101.83	37.58	2.71	16.3	
161	37.5	124.10	29.34	4.23	18.2	
162	29.5	208.54	116.11	1.80	18.2	

Table 5.6 Electrical measurements of oxidized niobium films.

A) Normal state

Series of Oxidation	ρ/d (300°K) Ω	ρ/d (250°K) Ω	ρ/d (200°K) Ω	ρ/d (150°K) Ω	ρ/d (100°K) Ω	ρ/d (50°K) Ω	ρ/d (res.) Ω
Sample No. 42							
1st	1.06	0.92	0.80	0.67	0.52	0.39	0.32
2nd	1.21	1.07	0.98	0.88	0.73	0.57	0.51
3rd	1.33	1.22	1.12	0.99	0.83	0.70	0.64
4th	1.49	1.36	1.25	1.13	0.98	0.86	0.81
5th	1.80	1.68	1.57	1.45	1.30	1.19	1.10
Sample No. 44							
1st	0.89	0.75	0.65	0.55	0.43	0.29	0.28
2nd	0.97	0.86	0.78	0.66	0.54	0.42	0.40
3rd	1.11	0.99	0.89	0.79	0.66	0.56	0.51
4th	1.25	1.15	1.07	0.97	0.87	0.76	0.72
5th	1.43	1.34	1.26	1.16	1.04	0.95	0.90

Table 5.6 (Continued.)

B) Superconducting state

Sample No.	Series of Oxidation	$\rho_{300}/\rho_{res.}$	T_c (°K)
42	1st	3.31	8.8
	2nd	2.38	8.1
	3rd	2.08	7.5
	4th	1.84	7.2
	5th	1.64	6.7
44	1st	3.18	8.7
	2nd	2.42	8.3
	3rd	2.18	7.9
	4th	1.74	7.1
	5th	1.59	6.9

Table 5.7 Electrical measurements of oxidized films of Nb_3Sn.

A) Normal state

Sample No.12

Series of Oxidation	ρ/d (300°K) Ω	ρ/d (250°K) Ω	ρ/d (200°K) Ω	ρ/d (150°K) Ω	ρ/d (100°K) Ω	ρ/d (50°K) Ω	ρ/d (res.) Ω
1st	12.93	12.04	10.87	9.52	7.73	7.12	4.01
2nd	13.40	12.27	11.27	9.93	8.20	6.93	4.21
3rd	14.47	13.46	12.47	11.00	9.12	7.00	4.67
4th	14.93	13.81	12.75	11.33	9.47	7.33	4.94
5th	15.27	14.00	12.87	11.43	9.48	7.46	5.43
6th	16.02	14.73	13.60	12.00	10.07	8.00	6.18
7th	16.93	15.67	14.53	12.93	10.80	8.40	6.85
8th	17.73	16.45	15.20	13.46	11.40	9.20	7.24
9th	18.73	17.56	16.27	14.43	12.15	9.47	7.64
10th	22.00	20.67	19.20	17.00	14.27	11.73	9.61
11th	24.27	22.53	20.67	18.12	15.20	12.40	11.29
12th	28.00	26.20	24.30	22.00	18.90	15.81	13.48
13th	49.31	46.41	43.60	40.01	35.62	31.33	28.80
14th	56.22	52.81	49.62	45.63	40.93	37.11	34.50
15th	77.11	74.61	72.50	69.89	66.40	63.81	61.72

Table 5.7 (Continued.)

Sample No. 143

Series of Oxidation	ρ/d (300°K) Ω	ρ/d (250°K) Ω	ρ/d (200°K) Ω	ρ/d (150°K) Ω	ρ/d (100°K) Ω	ρ/d (50°K) Ω	ρ/d (res.) Ω
1st	2.92	2.63	2.35	1.96	1.47	0.96	0.64
2nd	3.19	2.90	2.58	2.16	1.64	1.11	0.72
3rd	3.45	3.12	2.81	2.36	1.80	1.20	0.82
4th	4.11	3.68	3.26	2.72	2.11	1.60	1.12
5th	5.88	5.28	4.72	4.00	3.20	2.43	1.88
6th	6.77	6.17	5.57	4.75	3.81	2.93	2.40

B) Superconducting state

Sample No.	Series of Oxidation	$\rho_{300}/\rho_{res.}$	T_c (°K)
143	1st	4.56	16.8
	2nd	4.46	16.8
	3rd	4.20	16.2
	4th	3.63	15.7
	5th	3.12	15.4
	6th	2.82	15.0

Table 5.7 (Continued.)

Sample No.	Series of Oxidation	Film* Thickness (nm)	$\rho_{300}/\rho_{res.}$	T_c (°K)
12	1st	58.1	3.22	16.3
	2nd	55.8	3.18	16.1
	3rd	52.5	3.10	16.2
	4th	50.0	3.02	16.1
	5th	49.2	2.81	16.1
	6th	47.5	2.59	16.0
	7th	44.5	2.47	15.9
	8th	42.4	2.45	15.8
	9th	40.0	2.45	15.9
	10th	34.0	2.29	15.8
	11th	31.2	2.15	15.6
	12th	27.0	2.08	15.5
	13th	15.7	1.71	14.9
	14th	13.5	1.63	12.8
	15th	10.5	1.25	-

* Estimated from ellipsometric measurements.

Table 5.8 Calculated (l_{cal}) and Observed ($l_{obs.}$) electrical mean free paths in Nb_3Sn - Film No.12.

Temperature (^oK)	l^*_{cal}(nm)	$l_{obs.}$(nm)
20	29.26	28.7
50	18.46	19.3
75	12.80	–
100	8.97	8.5
125	6.45	–
150	4.76	5.0
175	3.62	–
200	2.84	2.25
225	2.30	–
250	1.92	1.90
275	1.64	–
300	1.43	1.35

$$* \; l_{cal} = l_o - aT + be^{-(T/T_o)}$$

where l_o = 2.1 nm , a = 3.06 x 10^{-3} nm/^oK , b = 38 nm and T_o = 60^oK.

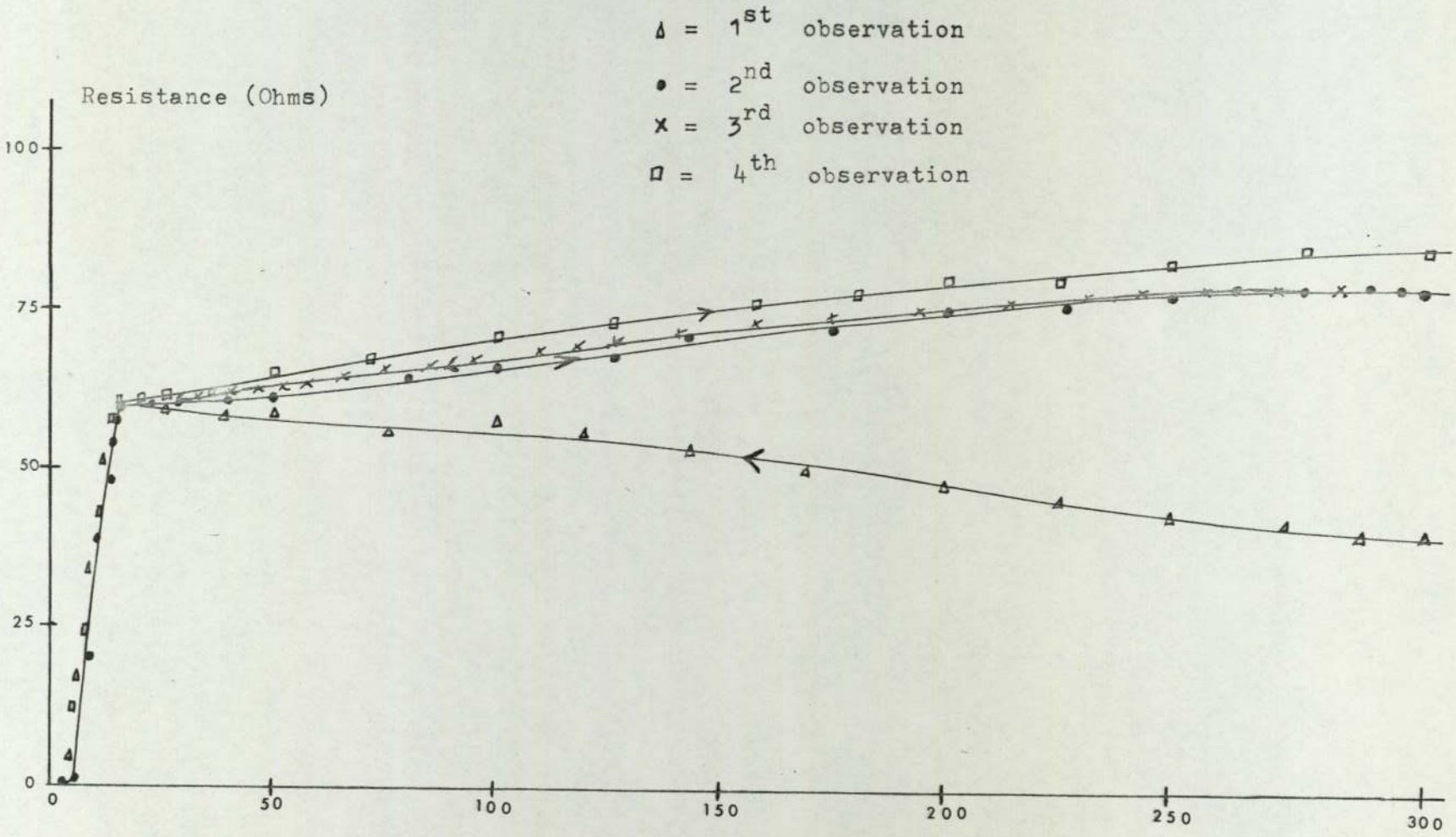

Figure 5.1 Irreversible temperature-dependence of the resistance due to thermal cycling.

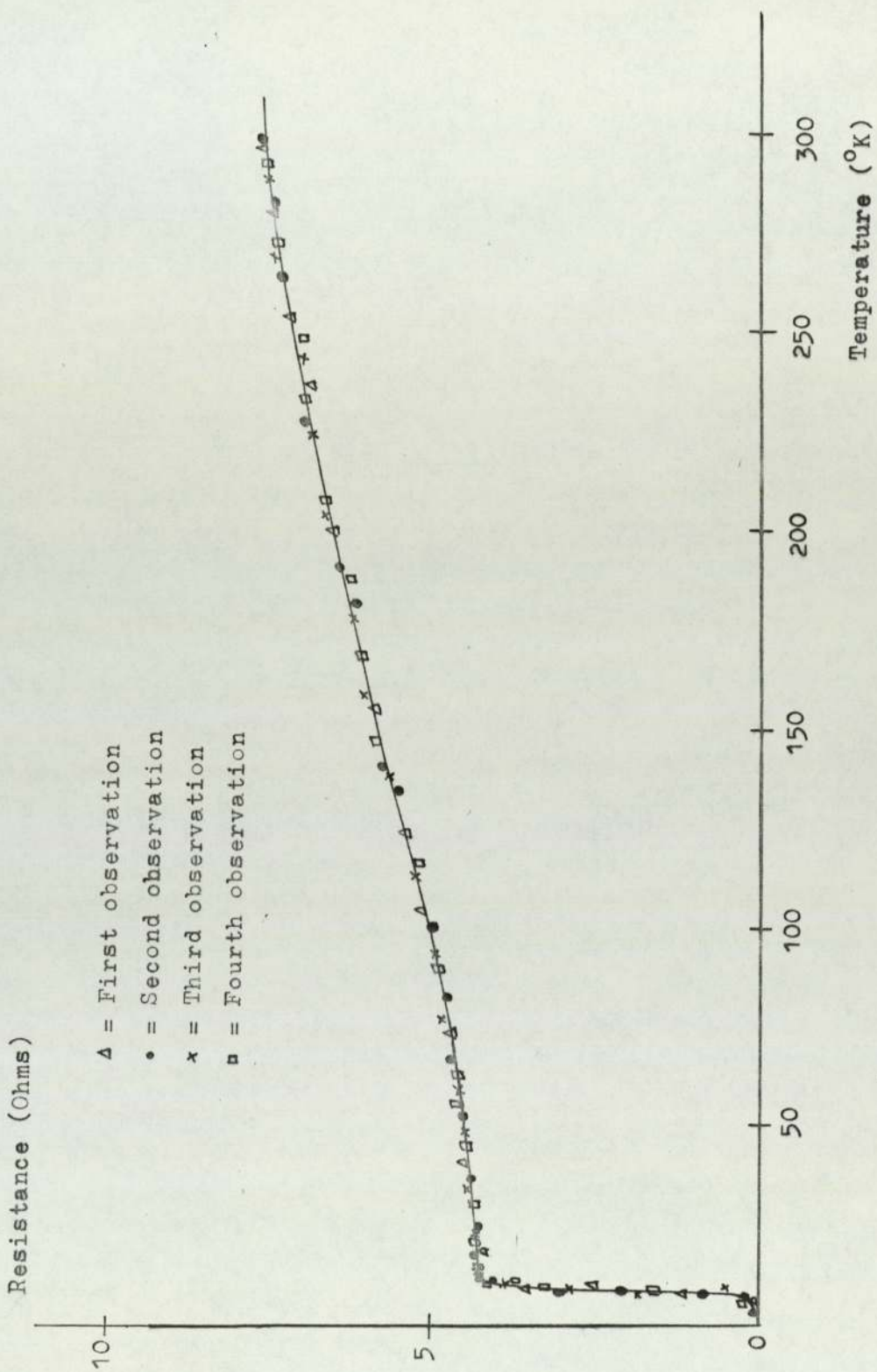

Figure 5.2 Thermal cycling of a stable film.

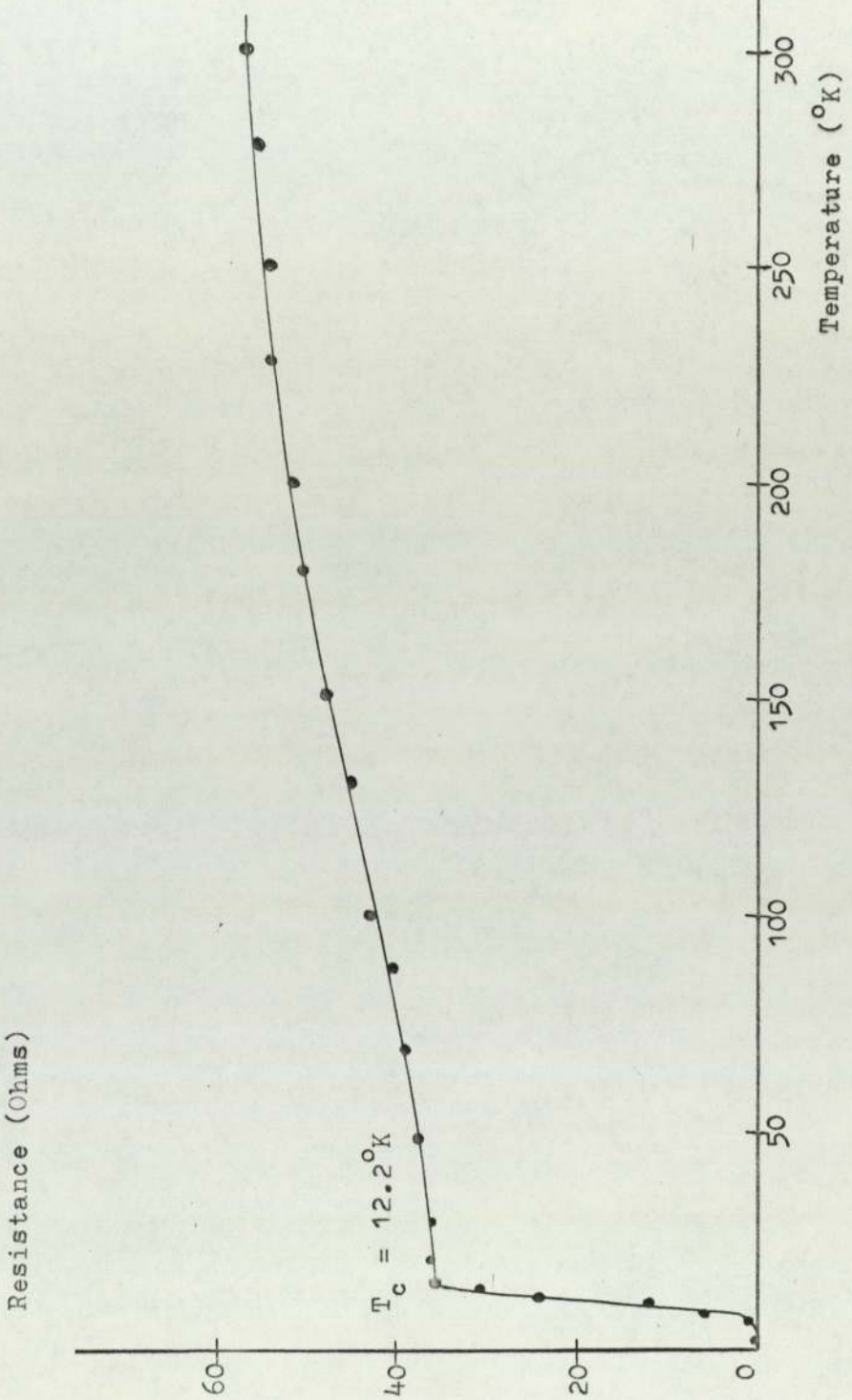

Figure 5.3 Resistive curve of film No.111.

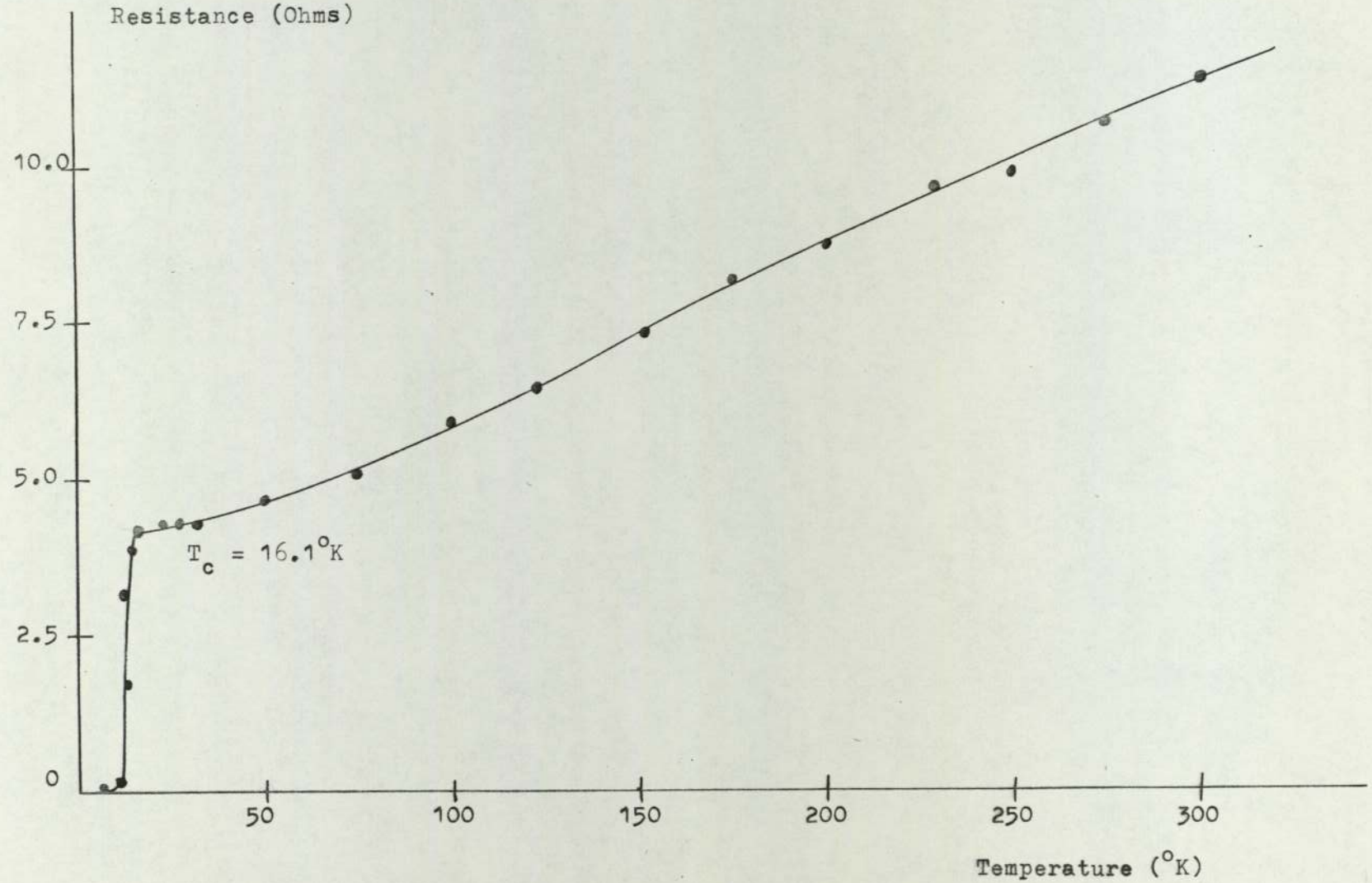

Figure 5.4 Resistive curve of film No.6.

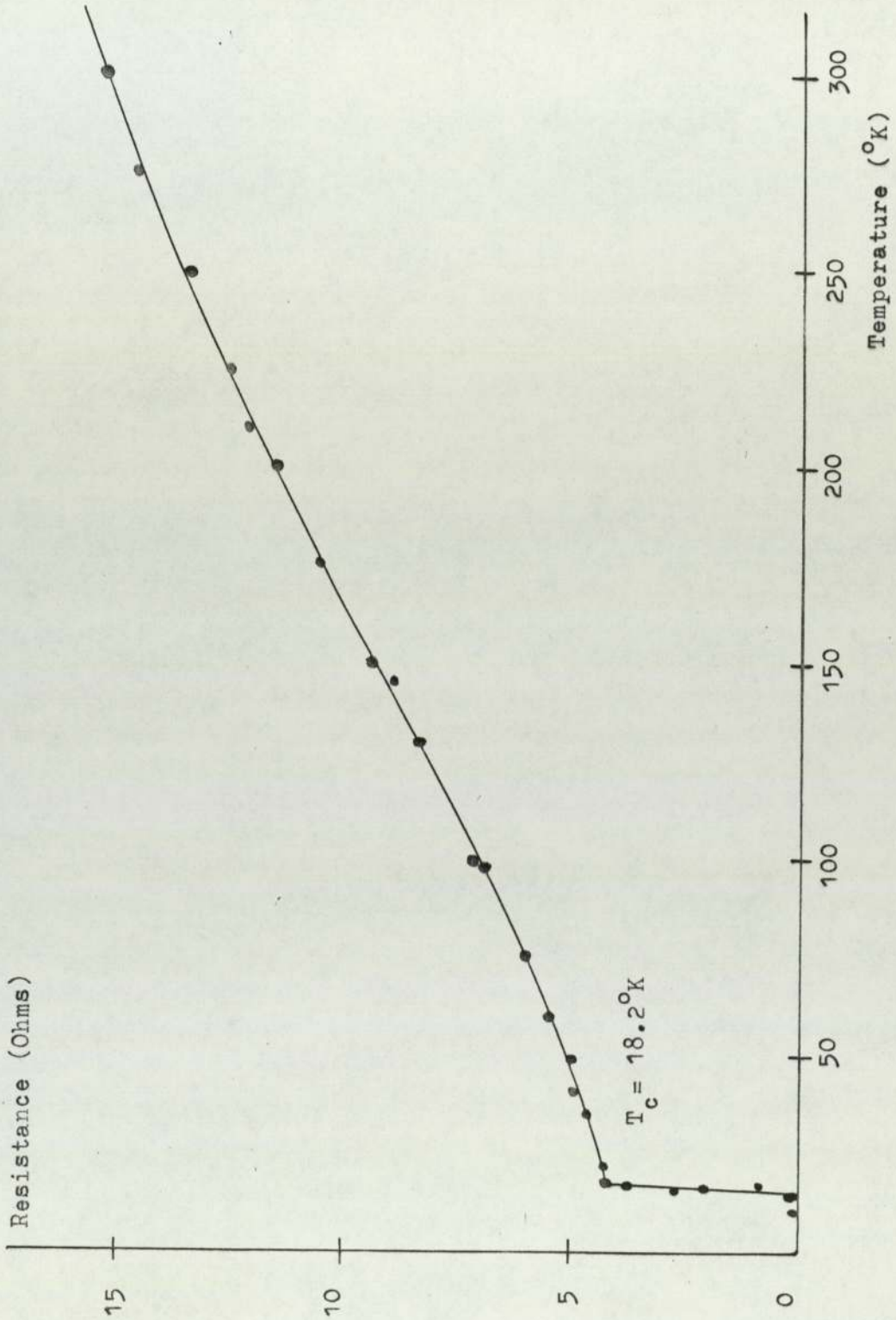

Figure 5.5 Resistive curve of film No.114.

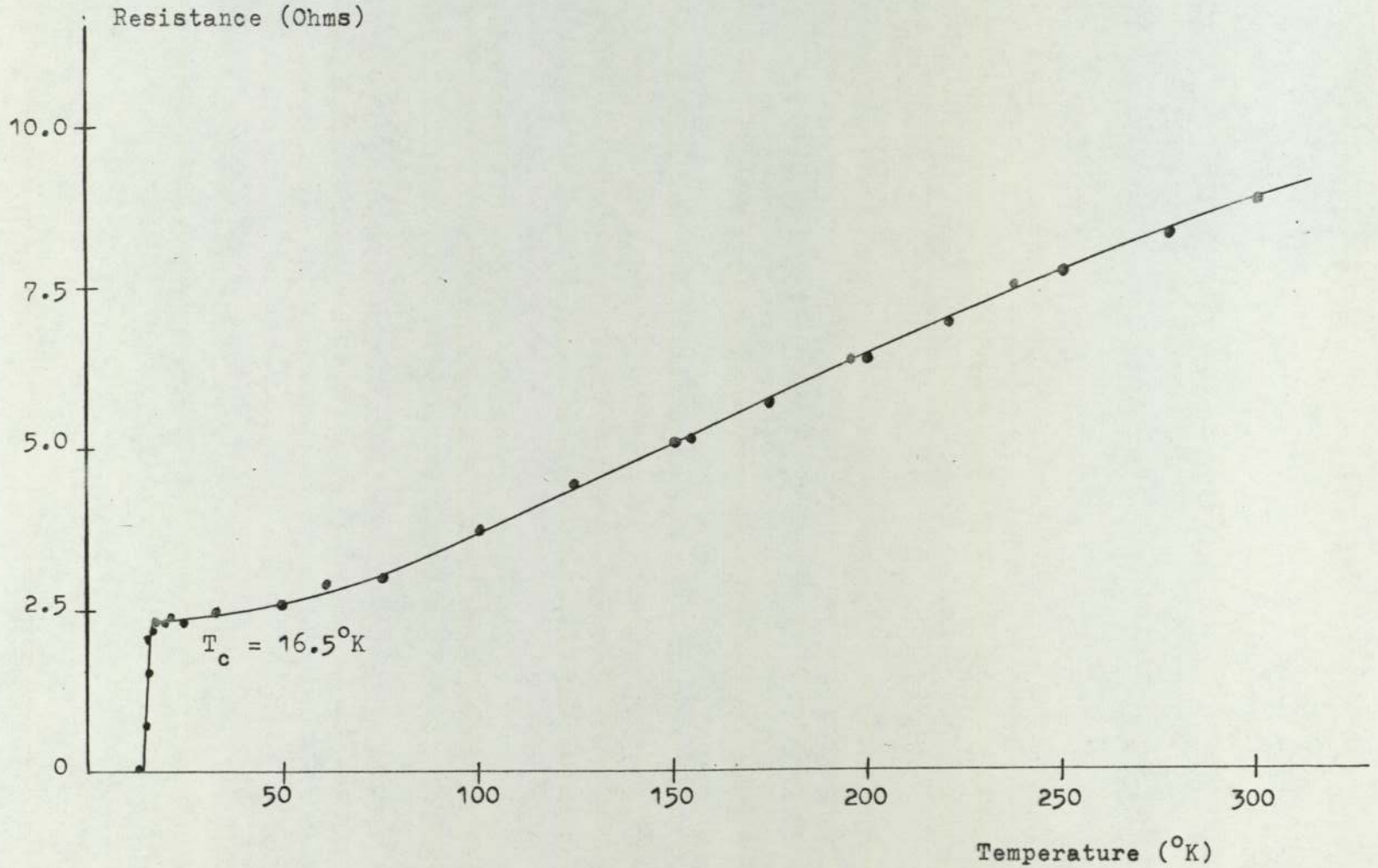

Figure 5.6 Resistive curve of film No.113.

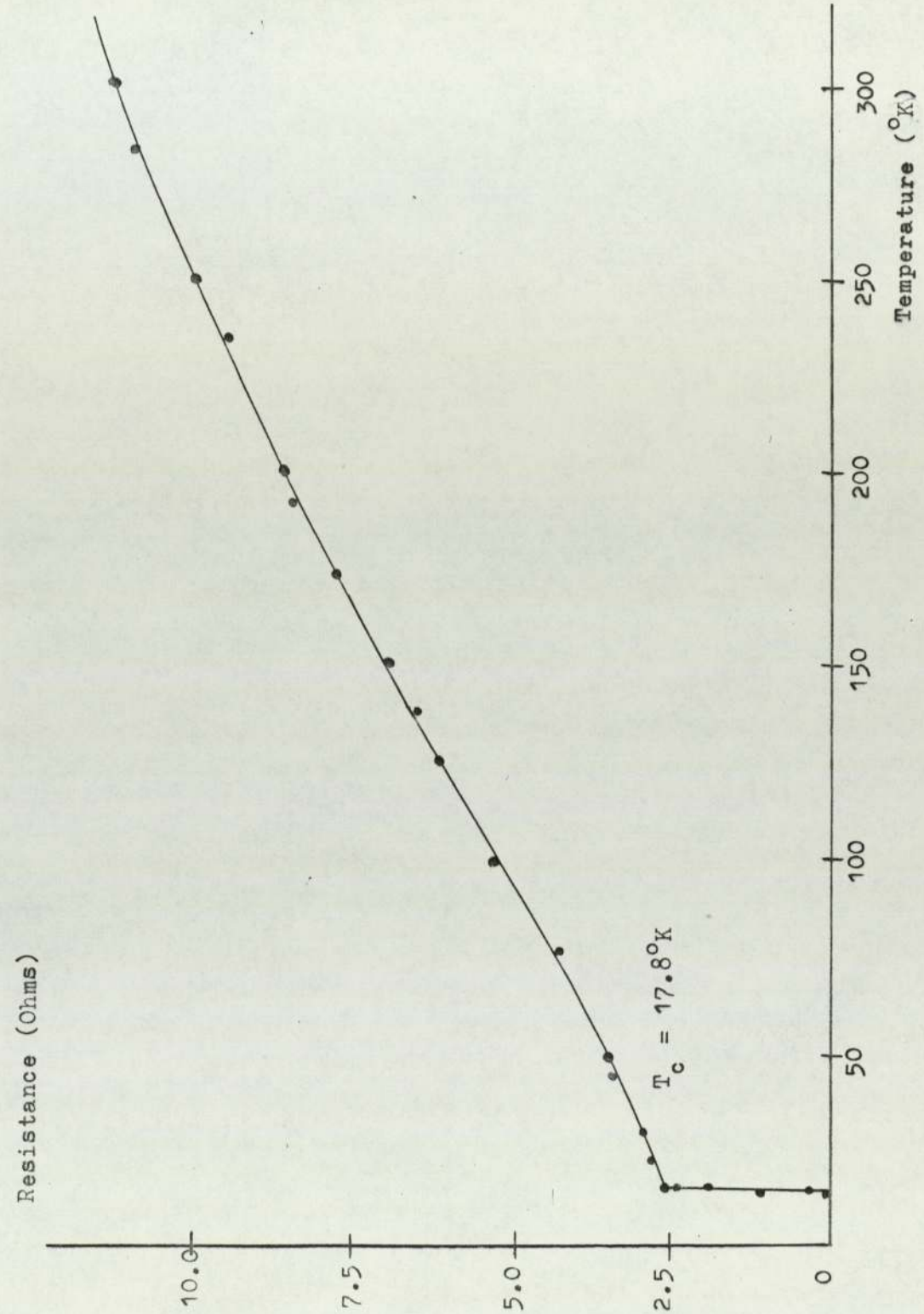

Figure 5.7 Resistive curve of film No.112.

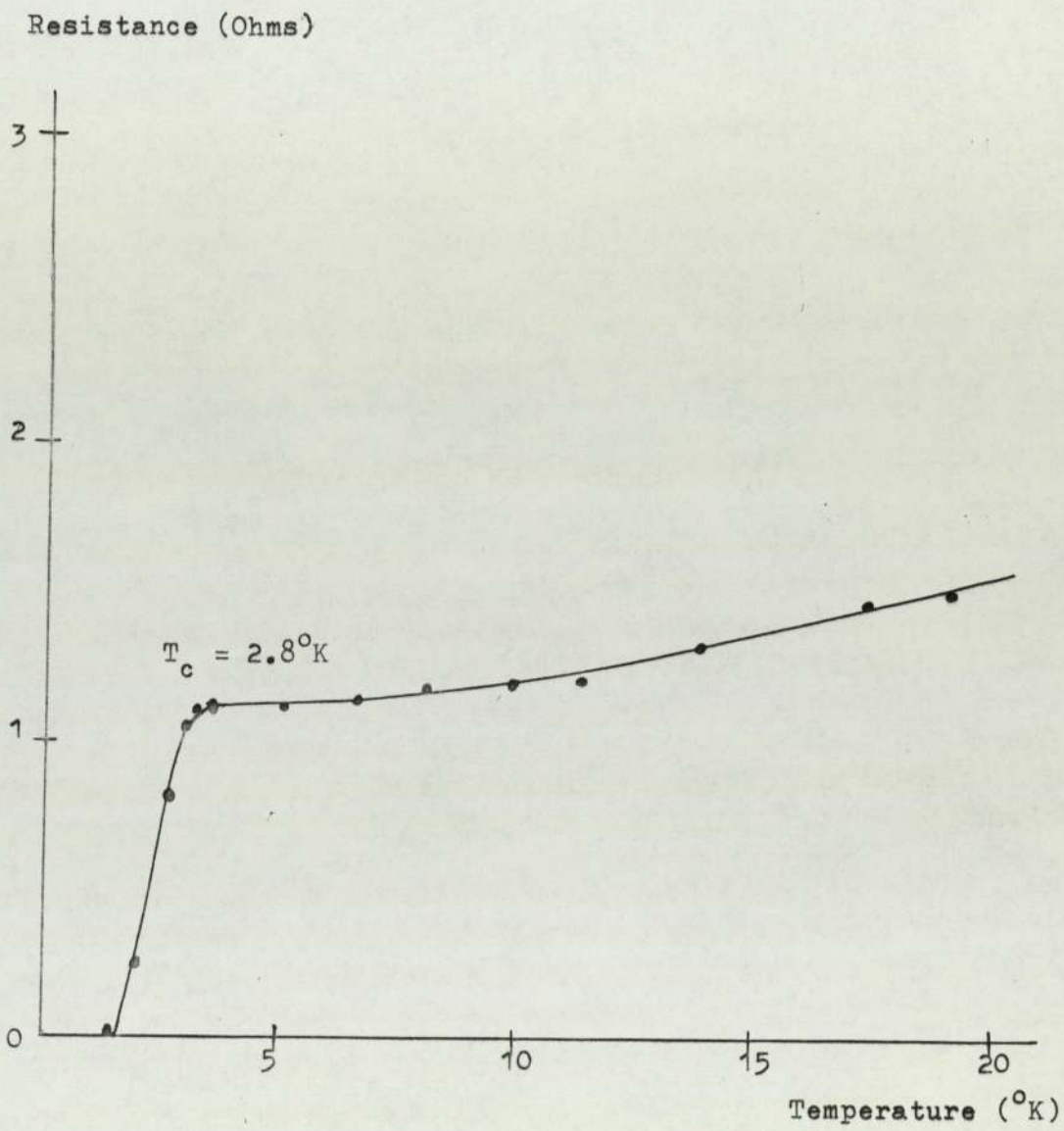

Figure 5.8 Transition curve of film No.82.

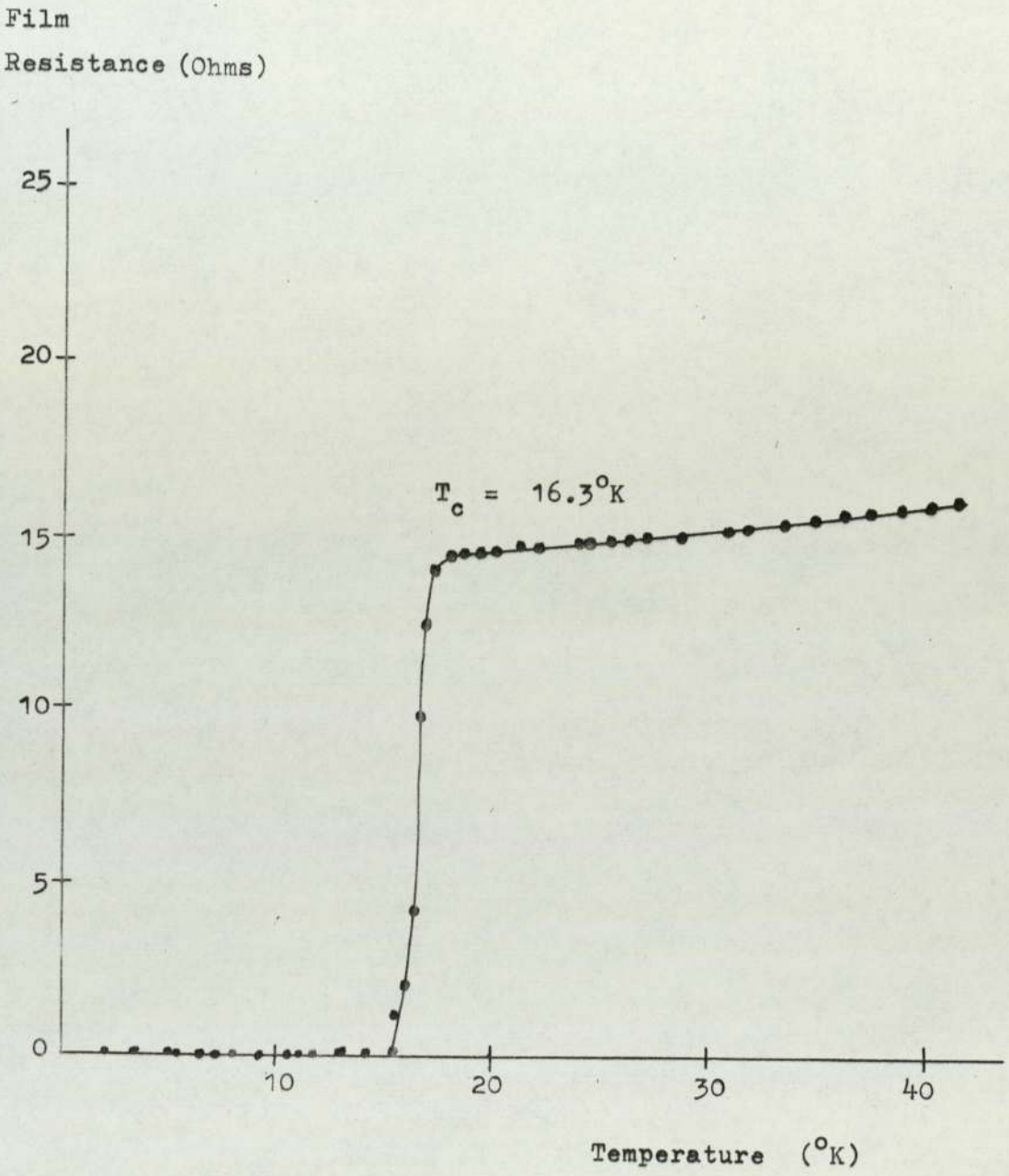

Figure 5.9 Transition temperature of (Nb_3Sn) film No.12 (prior to oxidation).

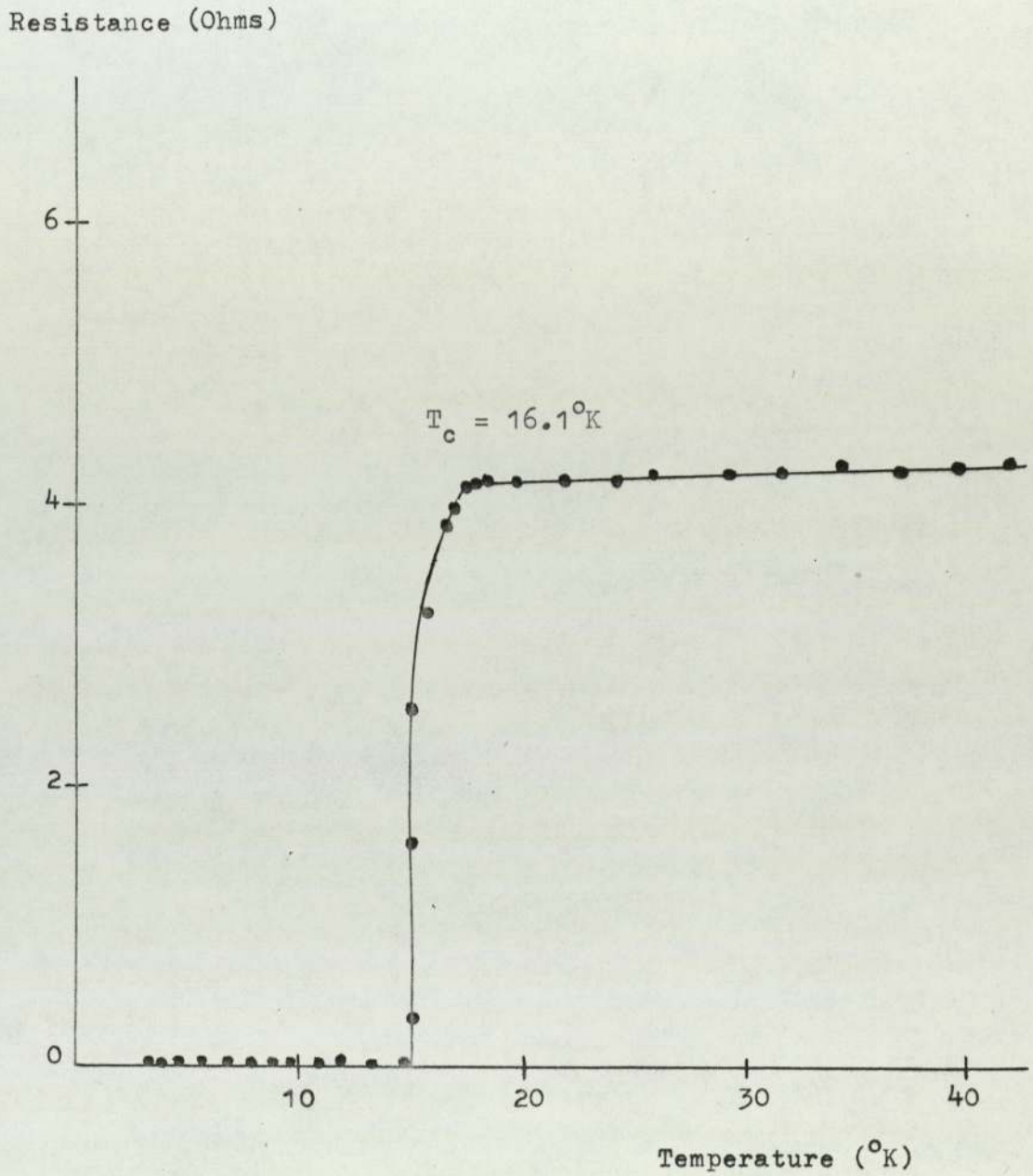

Figure 5.10 Transition temperature of (Nb_3Sn) film No.6.

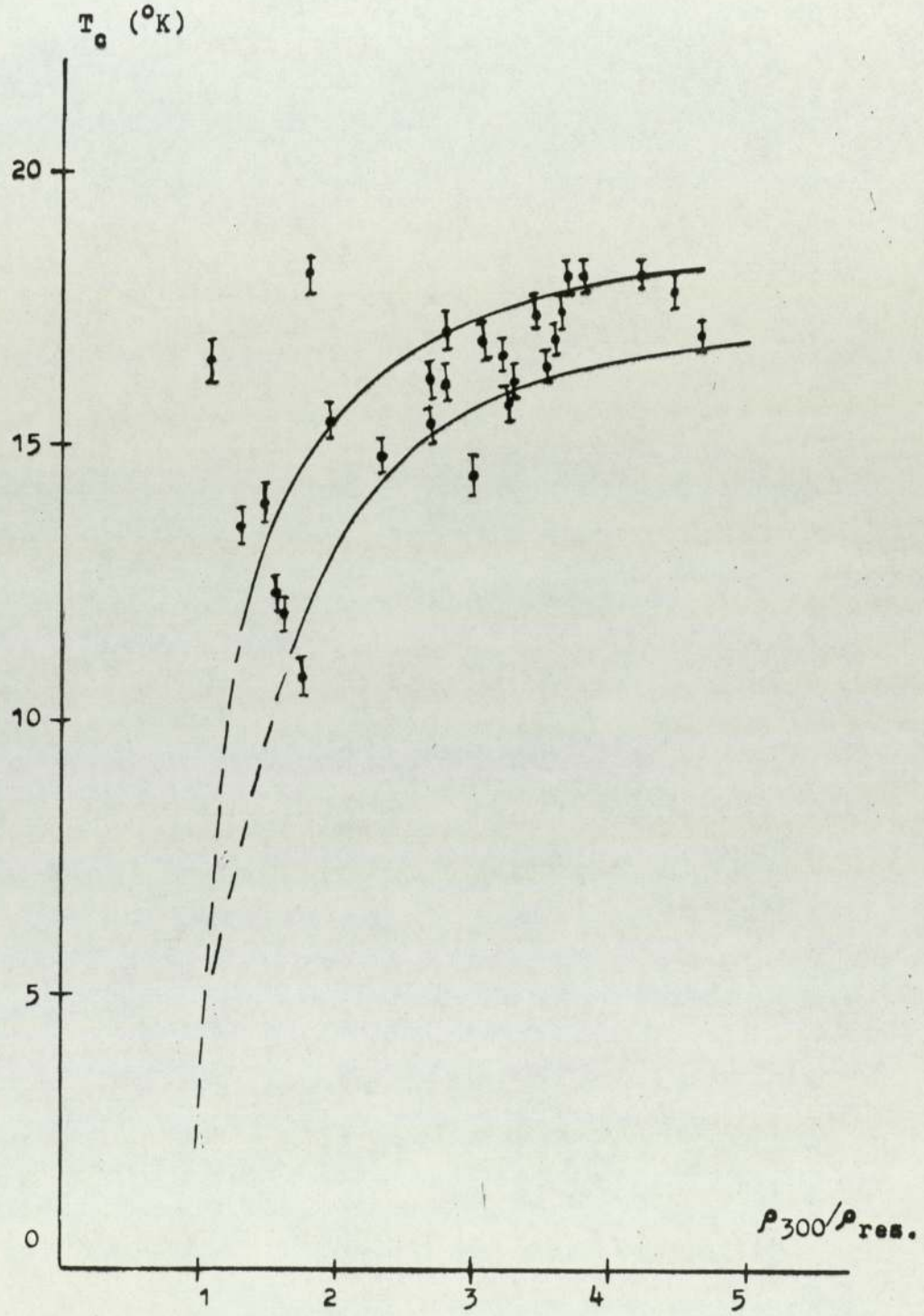

Figure 5.11 Plot of T_c against $\rho_{300}/\rho_{res.}$ for Nb_3Sn films of various thicknesses.

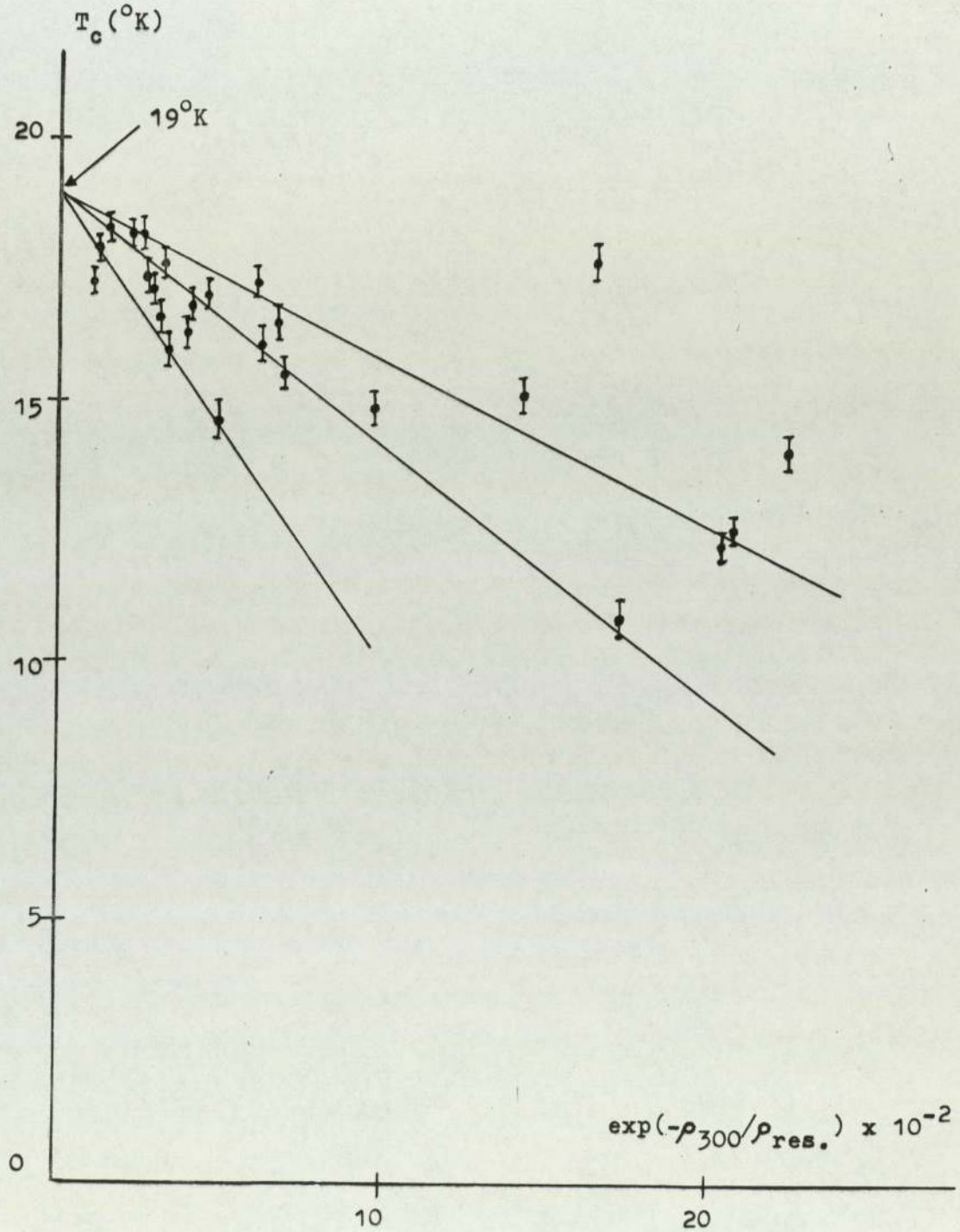

Figure 5.12 Plot of T_c against exp(-$\rho_{300}/\rho_{res.}$) for Nb_3Sn films of various thicknesses.

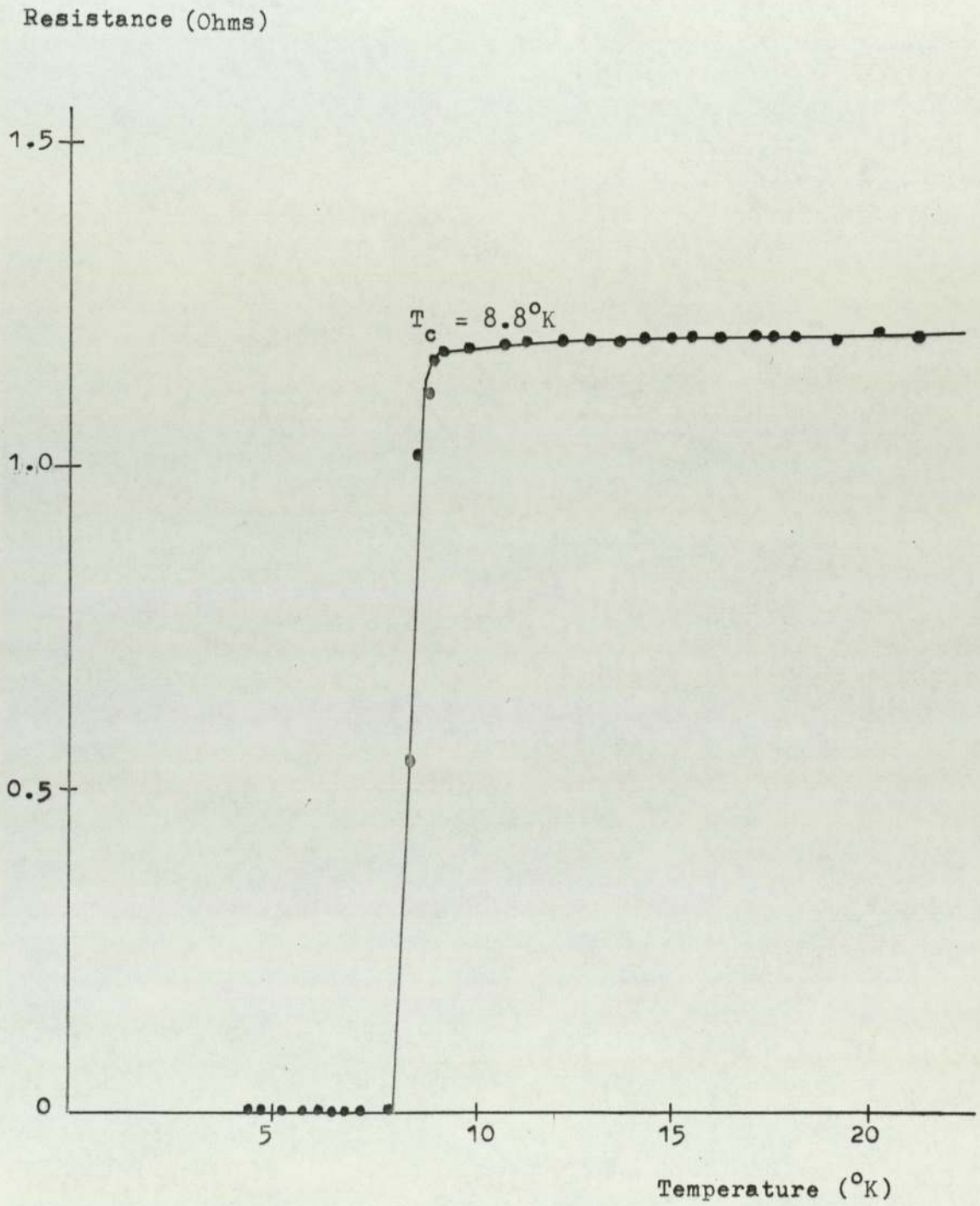

Figure 5.13 Transition temperature of niobium film No.42. (Prior to oxidation)

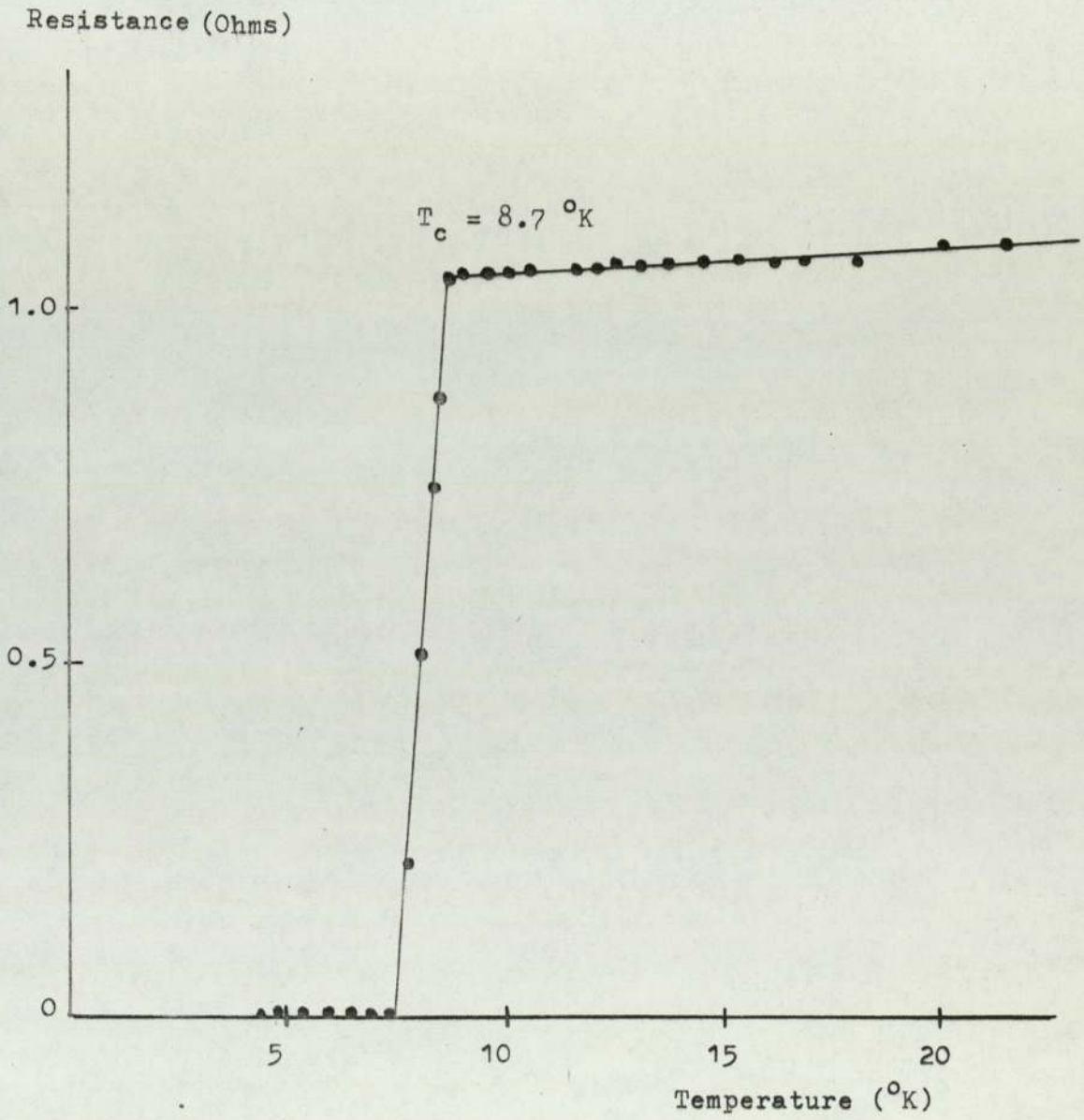

Figure 5.14 Transition temperature of (niobium) film No. 44.

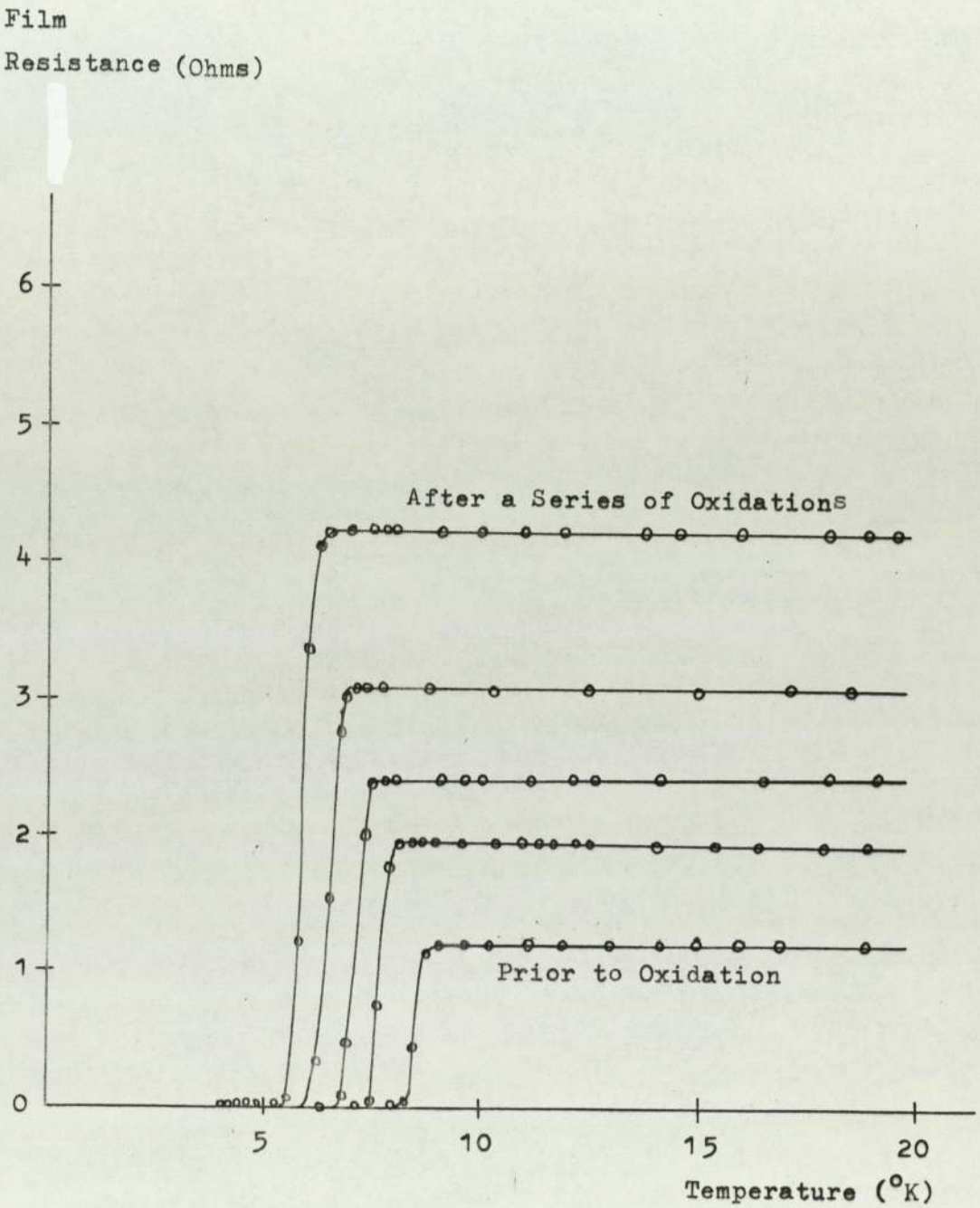

Figure 5.15 Depression of T_c of niobium film (No.42) due to reduction in (metal) film thickness.

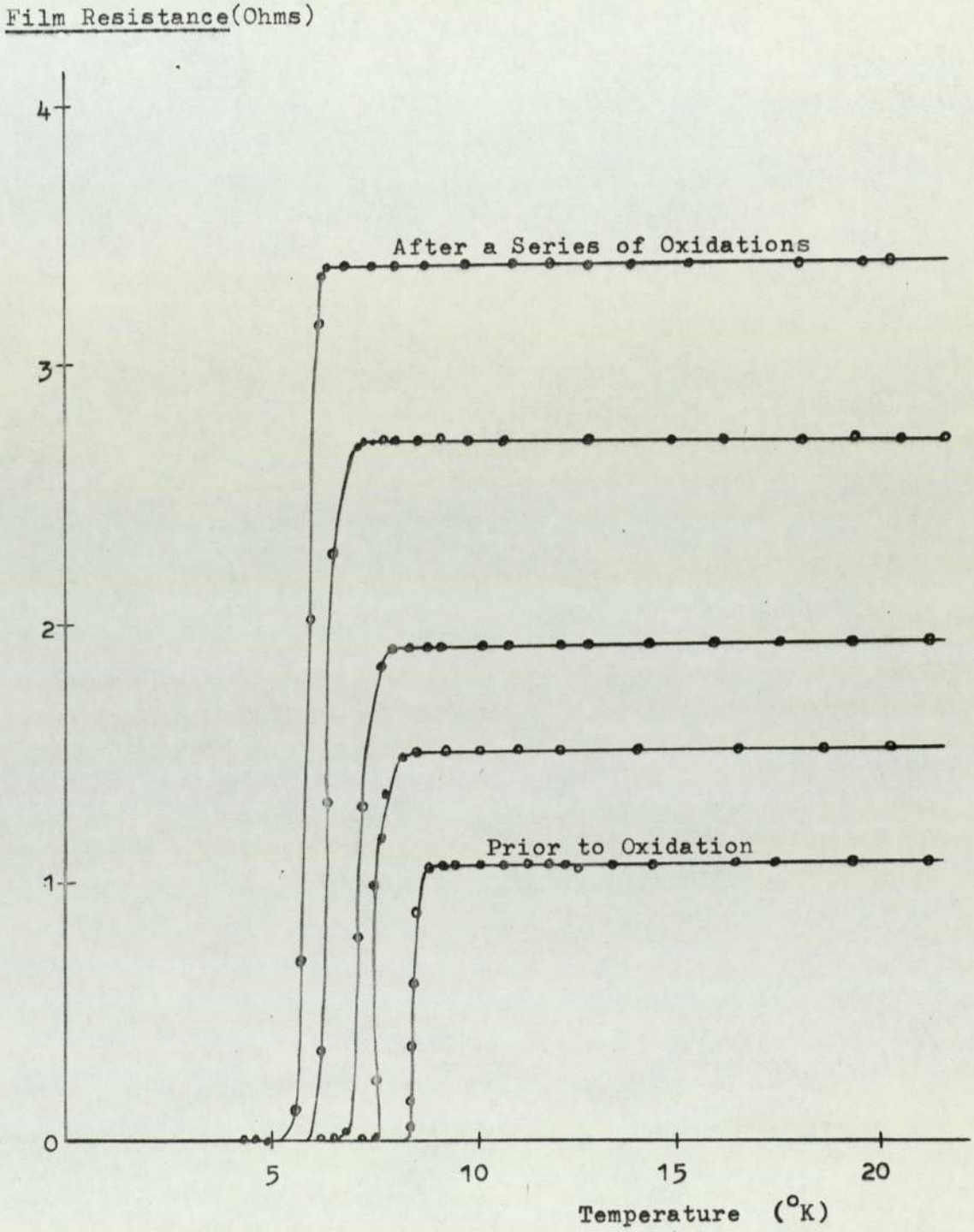

Figure 5.16 Depression of T_c of niobium film (No.44) due to metal thickness reduction by oxidation.

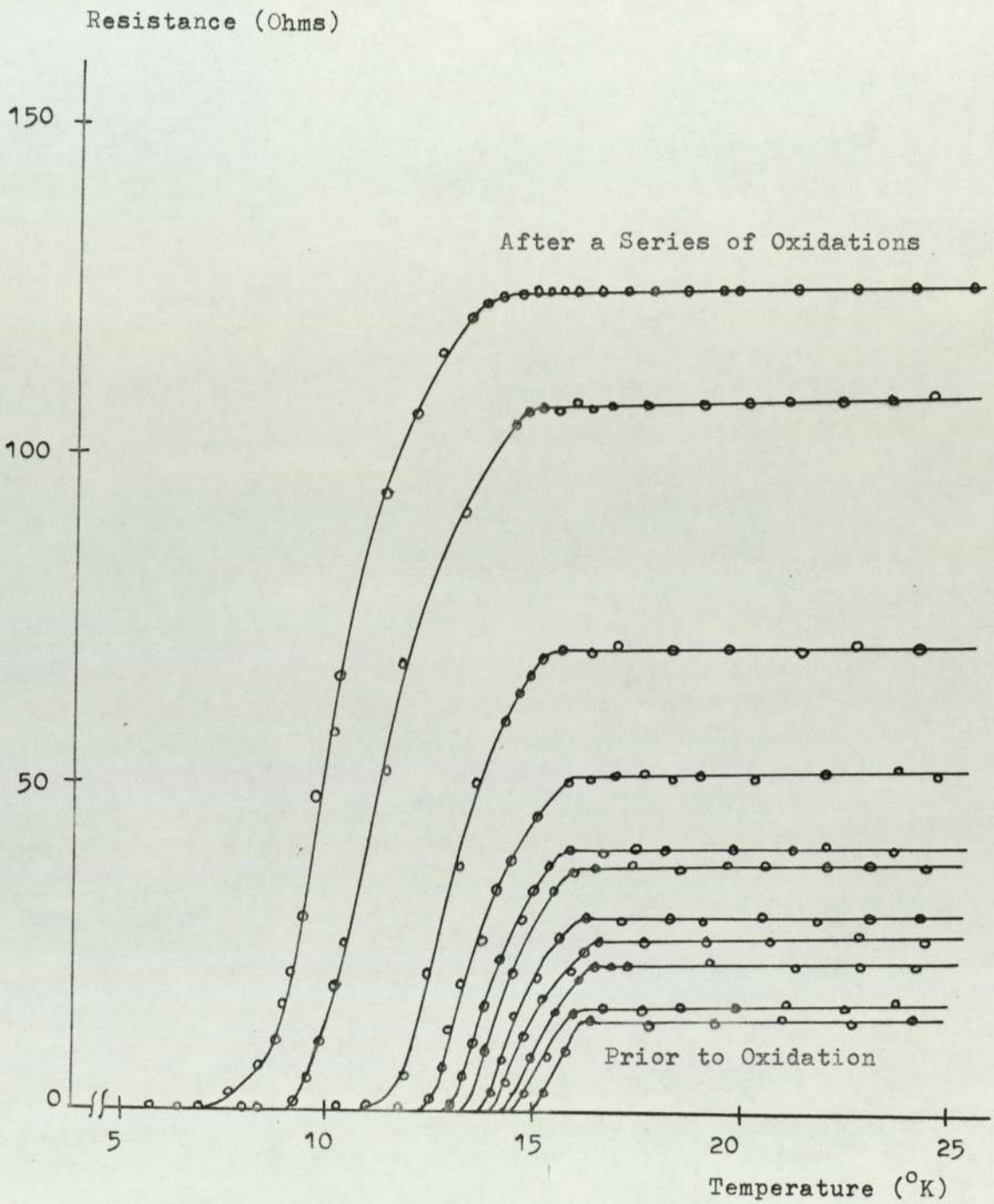

Figure 5.17 Depression of T_c of Nb_3Sn (No.12) due to the metal thickness reduction by oxidation.

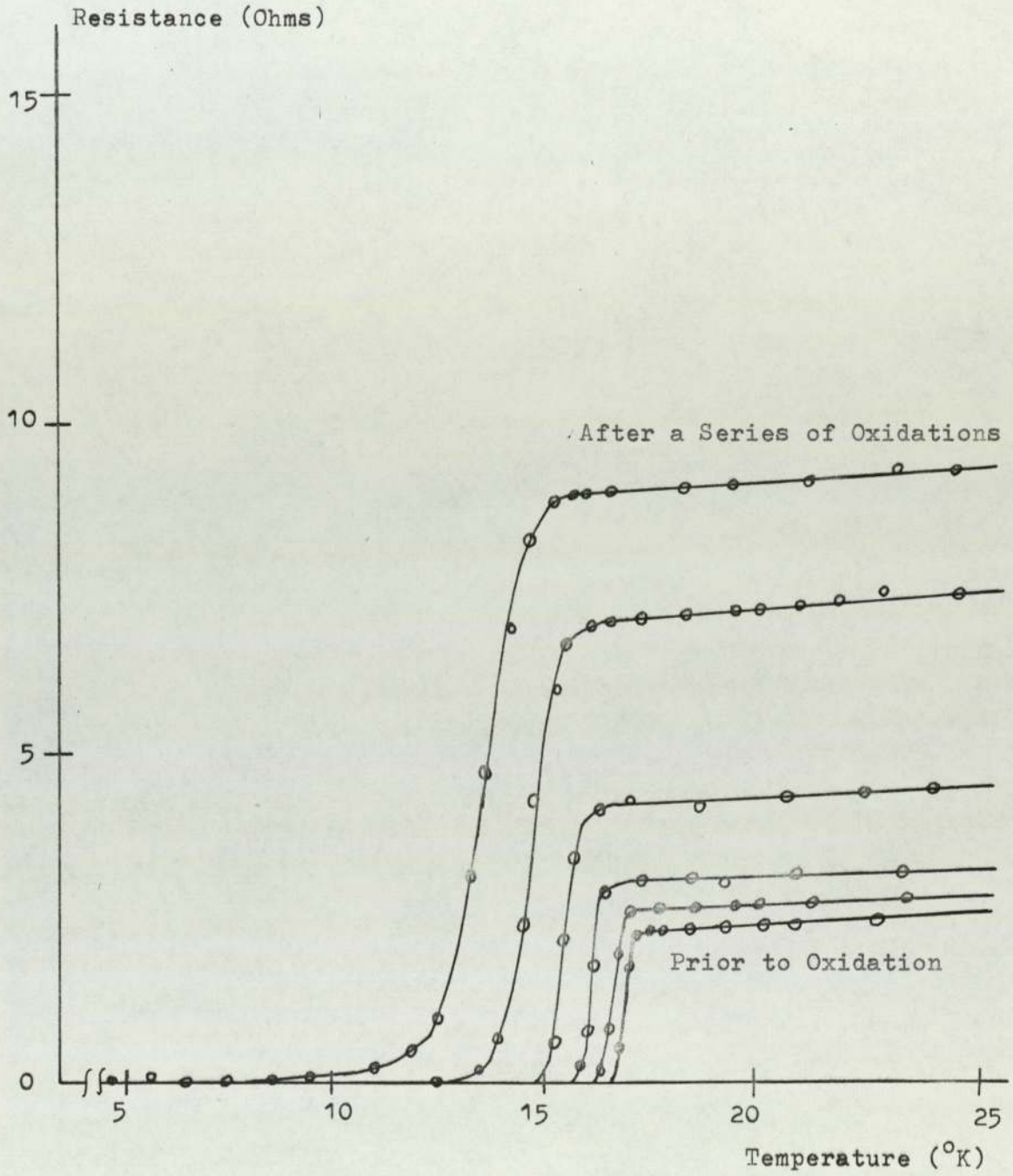

Figure 5.18 Depression of T_c of Nb_3Sn (No. 143) due to thickness reduction.

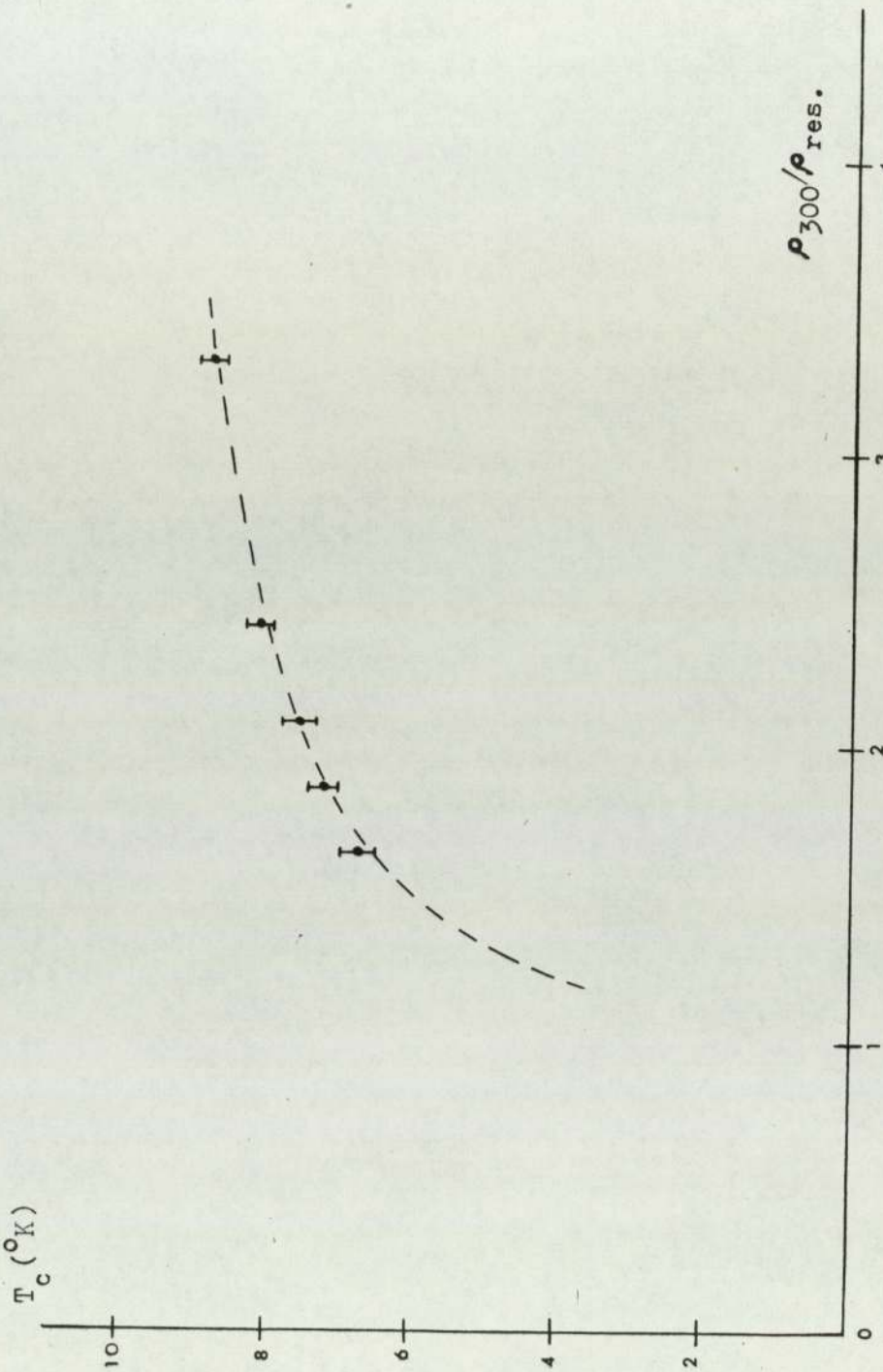

Figure 5.19 T_c vs resistivity ratio for an oxidized film of niobium (No.42).

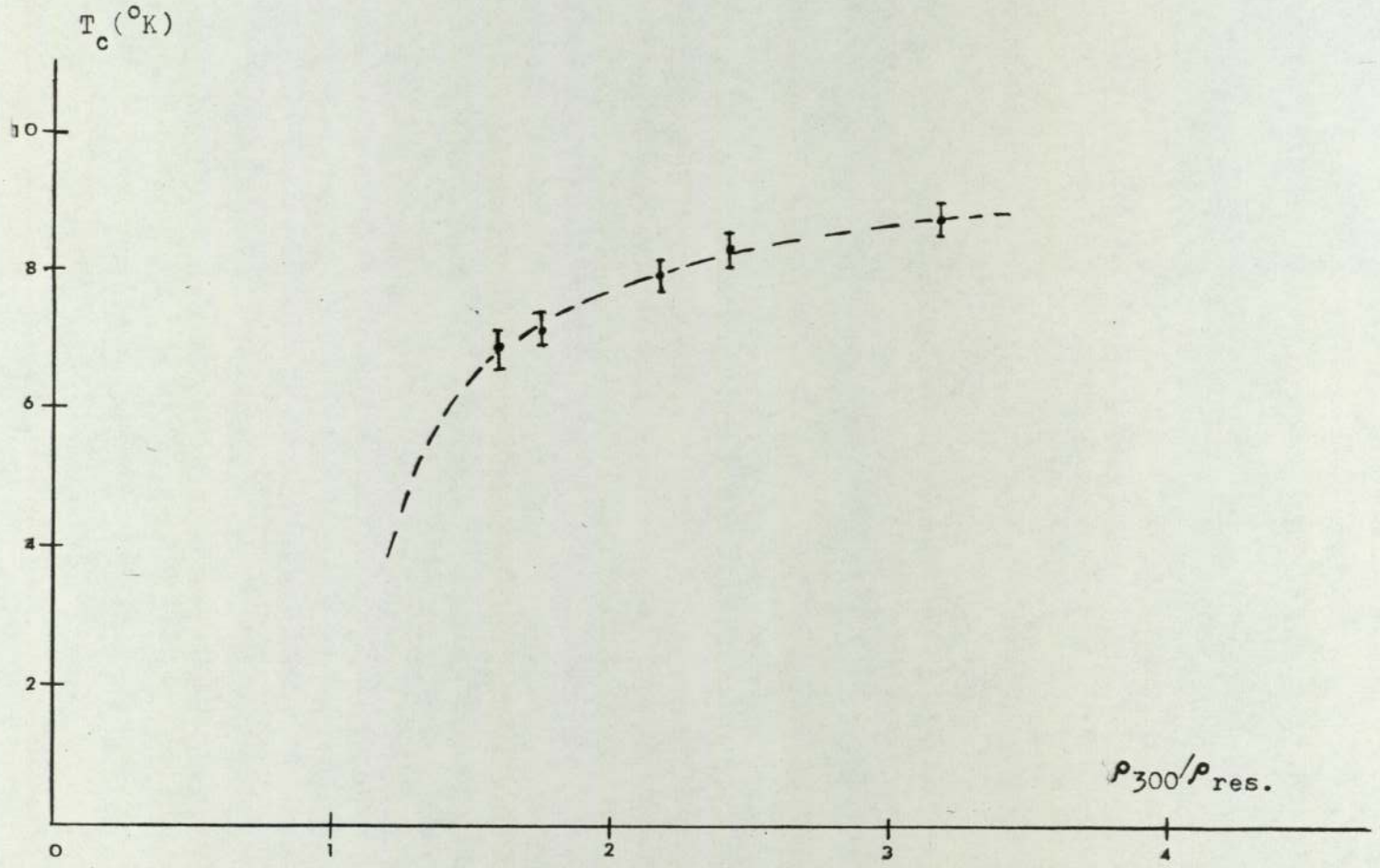

Figure 5.20a T_c vs resistivity ratio for an oxidized film of niobium (No.44).

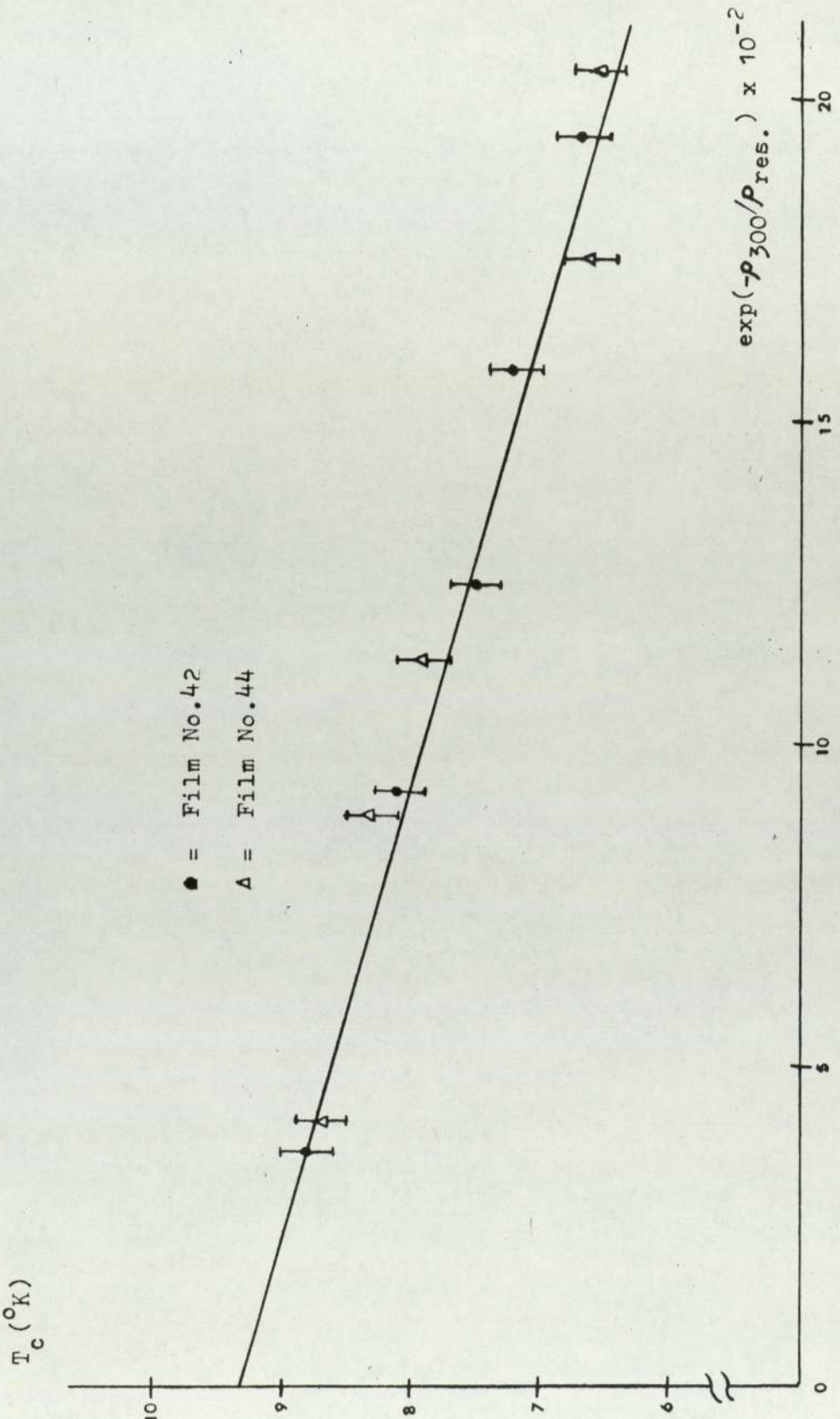

Figure5.20b Plot of T_c against $\exp(-\rho_{300}/\rho_{res.})$ for oxidized films of niobium.

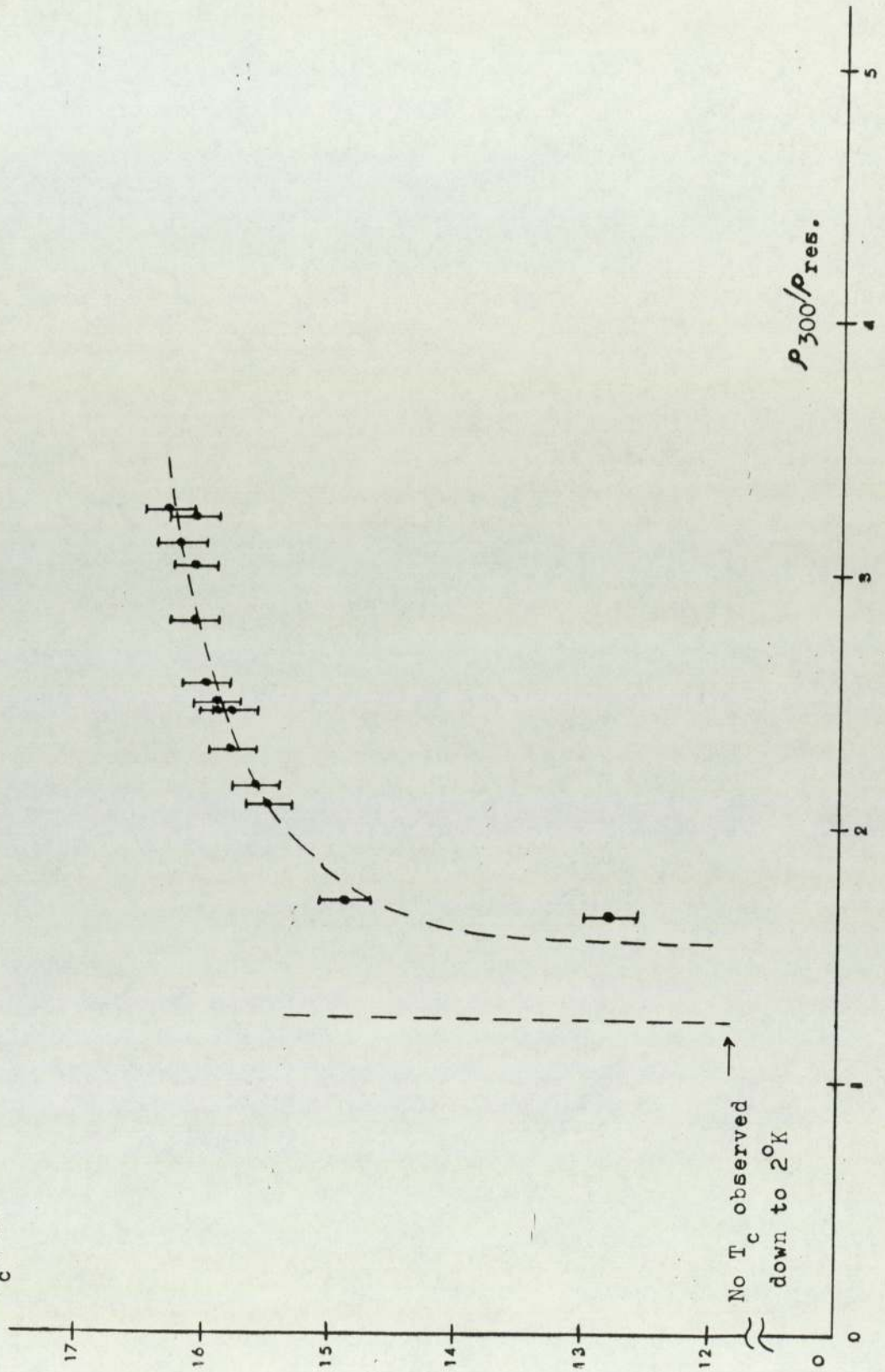

Figure 5.21 Variation of T_c with resistivity ratio for (Nb_3Sn) film No.12.

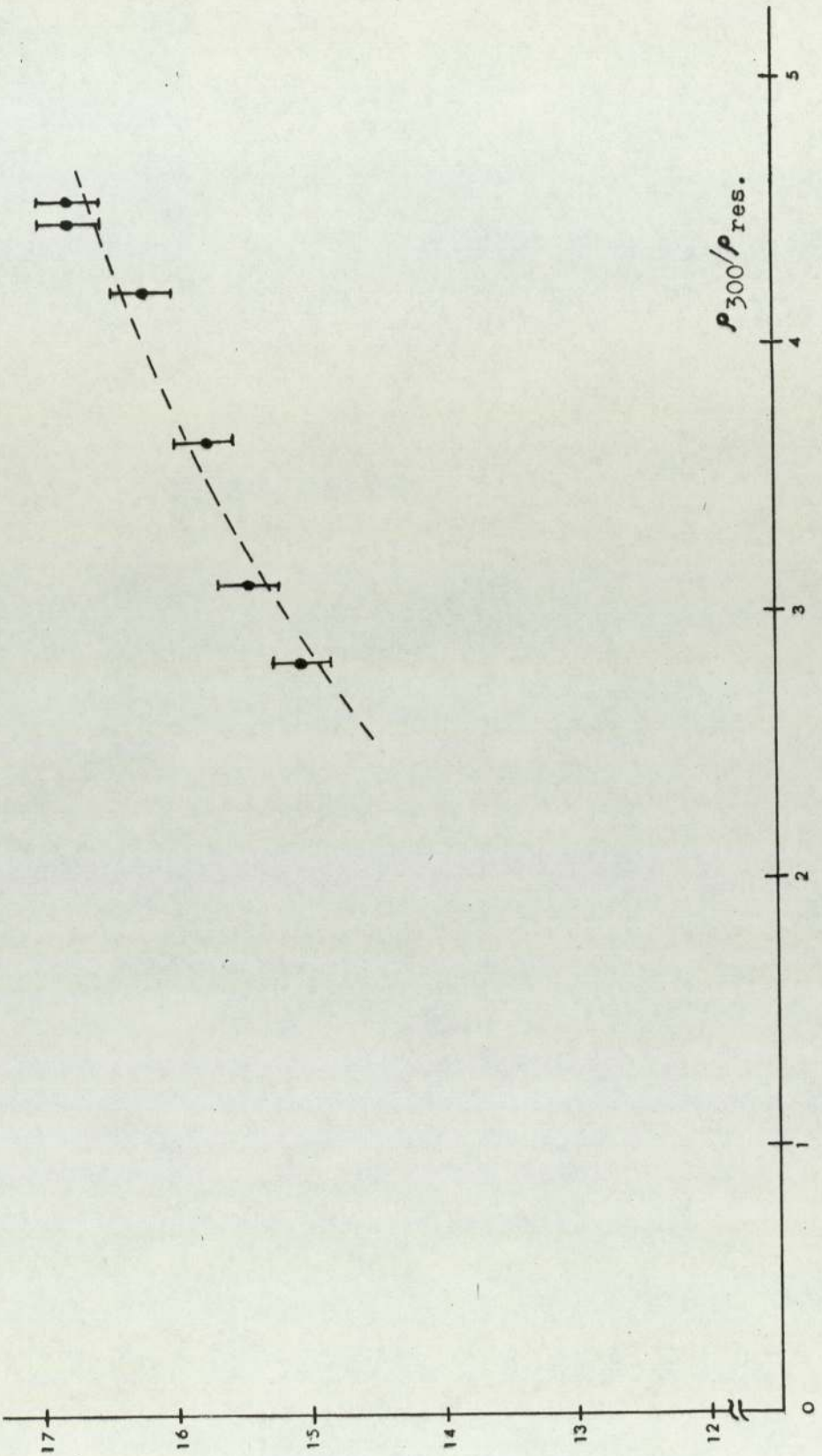

Figure 5.22 Variation of T_c with resistivity ratio for (Nb_3Sn) film No.143.

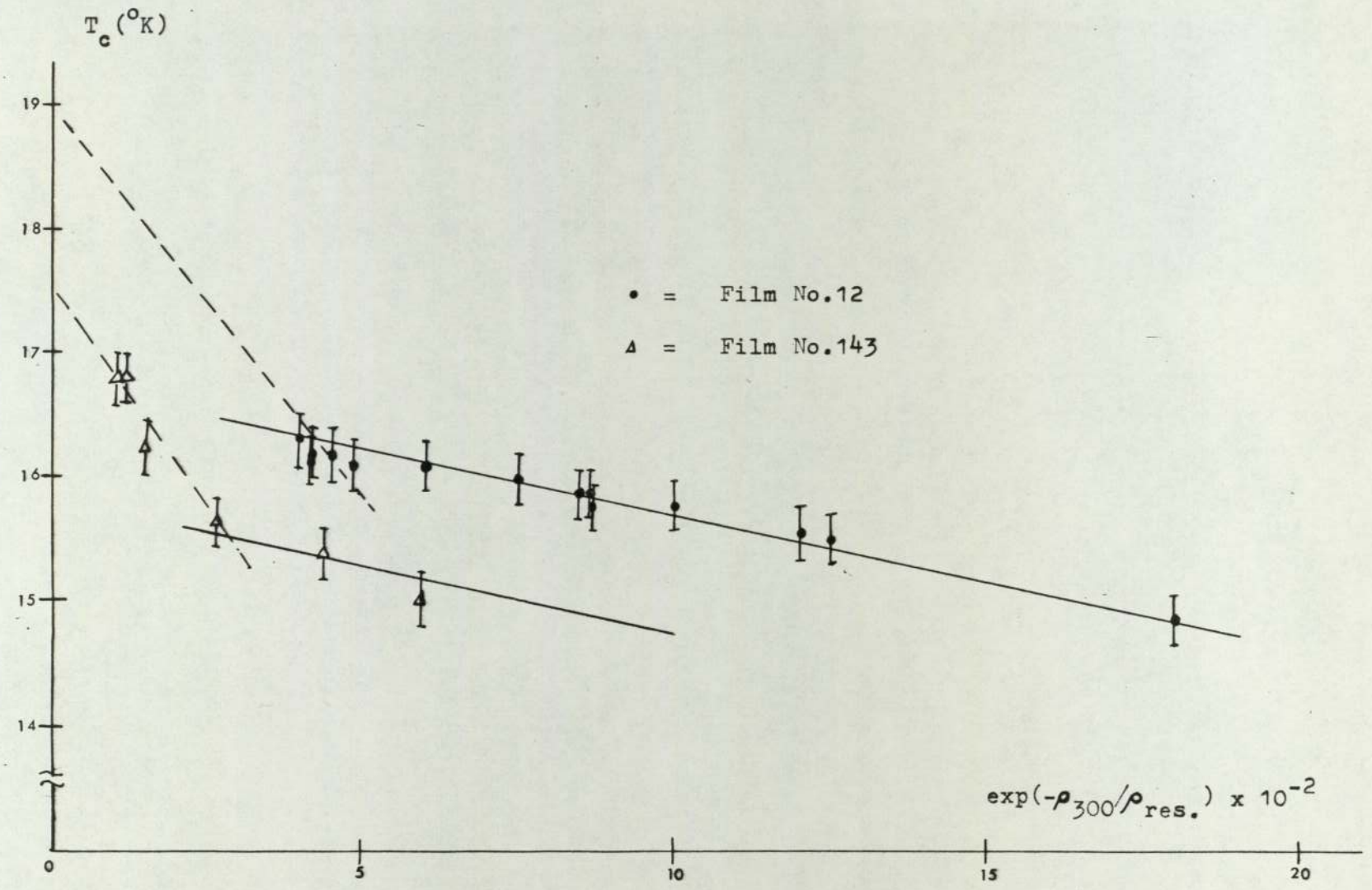

Figure 5.23 Plot of T_c against $\exp(-\rho_{300}/\rho_{res.})$ for Nb_3Sn films.

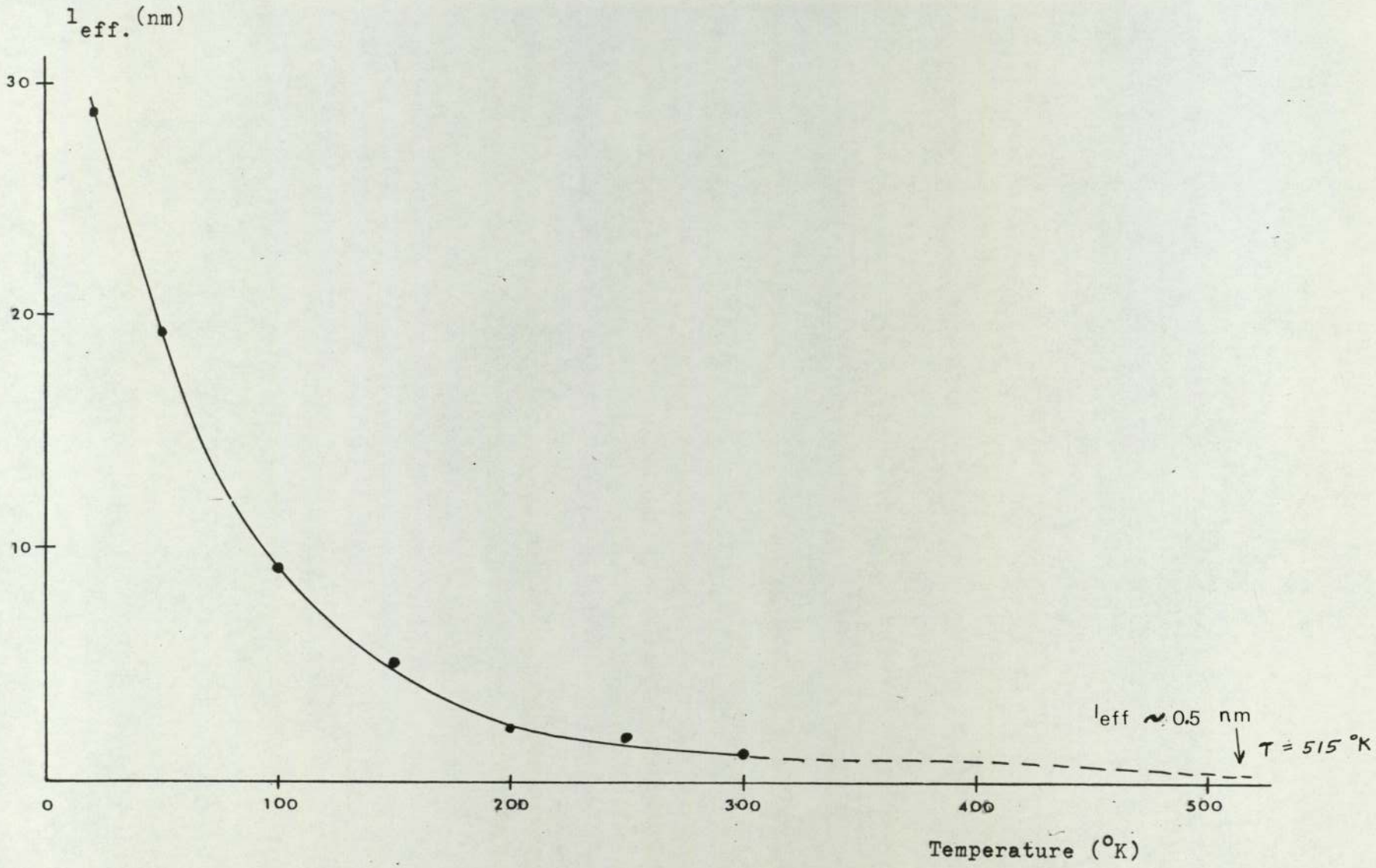

Figure 5.24 Variation of the electron mean free path with temperature.

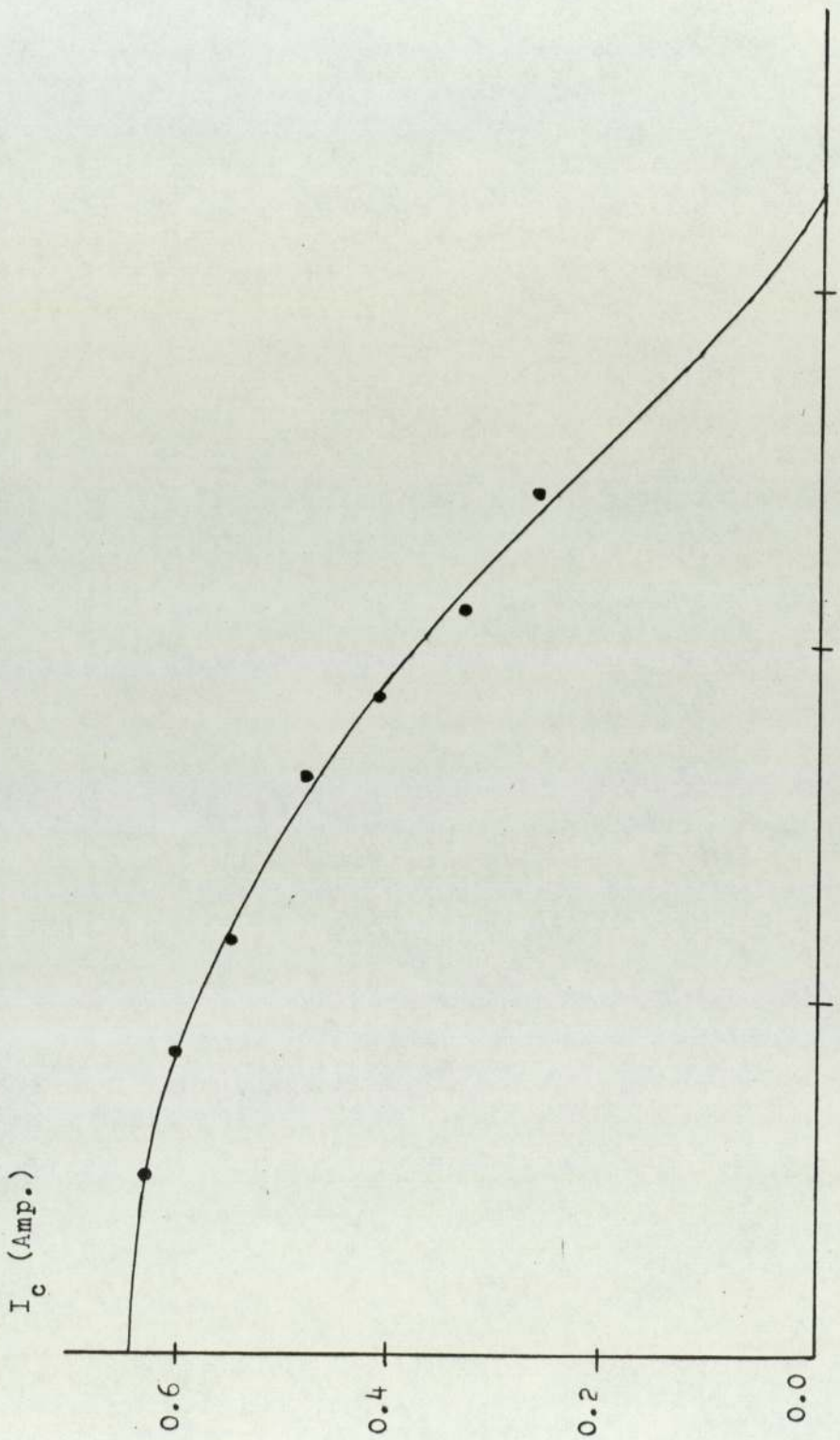

Figure 5.25 Variation of I_c with temperature for (Nb_3Sn) film No.12.

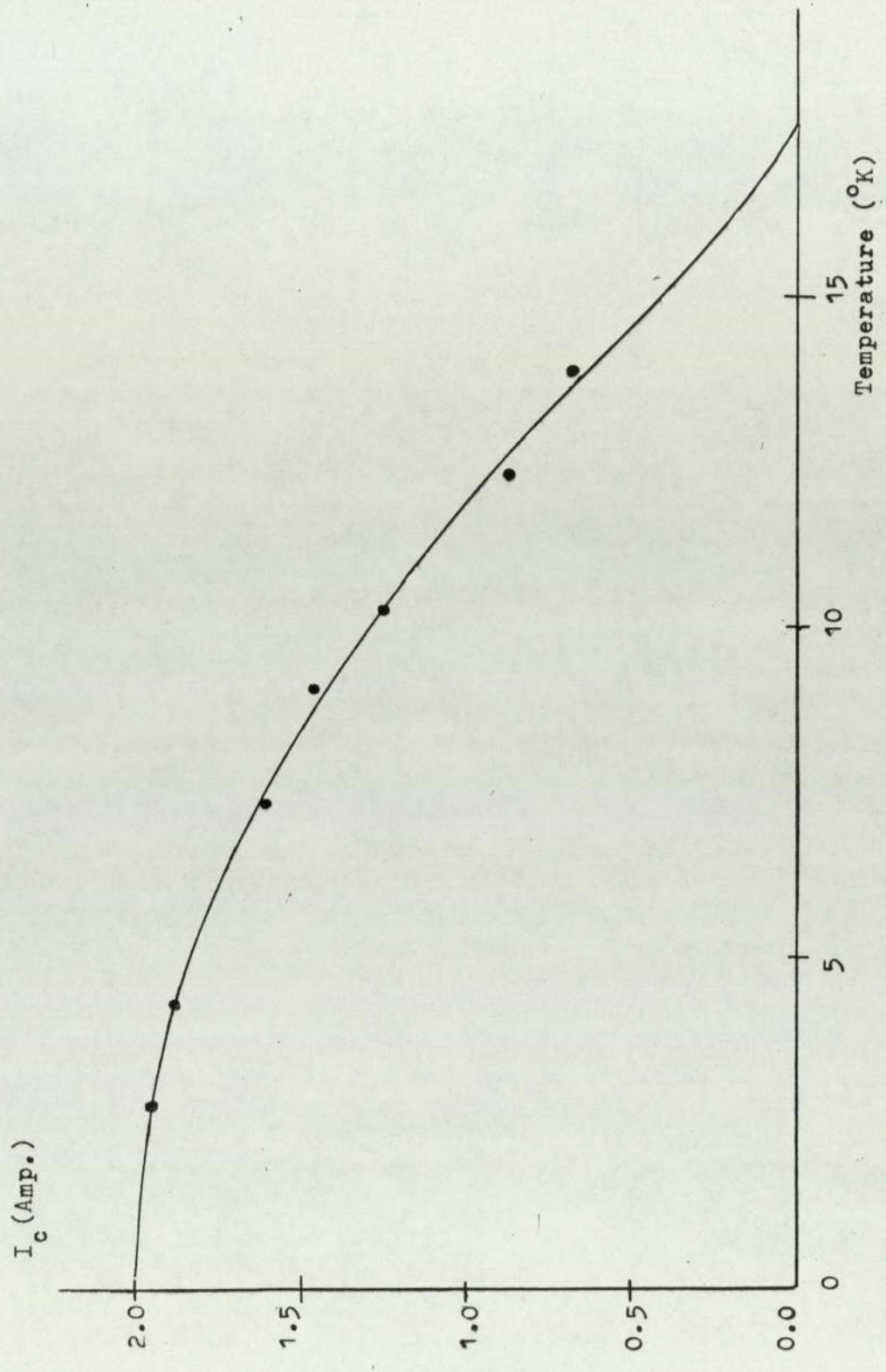

Figure 5.26 Variation of I_c with temperature for (Nb_3Sn) film No.112.

5.4 Optical Constants

Optical constants of several Nb_3Sn films were determined from the ellipsometric parameters which were obtained from measurements at two angles of incidence; 61° and 73°. These parameters for a film free surface were determined from the extrapolation to time t = 0 of the variation of oxide growth with respect to time, t, as shown in Figures (5.27) and (5.28), for the angles of incidence of 61° and 73° respectively. Table (5.9) shows the optical constants of some Nb_3Sn films, for the radiation of wavelength of 549 nm. Variation of the optical constants of a film of Nb_3Sn for different wavelength is presented in Table (5.10).

An oxidation process, as described in section 4.7, was used for two films of Nb_3Sn. The refractive index of the oxide was obtained by comparing the curvatures of Ψ_{cal} and Δ_{cal}, calculated from assumed values, with the observed data, Figures (5.29) and (5.30). The ratio of reduction of Nb_3Sn thickness to the production of oxide thickness in the oxidation process was found to be 2:3. This was obtained by measuring thicknesses. By this way the optical constant of the oxide was estimated from the best fit of the calculated values. Consequently, the thickness of the Nb_3Sn layer after each oxidation was deduced, as shown in Table (5.12).

Table 5.9a Optical constants of some Nb_3Sn films, at the radiation wavelength of 549 nm.

Sample No.	Film Thickness (nm)	n	k
6	187	1.95	2.44
12	58	2.20	2.41
105	210	3.00	2.66
115	410	1.69	2.47
145	135	2.32	2.51
165	166	1.74	2.26

Table 5.9b Calculated pseudo constants for a Nb_3Sn surface with the presence of oxide, assuming $n_{Nb_3Sn} = 2.3$, $k_{Nb_3Sn} = 2.5$, $n_{oxide} = 2.5$ and $k_{oxide} = 0$.

Oxide Thickness (nm)	n_{psuedo}	k_{pseudo}
0	2.30	2.50
1	2.19	2.44
2	2.09	2.37
3	1.99	2.31
4	1.90	2.24
5	1.82	2.17
6	1.74	2.11
7	1.67	2.04
8	1.60	1.98
9	1.54	1.91
10	1.47	1.85

Table 5.10 Ellipsometric measurements at various wavelengths of radiation for Nb_3Sn, film No.6. (Angle of incidence = 61°)

Wavelength (nm)	ψ	Δ	n	k
499	24.44	168.84	4.11	0.88
545	30.08	127.68	1.77	2.23
549	30.68	132.38	1.95	2.44
554	30.83	131.78	1.91	2.44
576	32.41	124.09	1.45	2.31
604	34.80	125.70	1.29	2.56

Table 5.11 Variation of ψ_{cal} and Δ_{cal} with respect to oxide and film thicknesses for film No.12 (Nb_3Sn), at wavelength of radiation of 549 nm.

$n_{oxide} = 2.50$, $n_{Nb_3Sn} = 2.20$,

$n_{quartz} = 1.46$, $k_{Nb_3Sn} = 2.40$.

Thickness(nm)		Angle of incidence = 61°		Angle of incidence = 73°	
Nb_3Sn	Oxide	ψ_{cal}	Δ_{cal}	ψ_{cal}	Δ_{cal}
59	1.5	30.02	133.61	25.91	88.52
58	3	29.89	130.77	26.45	84.93
56	6	29.65	124.93	27.53	78.14
54	9	29.44	118.88	28.60	71.82
52	12	29.34	112.58	29.70	65.89
50	15	29.34	105.96	30.85	60.30
48	18	29.57	98.92	32.09	54.95
46	21	30.11	91.29	34.46	49.72
44	24	31.10	82.80	35.04	44.40
42	27	32.68	72.97	36.85	38.68
40	30	34.99	61.03	38.88	32.10
38	33	37.90	45.77	40.94	24.09
36	36	40.66	25.97	42.60	14.27
34	39	41.68	1.99	43.21	2.93

Table 5.11 (Continued.)

Thickness(nm)		Angle of incidence = 61°		Angle of incidence = 73°	
Nb_3Sn	Oxide	ψcal	Δcal	ψcal	Δcal
32	42	39.84	-22.50	42.38	- 8.67
30	45	36.10	-43.56	40.31	-19.08
28	48	32.14	-60.45	37.55	-27.68
26	51	28.78	-74.20	34.59	-34.64
24	54	26.18	-85.95	31.66	-40.42
22	57	24.18	-96.48	28.79	-45.41
20	60	22.62	-106.28	25.96	-49.89
18	63	21.35	-115.67	23.09	-53.96
16	66	20.52	-124.90	20.10	-56.91
14	69	19.26	-134.21	16.93	-60.59
12	72	18.33	-143.84	13.55	-62.38
10	75	17.45	-154.07	9.97	-61.41
8	78	16.62	-165.27	6.35	-52.34
6	81	15.94	-177.92	3.82	-14.01

Table 5.12 Deduction of thickness of Nb_3Sn layer from the ellipsometric measurements of film No.12.

Series of Oxidation	Thickness (nm)	$\phi = 61^\circ$		$\phi = 73^\circ$	
		$\Delta_{obs.}$	$\Delta_{cal.}$	$\Delta_{obs.}$	$\Delta_{cal.}$
1st	58.1	131.15	131.05	85.22	85.28
2nd	55.8	124.38	124.34	77.54	77.49
3rd	52.5	114.24	114.18	67.34	67.34
4th	50.0	105.92	105.96	60.30	60.30
5th	49.2	103.42	103.20	58.72	58.14
6th	47.5	97.18	97.07	53.34	53.64
7th	44.5	85.22	85.02	45.72	45.75
8th	42.4	75.01	75.08	39.78	39.89
9th	40.0	62.38	61.03	32.24	32.10
10th	34.0	1.88	1.99	3.02	2.93
11th	31.2	-31.42	-31.46	-13.15	-13.03
12th	27.0	-67.44	-67.64	-31.65	-31.34
13th	15.7	-126.28	-126.28	-58.00	-58.09
14th	13.5	-136.02	-136.57	-61.15	-61.19
15th	10.5	-152.00	-151.44	-62.11	-62.07

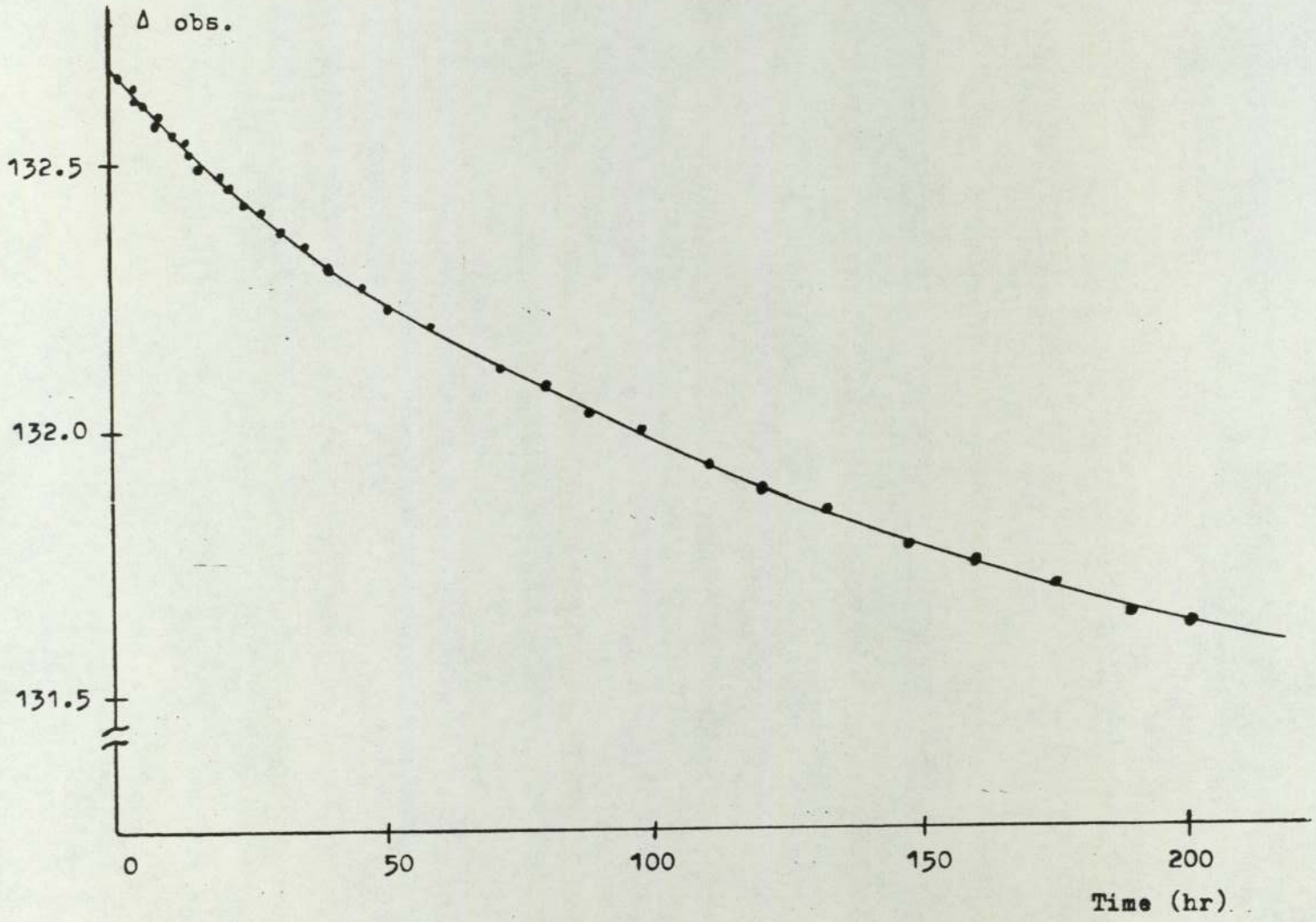

Figure 5.27 Variation of $\Delta_{obs.}$ with respect to time at the angle of incidence of 61° for film No. 6.

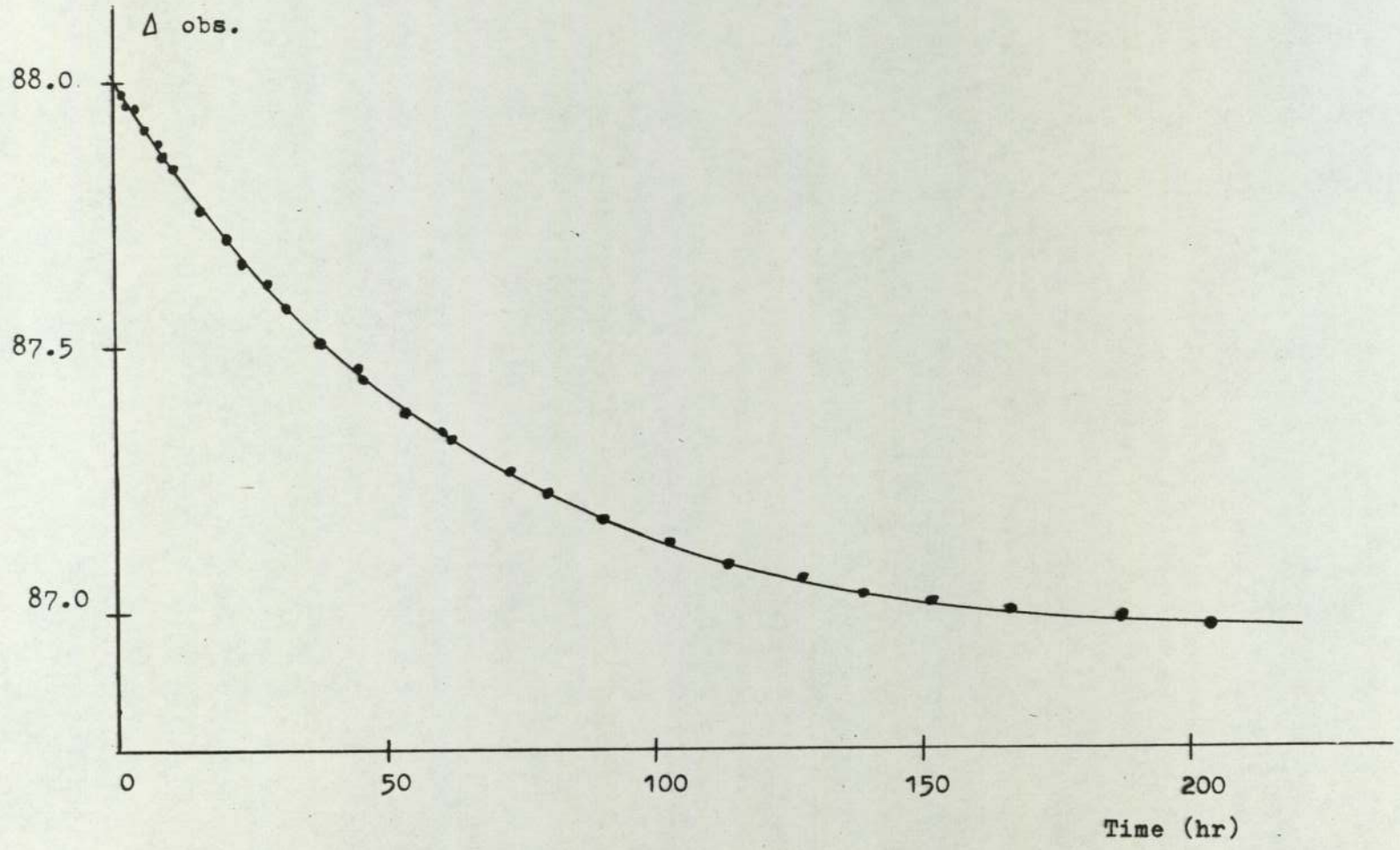

Figure 5.28 Variation of $\Delta_{obs.}$ with time at the angle of incidence of 73° for film No. 6.

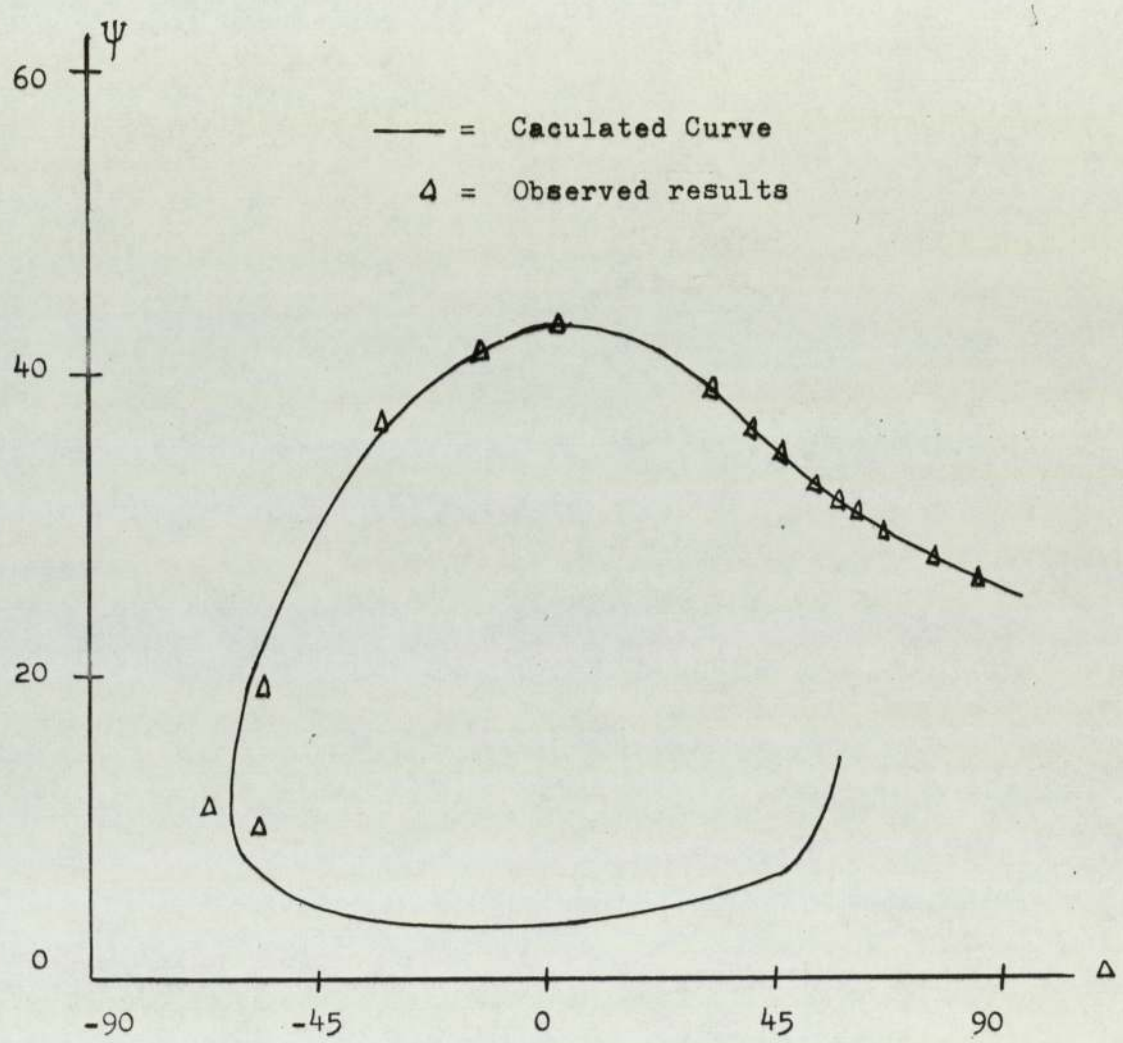

Figure 5.29 Variation of ψ and Δ due to oxidation for film No.12 , at the radiation wavelength 549 nm. (Angle of incidence = 73°).

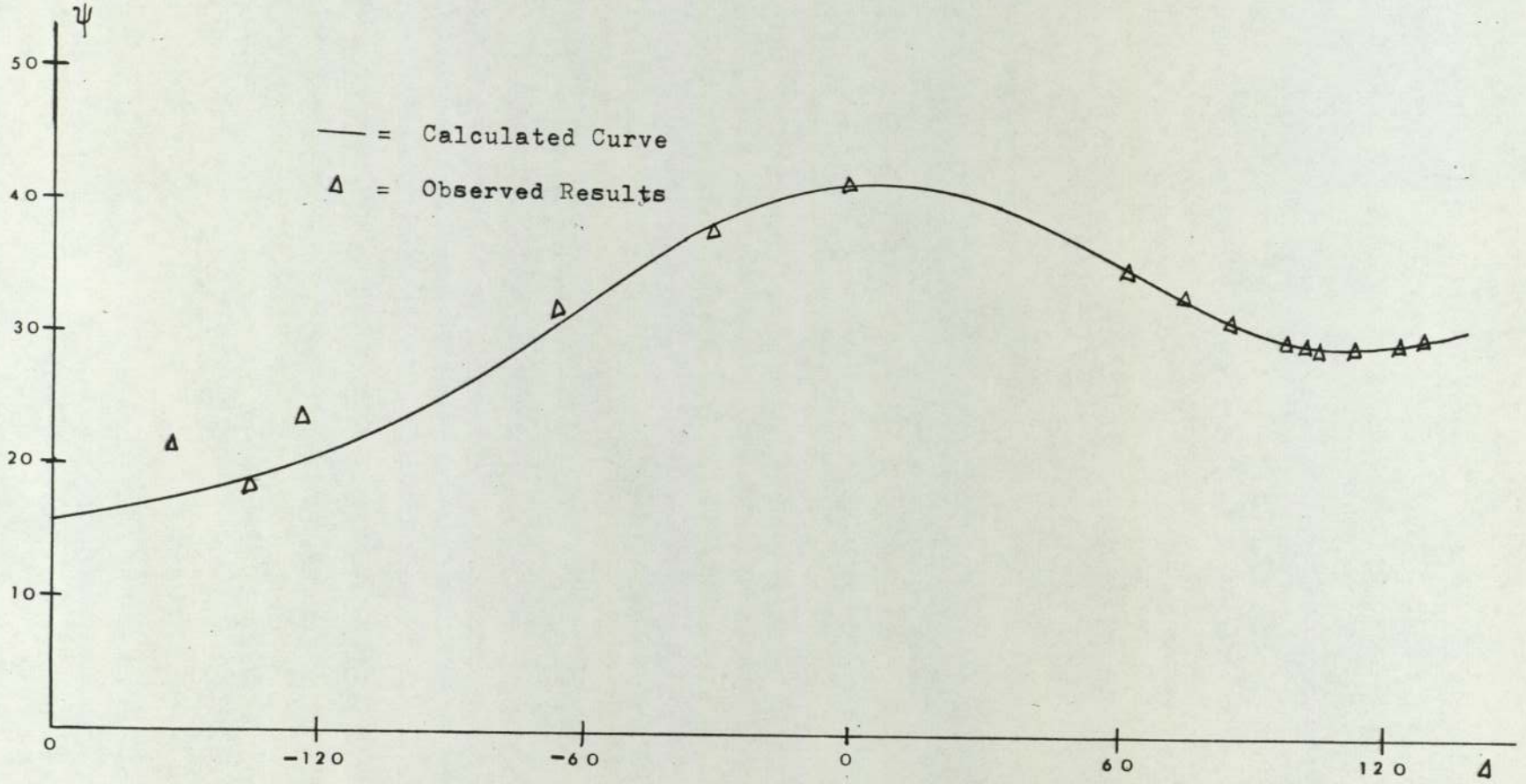

Figure 5.30 Variation of ψ and Δ due to oxidation for film No.12 at the wavelength of radiation of 549 nm. (Angle of incidence = 61°).

CHAPTER 6 : DISCUSSION OF RESULTS

6.1 Film Structure

According to Chopra(1969), thin films of most materials assume the same crystal structure as the bulk material, and the structural order,e.g., size and orientation of the crystallites, of prepared films can be varied from a highly disordered structure when deposited on a low temperature substrate to a well-ordered structure when (epitaxially) grown on a single crystal substrate. Some of the Nb_3Sn thin films prepared in this work showed quite marked effects of structural defects on cooling. For example, the variation of the resistance due to thermal cycling from room temperature to $4.2^{o}K$ was observed and the results for one such film are illustrated in Fig.(5.1). The majority of films did not show this effect and Fig.(5.2) is an example of recycling a stable film. Results for stable films have been given in Table.(5.5).

6.1.1 Structure of Nb_3Sn Alloy Films

The structure of thin films of Nb_3Sn as revealed by x-ray diffraction in this investigation was found to belong to β -tungsten or A-15 type with preferred orientation in the (200) direction. The lattice constant, a_o , of films thicker than 100 nm was found to be 5.28-5.29 Angstroms. This is in agreement with the bulk value (5.2906 $\mathring{A}$) listed in the A.S.T.M. index card numbers 17-909 and 19-875 (see Appendix B). For thinner films (less than 100 nm) , x-ray diffraction lines were weak but further indication of the composition of these films was obtained by observing the transition

temperature , T_c , at low temperatures , since Nb_3Sn is the only compound in the niobium-tin system which has a critical temperature above 4.2°K (Enstrom,1966).

A structural transformation (the Batterman-Barrett transformation, Batterman and Barrett,1964) in Nb_3Sn has been reported by Mailfert et al.(1969). According to them the compound undergoes a cubic-to-tetragonal transformation starting at 43°K, with distortion progressively increasing from the ratio a:c = 1:1 to 1: 1.006 at the lowest temperature, here a and c are the lattice parameters of the tetragonal structure. This structural transformation is illustrated in Fig.(6.1). The electrical measurements in the present investigation gave no evidence of this structural change. The resistivity measurements observed on chemically deposited Nb_3Sn (Woodard and Cody,1964) support the results obtained in the present investigation.

6.1.2 Film Structure of Nb_6Sn_5 and $NbSn_2$

A set of films prepared at alloying temperatures below 650 °C was found to have mixed phases of Nb_6Sn_5 and $NbSn_2$ with the crystal structures in accordance with the A.S.T.M. index card numbers 19-877 and 15-481. From the low temperature measurements, the critical temperature of these films were in the range 2.6-2.8°K.

According to van Vucht(1965) T_c of $NbSn_2$ is about 2.6°K and is less than 0.3°K for Nb_6Sn_5. Later Enstrom(1966) reinvestigated the superconducting properties of the compound Nb_6Sn_5 and observed a T_c of about 2.8°K but this could be attributed to $NbSn_2$ since about 1% of this compound was also observed. It is therefore

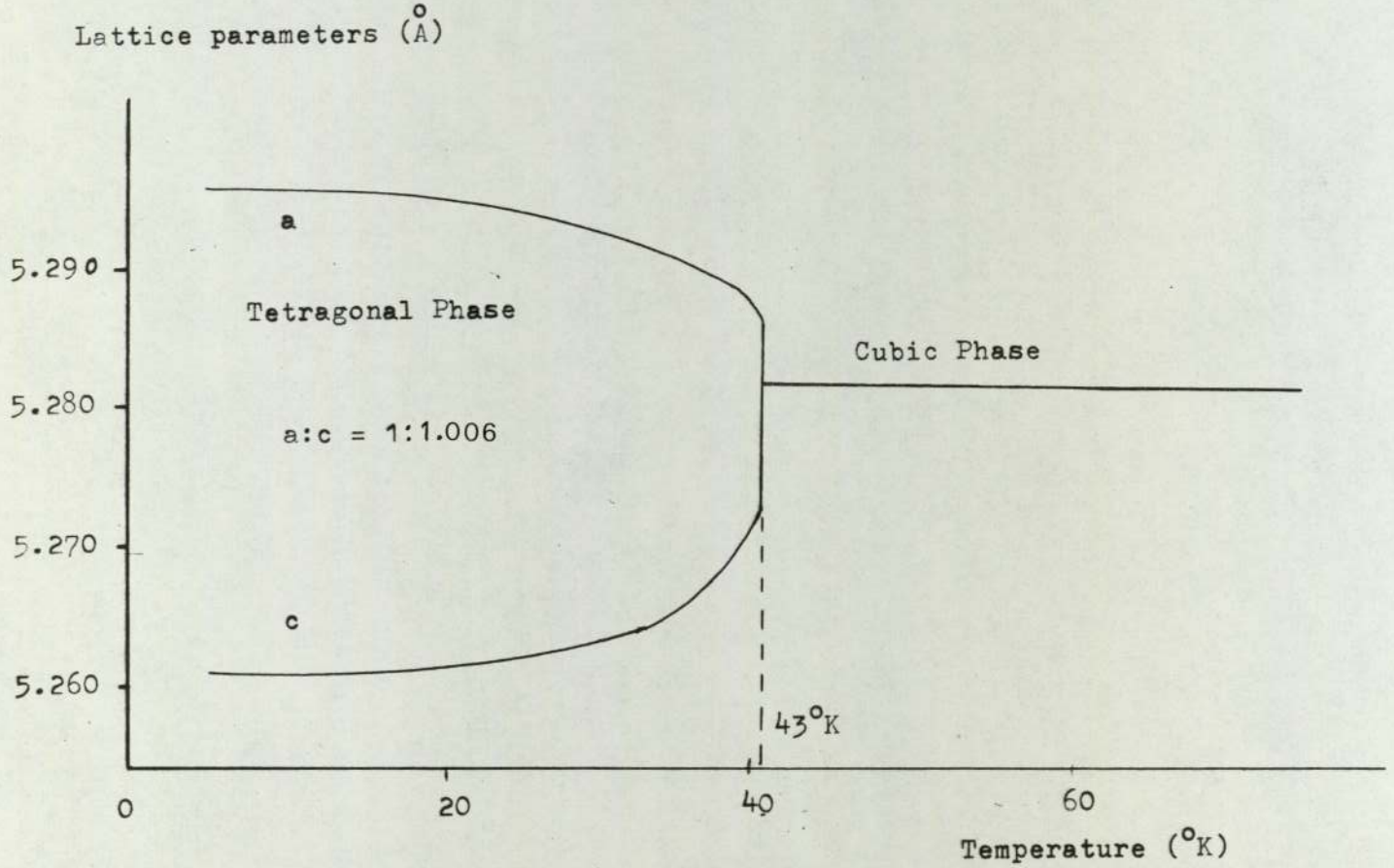

Figure 6.1 The structural transformation at 43°K of Nb_3Sn .(After Maiflert et al.,1969).

difficult to establish which of these two compounds has a T_c above $2^{\circ}K$ because both of them are normally present in samples prepared in this region of temperatures ($650^{\circ}C$). However, from the x-ray diffraction data and low temperature measurements of the present work, it appeared that these two compounds were formed into separated layers rather than a mixed layer, otherwise a 'kink' of resistance would have been observed at low temperatures instead of a smooth and complete disappearance of resistance below the transition temperature, as shown in Fig.(5.8).

6.1.3 Grain Size of Nb_3Sn

Grain sizes of Nb_3Sn formed by solid state diffusion in the range $600-1000^{\circ}C$ have been determined by Scanlan et al.(1975). Average grain sizes from 400 Angstroms to several thousand Angstroms for film thicknesses in the range 2 to 12 μm thick were observed. Similar results were also reported by Shaw(1976) who obtained grain sizes of 300-1200 Angstroms for Nb_3Sn layers of 0.2 μm to 0.7 μm thick. Both set of results are shown in Fig (6.2). No measurement of grain sizes were made on films in the present work but it is reasonable to assume that grain size is related to thickness as indicated in Fig.(6.2)

6.2 Normal-state Resistivity of Nb_3Sn

Resistivity measurements on chemical vapour deposited Nb_3Sn films have been carried out by Woodard and Cody(1964) in the range $18-850^{\circ}K$, and is well described by the expression :

$$\rho(T) = \rho_o + \rho_1 T + \rho_2 \exp(-T_o/T) \qquad (6.1)$$

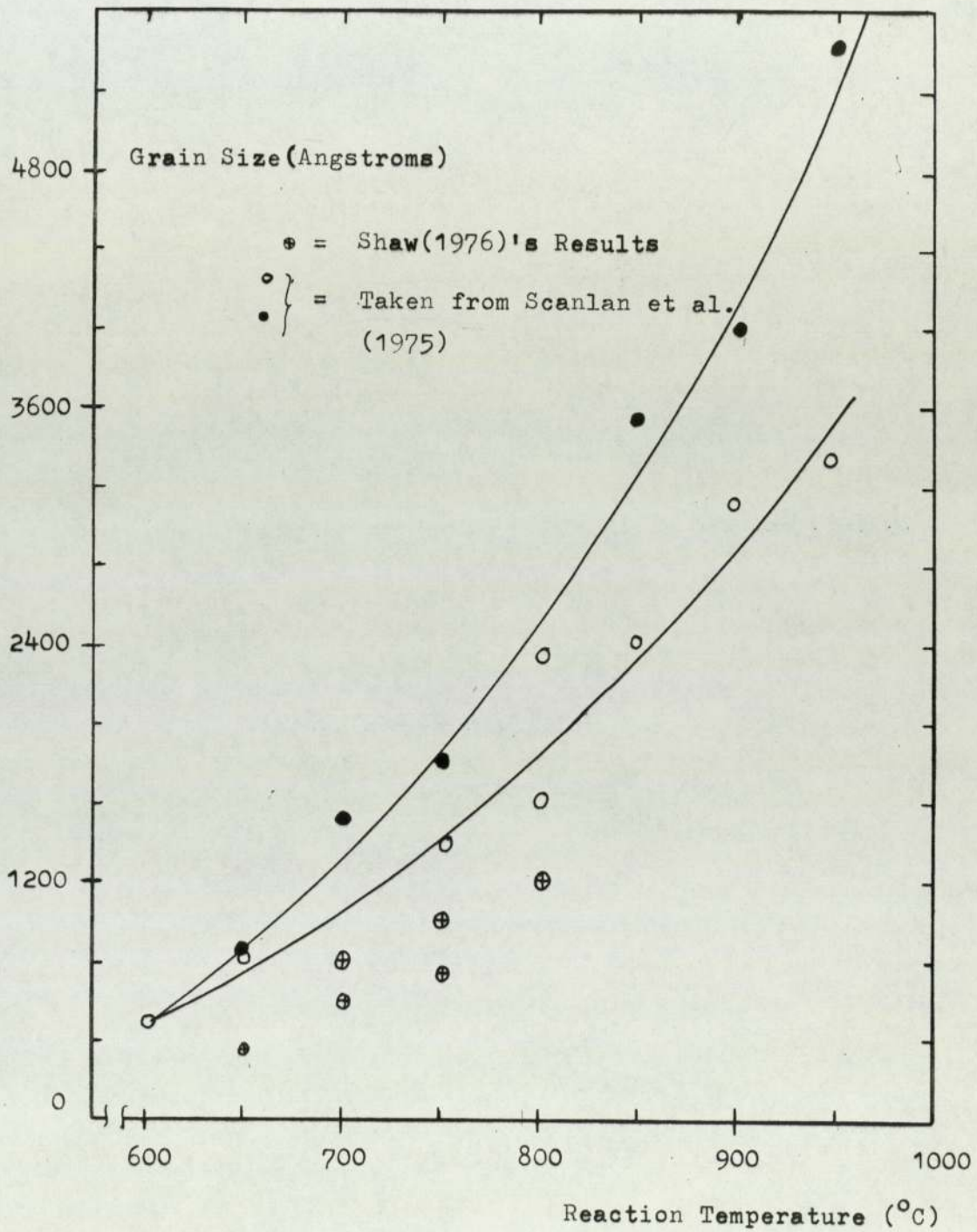

Figure 6.2 Average grain size as a function of reaction temperature. (After Shaw, 1976).

where $\rho_o = 1.8 \times 10^{-5}\ \Omega$-cm, $\rho_1 = 4.7 \times 10^{-8}\ \Omega$-cm/°K, $\rho_2 = 7.5 \times 10^{-5}\ \Omega$-cm, and T_o is a constant, found to be 85°K. This behaviour is entirely different from the usual temperature dependence of both transition and non-transition metals, where the resistivity dependence on the temperature can be described by a power law.

In the present investigation, the relationship in equation (6.1) was used to fit the temperature dependence of resistivity of a film of Nb_3Sn and the following values were obtained ; $\rho_o = 2.2 \times 10^{-5}\ \Omega$-cm, $\rho_1 = 4.1 \times 10^{-8}\ \Omega$-cm/°K , $\rho_2 = 5.8 \times 10^{-5}\ \Omega$-cm and $T_o = 105$°K , respectively. This equation was also applicable to the resistivity of films of (mixed phases) Nb_6Sn_5 and $NbSn_2$, and the results obtained for one such film were $\rho_o = 11 \times 10^{-5}\ \Omega$-cm, $\rho_1 = 4.9 \times 10^{-8}\ \Omega$-cm/°K , $\rho_2 = 8.4 \times 10^{-5}\ \Omega$-cm and $T_o = 83$°K , respectively.

6.2.1 Size Effect

As the thickness of a metal film becomes comparable in magnitude with the electron mean-free-path (m.f.p.), the film boundaries impose a geometrical limitation on the movement of the conduction electrons. The dependence of electron m.f.p. on film thickness (size effect) has been derived by Fuchs(1938) in terms of the reduced resistivity (ρ_F/ρ_B) and reduced film thickness (d/l_B) , where the suffices F and B refer to film and bulk material, respectively. The limiting form of ρ_F/ρ_B for thick and very thin films were given by equations (2.33) and (2.34) :

$$\rho_F/\rho_B = 1 + (3/8)(1-p) \qquad (\gamma > 1) \qquad (6.2)$$

and

$$\rho_F/\rho_B = \frac{4}{3}\frac{(1-p)}{(1+p)}\frac{1}{\ln(1/\gamma) + 0.4228} \qquad (\gamma \ll 1) \qquad (6.3)$$

where p is a fraction of electron suffering specular (elastic) scattering. If ρ_B and l_B are known then p can be determined from these equations. Most of the early work has been carried out on monovalent metal films to which the free electron theory is considered to be best applicable. Although the free electron model can not explain the normal resistivity behaviour of Nb_3Sn (Woodard and Cody, 1964), the effect of m.f.p. was observed in an oxidized Nb_3Sn film of the present work and was determined by means of equation (6.6) ,described below.

If we rewrite equation (6.2) as :

$$\rho_F \cdot d = \rho_B \cdot d + \frac{3}{8} l_B(1-p) \qquad (6.4$$

and define

$$l_{eff} \equiv l_B(1-p) \quad , \qquad (6.5)$$

then equation (6.2) becomes :

$$\rho_F \cdot d = \rho_B \cdot d + \frac{3}{8} l_{eff} \qquad (6.6)$$

Following the same technique of determination of ρ_B and l_B used by Mayer(1959) (equation (6.6)),the mean free paths at various temperatures were evaluated, for film No.12 of the present work, as shown in Table (5.8). The values of l_{eff} were found to be in the range 1.35 - 28.7 nm for the corresponded temperatures in the range 300 - 20°K. Attempts were made to fit the curve of l_{eff} vs temperature, and was found to be in the form of :

$$l_{eff}(T) = l_o - a\,T + b\,e^{-T/T_o} \qquad (6.7)$$

where l_o = 2.1 nm, a = 3.06 x 10^{-3} nm/^oK, b = 38 nm and T_o = 60^oK. The effective m.f.p., l_{eff}, is of the order of atomic spacing (0.53 nm) when T ≃ 515^oK, see Fig.(5.24).

In order to find the specular parameter, p, we used the value of m.f.p. calculated from the free electron model by Cody (1964). According to his calculation, l = 2.8 nm if the total number of conduction electron per atom = 1. Substituting this value into equation (6.5) and using the present value of l_{eff} = 1.4 nm, we obtain a value of p = 0.5 . Thus the scattering process was neither completely specular nor diffused.

6.2.2 Saturation of Resistivity of Nb_3Sn at High Temperatures

Cohen et al.(1967) made a 'Fermi smearing' model (which is known as RCA model) to explain the temperature dependence of the resistivity of Nb_3Sn, observed by Woodard and Cody. Here they argued that if the Fermi level was within ± kT of sharp structure in the density of states, N(E) , then as the temperature was raised, the Fermi level could be expected to shift into a region of lower density of states causing a deviation from linearity in the resistivity at high temperatures. In this model, the density of states, N(E), is a step-function of the form:

$$N(E) = \begin{cases} N_o & , \quad E > 0 \\ \alpha N_o & -E_o < E < 0 \end{cases} \qquad (6.8)$$

where $-E_o$ is the lowest energy, i.e., at the bottom of the band, and α is a fraction of the conduction electrons with energy lying between $-E_o$ and zero. The case $\alpha \ll 1$ and $E_F(0) > 0$ corresponds to a nearly empty d band overlapping an s band, and the case $\alpha \gg 1$, $E_F(0) < 0$ corresponds to a nearly full d band. $E_F(0)$ is the Fermi level at zero temperature. Applying the relation derived by Wilson (1938) for the electrical resistivity in transition metals and considering only s-d scattering due to phonons, they obtained :

$$\rho_{ph}(T) = A(T/\theta)^3 \int_0^{\theta/T} \left\{ \frac{x/2}{\sinh(x/2)} \right\}^3 \cdot \log \frac{1+F_\alpha(T)(1+e^x)}{1-F_\alpha(T)(1-e^{-x})} \, dx \qquad (6.9)$$

where F (T) is the Fermi distribution at the band edge, defined by

$$F_\alpha(T) \equiv \left[1 + \exp \left\{ -E_F(T)/kT \right\} \right]^{-1} ,$$

A is a constant and a Debye spectrum for the phonon is assumed, with characteristic temperature θ. By this way good agreement between the model and the resistivity data of Nb_3Sn (Woodard and Cody, 1964) was observed, see Fig.(6.3).

Although the RCA model is applicable to Nb_3Sn the non-linear variation of $\rho_o(T)$ with temperature can not be tied in with niobium, even with a more accurate solution of the semi-classical Boltzmann equation and accurate band structure information. According to Mattheiss(1975) niobium based compounds seem not to be fundamentally different in these respects from niobium , based on

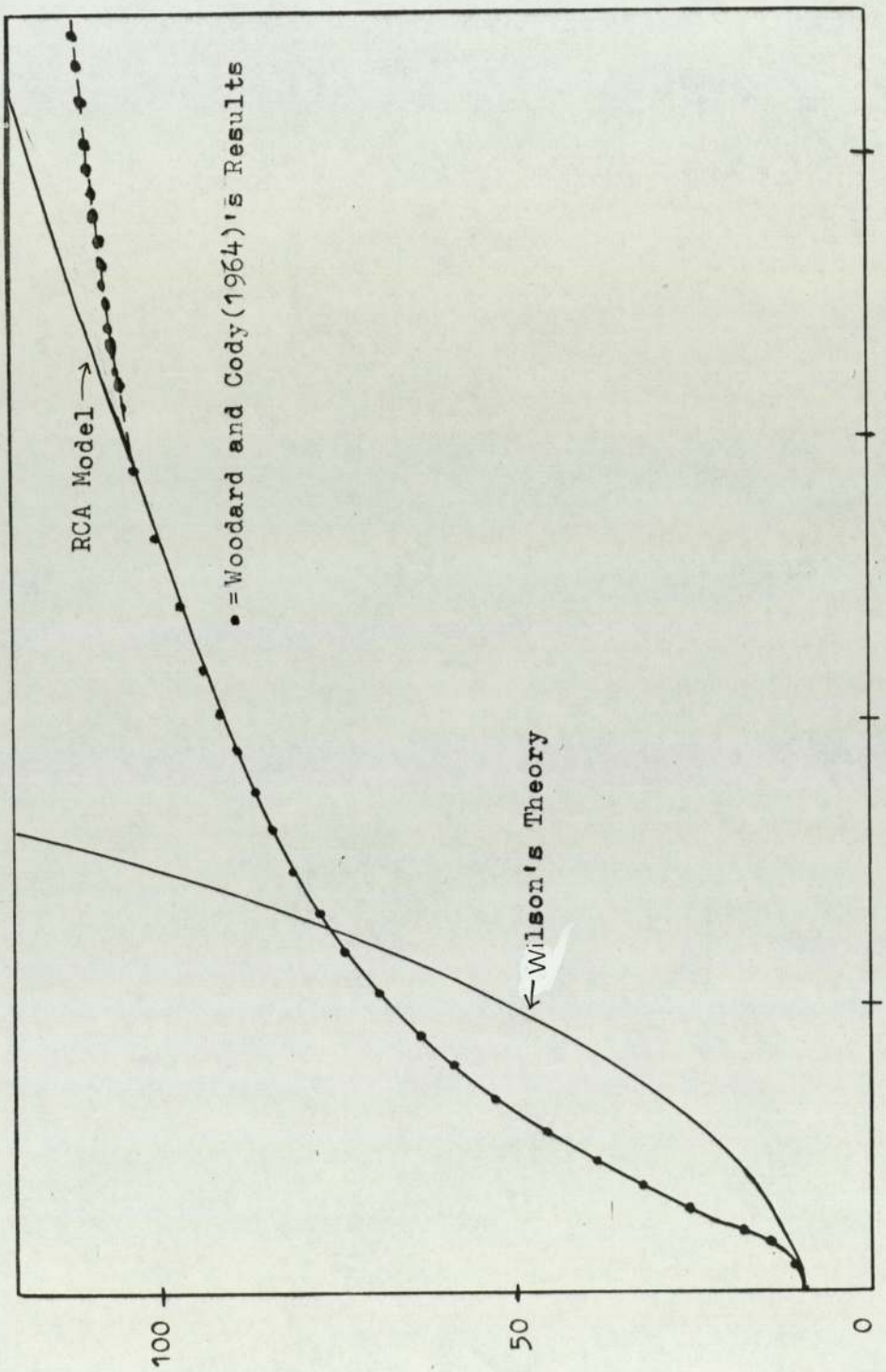

Figure 6.3 Resistivity against temperature of Nb_3Sn showing the 'saturation' of resistivity at high temperature. (After Cohen et al.(1967)).

the calculated shape of N(E) for both cases.

It has been observed by Mooij(1973) that $d\rho/dT$ for concentrated transition-metal alloys decreases to zero in the vicinity of 150 $\mu\Omega$-cm at high temperatures. He concluded that this was due to the electron mean free path at high temperatures was comparable with the interatomic spacing. Fisk and Webb(1976) have recently extended Mooij's argument to A-15 materials. They suggest that at high temperatures, the mean free path , l , is of the order of the interatomic spacing, and this essentially provides a maximum ("saturation") value for the resistivity.

This idea of saturation led Wiesmann et al.(1977) to propose a simple model for characterising the electrical resistivity in Nb_3Ge and Nb_3Sn. They assumed that $\rho(T)$ was resulted from a competition between an ideal dependence, ρ_{ideal}, and some limiting value given by ρ_{max} which is essentially 'shunting' ρ_{ideal} at high temperatures, described by :

$$\rho(T)/\rho_{max} = A/(1 + A) \qquad (6.10)$$

where

$$A = \rho_{ideal}/\rho_{max} \quad , \qquad (6.11)$$

and

$$\rho_{ideal}(T) = \rho_{ideal}(0) + \rho_{e\text{-}ph}(T) \qquad (6.12)$$

with $\rho_{e\text{-}ph}(T)$ approaching $\rho_1(T)$ in the high-temperature limit. From expressions above, Wiesmann et al.(1977) observed that the temperature dependence of resistivity of Nb_3Sn could be fitted to better than 1%.

In the present investigation, the electron mean-free-path was deduced from the resistivity measurements in the temperature range 4-300°K. The temperature dependence of the mean free path which

has been plotted in Fig.(5.24) (see previous section) seems to support the idea of "saturation" suggested by Wiesmann et al.(1977). The effective mean free path was found to be decreasing as temperature increased, and was of the order of the lattice parameter (by extrapolation) at temperatures above 500°K.

6.3 Depression of T_c of Nb_3Sn due to Induced Damage

It has been discovered by Swartz et al.(1964) that high energy neutrons (E > 1Mev) cause the T_c of β-tungsten compounds to be depressed. For a total flux of 1.5×10^{18} neutrons/cm^2, depressions of 0.1 - 0.22°K were observed. Using higher dose, 5×10^{19} neutrons/cm^2 , larger depressions of 1 - 13°K for commercially prepared Nb_3Sn tapes have been achieved by Bett(1974). Large depression up to 17°K has also been reported by Sweedler et al. 1974) for several Nb_3X compounds (X= Al, Sn, Ga and Ge).

There are at least three possible effects of neutron irradiation : 1) interchange of atoms between sites, 2) creation of interstitial-vacancy pairs and 3) creation of new elements. Sweedler et al.(1974) have demonstrated that in case of their Nb_3X compounds, the principal result is the exchange of atoms between sites. To describe the position of the atoms in the unit cell of A_3B structure, they introduced the Bragg-Williams long-range-parameter, $S \equiv (P-r)/(1-r)$, where $0 \leqslant S \leqslant 1$, P is the probability of an A site being occupied by an A atom (Nb), and r is the fraction of A atoms in the binary alloy. Following Aronin(1954) who derived a relationship between S and the flux n, to describe results of neutron-induced order-disorder transformations in Ni_3Mn and Cu_3Au,

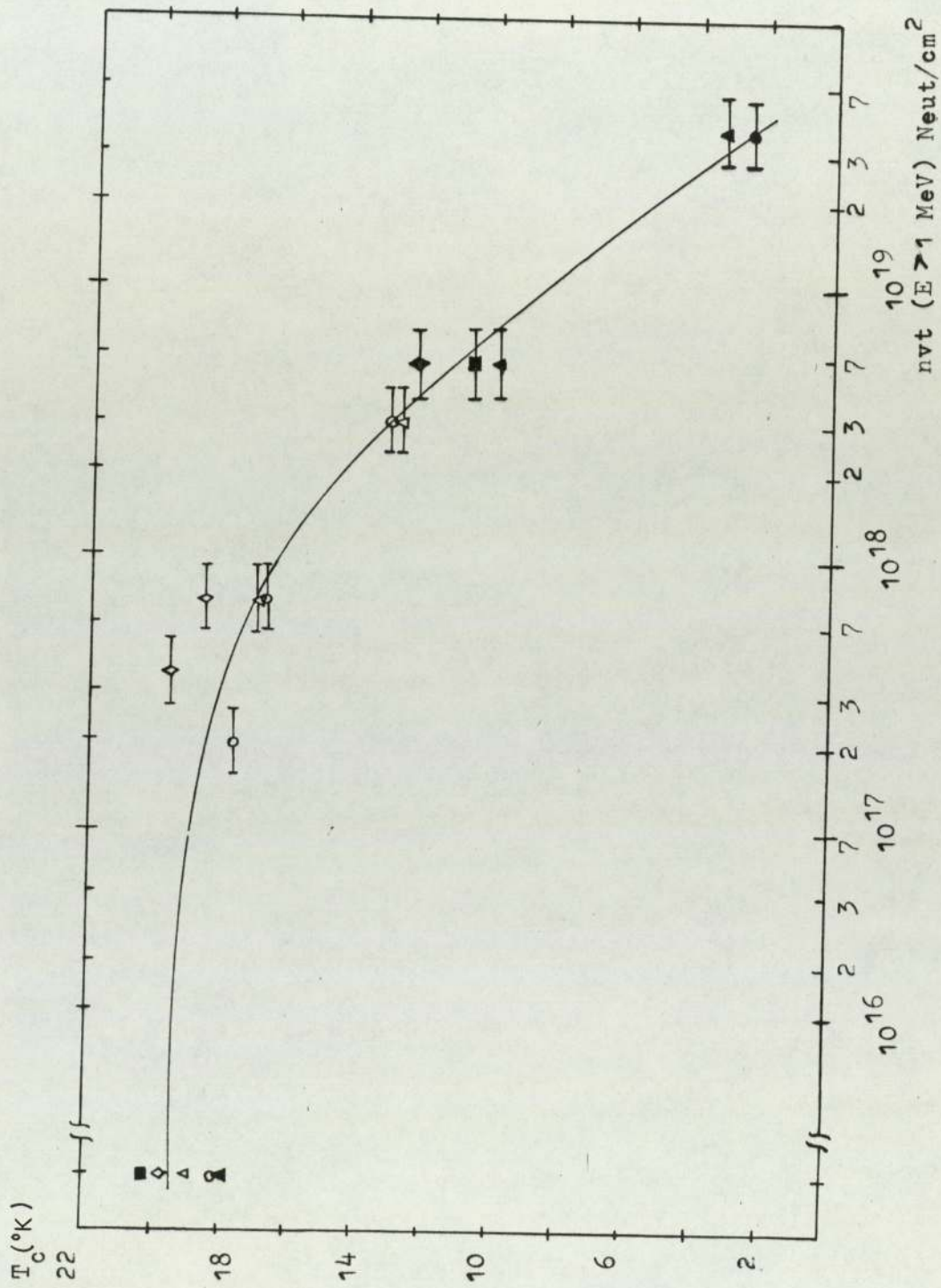

Figure 6.4 Superconducting transition temperature against neutron dose.
(After Sweedler et al.,1974).

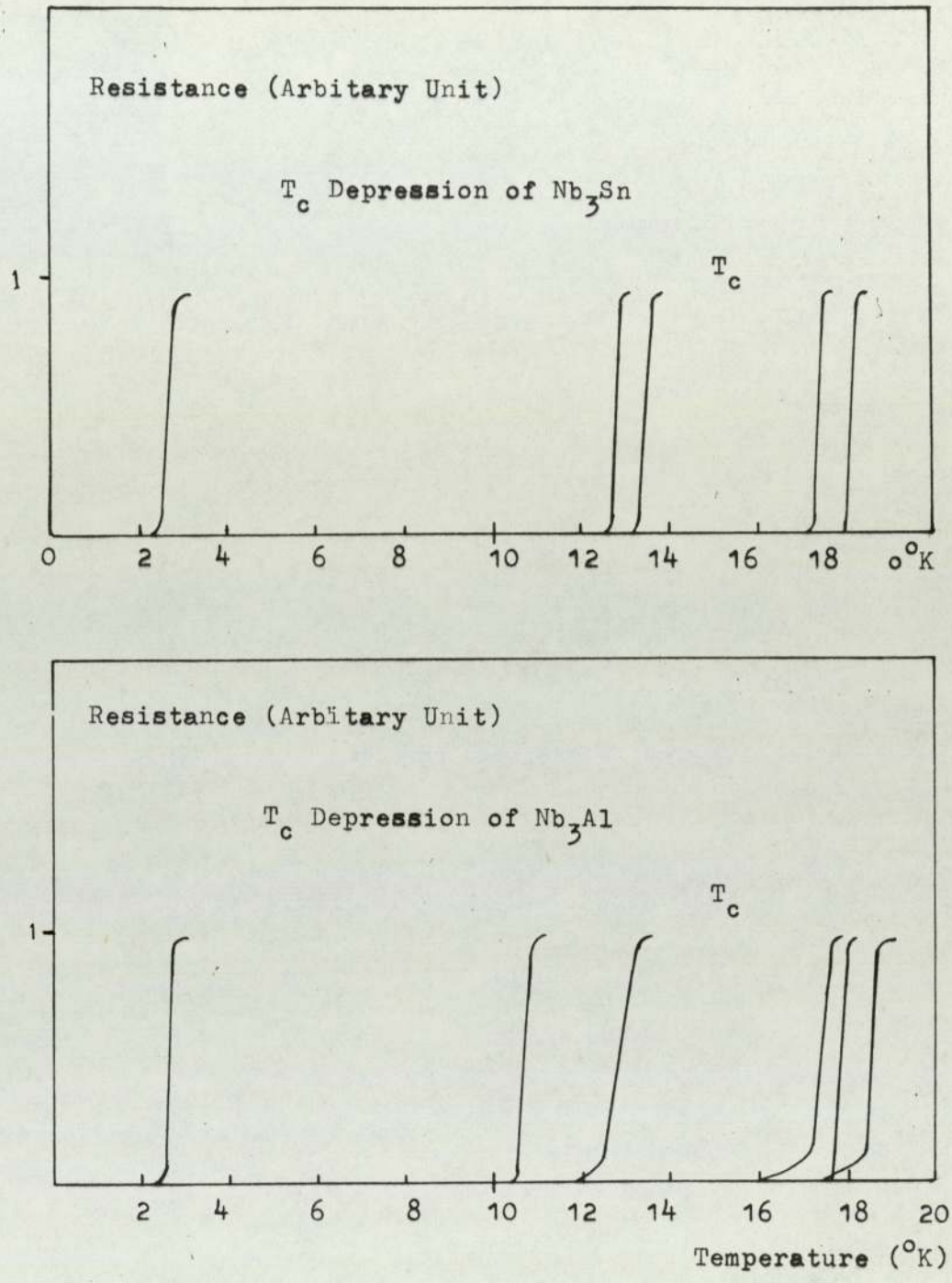

Figure 6.5 Depression of T_c for Nb_3Sn and Nb_3Al due to neutron irradiation.(After Sweedler et al., 1974).

they used the expression :

$$S = S_o e^{-k'n} \qquad (6.13)$$

where S_o is the value of S before irradiation, n the neutron flux and k' is a proportionality constant. With $k' = 9 \times 10^{-21}$ cm^2/neutron , for Nb_3Sn, the T_c could be related directly to S through the neutron dose, n. Fig.(6.6) illustrates the plot of the reduced transition temperature, T_c/T_{co}, against the reduced order parameter, S/S_o , and $S_o = 1$ for complete order at $T_c = T_{co}$. The exponential dependence of T_c on S is given by

$$T_c = T_{co} \exp\left[-\alpha(1-S/S_o)\right] \qquad (6.14)$$

where $\alpha = 5 \pm 1.5$, $T_{co} = 18.1^{\circ}K$.

Recently Meyer et al.(1974) have demonstrated that the T_c's of superconducting Nb_3Sn films can be reduced from an initial T_c of $17.8^{\circ}K$ to $2^{\circ}K$ by implantation of Argon ions and this decrease could be attributed to damage effects and probable change in long range order. Testardi et al.(1975) have observed that, although composition is important, it is not the most crucial factor responsible for the high T_c's in the sputtered Nb_3Ge films. From Rutherford backscattering, and other means of measurements , they concluded that a key factor which determined whether the T_c was low or high, was the presence or absence of microscopic defects.

6.3.1 Depression of T_c due to Film Thickness Reduction

As has been indicated in the previous section that a reduction in T_c resulting from neutron bombardment has been attributed to an increase in defects. In the present work, the

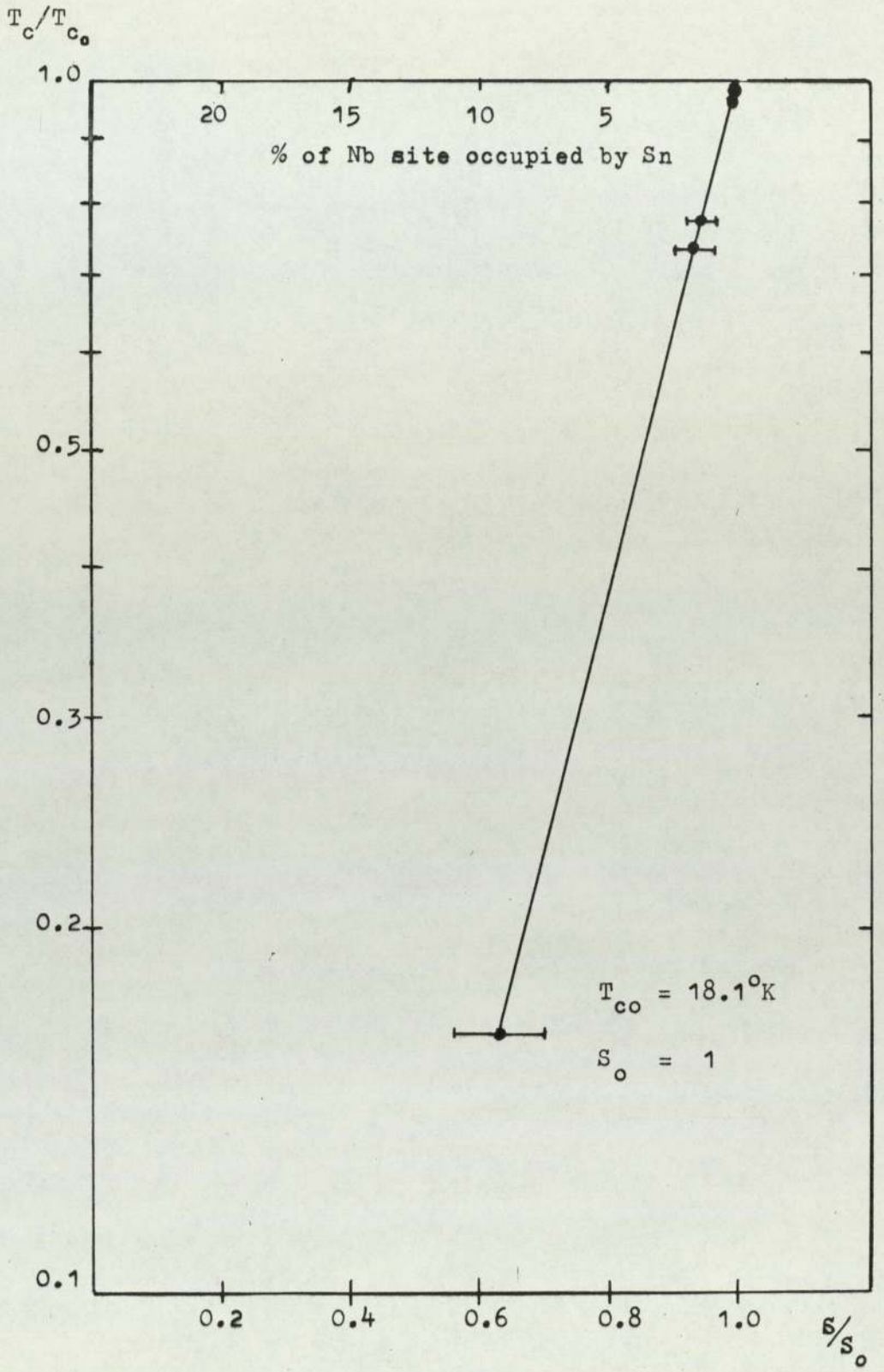

Figure 6.6 Reduced transition temperature , T_c/T_{c_o}, against reduced long-range-order parameter, S/S_o , for neutron irradiated Nb_3Sn. (After Sweedler et al., 1974).

T_c depression resulted from the (metal film of Nb_3Sn) thickness reduction which in turn could be due to the increase in proportion of defects in the metal layer as one approaches the substrate. In order to explain this phenomenon , let us consider a model of the film structure as shown in Fig.(6.7).

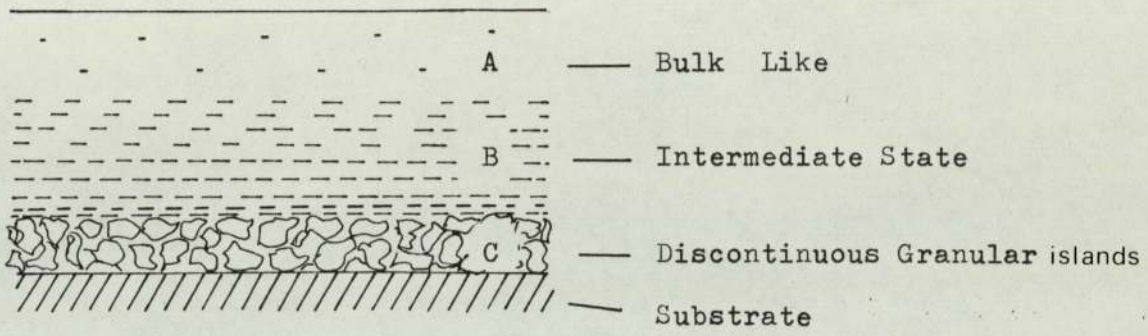

Figure 6.7 Profile of a film structure.

Initially when a film is being prepared, atomic condensation takes place in the form of three dimensional nuclei (islands), and as the deposition process continues, these islands will grow to form a continuous film. Up to this stage, the structural disorder could be considerably increased. After further deposition of film beyond this thickness, the structure of the film will be consistent and usually approaching the structure of bulk material.

The experimental observations, following a series of oxidations, seems to confirm this. At first oxidation caused small decreases in T_c and then large changes were observed at about $14^{o}K$.

When the metal layer was reduced to about 10 nm (estimated from ellipsometric measurements) no transition to the superconductive state was observed down to the lowest temperature of 2°K which could be produced with the equipment.

Using the model assumed above (see Fig.(6.7)), the apparent knee of the T_c against resistivity ratio curve in Fig.(5.21) would correspond to the metal layer of thickness in the A and B regions (about 25 nm). Larger T_c depression would occur when the Nb_3Sn layer was reduced to the region B (about 17 nm). The disappearance of T_c could be attributed to the rapid increase in the proportion of defects as the region B of the layer was reduced. Because the film was still electrically continuous, we would think that the thickness of region C should be less than 10 nm. If we compare this film at this thickness with a niobium film of the same thickness which has been observed by Salter(1973) to have T_c of about 8°K, then the disappearance of T_c of our film could be due to either Nb_3Sn is more sensitive to defects or more defects were created during the processes of Nb_3Sn formation after the niobium film had been deposited , i.e., during the diffusion and alloying processes. Another point to observe is that if the diffusion of tin had not taken place through out the niobium film a film of niobium would be left near the quartz substrate.This itself would give a T_c above 2°K for a niobium film of about 5 nm has a T_c above 4.2°K (Salter,1973).

The depression of T_c for Nb_3Sn due to neutron irradiation has been related to the long-range-order defects by Sweedler et al. (1975),as described in the previous section. If we extend our

argument to this case, using our model, it would be seen that , before any neutron bombardment, high T_c was observed in their films because these films were thick (more than a few hundred nanometers), i.e., the proportion of defects present in the films was low. Equivalent to this would be the initial T_c observed before any oxidation of our film. Subsequent irradiation would introduce more defects and the film layers would be partly well ordered and partly disordered, thus, T_c depression resulted. The reduction of T_c due to irradiation would be caused by the presence of larger proportions of defects in the films similar to that assumed in our model. A comparision between the situations of the irradiated films and our oxidized film is illustrated in Fig.(6.8).

In fact the argument of our model can be applied to other higher T_c β-tungsten compounds such as Nb_3Ge, Nb_3Ga, V_3Si and V_3Ge in which the T_c depression due to induced damage has been reported (e.g., Sweedler et al.1974, Testardi et al.,1976 , Testardi et al., 1977). The model is also relevant when considering the variation of T_c for films of different thicknesses since for thin films the regions B and C (Fig.6.7) near the substrate would constitute larger proportion of the films.

6.4 Correlation Between T_c and Resistivity Ratio

In the present work a correlation between T_c and resistivity ratio, $\rho_{300}/\rho_{res.}$, was observed for films of different thicknesses from 27 nm to 510 nm and for a film of consecutive reductions in thickness from 58 nm to 10.5 nm by oxidation. This is illustrated in Figures (5.11) and (5.21). The resistivity ratio in Fig.(5.11) ranges from 1 to 4 at which the critical temperature approaches the bulk value of 18°K.

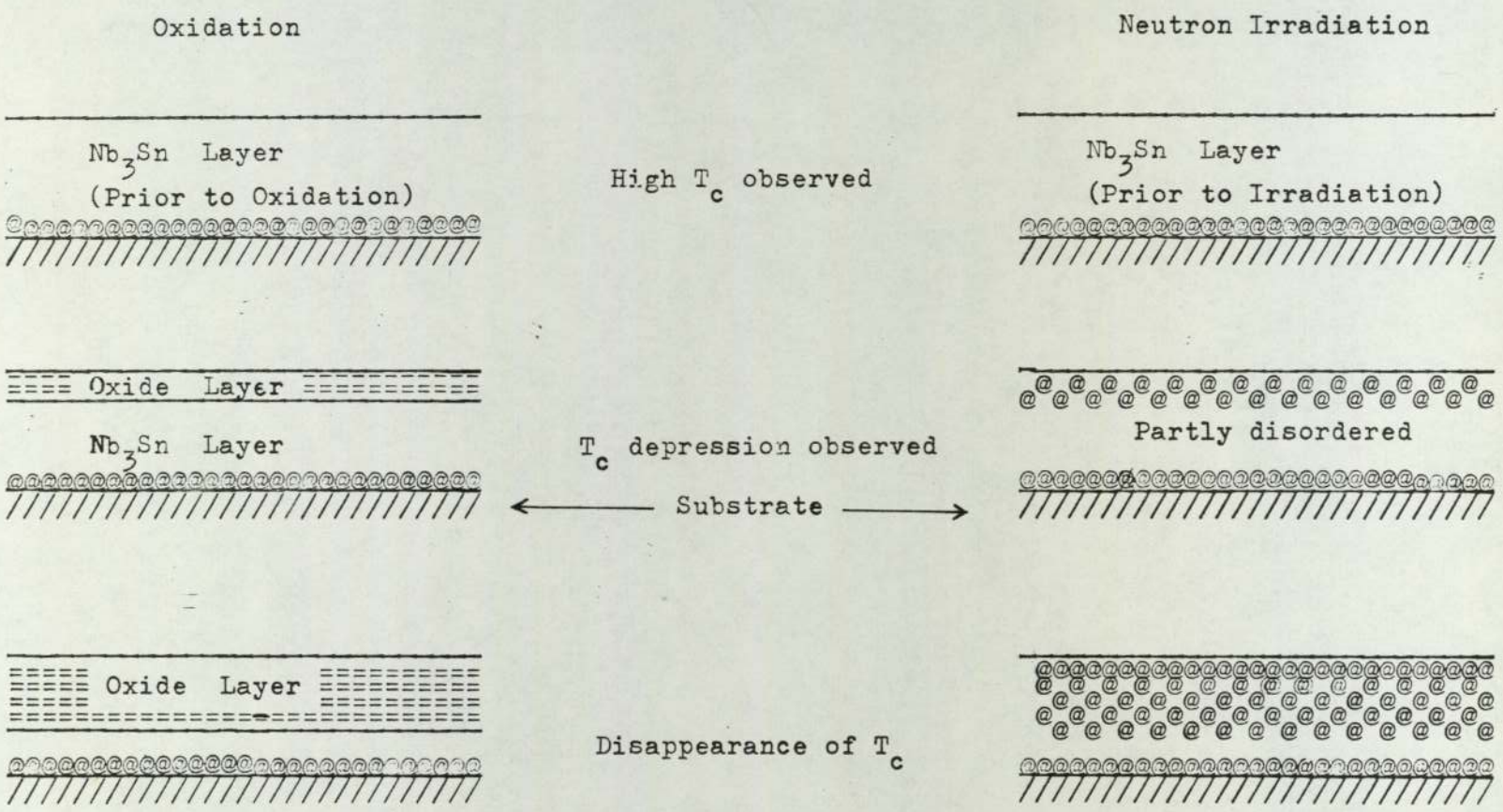

Figure 6.8 A comparision between the situations of an oxidized Nb_3Sn film and an irradiated Nb_3Sn film.

From the studies of T_c depression of Nb_3Sn films discussed in the previous section, it is evident that this phenomenon results from defects present in the samples after induced damage. If we consider resistivity ratio as a measure of the quality of a film (a low resistivity ratio indicating poor quality) then it would appear that T_c approaches the bulk value of 18°K as the film quality improves. This argument is also evident from other high T_c compounds with niobium or vanadium based compounds because a similar correlation has also been observed in these compounds. The correlation between T_c and resistivity ratio, ρ_{300}/ρ_{25}, over the range of resistivity ratios from 1 to 3 for Nb_3Ge sputtered films was first reported by Testardi et al. (1975). Subsequently, this universal behaviour has been found in V_3Si and V_3Ge by Testardi et al.(1977). Dynes et al.(1977) obtained similar results from the study of the ^4He bombardment for Nb_3Ge, Nb_3Sn, V_3Si and V_3Ge. So far no theoretical explanation has been proposed for this correlation.

In fact a similar correlation between T_c and ρ_{300}/ρ_{10} has been observed in niobium films by Salter(1973) and later in tantalum films by Aguado Bombin(1975). From the study of tantalum films, two empirical relationships between T_c and resistivity ratio have been proposed by Aguado Bombin and Neal(1976) :

$$T_{cf} = T_{cb}\left[1 - \exp(-k^*\rho_{300}/\rho_{res.})\right] , \quad (6.15a)$$

where T_{cf} and T_{cb} are the critical temperatures of thin films and bulk material, respectively and k^* is a constant, found to be 0.65 for tantalum.

Another equally good expression relating T_{cf} and $\rho_{300}/\rho_{res.}$

was given as

$$T_{cf} = T_{cb}\left[1 - k_1^* \exp(-\rho_{300}/\rho_{res.})\right] , \quad (6.15b)$$

where k_1^* is another constant. Aguado Bombin and Neal have also applied equation (6.15b) to Salter's results for niobium thin films and to Testardi et al.(1975)'s results for Nb_3Ge , and a similar agreement was observed.

When these two expressions were applied to the results of two niobium films prepared in the present work which were successively oxidized (Table (5.6)), a very good agreement was observed, as shown in Figure (5.20b). k^* and k_1^* were found to be 1.03 and 1.46 respectively, with $T_{cb} = 9.3^oK$. For Nb_3Sn films which were subjected to a similar treatment , the plots of T_c and $\exp(-\rho_{300}/\rho_{res.})$ are shown in Fig.(5.23). The maximum value of $\rho_{300}/\rho_{res.}$ for film No.12 was 3.3 but for film No.143,the maximum resistivity ratio was in the region of 4.6 since it was a thicker film. For values of $\rho_{300}/\rho_{res.}$ less than 3.6 both films had k_1^* of about the same order(0.63) but the intercept (T_{cb}) for film No.12 was higher than that for film No.143. If it is assumed that film No.12 was inherently a film of better quality and reisistivity ratios higher than 3.6 could have been achieved (i.e., if the initial film thickness of both films were of the same order) then a k_1^* value of 3.5 as for film No.143 with higher resistivity ratios might have given a T_{cb} of about 19^oK. This value is greater than that has been observed for bulk Nb_3Sn(Matthias,1954). The present results suggest that values of T_c for bulk Nb_3Sn greater than 18.3^oK might be achieved if preparation technique could be improved to give bulk of higher quality.

6.4.1 Critical Currents

The critical currents in zero magnetic field of some Nb_3Sn films were measured during the present work. Figures (5.25) and (5.26) show the variation of the critical currents with temperature. The smooth curves were calculated from equation (2.72) by assuming that $I_c(T)/I_c(0) = J_c(T)/J_c(0)$, i.e.,

$$I_c(T)/I_c(0) = (1 - T_R^2)^{\frac{3}{2}} (1 + T_R^2)^{\frac{1}{2}} \qquad (6.16)$$

where $I_c(0)$ is the critical current at absolute zero. From the calculated curves, using equation (6.16), the critical currents at absolute zero were found to be 0.64 and 2.0 Amp. for two films of thicknesses of 58 and 321 nm, respectively. The critical current densities, $J_c(0)$, were estimated from $I_c(0)$ divided by the cross-sectional area of the films and were of the order of about 5×10^5 Amp./cm^2 which is about a factor of two smaller than that observed by Cody and Cullen(1964). This could be due to the effect of Joule heat along the electrical leads and/or 'weak spots', such as small regions which were thinner or narrower than the rest of the films, or had slightly different metallurgical properties, thus the films could be driven normal before the true critical currents of the films were reached.

6.5 Optical Constants of Nb_3Sn

The absorption of Nb_3Sn in the visible region was so high that transmittance of a film of a few tens of nanometers in thickness is nearly negligible. That is films of thickness more than 50 nm could be considered as opaque. Table (5.9a) shows the optical

constants at a radiation wavelength of λ = 549 nm , of some films evaluated from the ellipsometric measurements. All of the films were of the thickness more than 50 nm. The k values of all films agreed to within ± 0.1 but the n values varied from 3 to 1.7. In attempts to explain this variation, a series of computed ψ and Δ due to the presence of an oxide layer were used.In general,when an oxide grows on a clean metal surface the values of n and k (i.e., pseudo constants) are reduced. From the results obtained,the highest value of k was in the region of 2.5 and the corresponding n value was 2.3. It is reasonable to assume in the first instance that these characterise a clean surface for the purpose of this exercise. Thus, the optical constants of Nb_3Sn were assumed to be n=2.3 and k = 2.5 with n_{oxide}=2.5 and k_{oxide}= 0. As oxide thickness increased the psuedo constants computed from equations (2.89) - (2.95b) were decreased , see Table (5.9b), and the n values decreased more rapidly than the k values. Therefore if we assumed that an oxide layer of about 2 nm was already formed during the preparation process before exposure to the atmosphere, then this would lead to the difference of n by ± 0.2 or more but the k value would differ by only ± 0.1. Hence film numbers 6, 12 and 115 would have oxide layers of thicknesses of about 3.5, 1 and 6 nm, respectively. This assumption could not explain the high value of n = 3 for film number 105. Avery(1950) has observed a dramatic change of optical constants for very thin layers (2.5 nm) of tin. He found n = 3 and k = 0.5 despite the bulk values of 1 and 4.2, respectively. It could be that this film (No.105) had a thin layer of tin on its surface due to excess tin which did not evaporate

away completely during the film preparation. An unoxidized Nb_3Sn surface could therefore have optical constants n = 2.3 ± 0.2 and k = 2.5 ± 0.1 at a wavelength of 549 nm.

6.5.1 Ellipsometric Measurements of Nb_3Sn at Various Wavelengths

The variation of optical constants of Nb_3Sn with wavelength of radiation are presented in Table (5.10). The absorption coefficient, k , was larger than 2 and n was less than 2 for λ_o longer than 500 nm but for λ_o = 499 nm , n was about 4 and k was about 0.9 which suggested that Nb_3Sn could become transparent, i.e., k = 0 , in the shorter wavelengths of radiation. Optical constants at longer wavelength, in the region of 1-20 μm have been determined by Golovashin(1971), using the reflectivity method. Their results are shown in Figures (6.9) and (6.10) respectively. Optical constants at λ_o = 549 nm obtained by extrapolation of their results are n = 2.5 and k = 3, compared with n = 2.3 and k = 2.5 of us obtained from the present work.

6.5.2 Optical Constants of Oxide Layer

It has been demonstrated by Archer(1962) that Ψ and Δ curves of transparent films of different refractive indices (n larger than 1.2) do not cross, so that a given set of measurements of ψ and Δ is a unique characteristic due only to the refractive indices and the thickness of the films.

Although a set of ψ and Δ was obtained from the successive

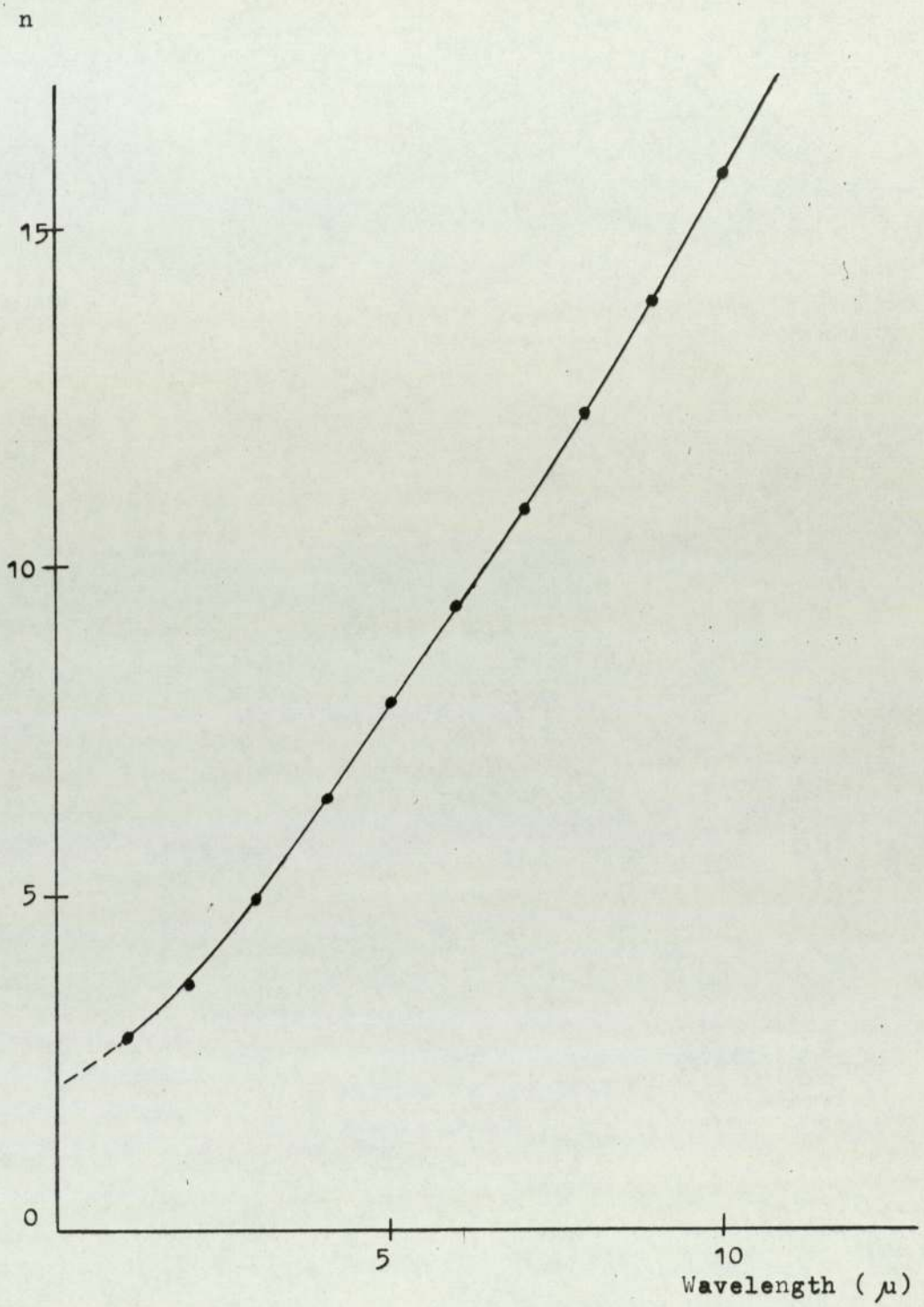

Figure 6.9 Variation of n with respect to wavelength for Nb_3Sn.(After Golovashkin et al.,1971).

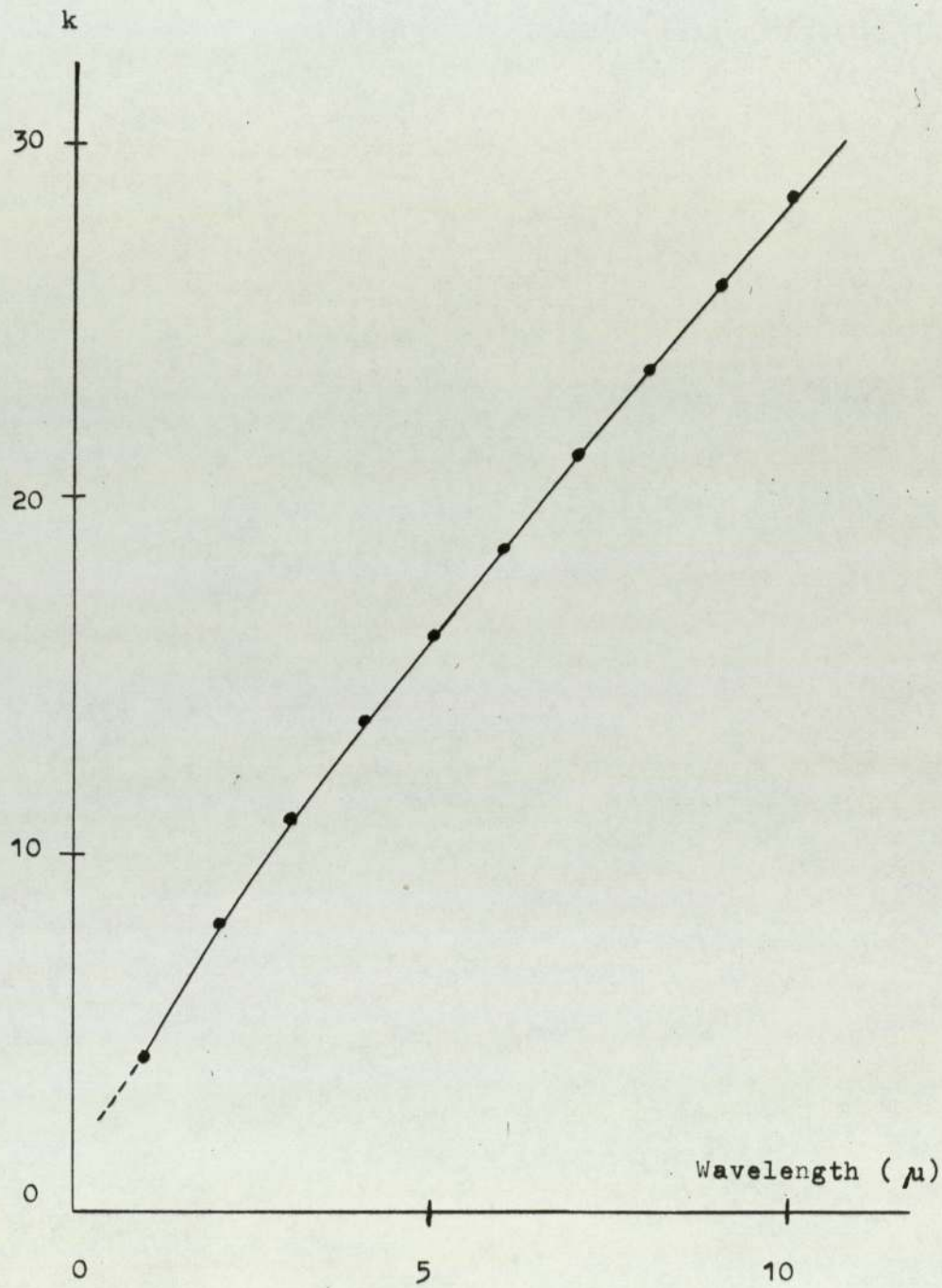

Figure 6.10 Variation of k with respect to wavelength of radiation. (After Golovashkin et al., 1971)

oxidations of a film in the present work, the interpretation of the results was more complicated since the initial Nb_3Sn film thickness was only≈60 nm. As the Nb_3Sn layer was reduced, the effect of multiple reflection from the quartz substrate had to be taken into account for Nb_3Sn could be no longer considered as opaque. Thus, the computing programme for two layer films, as described by O'Shea(1971), was used for this purpose. The advantage of using a film of this thickness was that the ψ and Δ were sensitive to the change in thickness of the Nb_3Sn layer which enabled the size effect to be determined from the electrical measurements. The variation of Ψ_{cal} and Δ_{cal} with respect to oxide and film thicknesses, at a wavelength of radiation of 549 nm , is shown in Table (5.11) and in Figures (5.29) and (5.30). The consequent deduction of the thickness of the Nb_3Sn layer is presented in Table (5.12). The calculated curves could be fitted to the observed data in the region where the metal film was thicker than about 18 nm. When the metal film was thinner than this thickness, deviation was observed, which suggests that the assumed parameters (i.e. the optical constants of the oxide and metal layers) were no longer constant. This could be resulted from the increase in structural defects as has been discussed in section 6.3.1.

The refractive index of the oxide at the wavelength of 549 nm was found to be 2.5 ± 0.2. The composition of the oxide was not known. Results from x-ray diffraction indicated that the layer was amorphous since no diffraction line was observed from angle $2\theta = 20^{\circ}$ to 140°. No report of the optical measurements of oxides of Nb_3Sn has appeared in the literature so far but the

refractive index of the oxide in the present work was very close to the refractive index of niobium oxide which has been observed by Young and Zobel(1966) to be 2.37 . (Refractive index of tin oxide is about 1.8 in the visible region).

****

CHAPTER 7 : CONCLUSIONS AND SUGGESTIONS FOR FURTHER WORK

7.1 Conclusions

Thin alloy films of the niobium-tin system investigated in the present work could be divided into two groups; (i) for alloying temperatures above 650°C, single phase of Nb_3Sn was obtained with a lattice parameter, a_o, in the range of 5.28-5.29 Angstroms , whereas (ii) if the alloying temperature was below 650 °C , mixed phases of Nb_6Sn_5 and $NbSn_2$ were found. In the latter case, superconductivity was observed at tempertures 2.6-2.8°K whilst transition temperatures above 10°K were observed in Nb_3Sn films. Niobium oxide was detected in some Nb_3Sn films (Table(5.3)).

A structural transformation of Nb_3Sn from cubic to tetragonal at 43°K has been reported by Maifert et al.(1969), using an x-ray diffraction technique but this effect was not be observed from the resistivity measurements in the present work, which suggests that either the structural transformation did not occur in the Nb_3Sn of the present investigation or that the temperature dependence of resistivity is insensitive to this change.

Anomalous temperature dependence of resistivity has been found by Woodard and Cody(1964) who observed that resistivity at high temperatures deviates from linearity. Both Nb_3Sn films and films of mixed phases of Nb_6Sn_5 and $NbSn_2$ could be fitted with a similar expression used by them, i.e., $\rho(T) = \rho_o + \rho_1(T) + \rho_2 \exp(-T_o/T)$.

Wiesmann et al.(1977) have proposed a model to explain the deviation of resistivity from linearity at high temperatures on the assumption that the mean free path of Nb_3Sn is of the order of the lattice spacing, causing the resistivity to saturate. This

is in good agreement with the observation of the temperature dependence of the mean free path evaluated from the resistivity measurements of an oxidized Nb_3Sn film of the present work. Even-though the measurements were carried out within the lower temp-erature range, 2-300°K, the tendency for the mean free path to become smaller as temperature increases can still be seen, as shown in Fig.(5.24). By extrapolation to higher temperatures, mean free paths of the order of the atomic spacing were estimated to be at temperatures above 500°K. This temperature dependence of mean free path was well described by an expression of the form :

$$l = l_o - aT + b\exp(-T/T_o) \qquad (7.1)$$

where l_o = 2.1 nm, a = 3.06 x 10^{-3} nm/°K , b = 38 nm and T_o = 60°K. In addition to this, if the free-electron model was applied assuming one conduction electron per atom , the specular parameter, p, was found to be 0.5, i.e., the process of scattering was neither completely diffused nor entirely specular.

The depression of the critical temperature of Nb_3Sn has been discussed according to the model proposed in the present work. The essence of the argument was that the T_c depression was due to the increase of the proportion of the defects present in the films. In this way, T_c depression produced by any means (e.g., neutron irradiation, ^4He bombardment or variation of thickness either by oxidation of a thick film or depositing films of varying thicknesses) in any superconducting material either β-tungsten compounds or elements, could be understood. Nb_3Sn and niobium films in the present work were demonstrated as some examples of this.

The quality of superconducting films of Nb_3Sn could be indicated simply by means of the resistivity ratio, $\rho_{300}/\rho_{res.}$. A high T_c film was usually observed to have a high resistivity ratio. No resistivity ratio of less than unity was observed for any of the superconducting films. In fact, the correlation between T_c and resistivity ratio has been found in many superconducting materials, such as , tantalum,niobium and several β-tungsten compounds. Up to now,a clear theoretical explanation of this correlation has not been put forward. However, two empirical relations proposed by Aguado Bombin and Neal(1976), i.e.,

$$T_{cf} = T_{cb}\left[1 - \exp -k^{*}(\rho_{300}/\rho_{res.})\right] \qquad (7.2)$$

and

$$T_{cf} = T_{cb}\left[1 - k_1^{*}\exp(-\rho_{300}/\rho_{res.})\right] , \qquad (7.3)$$

have been used to test the correlation between T_c and the resistivity ratio of oxidized films of Nb_3Sn and niobium as well as Nb_3Sn of various thicknesses. These two relations gave good agreement with experimental results obtained previously in this laboratory for tantalum films.

For oxidized niobium films , good agreement was found between these empirical rules and the experimental results, giving $k^{*}$and k_1^{*} of 1.03 and 1.46 , respectively. In the case of Nb_3Sn, more than one straight line was needed to correlate the T_c and resistivity ratio. This suggests that the electronic characteristics of Nb_3Sn is more complicated than that of niobium, i.e., a more sophisticated relationship is required.

The optical constants of Nb_3Sn were found to be n = 2.3 ± 0.2 and k = 2.5 ± 0.1 respectively, for a radiation wavelength of

549 nm. Attempts were made to explain the uncertainty of the optical constants of some films. The lower values of optical constants were due to the presence of an oxide layer on the Nb_3Sn surface , estimated to be of the order of 20-50nm. Higher n value for a film was considered to be attributed to the presence of a very thin layer of tin on the Nb_3Sn surface.

The refractive index of the oxide was found to be 2.5 ± 0.2 at 549 nm, compared to 2.4 for niobium oxide and 1.8 for tin oxide. The composition of oxide was not known since no x-ray diffraction peaks were observed (after the oxidation had been completed). This suggests that the oxide layer could be amorphous. The presence of niobium oxide in some Nb_3Sn films was revealed by x-ray diffraction as shown in Table (5.3) (Mangkorntong and Neal,1977).

7.2 Suggestions for Further Work

In the recent years, a number of high T_c compounds with β-tungsten structure have been found to have similar electrical characteristics, e.g., "saturation" of resistivity at high temperatures, correlation between T_c and resistivity ratio and the depression of T_c due to structural defects. There are some aspects of these discoveries and of the present work which would merit further investigation :

1) Exploration for a new material with higher T_c. At the present, the highest T_c, 23°K, has been observed in Nb_3Ge (Gavaler et al.,1974 and Testardi et al.1974) but Nb_3Si has been predicted as having an even higher T_c if the β-tungsten phase of this material can be formed. The solid diffusion techniuqe employed in the

present work could be an attractive method for the preparation of this compound since, as silicon has a smaller atomic mass (28) than germanium (72) , it can be diffused into a niobium surface more effectively.

2) Observation of the electrical mean free path at high temperatures. The electrical mean free path of a film of Nb_3Sn was observed in the present work to decrease as the temperature increased up from low temperatures to room temperature and the resistivity seemed to approach a saturation value at a higher temperature. It would be very interesting to determine this parameter at higher temperatures, say $500^{\circ}K$ or above , so that the effect of saturation of resistivity, which is associated with the mean free path, could be clarified.

3) Examination of the film thickness dependence of T_c depression. In the present investigation, this effect has been demonstrated and a model of structural defects has been proposed. It is likely that similar trends would be found in other high T_c compounds, such as , Nb_3Ge, Nb_3Ga, Nb_3Al and V_3Si.

Finally, the author would like to recommend the oxidation technique for the investigation of the electrical and optical properties of thin metal films. This method is a very simple and useful technique provided the films can be oxidized with an appropriate condition. A single good quality specimen is sufficiently for use in the studies instead of a set of specimens prepared under the same conditions. It is hoped that this technique and the combination of techniques described in the present work can be useful for studying the electrical and optical properties of new materials and for verifying the model which has been proposed.

as a result of the present investigation is applicable to other materials.

****

APPENDIX A

THIN FILM OPTICS NOTATIONS

(i) Direction

In order to signify the direction of propagation of a wave a superscript + or - is used showing whether the wave travels in the positive or negative sense with respect to some fixed direction which is usually the normal to a surface or a film surface. A wave travelling towards the surface is regarded as positive.

(ii) Polarization

To give the plane of polarization a subscript is used:-

p , parallel to the plane of incidence

s , perpendicular to the plane of incidence.

Any orientation can be resolved into these two components.

(iii) Multilayers

If a system is composed of several layers of thin films each layer is denoted by a simple suffix. For example E^{+}_{np} is the amplitude of the electric vector of a wave travelling in the positive direction (towards the surface) in the n^{th} layer and polarized with the electric vector parallel to the plane of incidence. E^{-}_{ns} is the amplitude of the electric vector perpendicular to the plane of incidence.

Refractive Index

The refractive index 'n' of a non absorbing medium is given by:-

$$n = \frac{\text{wave velocity in vacuum}}{\text{wave velocity in medium}}$$

In an absorbing medium the refractive index 'n' is replaced by a complex quantity n-ik in which the imaginary part is related to the absorption of energy by the medium. For a path of one vacuum wavelength the attenuation of the amplitude of the wave is $\exp(-2\pi k)$.

The reduction of amplitude of the wave in a medium depends directly on the distance travelled so the loci of points of equal amplitude will be planes parallel to the surface of separation of two media. Only for NORMAL incidence are planes of equal phase parallel to those of equal amplitude.

APPENDIX B

A.S.M.T. Index Cards of the Compounds in the Niobium-Tin System, Niobium Oxides and Tin Oxides.

1-1183 MAJOR CORRECTION

3236 d 1-1185	2.33	1.34	1.65	2.33	Nb
I/I₁ 1-1183	100	32	20	100	NIOBIUM

Rad. MoKα λ 0.709 Filter ZrO_2
Dia. 16 INCHES Cut off Coll.
I/I₁ CALIBRATED STRIPS d corr. abs.? No
Ref. H

Sys. CUBIC S.G. O_h^9 - Im3m
a_o 3.301 b_o c_o A C
α β γ Z 2
Ref. Wy, Wys

ε α nω β ε γ Sign
2V D 8.57[20]mp 2500 Color WHITE
Ref. C.C.

B.P. > 3300

d Å	I/I₁	hkl	d Å	I/I₁	hkl
2.33	100	110			
1.65	20	200			
1.34	32	211			
1.16	6	220			
1.04	10	310			
0.95	1	222			
.88	6	321			
.78	2	411,330			
.74	1	420			
		INDEXED BY SW			

565

4-0673 MINOR CORRECTION

d 4-0669	2.92	2.79	2.02	2.915	β-Sn
I/I₁ 4-0673	100	90	74	100	BETA TIN

Rad. CuKα₁ λ 1.5405 Filter Ni
Dia. Cut off Coll.
I/I₁ G. C. DIFFRACTOMETER d corr. abs.?
Ref. SWANSON AND TATGE, NBS J. C FEL. REPORTS, 1951

Sys. TETRAGONAL S.G. D_{4h}^{19} - I4/AMD*
a_o 5.831 b_o c_o 3.182 A C
α β γ Z 4
Ref. IBID.

ε α nω β ε γ Sign
2V D_x7.286 mp Color
Ref. IBID.

*MARK AND POLANYI, Z. PHYS. 18, 75-96 (1925).
SPECTROGRAPHIC ANALYSIS SHOWS FAINT LINES OF Pb, Bi, Na.
SAMPLE ANNEALED FOR 12 HRS. AT 160°C.
AT 26°C
TO REPLACE 1-0926, 2-0709

d Å	I/I₁	hkl	d Å	I/I₁	hkl
2.915	100	200	1.0252	5	521
2.793	90	101	0.9824	5	213
2.062	34	220	.9718	2	600
2.017	74	211	.9310	3	303
1.659	17	301	.9286	13	512
1.484	23	112	.9219	5	620
1.458	13	400	.9178	5	611
1.442	20	321	.8868	4	323
1.304	15	420	.8755	2	541
1.292	15	411	.8485	4	413
1.205	20	312	.8466	10	532
1.0950	13	501	.8386	4	631
1.0434	3	103	.8086	6	640
1.0401	5	332	.8058	3	701
1.0309	2	440			

1675

5-0390 MINOR CORRECTION

d	3.75	2.29	1.96	3.751	α-Sn
I/I₁	100	83	53	100	ALPHA TIN

Rad. CuKα₁ λ 1.5405 Filter Ni
Dia. Cut off Coll.
I/I₁ G.C. DIFFRACTOMETER d corr. abs.?
Ref. SWANSON AND FUYAT, NBS CIRCULAR 539, VOL. II, 12 (1953)

Sys. CUBIC (FACE-CENTERED) S.G. O_h^7 - Fd3m
a_o 6.489 b_o c_o A C
α β γ Z 8
Ref. IBID.

ε α nω β ε γ Sign
2V D_x5.770 mp Color
Ref.

SAMPLE IS NBS MELTING POINT STANDARD #42D.
SPECT. ANAL.: <0.01% Cu, Fe, Pb.
SAMPLE WAS REFRIGERATED AT 10°C UNTIL JUST BEFORE USE.
X-RAY PATTERN AT 25°C.

d Å	I/I₁	hkl	d Å	I/I₁	hkl
3.751	100	111			
2.294	83	220			
1.956	53	311			
1.622	12	400			
1.489	20	331			
1.325	21	422			
1.249	11	511			
1.1470	6	440			
1.0968	10	531			
1.0260	9	620			
0.9895	4	533			
.9365	3	444			
.9087	7	711			
.8671	13	642			
.8450	12	731			

1885

15-481

d	2.39	2.18	2.71	4.78	$(NbSn_2)48S$
I/I$_1$	100	100	90	6	Niobium Tin

Rad. CuKα λ 1.5418 Filter Ni Dia.
Cut off I/I$_1$ Diffractometer
Ref. Van Ooijen, et al, Philips Res. Lab., Eindhoven, Netherlands

Sys. Orthorhombic S.G. Fddd (70)
a_o 19.126 b_o 5.645 c_o 9.852 A 3.388 C 1.745
α β γ Z 16 Dx 8.26
Ref. Van Ooijen, Phys. Letters 3 128 (1962)

εα nωβ εγ Sign
2V D 8.08 mp Color
Ref. Ibid.

Single crystal data taken.

d Å	I/I$_1$	hkl	d Å	I/I$_1$	hkl
4.777	6	400	1.7013	<1	913
4.746	4	111	1.6732	4	515
3.880	<1	311	1.6642	4	531
3.0130	25	511	1.6380	6	11.1.1
2.8090	65	113	1.6272	10	133
2.7056	90	220	1.6192	8	206
2.6758	80	602	1.6042	16	624
2.5945	55	313	1.5933	4	12.0.0
2.4642	10	004	1.5821	20	10.2.0,333
2.4492	25	022	1.5382	12	715
2.3852	100	800,711	1.5310	14	731
2.2794	8	513	1.5019	2	533
2.1897	35	404	1.4826	14	11.1.3
2.1796	100	422	1.4200	18	026
1.9681	2	713	1.4114	10	040
1.9490	16	911	1.4000	4	915
1.8517	<1	115	1.3944	4	931
1.8398	<1	131	1.3609	<1	426
1.7161	<1	804	1.3575	<1	135
1.7107	<1	822	Plus 99 lines to 0.8307		

2871

12-607

d	2.10	1.49	1.27	4.23	NbO
I/I$_1$	100	100	100	30	Niobium Oxide

Rad. CuKα λ 1.542 Filter Ni Dia.
Cut off I/I$_1$ Visual
Ref. Battelle Memorial Inst., Columbus, Ohio

Sys. Cubic S.G.
a_o 4.21 b_o c_o A C
α β γ Z 3 Dx 7.24
Ref. Brauer, Z. anorg. Chem. 248 1 (1941)

εα nωβ εγ Sign
2V D 7.30 mp Color
Ref.

d Å	I/I$_1$	hkl	d Å	I/I$_1$	hkl
4.23	30	100			
2.96	50	110			
2.43	70	111			
2.10	100	200			
1.88	30	210			
1.73	50	211			
1.49	100	220			
1.40	30	300,221			
1.33	40	310			
1.27	100	311			
1.21	60	222			
1.17	20	320			

9-235 MAJOR CORRECTION

d	3.42	2.54	1.75	5.63	$(NbO_2)96I$
I/I$_1$	100	80	80	20	Niobium(IV) Oxide

Rad. CuKα λ 1.5405 Filter MONOCHR. Dia. 80MM GUINIER
Cut off I/I$_1$ VISUAL
Ref. MAGNELI ET AL., ACTA CHEM. SCAND. 9 1402 (1955)

Sys. TETRAGONAL S.G. $P4_2/MNM$ (136)
a_o 13.71* b_o c_o 5.985* A C 0.4368
α β γ Z 32 Dx 5.90
Ref. IBID.

εα nωβ εγ Sign
2V D 5.98 mp Color
Ref.

*$a_O=2\sqrt{2}a_R$, *$c_O=2c_R$
WHERE a_R=4.846 AND c_R=2.993 REPRESENT THE LATTICE PARAMETERS OF THE SUBCELL OF THE RUTILE TYPE.

d Å	I/I$_1$	hkl	d Å	I/I$_1$	hkl
5.63	20	101	1.754	80	622R,650
4.29	20	211	1.712	50	800R
3.63	30	301			
3.42	100	400R	R— COMPATIBLE WITH THE BASIC RUTILE TYPE STRUCTURE.		
3.21	30	321			
2.91	30	411			
2.54	80	222,520R			
2.491	30	501,431			
2.422	50	440			
2.341	20	521			
2.253	30	402R			
2.166	20	620R			
2.014	10	541			
1.975	20	103			
1.932	20	631			
1.897	20	640,213			
1.862	20	701			
1.829	20	303			
1.766	30	612,730 721			

1465

17-909

d	2.37	2.16	2.65	3.75	$(Nb_3Sn)8\underline{C}$
I/I_1	100	90	50	4	Niobium Tin

Rad. Cu λ 1.5405 Filter Ni Dia.
Cut off I/I_1 Diffractometer
Ref. S. L. Bender, J. K. Hill, Avco Corporation, Wilmington, Massachusetts (1963)

Sys. Cubic S.G. Pm3n (223)
a_0 5.2908 b_0 c_0 A C
α β γ Z 2 Dx
Ref. Ibid.

ε α nωβ ε γ Sign
2V D mp Color
Ref.

d Å	I/I_1	hkl	d Å	I/I_1	hkl
3.75	4	110			
2.647	50	200			
2.367	100	210			
2.160	90	211			
1.528	6	222			
1.468	20	320			
1.414	45	321			
1.323	18	400			
1.183	10	420			
1.155	16	421			
1.128	10	332			
0.983	14	520,432			
.966	14	521			
.934	8	440			
.882	6	600,442			
.870	4	610			
.858	14	611,532			
.798	4	622			
.789	14	630,542			
.780	10	631			

W

19-875

d	2.15	1.41	2.36	2.63	$(Nb_3Sn)8\underline{C}$
I/I_1	100	90	80	30	Niobium Tin

Rad. CuKa λ 1.5418 Filter Ni Dia. 114.6mm
Cut off I/I_1 Visual
Ref. Institute of Physics, University College, Cardiff, Wales (1967)

Sys. Cubic S.G. Pm3n (223)
a_0 * b_0 c_0 A C
α β γ Z 2 Dx 8.92
Ref. van Vucht et al., Philips Res. Repts., 20 136 (1965)

ε α nωβ ε γ Sign
2V D 8.95 mp ** Color White
Ref. Ibid.

*5.2902-5.2816
**Peritectic decomposition at 1980±10°C.
Deposited on Niobium ribbon by the Oxford Instrument Co. Ltd.
ß-Tungsten-type.
Taken at 25.4°C, stable below 775°C.

d A	I/I_1	hkl	d A	I/I_1	hkl
2.632	30	200			
2.357	80	210			
2.149	100	211			
1.524	20	222			
1.463	30	320			
1.410	90	321			
1.319	40	400			
1.181	40	420			
1.153	40	421			
1.126	30	332			
0.983	40	520,432			
.965	30	521			
.936	20	440			
.882	40	600			
.870	30	610			
.859	60	611			
.798	30	622			
.789	70	630,542			
.780	70	631			

FORM T-2
W

19-877

d	2.39	2.30	2.31	4.03	$(Nb_6Sn_5)44\underline{P}$
I/I_1	100	80	45	2	Niobium Tin

Rad. CuKa λ 1.5418 Filter Dia.
Cut off I/I_1 Diffractometer
Ref. Van Vucht et al., Philips Res. Rept. 20 136 (1965)

Sys. Orthorhombic (b.c.) S.G.
a_0 5.6549 b_0 9.2057 c_0 16.814 A C
α β γ Z 4 Dx 8.74
Ref. Ibid.

ε α nωβ ε γ Sign
2V D 8.6 mp Color
Ref. Ibid.

Isomorphous with ß-Ti_6Sn_5. Peritectic decomposition at 930±15°C. Single crystal data taken.

See following card

d A	I/I_1	hkl	d A	I/I_1	hkl
4.03	2	022	2.017	6	044
3.16	10	114,015	1.991	4	127,143+
3.10	16	024	1.949	4	233,136
3.01	20	031,123	1.911	2	028
2.886	8	105	1.847	<2	310
2.822	4	200	1.826	<2	226
2.798	2	006	1.795	<2	217
2.680	30b	130,033+	1.771	2	109,235
2.560	4	132	1.747	4	150,053+
2.445	6	125	1.684	10	208,0010
2.420	16b	116	1.657	<2	323
2.392	100	026	1.654	4	138,129
2.343	30b	017,204	1.642	25	305,244
2.313	45	222	1.614	4	154,055
2.298	80	040	1.606	2	330
2.268	35	134,035	1.588	16b	039,147+
2.218	2	042	1.552	<2	048
2.210	6	107	1.548	<2	325
2.106	16b	141,215+	1.541	6	316,219+
2.061	2	231	1.534	4	060

FORM T-2
W

7-61 MAJOR CORRECTION

d	3.12	3.92	2.45	3.92	$(Nb_2O_5)3.5H$
I/I_1	100	90	40	90	NIOBIUM PENTA OXIDE

Rad. CuKα λ 1.542 Filter Ni Dia.
Cut off I/I_1 CALIBRATED SCALE
Ref. FREVEL AND RINN, ANAL. CHEM. 27 1329 (1955)

Sys. PSEUDOHEXAGONAL S.G.
a_o 3.607 b_o c_o 3.925 A C 1.088
α β γ Z 1/2 Dx MOLECULE
Ref. IBID.

ε a n ω β ℓ γ Sign
2V D mp Color
Ref.

DELTA MODIFICATION TRANSFORMED TO THE LOW TEMPERATURE MODIFICATION ON HEATING AT 700°C FOR 16 HOURS.

d Å	I/I_1	hkl	d Å	I/I_1	hkl
3.92	90	001			
3.12	100	100			
2.446	40	101			
1.962	30	002			
1.800	25	110			
1.663	30	102			
1.637	14	111			
1.565	12	200			
1.456	8	201			
1.327	18	112			
1.309	4	003			
1.222	8	202			
1.205	6	103			

597

6-0395 MINOR CORRECTION

d	2.99	2.69	1.80	4.85	$(SnO)4I$
I/I_1	100	35	25	10	TIN(II) OXIDE

Rad. CuKα λ 1.5405 Filter Ni
Dia. Cut off Coll.
I/I_1 DIFFRACTOMETER d corr. abs.?
Ref. SWANSON ET AL., NBS CIRCULAR 539 VOL IV p 28-9 (1953)

Sys. TETRAGONAL S.G. $P4/nmm$ (129)
a_o 3.802 b_o c_o 4.836 A C 1.272
α β γ Z 2
Ref. IBID.

ε a >2.0 n ω β ℓ γ Sign
2V Dx6.398 mp Color
Ref. IBID.

SAMPLE FROM THE BAKER CHEMICAL CO. SPECT. ANAL.: <0.01 % Ca, Cu, Fe, Mg, Sb, Si; <0.001 % Al, Ba, Ni, Pb.
X-RAY PATTERN AT 26°C.

d Å	I/I_1	hkl	d Å	I/I_1	hkl
4.85	10	001	1.076	6	312
2.989	100	101	1.030	4	321
2.688	35	110	1.020	4	204
2.418	14	002	0.994	2	303
2.039	<1	102	.985	2	214
1.901	14	200	.967	<1	005
1.797	25	112	.950	4	400
1.604	25	211	.937	4	105
1.494	12	202	.905	4	411
1.484	12	103	.898	4	224
1.382	4	113	.882	6	323
1.344	6	220	.852	4	314
1.225	4	301	.850	4	420
1.209	4	004	.840	6	215,332
1.202	4	310	.806	2	006
1.174	6	222	.802	<1	422
1.169	8	213	.800	2	413
1.152	2	104			
1.102	4	114			

225

5-0467 MINOR CORRECTION

d	3.35	2.64	1.77	3.351	SnO_2
I/I_1	100	81	63	100	TIN OXIDE (CASSITERITE)

Rad. $CuK\alpha_1$ λ 1.5405 Filter Ni
Dia. Cut off Coll.
I/I_1 DIFFRACTOMETER d corr. abs.?
Ref. SWANSON AND TATGE, NBS CIRCULAR 539 Vol. 1, 54 (1953)

Sys. TETRAGONAL S.G. D_{4h}^{14} - $P4/mnm$
a_o 4.738 b_o c_o 3.188 A C 0.673
α β γ Z 2
Ref. IBID.

ε a n ω β ℓ γ Sign
2V D_x6.995 mp Color
Ref. IBID.

SAMPLE FROM JOHNSON, MATTHEY AND CO., LTD. SPECT. ANAL. SHOWS NO LINES FOR IMPURITIES STRONGER THAN FAINTLY VISIBLE.
X-RAY PATTERN TAKEN AT 26°C.

TO REPLACE 1-0625,1-0657, 2-1337,2-1340,3-0439, 3-1114,3-1116

d Å	I/I_1	hkl	d Å	I/I_1	hkl
3.351	100	110	0.9505	8	402
2.644	81	101	.9291	3	510
2.369	24	200	.9143	3	332
2.309	5	111	.9081	8	501
2.120	2	210	.8819	7	422
1.765	63	211	.8814	6	303
1.675	63	220	.8480	6	521
1.593	8	002	.8375	1	440
1.498	13	310	.8261	4	323
1.439	17	112	.8125	2	530
1.415	15	301	.9026	6	512
1.322	7	202			
1.215	11	321			
1.184	3	400			
1.155	8	222			
1.117	3	330			
1.092	8	312			
1.081	8	411			
1.059	3	420			
1.036	4	103			

1913

ACKNOWLEDGEMENTS

This research was carried out at the University of Aston in Birmingham while on leave of study from the University of Chiengmai, Thailand.

I would like to thank my supervisor, Dr. W.E.J. Neal, for his enthusiastic support and patient while the present work was in progress.

I wish to express my gratitute to the technical staff of the Physics Department, in particular to Messrs. F. Lane and H. Arrowsmith of the main workshop and to Mr. G. Cochrane of the X-ray laboratory.

I should also like to thank the British Council for the fee awards.

REFERENCES

M.I. Agafonova, V.V. Baron and E.M. Savitskii : Izv Akad. Nauk SSSR Otd. Tekh. Nauh, Metallurgiya i Topliv.,No.5, p 139, (1959)

R.M. Aguado Bombin : PhD Thesis, Univ. of Aston, (1971)

R.M. Aguado Bombin and W.E.J. Neal : J. Appl.Phys.Lett.,28 , 410, (1976)

R.M. Aguado Bombin and W.E.J. Neal : Thin Solid Films, 42, 91, (1977)

N.E. Alekseevskii, N.Y. Ageev and V.J. Shamrai : Izv. Akademii. Navk. SSSR Neorg. Mater. 2, 2156, (1966)

R.J. Archer : J. Opt. Soc. Am., 52, 970, (1962)

L.R. Aronin : J. Appl. Phys., 25, 344, (1954)

V.D. Arp, R.H. Kropschot, J.H. Wilson, W.F. Love and R. Phelan : Phys. Rev. Lett., 6, 452-3, (1961)

D.G. Avery : Phil. Mag., 41, 1018, (1950)

J. Bardeen, L. Cooper and J. Schrieffer : Phys. Rev., 108, 1175, (1957)

J. Bardeen : Phys. Rev. Lett., 1, 399, (1958)

B.W. Batterman and C.S. Barrett : Phys. Rev. Lett., 13, 390, (1964)

R. Becker, G. Hiller and F. Santer : Z. Physik, 85, 772, (1933)

R. Bett : Cryogenics, 14, 361, (1974)

F. Bloch : Zeit. Physik, 52, 555, (1928)

R.M. Bozorth, A.J. Williams and D.D. Davis : Phys. Rev. Lett., 5, 148, (1960)

K.L. Chopra : 'Thin Film Phenomena' , McGraw-Hill, New York, (1969), p 138

W. Cirkler : Z. Physik, 147, 481, (1957)

G.D. Cody : RCA Review, Vol.XXV, 431, (1964)

G.D. Cody and G.W. Cullen : RCA Review, Vol. XXV, 476, (1964)

R.W. Cohen, G.D. Cody and J.J. Halloran : Phys. Rev. Lett., 19, 840, (1967)

L.N. Cooper : Phys. Rev., 104, 1189, (1956)

T. Courtney, G.W. Pearsall and J. Wuff : J. Metals, 16, 97-8, (1964)

A.J. Dekker : 'Solid State Physics' , Macmillan & Co Ltd.,(1962), p 27

W. De Sorbo : Phys. Rev., 132, 107, (1963)

J.M. Dickey, Myron Strongin and O.F. Kammerer : J. Appl. Phys., 42, 5808, (1971)

P. Drude : Ann Physik, 272, 532, (1889) ; ibid. 272, 865, (1889) ; ibid. 275, 481, (1890)

P. Drude : Wiedeman Ann. Physik,36, 884-6, (1889)

P. Drude : Ann. Physik, 1, 566, (1900)

R.C. Dynes, J.M. Poate, L.R. Testardi, A.R. Storm and R.H. Hammond, IEEE Transact. on Magnetics, Vol. MAG-13, 640, (1977)

T.G. Ellis and H.A. Wilhelm : J. Less-comm. Metals, 7, 67, (1964)

R. Enstrom, G.W. Pearsall and J. Wuff : Bull. Am. Phys. Soc. Ser.2, 7, 323, (1962)

R. Enstrom, T. Courtney, G. Pearsall and J. Wuff : 'Metallurgy of Advanced Electronic Materials',Vol. 19, Interscience Publishers, New York, (1963), p 121

R.E. Enstrom : J. Appl. Phys., 37, 4880, (1966)

Z. Fisk and G.W. Webb . Phys. Rev. Lett., 36, 1084, (1976)

H. Fröhlich : Phys. Rev., 79, 845, (1950)

K. Fuchs : Proc. Cambridge Phil. Soc., 34, 100, (1938)

J.R. Gavaler : J. Appl. Phys. Lett., 23, 480, (1973)

J.R. Gavaler, M.A. Janocko and C.K. Jones : J. Appl. Phys., 45, 3009, (1974)

S. Geller . B.T. Matthias, and R . Goldstein : J. Am.Chem.Soc., 77 , 1502,(1955)

V.L. Ginzburg and L.V. Landau : J.E.T.P., 20, 1064, (1950)

A.I. Golovashkin, E.D. Donner, I.S. Evchenko and G.P. Motulevich : Soviet Phys. J.E.T.P. 32, 1064, (1971)

C.J. Gorter and H.B.G. Casimir : Physica, 1, 305, (1934)

C.J. Gorter and H.B.G. Casimir : Phys. Z., 35, 963, (1934) ; Z. Techn. Phys., 15, 539, (1934)

J. Halder, L. Holland and L. Laurenson : J. Sci. Instr.,36, 281, (1959)

F.B. Haller : Rev. Sci. Instr., 35, 1356, (1964)

R.H. Hammond : IEEE Trans. on Magnetics, Vol. MAG-11(2), 201, (1975)

J.J. Hanak : 'Metallurgy of Electronic Materials', G.E. Brock, ed., Interscience Publishers, New York,(1963), p 161

J.J. Hanak, K. Strater and G.W. Cullen : RCA Review, Vol.XXV, 342, (1964)

G.E. Hardy and J.K. Hulm : Phys. Rev., 93, 1004, (1954)

H.R. Hart, J.S. Jacobs, C.L. Kolbe and P.E. Lawrence : 'High Magnetic Fields', Technol. Press, Cambridge, Mass., (1962), p 584

A.G. Jackson and M.P. Hooker : 'Structure and Chemistry of Solid Surfaces',edited by G.A. Somorjai , Wiley, New York, (1969)

H. Kammerlingh Onnes : Leiden Comm. 122b, 124c, (1911)

G.W.C. Kaye and T.H. Laby : 'Tables of Physical and Chemical Constants', (1973), p 92

C.H. Kittel : 'Introduction to Solid State Physics', John Wiley & Sons Ltd., (1971), p 332

V.S. Kogan, A.I. Krivko, B.G. Lazarev, L.S. Lazareva, A.A. Matsa and O.N.Ovcharenko : Fiz. Met. Metallov., 15, 143, (1963)

C.L. Kolbe and C.H. Rosner : 'Metallurgy of Advanced Electronic Materials',Vol.19, Interscience Publishers, New York, (1963), p 17

J.E. Kunzler, E. Buehler, F.S.L. Hsu and J.H. Wernick : Phys. Rev. Lett., 6, 89-91, (1961)

W.H. Lawson: J.Sci. Instrum. (G.B.), 44 ,917,(1967)

H.J. Levinstein and E. Buehler : Trans. Met. Soc. AIME , 230, 1314, (1964)

H. Lipson and H. Steeple : 'Interpretation of X-ray Powder Diffraction Patterns', MacMillan and Co Ltd.,(1970), pp 114-115

F. London and H. London : Proc. Royal Soc. (London), A149, 71, (1935)

H.A. Lorentz : Proc. Acad. Sci.,Amsterdam, 7, 438, 585, 684, (1904 - 1905)

M.S. Lucas : J. Appl. Phys., 36, 1632, (1965)

E.A. Lynton : 'Superconductivity', 3rd ed. , Methuen & Co Ltd., London, (1969), p 112

R. Mailfert, B.W. Batterman and J.J. Hanak : Phys. Status Solidi, 32, K67, (1969)

N. Mangkorntong and W.E.J. Neal : Surf. Tech., 5, 78-80, (1977)

W.P. Mason : 'Piezoelectric Crystals and Their Application to Ultrasonics', D. Van Nostrand Company, Inc., Princeton, N.J., 1956

L.F. Mattheiss : Phys. Rev. B , 12, 2161, (1975)

B.T. Matthias, T.H. Geballe, S. Geller and E. Corenzwit : Phys. Rev., 95, 1435, (1954)

B.T. Matthias, 'Progress Low Temperature Physics', Vol.II, edited by C.J. Gorter, Interscience Publishers, New York, Chapter V

B.T. Matthias, T.H. Geballe, L.D. Longinotti, E. Corenzwit, G.W. Hull and J.P. Maita : Science, 156, 645, (1967)

B.T. Matthias : Physics Today , 24, 25, (1971)

E. Maxwell : Phys. Rev., 78, 477, (1950)

H. Mayer : 'Structure and Properties of Thin Films', (C.A. Neugebauer, J.B. Newkirk and D.A. Vermilyea, eds.), John Wiley & Son, Inc., New York , (1959), p 225

F.L. McCrackin, E. Passaglia, R. Stromberg, and H.L. Steinberg : J. Res. Natt. Bur. Std. 67A, 363, (1963)

H. Meissner and R. Ochsenfeld : Naturwissenschaften, 21, 787, (1933)

O. Meyer, H. Mann and E. Phrilingos : 'Applications of Ion Beams to Metals', edited by S.T. Picraux, E.P. EerNisse and F.L. Vook, Plenum, New York, (1974), p 15

R.F. Miller, A.J. Taylor and L.S. Julien : J. Appl. Phys. (D), 3, 1957, (1970)

D.B. Montgomery : Bull. Am. Phys. Soc. Ser.2, 10, 359, (1965)

J.H. Mooij : Phys. Status Solidi (a), 17, 521, (1973)

K.R. O'Shea : PhD Thesis, Univ. of Aston, 1971.

T.B. Reed and H.C. Gatos : J. Appl. Phys.,33, 2657, (1962)

T.B. Reed, H.C. Gatos, W.J. Lafleur and J.T. Roddy : 'Superconductors', Interscience, New York, (1962), pp 143-9

C.A. Reynolds, B. Serin, W.H. Wright and L.B. Nesbitt : Phys. Rev., 78, 487, (1950)

B. Roberts : Progress in Cryogenics, Vol. IV, pp 160-231, (1964)

B. Roberts : J. Phys. Chem. Ref. Data, 5, 581, (1976)

A.C. Rose-Innes and E.H. Rhoderick : ' Introduction to Superconductivity', Pergamon Press, (1976), p 47

I.W. Salter : PhD Thesis, Univ. of Aston, 1973

R.M. Scanlan, W.A. Fietzand E.F. Koch : J. Appl. Phys., 46, 2244, (1975)

H.W. Schadler and H.S. Rosenbaum : J. Metals, 16, 97, (1964)

B.J. Shaw : J. Appl. Phys., 47, 2143, (1976)

D. Shoenberg : 'Superconductivity', Cambridge Univ. Press, (1960)

F.B. Silsbee : J. Wash. Acad. Sci., 6, 597, (1916)

E.H. Sondheimer : Phys. Rev., 80, 401, (1950)

E.H. Sondheimer : Adv. Phys., 1, 1, (1952)

J.A. Strozier, D.L. Miller , O.F. Kammer and M. Strongin : J. Appl. Phys., 47, 1611, (1976)

A. Sommerfeld : Z. Physik, 47, 1, (1928)

P.S. Swartz, H.R. Hart and R.L. Fleischer : Appl. Phys. Lett., 4, 71, (1964)

A.R. Sweedler, D.G. Schweitzer and G.W. Webb : Physical Review Lett., 33, 168, (1974)

L.R. Testardi, J.H. Wernick, W.A. Royer, D.D. Bacon and A.R. Strom : J. Appl. Phys., 45, 446, (1974)

L.R. Testardi, R.L. Meek, J.M. Poate, W.A. Royer, A.R. Strom and J.H. Wernick : Phys. Rev. B , 11, 4304, (1975)

L.R. Testardi, J.M. Poate and H.J. Levinstein : Physical Rev. Lett., 37, 637, (1976)

L.R. Testardi, J.M. Poate and H.J. Levinstein : Phys. Rev., 15, 2570, (1977)

J.J. Thomson : Proc. Cambridge Phil. Soc., 11, 120, (1901)

S. Tolansky : 'Multiple Beam Interferometry', Clarendon Press, (1949)

J.H.N. van Vucht, D.J. van OOIJEN and H.A.C.M. Bruning : Philips Res. Rept. 20, 136-161, (1965)

A. Vasicek : 'Optics of Thin Films', North-Holland Publishing Company, (1960), p 26

L.J. Vieland : RCA Review, Vol. XXV, 366, (1964)

G.W. Webb, L.T..Vieland, R.E. Miller and A. Wicklund : Solid State Comm., 9, 1769, (1971)

H. Wiesmann, M. Gurvitch, H. Lutz, A. Ghosh, B. Schwarz, Myron Strongin, P.B. Allen and J.W. Halley : Phys. Rev. Lett., 38, 782, (1977)

A.W. Wilson : Proc. Roy.Soc. Ser. A, 167, 580, (1938)

A.B. Winterbottom : Norske Videnskabers Selskab (Trondheim), (1955)

D.W. Woodard and G.D. Cody : Phys. Rev., 136, 166A, (1964)

L.L. Wyman, J.R. Cuthil, G.A. Moore, J.J. Park and H. Yakowitz : J. Res. Nat. Bur. of Standards, Phys. and Chem. , 66A, 351, (1962)

L. Young and F.G.R. Zobel : J. Electrochem. Soc., 113, 277, (1966)

*

W.E.J. Neal and Fane : J. Phys. E, 6 , 409, (1973)

W.E.J. Neal and R.M. Aguado Bombin: Thin Solid Films, 44 , 169, (1977)

A. Neugebauer: J. Appl. Phys., 35, 3599, (1964)

J. Niebuhr: Z. Physik, 132, 468, (1952)

formed. In the other case the reaction leads to a ≡Ge—O— complex with an unsaturated bond which would be expected to be electronically active (H1 states).

The author wishes to acknowledge much support by Professor Dr. W. Waidelich. He thanks Professor Dr. H. Finkenrath for critical reading of the manuscript and is very grateful to Mrs. H. Schäfer for co-operation in typing the manuscript.

1 E. W. Kreutz and W. Waidelich, Phys. Letters, 31A (1970) 117.
2 E. W. Kreutz, H. Pagnia and W. Waidelich, Z. angew. Phys., 30 (1970) 145.
3 E. W. Kreutz, Japan. J. Appl. Phys., Suppl. 2, (2) (1974) 445.
4 E. W. Kreutz and B. Waack, Phys. Status Solidi, 25a (1974) 251.
5 E. W. Kreutz, Appl. Phys., 10 (1976) 289.
6 A. F. Bogenschütz, Ätzpraxis für Halbleiter, C. Hanser, München, 1967.
7 P. K. Kashkarov and S. N. Kozlov, Soviet Phys. Semiconductors, 8 (1974) 646.
8 J. Bardeen, Phys. Rev., 71 (1947) 717.
9 E. W. Kreutz, H. Mödl and H. Pagnia, Z. angew. Phys., 30 (1970) 269.
10 G. Heiland and P. Handler, J. Appl. Phys., 30 (1959) 446.
11 W. H. Brattain and J. Bardeen, Bell System Tech. J., 32 (1953) 1.
12 E. W. Kreutz, Appl. Phys., 1 (1973) 161.
13 E. W. Kreutz, Thin Solid Films, submitted for publication.
14 T. P. Ma, Appl. Phys. Letters, 27 (1975) 615.
15 E. W. Kreutz, Z. angew. Phys., 32 (1971) 280.
16 H. A. Papazian, J. Appl. Phys., 27 (1956) 1253.
17 F. J. Arlinghaus and W. A. Albers, J. Phys. Chem. Solids, 32 (1971) 1455.

Surface Technology, 5 (1977) 78 - 80

Short Communication

Preparation of high critical temperature and high resistivity ratio Nb_3Sn films on quartz

N. MANGKORNTONG and W. E. J. NEAL

Physics Department, University of Aston in Birmingham, Birmingham B4 7ET (Gt. Britain)

(Received July 29, 1976)

During the last decade there has been considerable interest shown in the alloys Nb_3X, (X = Sn, Ga, Ge and Si) having β-tungsten (A-15) structure, because of their high critical temperature (T_c) either measured or expected. In the case of Nb_3Sn, bulk material can be produced by sintering [1] or preferably by vapour growth as explained by Testardi [2]. In some applications, *e.g.* a resonant cavity, it is sufficient to form a thin layer of the alloy on the surface of niobium by heating the metal under vacuum conditions in tin vapour at a temperature in the region of 900 °C. Surface layers with high T_c have been prepared although it is not easy to determine the characteristics of such layers independently particularly if they are very thin. Various authors have shown that the superconductive properties of the alloy depend on the temperature of preparation whether as bulk or as layers on niobium [3 - 6]. Thin layers have been prepared by chemical vapour deposition [7], vapour deposition–coevaporation [8, 9], and diffusion layers [5, 6]. Diffusion is one of the simplest methods for preparing a superconducting layer and usually short diffusion times have been employed.

In the work described here thin films of Nb_3Sn have been prepared on quartz substrates by a process of evaporation, diffusion, alloying and annealing, thus enabling the independent investigation of the electrical and structural properties of the films.

Basic equipment

The substrate holder was designed in such a way that up to eight films with the same or different thicknesses could be prepared simultaneously depending on the separation of source and substrate. The positions of the polished fuzed quartz substrates (measuring 15 mm × 20 mm) were arranged on the segment of a sphere such that the normals from the centres of the films intersected at the electron gun hearth. They could be heated independently up to 1000 °C to provide a range of temperatures as in the alloying process or all maintained at the same temperature as in the evaporation or diffusion processes. A careful cleaning procedure was adopted which included washing in 5% detergent solution and distilled water, ultra-sonic cleaning, heating in

isoprophyl alcohol and final removal through the vapour. Prior to evaporation a prolonged outgassing procedure was adopted for the sources, substrates and the vacuum chamber.

Film preparation

Films of niobium (99.99% purity) were first prepared in a chamber (base pressure $\sim 10^{-9}$ torr) by electron gun evaporation on to quartz substrates held at a temperature of 400 °C. The evaporation rate was ~10 nm/min and this in conjunction with a high substrate temperature had previously been shown to reduce gaseous impurities [10]. The mass deposited was measured by a quartz crystal monitor to give any desired film thickness. At the completion of the evaporation the substrates were cooled to room temperature and a film of tin (99.999% purity) was evaporated over the niobium from a quartz crucible adjacent to the electron gun hearth. In the diffusion stage which followed the substrates were held at a temperature of 400 °C for several hours. Too high a temperature produced re-evaporation of tin and a short time resulted in penetration of only part of the niobium film.

After the diffusion process, the substrates were further heated in the vacuum chamber to temperatures ranging between 650 °C and 1000 °C for the alloying process for a period of several hours. Films formed after a short alloying period either did not exhibit superconductivity or consist of the required alloy Nb_3Sn. Film thicknesses were checked after removal from the vacuum using an interferometer and fringes of equal chromatic order.

Results and discussion

In all over 100 films were prepared (under varying conditions) of which over 30 exhibited superconducting properties. All films were examined in an X-Ray diffractometer and their critical temperatures (T_c) observed in a cryostat in which temperatures between 1.5 K and 300 K could be produced. For the very thin alloy films (<50 nm) the X-ray diffraction lines were weak. For the thicker films which gave an onset $T_c > 17$ K it was possible to establish A-15 structures and examples for two such films out of ten in this category are given in Table 1.

The presence of niobium tin alloys other than Nb_3Sn, when the alloying temperature is low has been reported by other workers [1, 4, 5]. We have also found this to be true for Nb_3Sn films on quartz. At temperatures less than 650 °C superconducting films of $NbSn_2$ were produced. An increase of alloying temperature from 650 to 1000 °C increases the critical temperature and even for very thin films prepared at high temperatures, high T_c values were obtained. Table 1 shows that niobium oxide (NbO) was the major impurity but even so, values of T_c are near the bulk value of 18 K.

This method of preparation shows that the care in preparation of alloy films is very important in order to achieve high critical temperatures. Another factor indicative of good quality film is the resistivity ratio ρ_{300}/ρ_{20}. The better films prepared by the method described have given resistivity ratios of 3.6 - 4.3.

TABLE 1

X-ray data and some superconducting properties of two samples prepared by the technique described in this report

Sample No.	d (Å) (obs.)	hkl	I/I_{max}	Remark	Additional information*
1	4.23	100	4	NbO	T_c = 17.8 K
	2.65	200	100	Nb_3Sn	t = 500 nm
	2.44	111	8	NbO	a_o = 5.29 Å
	2.37	210	50	Nb_3Sn	t_s = 800 ± 50 °C
	2.16	211	3	Nb_3Sn	ρ_{300}/ρ_{20} = 4.28
	2.11	200	10	NbO	
	1.32	400	8	Nb_3Sn	
2	4.21	100	50	NbO	T_c = 18.2 K
	2.64	200	100	Nb_3Sn	t = 450 nm
	2.43	111	41	NbO	a_o = 5.28 Å
	2.36	210	77	Nb_3Sn	t_s = 800 ± 50 °C
	2.15	211	10	Nb_3Sn	ρ_{300}/ρ_{20} = 3.66
	2.11	200	41	NbO	
	1.18	420	15	Nb_3Sn	

* t = film thickness, t_s = alloying temperature, a_o = lattice parameter.

Bombin and Neal [11] have reported a correlation between resistivity ratio (in the range 1 to 6) and critical temperature for evaporated tantalum films. Testardi *et al.* [12] have also shown a correlation between resistivity ratio and T_c for sputtered Nb_3Ge films although the maximum resistivity ratio giving $T_c \sim 23$ K was in the region of 3. It would seem that if higher quality films of Nb_3X alloys could be produced, higher T_c values for films could be achieved as has been illustrated in this report for Nb_3Sn.

1 J. H. N. van Vucht, D. J. van Oojen and H. A. C. M. Bruning, Philips Res. Repts., 20 (1965) 136.
2 L. R. Testardi, Rev. Mod. Phys., 47 (1975) 637.
3 J. E. Kunzler, E. Buehler, F. S. L. Hsu and C. Wahl, Phys. Rev. Lett., 6 (1961) 89.
4 V. N. Svechnikov, V. M. Pan and Yu. I. Beletskii, Soviet Phys. Dokl. (U.S.A.), 11 (1966) 152.
5 A. A. Matsakova and B. G. Lawarev, Phys. Met. Metallogr., 35 (1) (1973) 133.
6 G. Pasotti, M. V. Ricci, N. Sacchetti, G. Sacerdoti and M. Spadoni, J. Mater. Sci., 6 (1971) 54.
7 J. J. Hanak, K. Strater and G. W. Cullen, RCA Review, XXV (1964) 342.
8 R. H. Hammond, IEEE Trans., MAG-11 (1975) 201.
9 A. I. Golovashkin, I. S. Levchenko and G. P. Motulevich, Phys. Metals Metallogr., 28 (1969) 166.
10 R. M. Aguado Bombin, Ph. D. Thesis, Aston University (1975).
11 R. M. Aguado Bombin and W. E. J. Neal, Appl. Phys. Lett., 28 (1976) 410.
12 L. R. Testardi, R. L. Meek, J. M. Poate, W. A. Royer, A. R. Storm and J. H. Wernick, Phys. Rev. B., 11 (1975) 4304.